GeoERA RESOURCE GROUNDWATER

Resources of groundwater, harmonized at Cross-Border and Pan-European Scale

Deliverable 3.2

Report with associated database of hydraulic properties of prime aquifers and aquitards and fault zones

Authors and affiliation:
Ronald Vernes (TNO-GSN), Koen Beerten (SCK CEN), Bernd Linder (GD NRW), Alberto Casillas (SCK CEN), Andreas Kruisselbrink (TNO-GSN), Reinder Reindersma (TNO-GSN), Bart Rogiers (SCK CEN), Cis Slenter (VMM)

E-mail of lead author:
ronald.vernes@tno.nl

Version: May 2021

This report is part of a project that has received funding by the European Union's Horizon 2020 research and innovation programme under grant agreement number 731166.

Deliverable Data		
Deliverable number	D3.2	
Dissemination level	Public	
Deliverable name	Report with associated database of hydraulic properties of prime aquifers and aquitards and fault zones	
Work package	WP3 H3O-PLUS	
Lead WP/Deliverable beneficiary	VMM	
Deliverable status		
Submitted (Author(s))	28/05/2021	Ronald Vernes (TNO-GSN)
Verified (WP leader)	31/05/2021	Cis Slenter (VMM)
Approved (Coordinator)	31/05/2021	Hans-Peter Broers (TNO-GSN)

EXECUTIVE SUMMARY

This report describes a database of hydraulic properties of aquifers and aquitards based on common criteria created as part of the H3O-PLUS project. Attention is also given to the characterization of hydraulic properties of faults. The cross-border demonstration project H3O-PLUS may set a new standard for harmonization across borders of hydrogeological and hydrological data.

The Roer Valley Graben, an active rift basin comprising parts of Germany, the Netherlands and Belgium, is of great importance for drinking water supply. Although the occurrence and behaviour of groundwater are not restricted to national borders, groundwater managers were faced with inconsistencies between subsurface information from the different countries, which led to uncertainty in the understanding of the groundwater system in the border region.

Unambiguous (hydro)geological knowledge and information are essential for sustainable management and use of not only groundwater resources but of the entire subsurface.
A 3D hydrogeological model was developed in a series of so called 'H3O' projects in the transboundary region in the Roer Valley Graben. The results are stored as digital maps of the top, base and thickness of all relevant aquifers and aquitards. H3O-PLUS, a work package of the RESOURCE-project, aims to add attribute data to the modelled units to facilitate the use of the maps in decision making processes.

Groundwater flow models are commonly used in groundwater management. Various Dutch, Belgian and German models exist for (parts of) the Roer Valley Graben. These models require input data, of which the geometry and hydraulic properties of the aquifers and aquitards are important ones. The harmonization of the 3D geometry of the hydrogeological units in the H3O-projects constitutes a major step towards a common hydrogeological dataset of the Roer Valley Graben and thus the harmonization of these groundwater flow models. The next step is the characterization of these hydrogeological units with respect to their hydraulic properties, primarily their hydraulic conductivity. This report documents the method and results of this next step.

Based on common criteria, an inventory and analyses of the hydraulic conductivity (K-value) of the Cenozoic aquifer system were made by Dutch, Belgian and German partners. Attention was also given to the characterization of hydraulic properties of faults.

Not surprisingly, the metadata analysis of K-values for aquifers and aquitards shows that the availability of data on hydraulic conductivity decreases with depth. For some of the hydrogeological units, no data are available at all or only for specific subareas. It is striking to note that data are lacking for important aquitards such as the Boom Clay in the Dutch part of the Roer Valley Graben and the lignite layers of the Ville Formation in the Dutch and Belgian part of the project area. Although data reliability presented in this study is a first assessment only, it shows that the reliability of available hydraulic conductivity data decreases with depth.

Of the 59 hydrogeological units for which hydraulic conductivity data are available in more than one country:

- 18 units show a very good agreement for K values between the various subareas on different sides of common borders. These units are all aquifers and dominated by relatively pure quartz sand, coarse to fine, with various degrees of gravel. They are mostly deposited in a fluvial-estuarine setting, while some units refer to a shallow marine environment.
- 32 units show a good agreement for K values between the various subareas, in the sense that their expert ranges at least partially overlap. However, for some subareas either the expert and/or absolute minimum or maximum shows a significant offset and/or

the full range is much smaller or larger. Around 47% of these units (15 out of 32) are aquitards.

- 10 do not show any overlap for their expert ranges, and with various degrees of overlap of their absolute ranges. Out of 10 units, 7 qualify as an aquitard.

The juxtaposition and displacement analysis of a fault near Veghel, which is part of the Peel Boundary Fault zone, provide a better 3D insight in areas where sand-to-sand contacts are present, and hydraulic connectivity across the fault plane may therefore occur. However, 3D seismic data is required for an interpretation that would be detailed enough for the study of the relay ramp, areas of fault-linkage that play an important role in groundwater dynamics around faults.

The nature of groundwater dynamics around faults that act as horizontal flow barriers was assessed through exhaustive numerical modelling of groundwater flow along the Rauw Fault near Mol. The results of this exercise show how the flow pattern can be deflected in an upward direction, and fully explain observations of abrupt groundwater head gradients across the fault. The modelling exercise leads to an estimate of the hydraulic characteristic of the fault, which, in combination with the width of the barrier zone, leads to a value for hydraulic conductivity of the fault. Another way of characterising hydraulic properties of fault zones is demonstrated for the Peel Boundary Fault near Veghel, using a detailed juxtaposition analysis.

The results of this deliverable may be a first step in the parameterisation of Dutch, Belgian and German groundwater flow models of the area, thus supporting management of transboundary groundwater water resources.

TABLE OF CONTENTS

1 INTRODUCTION

The cross-border demonstration project H3O-PLUS may set a new standard for harmonization across borders, not only for hydrostratigraphy, but also for hydrological data such as groundwater heads and groundwater quality.
H3O-PLUS, the third work package (WP3) of the project RESOURCE, aims to be an advanced demonstration of a transboundary assessment of groundwater resources. It is 'advanced' in the sense that it builds on and extends previous work, trying to make it more useful for groundwater policy and management and for subsurface spatial planning. A 3D hydrogeological model has been developed in a series of so called 'H3O' projects[1] in the transboundary region in the Roer Valley Graben, comprising parts of Germany, the Netherlands and Belgium. The results are stored as digital maps of the top, base and thickness of all relevant aquifers and aquitards. H3O-PLUS aims to add attribute data to the modelled units to facilitate the use of the maps in decision making processes. Note that the project does not aim to produce new maps or spatial delineations. The objective is to characterize units on existing maps and hence support the interpretation and use of those existing maps.

The overall study area coincides with the study areas of previous H3O projects (Figure 1). Vertically, the study is limited to the clastic (hydro)geological layers of Cenozoic age or younger. This coincides with the vertical scope of the recently developed transboundary 3D (hydro)geological models of the H3O projects. The base of the models is thus located at the top of the Chalk aquifer (Houthem or Maastricht / Kunrade Formations) or the top of the Carboniferous deposits.

Figure 1 – The four H3O-PLUS model areas, distributed over 3 countries, leading to 7 subareas.

[1] For more information and data downloads of the H3O-projects, the reader may refer to H3O (H3O website of TNO), H3O-Roerdalslenk (website of the Flemish administration), or H3O-De Kempen (website of the Flemish administration).

Groundwater flow models are commonly used in groundwater management. Various Dutch, Belgian and German models exits for (parts of) the Roer Valley Graben, see Buma et al. (2021). These models require input data, of which the geometry and hydraulic properties of the aquifers and aquitards are important ones. The harmonization of the 3D geometry of the hydrogeological units in the H3O projects constitutes a major step towards a common hydrogeological dataset of the Roer Valley Graben and thus the harmonization of these groundwater flow models. The next step is the characterization of these hydrogeological units with respect to their hydraulic properties, primarily their hydraulic conductivity.

This report describes a database of hydraulic properties of aquifers and aquitards based on common criteria. Attention is also given to the characterization of hydraulic properties of faults.

The work has been supported in part by the Dutch provinces of Noord-Brabant and Limburg, as well as the water companies Brabant Water and Waterleiding Maatschappij Limburg (WML).

2 HYDRAULIC CONDUCTIVITY

The hydraulic properties of strata represent the physical properties of the materials related to groundwater flow (Vandersteen et al., 2013). These are the hydraulic conductivity, storage coefficients (specific storage, storativity and specific yield) and porosity. They are used in the groundwater flow diffusion equation for the transient flow (see, e.g., Rushton and Redshaw, 1979). When estimating the steady-state groundwater flow, the Laplace equation is used, in which the dynamic term including groundwater storage becomes zero. The most important parameter from a modelling perspective is the (saturated) hydraulic conductivity, denoted by the symbol K, since this parameter together with the hydraulic gradient allows quantifying groundwater flow.
Information on the hydraulic conductivity often originates from various sources, for example laboratory tests, estimates based on lithological descriptions of soil samples, pumping tests, calibrated groundwater flow models, etc. However, the hydraulic conductivity often depends on the scale of the groundwater flow that is considered (e.g. Bear, 1972). This is an important consideration when comparing and analysing heterogeneous data on hydraulic conductivity.

Laboratory tests on borehole samples (usually samples of 20 to 100 cm^3) provide information about hydraulic conductivities at the core scale. The measurements are carried out in a controlled environment and provide reliable values at that scale. However, this scale differs from the application in groundwater flow models, even though the scales of groundwater models vary over orders of magnitudes ranging from e.g. the local scale of building pit dewatering and cleaning up of groundwater contamination to the regional or supra-national scale of river basins for groundwater management in the context of the EU Water Framework directive.
Therefore, measurements, for example laboratory tests, need to be upscaled to obtain hydraulic conductivities at the application scale. In this project, the application scale considered is the regional scale of most of the groundwater flow models in the Roer Valley Graben. The upscaling of small-scale data however falls outside the scope of this project. This should be kept in mind when data of various scales are presented.

3 HYDRAULIC CONDUCTIVITY OF HYDROGEOLOGICAL UNITS

3.1 Method

3.1.1 General approach

The aim is to create a database of hydraulic properties of the hydrogeological units, both aquifers and aquitards, of the H3O-models. The format of this 'database' is an Excel workbook.

This database can provide information about regional differences and trends in parameter values which could be used for making maps, but it is explicitly not the objective of H3O-PLUS to produce such maps. Instead, the goal is to gather data from different regions and explain cross-border differences in inventoried parameter value ranges should they occur.

The procedure to create and fill this database of hydraulic properties is as follows:

1. A first round of data gathering based on an initial template of the database was completed for the hydrogeological units of the Kieseloolite Formation. The sandy parts of this formation build up the most important cross-border aquifer of the Roer Valley Graben and as such can be regarded as a good example to work out the methodology and database in more detail. The results were discussed focusing on the structure of the worksheet (Which fields are useful? Which are less useful? Which data are lacking?) rather than on the collected data content. The discussion led to several modifications of the worksheet:
    - Concerning the considered parameters: hydraulic conductivity is the most important, but transmissivity, resistance and porosity might also be considered. However, transmissivity and resistance can be deducted from the hydraulic conductivity and (saturated) thickness of the units. Given the fact that porosity data are very scarce it was decided to restrict the data inventory to hydraulic conductivity;
    - In order to record the spatial variation in parameter values in the database in a simple way without making maps, a distinction is made between values for different H3O subareas. This is a practical way to deal with spatial variation.
    - In order to define the subareas, some overlap issues had to be addressed. There is some overlap between H3O subareas: between ROSE and Roer Valley Graben (here we take the Meuse as boundary) and between De Kempen and Roer Valley Graben. However, the overlap is small. If the overlapping region would contain parameter values, then these will be used for both regions.
    - A distinction is made between the 'absolute' min-max range that includes the extremes that can be found in literature and the 'expert' range that a modeler or other expert would use. This is a 'representative' value that we would recommend using.
    - We discussed whether metadata should be included in the excel table: literature source, method (type of test, type of interpretation, …), … This seems to be difficult, because one parameter range can be derived from different literature sources. A comment field is included in the Excel worksheet where arguments (and literature sources) can be inserted for setting the range to certain values (see section 3.1.2.2).
    - Information about thickness of layers can be derived from the H3O models, so it is not necessary to include this in the Excel worksheet. It might however be insightful to include a histogram of thickness values, eventually a separate graph per H3O subregion.

2. A second round of data gathering - with an adjusted sheet – was performed for the units of the Kieseloolite Formation, the results of which were visualized in a graph. The graphical presentation of the hydraulic conductivity ranges was optimized.
3. Data for all the other hydrogeological units and H3O subareas were collected accordingly.
4. The ranges of values for the same hydrogeological unit but different H3O subareas were analysed. If the parameters are within the same order of magnitude, they can be used directly in H3O-PLUS. If there are important differences for a given hydrogeological unit, the data should be interpreted in more detail to assess the reason for the difference and the way it should be dealt with in H3O-PLUS. Important notes that needed to be made were reported in the Excel workbook.

3.1.2 Definition of the Excel workbook

3.1.2.1 General lay-out

The Excel workbook contains the following sheets:

- Table: the main part of the database with ranges in hydraulic conductivity of the hydrogeological units in the different subareas of the H3O-model, see paragraph 3.1.2.2 .
- Correlation table and category: an overview of the hydrogeological units in this project with their corresponding Dutch, Belgian and German names in the various subareas, classified according to the three categories considered in the analyses of the data, see paragraph 3.1.9.
- Notes on observed trends: specific and detailed notes on observed trends and differences, see paragraph 3.1.9.
- References: an overview of the various data sources used.
- Key to colours and remarks: legend and explanations of colours used, and remarks given in the first two worksheets.

3.1.2.2 Lay-out of worksheet “Table”

Column A “Nr”: record number

Column B “Model area (H3O)”: H3O model area for which the information on hydraulic conductivity is valid:

- RVG: H3O-Roerdalslenk (Roer Valley Graben)
- De Kempen: H3O-De Kempen (Campine)
- RVGNW: H3O-Roerdalslenk Noordwest (Roer Valley Graben Northwest)
- ROSE: H3O-ROSE (Roer Valley Graben SouthEast)

Column C “Geological unit code (H3O-PLUS)”: Code of the geological model unit of the combined H3O *geological* models. Note that this is a geological unit, and not a hydrogeological unit.

Column D “Hydrogeological unit code (H3O-PLUS)”: Code of the model unit of the combined H3O *hydrogeological* models. As definition and coding of the model units differ between the various H3O-projects an Excel table (“Correlation table and category”) was created which provides information on corresponding model units. For every model unit of the combined hydrogeological model a code was given. It is this unique code that corresponds to the information given in the factsheets (see Appendix).

Column E “Hydrogeological unit (H3O)”: Code of the hydrogeological unit as used in the preceding H3O projects.

Column F “Unit Type”: The type of hydrogeological unit: aquifer or aquitard.

Column G “Conductivity”: Horizontal hydraulic conductivity (Kh) or vertical hydraulic conductivity (Kv). For aquifers horizontal conductivity values will be provided, for aquitards vertical hydraulic conductivity values.

Column H "BE unit code (HCOV)": The code of the corresponding Belgian hydrogeological unit according to the HCOV hydrostratigraphical system.
Column I "BE unit description (HCOV)": A short description or the Belgian name of the hydrogeological unit according to the HCOV hydrostratigraphical system.
Column J "BE lithofacies (HCOV)": the lithofacies of the sediments of the hydrogeological unit according to Belgian sources.
Column K "BE reference lithofacies": Number that refers to the source from which the Belgian information on the lithofacies was obtained. Full references are presented in a separate worksheet "References BE".
Column L "BE expert range min.": Minimum value of the range of values that the hydraulic conductivity (m/d) is likely to have according to quoted references and expert judgement.
Column M "BE expert range max.": Maximum value of the range of values that the hydraulic conductivity (m/d) is likely to have according to quoted references and expert judgement.
Column N "BE reference expert range": Number that refers to the source from which the Belgian information on the expert range was obtained. Full references are presented in a separate worksheet "References BE".
Column O "BE absolute min.": Absolute minimum value of the hydraulic conductivity (m/d) in the Belgian part of the project area that is still considered to be plausible.
Column P "BE absolute max.": Absolute maximum value of the hydraulic conductivity (m/d) in the Belgian part of the project area that is still considered to be plausible.
Column Q "BE reference absolute range": Number that refers to the source from which the Belgian information on the absolute range was obtained. Full references are presented in a separate worksheet "References BE".
Column R "BE qualitative reliability assessment": Qualification that indicates the overall reliability of the given values. Explanation is provided in the separate worksheet "Reliability assessment".
Column S "BE remarks": Important remarks on the hydraulic conductivity (m/d) of the unit in the Belgian part of the project area.
Column T "DE unit code (Rurscholle)": The code (Symbol) of the corresponding German "Kartiereinheit" according to the lithostratigraphical classification scheme of IS GK50 (Informationssystem Geol. Karte 1:50.000), Rahmenlegende.
Column U "DE unit description (Rurscholle)": A short description of the German name of the "Kartiereinheit" according to the lithostratigraphical classification scheme of IS GK50 (Informationssystem Geol. Karte 1:50.000), Rahmenlegende.
Column V "DE lithofacies (Rurscholle): The lithofacies of the sediments of the "Kartiereinheit" according to German sources.
Column W "DE reference lithofacies": Number that refers to the source from which the German information on the lithofacies was obtained. Full references are presented in a separate worksheet "References DE".
Column X "DE expert range min.": Minimum value of the range of values that the hydraulic conductivity (m/d) is likely to have according to quoted references and expert judgement.
Column Y "DE expert range max.": Maximum value of the range of values that the hydraulic conductivity (m/d) is likely to have according to quoted references and expert judgement.
Column Z "DE reference expert range": Number that refers to the source from which the German information on the expert range was obtained. Full references are presented in a separate worksheet "References DE".
Column AA "DE absolute min.": Absolute minimum value of the hydraulic conductivity (m/d) in the German part of the project area that is still considered to be plausible.
Column AB "DE absolute max.": Absolute maximum value of the hydraulic conductivity (m/d) in the German part of the project area that is still considered to be plausible.

Column AC "DE reference absolute range": Number that refers to the source from which the German information on the absolute range was obtained. Full references are presented in a separate worksheet "References DE".
Column AD "DE qualitative reliability assessment": Qualification that indicates the overall reliability of the given values. Explanation is provided in the separate worksheet "Reliability assessment".
Column AE "DE remarks": Important remarks on the hydraulic conductivity (m/d) of the unit in the German part of the project area.
Column AF "NL unit code (REGIS II v2.2)": The code of the corresponding Dutch hydrogeological unit according to the hydrostratigraphical classification scheme of REGIS II v2.2.
Column AG "NL unit description (REGIS II v2.2)": A short description or the Dutch name of the hydrogeological unit.
Column AH "NL Lithofacies": The lithofacies of the sediments of the hydrogeological unit according to Dutch sources.
Column AI "NL Reference lithofacies": Number that refers to the source from which the Dutch information on the lithofacies was obtained. Full references are presented in a separate worksheet "References NL".
Column AJ "NL Expert range min. (m/d)": Minimum value of the range of values that the hydraulic conductivity (m/d) is likely to have according to quoted references and expert judgement.
Column AK "NL Expert range max. (m/d)": Maximum value of the range of values that the hydraulic conductivity (m/d) is likely to have according to quoted references and expert judgement.
Column AL "NL reference expert range": Number that refers to the source from which the Dutch information on the expert range was obtained. Full references are presented in a separate worksheet "References NL".
Column AM "NL absolute min. (m/d)": Absolute minimum value of the hydraulic conductivity (m/d) in the Dutch part of the project area that is still considered to be plausible.
Column AN "NL absolute max. (m/d)": Absolute maximum value of the hydraulic conductivity (m/d) in the Dutch part of the project area that is still considered to be plausible.
Column AO "NL absolute min/max reference": Number that refers to the source from which the Dutch information on the absolute minimum and maximum values was obtained. Full references are presented in a separate worksheet "References NL".
Column AP "NL qualitative reliability assessment": Qualification that indicates the overall reliability of the given values. Explanation is provided in the separate worksheet "Reliability assessment".
Column AQ "NL Remarks": Important remarks on the hydraulic conductivity (m/d) of the unit in the Dutch part of the project area.

3.1.3 Procedure followed to populate the Excel workbook with data

For each of the listed units (column E), several attributes were added for each of the project or model areas (column B). First of all, the units were split according to their dominant characteristic with respect to flow: they were assigned to be either an aquifer or an aquitard. In the current scheme, the concept of aquiclude was not adopted, and considered to be an extreme case of an aquitard. Next, at least for the Belgian and Dutch model areas, a distinction was made between horizontal (Kh) and vertical (Kv) hydraulic conductivity. In aquifers and aquitards horizontal respectively vertical groundwater flow predominates. Accordingly, for aquifers Kh is considered while for aquitards Kv is considered. Instead of providing a single value for each of the units, a system of expert range and absolute range was adopted. The expert range can be regarded to encompass K values that are considered to be appropriate values for the unit at a larger scale, typically applied in cross-border hydrogeological modelling. Usually, the expert range will be smaller than the absolute range. The latter can be regarded as a bulk range where any validated individual measurement of that unit is

expected to fall within, regardless the applied method (even small-scale laboratory tests). Even though for some units this range may be rather large, it is still less generic than schemes developed by, e.g., Domenico and Schwartz (1997). For heterogenous units, which consist of, e.g., fine sand with clay lenses and coarser intervals, the range may become very large. Finally, absolute ranges can be very useful if applied to smaller cross-border hydrogeological studies and modelling exercises, and small-scale and local facies changes within a unit can be accounted for.

3.1.4 Inventory of Belgian, German and Dutch data of the area (Excel workbook)

3.1.4.1 Hydraulic conductivity of units in the Belgian subareas

For the project areas that are located in Belgium, De Kempen (BE) and RVG (BE), sources of hydraulic conductivity mainly include groundwater modelling reports, or reports that are partially devoted to groundwater modelling in the framework of, e.g., site characterisation campaigns. Other sources of information are scientific publications (peer-reviewed papers and master theses) as well as undisclosed data provided by a private company. The exact references can be found in the worksheet "References BE".

In most cases, expert ranges for individual units are derived from minimum and maximum values of pumping tests (point observations). In a limited number of cases expert ranges are based on model output and/or lithological analogues (regional values). Occasionally, only a single K-value could be found in the literature – in such case that value was treated as a central value and ranges were estimated by arbitrarily applying a factor of 2.

Absolute ranges are usually based on extreme minima and maxima that are reported for individual units in the literature. Most often, these values are obtained from very small-scale permeameter tests on corings or outcrops and may thus not be representative for the entire unit. However, they may still serve as a conservative minimum and maximum estimate. For some units the available information converges to a consistent range, regardless the method that was used to estimate hydraulic conductivity. In such cases absolute ranges are set equal to expert ranges.

3.1.4.2 Hydraulic conductivity of units in the German subareas

The part of the project area located in Germany (H3O-ROSE) covers only the western part of the German "Rur-Scholle" near the Dutch border. Information about the geometry and hydraulic conductivity of predominantly Quaternary and Neogene hydrogeological units in the "Rur-Scholle" is provided by the hydrogeological model for the Rur-Scholle and the maps based on it (IS HK50). The hydrogeological units are defined by classes of hydraulic conductivity, covering mainly a range of one or two magnitudes. For aquitards, there is often only sparse data available. They are also more heterogeneous and therefore they often cover two orders of magnitudes. For this project, the German conductivity values were converted from the unit m/s to m/d.

In most cases, the expert ranges were taken from these recalculated classes, adapting them were necessary, mainly because of changing facies or more detailed information in the project area, e.g. from pumping tests. For a number of units for which no information on hydraulic conductivity is available, estimates were made based on the lithology of these units and/or from the comparison of the unit with its occurrence in other regions.

Absolute minimum and maximum values were obtained from the "Permeability values database", as well as from other available data. These values are derived from pumping tests, grain-size analysis and other studies, thus they may not be representative for the entire unit.

Especially for the deeper Palaeogene units there is only little information about the hydraulic conductivity available. Therefore, estimates were made, based mainly on some literature and lithology.

3.1.4.3 Hydraulic conductivity of units in the Dutch subareas

In the Dutch part of the project area the Dutch national hydrogeological model REGIS II v2.2 provides information on the geometry and hydraulic conductivity of predominantly Quaternary and Neogene hydrogeological units. Due to the need for hydrogeological information of the deeper Paleogene units, Paleogene units were also interpreted and modelled in the H3O-projects. Except for the area of South-Limburg, no recent inventory, interpretation and/or mapping of the hydraulic conductivity of Paleogene hydrogeological units has been carried out in the Dutch part of the project area. This explains why little information is available on these units yet.

For Quaternary and Neogene hydrogeological units:

- Minimum and maximum values of the expert range are derived from the statistics of the corresponding hydraulic conductivity grids of REGIS II v2.2 for most units.
- Absolute minimum and maximum values were obtained from the database ("catalogus") with hydraulic properties of REGIS II v2.2.
- For a number of Quaternary and Neogene units for which no information on hydraulic conductivity is available in REGIS II v2.2, estimates were made based on the lithology of these units.

For Paleogene hydrogeological units:

- For the aquifers of the geothermal model ThermoGIS v2.1 background information on the permeability is available in the form of grids. These grids were used to make estimates of both minimum and maximum values of the expert range and absolute minimum and maximum values.
- If no other information is available and REGIS II v2.2 provides information on the hydraulic conductivity of these units in other parts of the Netherlands (for example South-Limburg, Province of Zeeland) first estimates were made of both minimum and maximum values of the expert range and absolute minimum and maximum values based on these data.
- Estimates were made based on literature that was readily available. A comprehensive literature review and analyses of databases is out of scope of the H3O-PLUS work package. This means that for the Dutch part of the project area better estimates on the hydraulic conductivity of Paleogene units might be possible.

3.1.5 Analysis and interpretation of results of the inventory, and determination of trends and misfits

After having completed the Excel table (iteratively), the results were plotted according to their expert and absolute ranges (see 3.1.3), for each unit and each model area (7 in total). These results are visualised in a series of fact sheets, for every unit, which are given in Appendix 2. These fact sheets contain the following information: model unit, cross-border correlation, the expert and absolute ranges of hydraulic conductivity by model area, an isopach map with thickness histograms for each model area, and a short note on the observed trend and differences between K estimates of model units per model area and country. Next, those units for which data could be provided for the three countries (59 out of 80 units) were informally classified according to observed trends and misfits between model areas over the three countries. Three categories are foreseen. Category 1 includes units that show a very good agreement for K values between the various subareas. Mostly, both expert and absolute ranges correspond quite well. Category 2 includes units that show a good agreement for K values between the various subareas, in the sense that their expert ranges at least partially overlap. However, for some subareas either the expert and/or absolute minimum or maximum shows a significant offset and/or the full range is much smaller or larger. Finally, units of category 3 are those that do not show any overlap for their expert ranges, and with various degrees of overlap of their absolute ranges. A preliminary attempt is made to explain the observed trends and misfits, in terms

of the source of the hydraulic conductivity values (estimates, analogues, field, lab), certain traditions over the various countries with respect to data gathering and processing, lithological properties and the palaeogeographical context.

3.1.6 Results

The data from Appendix 1 (Excel table) are visualised in a series of graphs, one graph for each unit, in which the expert and absolute ranges, as well as the qualitative reliability estimate, are included. The graphs can be accessed through a pdf-file in Appendix 2.

3.1.7 Availability of data

The overall picture of data availability can easily be grasped while scrolling down through the pdf. This movement largely coincides with moving down the stratigraphical column and thus depth. There are quite some units that do not cover the entire H3O-PLUS model area and are sometimes only present in one subarea in one specific country. As the Cenozoic strata are thickest in the central part of the Roer Valley Graben, in the Netherlands, the highest resolution is also found there. This is reflected in the fact that the amount of units found in the Dutch model areas is highest. Blanks for model subareas in the pdf mean that the unit was not found there, not mapped or that only a small fragment is present in that subarea (see worksheet 'General remarks' in the Excel table). In the case that the unit is present but no data are available, the respective field in the graph is indicated with 'no data'. For the Quaternary and Neogene units, only two cases are present where no data were available: Vlb1 and Vlb2 in the Belgian subareas RVG and De Kempen. The availability of data in the individual pdf pages is thus largely controlled by the spatial distribution of the various Quaternary and Neogene units. For deeper, Paleogene units, another component is added to data availability. Data become increasingly scarce for the deeper units, culminating in a full blank 'no data' record for the HAc unit.
Note that the industrial and societal relevance of deep subsurface layers is also partially reflected in the amount of available data. Furthermore, temporal trends may cause a shift of focus over time, as units may become more relevant for other uses, i.e., geothermal energy.

3.1.8 Reliability of data

The same trend as in data availability is roughly visible for data reliability. Gradually, the amount of pink (low) boxes/whiskers increases with depth, at the expense of green (high) and brown (medium reliability). It has to be noted though that the data reliability is a first assessment only. The strict definition of low, medium and high, as defined in worksheet 'Reliability assessment' (Excel table) is not always applied. This sometimes leads to the fact that there are large differences in data reliability over the various subareas for one unit. Representative examples are units Klz2 and Klz3, which coincide with the Maatheide and Donk Members of the Mol Formation, respectively, and are very intensively studied in the framework of various projects in the De Kempen project area in Belgium (see worksheet 'References BE' in the Excel table). Hence the K ranges for those units are considered to be highly reliable for these subareas, unlike the Dutch and German subareas.

3.1.9 Observed trends and fits-misfits of hydraulic conductivity values

Appendix 2 summarizes the expert and absolute ranges of 80 units, in the form of a pdf containing fact sheets, according to the data provided in Appendix 1. Additional information on the thickness of each of the units in the different H3O subareas is provided. Specific and detailed notes on observed trends and differences can be found in the corresponding worksheet "Notes on observed trends" of the Excel table in Appendix 1 These specific notes are also included in Appendix 2. Here, an attempt is

made to sketch the overall pattern of fits and misfits of hydraulic conductivity values for the 7 subareas in the H3O-PLUS project.
Out of 80 units, 20 units occur exclusively in the Dutch part of the project area. For one unit (HAc), no data were reported at all. This leaves a total of 59 units which we attempt to classify according to their degree of agreement over the various subareas, in 3 informal categories.
Category 1 includes units that show a very good agreement for K values between the various subareas. Mostly, both expert and absolute ranges correspond quite well. These units are listed in Table 1. Strikingly, but not surprisingly, the units are all aquifers and many of them are dominated by relatively pure quartz sand, coarse to fine, from a fluvial-estuarine setting and mostly (but not always) with a signature from the river Rhine: the Stramproy Formation and Maatheide Member of the Mol Formation, Pleistocene Rhine sands in the Belgian and Dutch Roer Valley Graben and Ältere Hauptterrassen in Germany, and sands from the Waalre and Kieseloolite Formations. Meuse gravels from the middle terraces in Belgium and the Netherlands are also included in this category, while several units are marine in origin and contain some glauconite: the Malle, Merksplas, Lillo, Oosterhout and Tienen/Dongen (TNc) Formations. Note that the TNc unit is indicated as terrestrial in Belgium and marine in the Netherlands, which makes the very good agreement rather surprising.
A few trends can be observed for some of the units. For instance, the expert range for the Belgian STz1 and STz2 is slightly narrower and with slightly lower values compared to the Dutch and German data. This could be due to the fact that the Belgian data are based on site-specific values. On the other hand, the absolute range is wider for the Belgian data, due to the incorporation of small-scale permeameter test results. Another interesting trend are the larger values for the expert range minimum and maximum for the German SYz2, SYz3 and SYz4 data. This can be explained by the fact that these deposits in this subarea are closer to the source and thus coarser. The same trend would then be expected for KIz2, KIz3, KIz4 and KIz5, but this appears not to be the case.

Table 1 – Hydrogeological units, category 1. All units are aquifers.

BEz2	SYz1	PZWAz2	KIz2	OOz2
BEz3	SYz2	PZWAz3	KIz3	TNc
STz1	SYz3	PZWAz4	KIz4	
STz2	SYz4	MSz2	KIz5	

Category 2 includes units that show a good agreement for K values between the various subareas, in the sense that their expert ranges at least partially overlap. However, for some subareas either the expert and/or absolute minimum or maximum shows a significant offset and/or the full range is much smaller or larger. These units are listed in Table 2. Around 47% of these units (15 out of 32) are aquitards such as the Pleistocene loess deposits in the Netherlands and Germany, several clay (in some cases lignite) units within the Sterksel, Weelde/Waalre and Kieseloolite Formation (e.g., Brunssum), clays from the Kasterlee and Inden Formations, Ypresian clays and clays from the Tongeren/Borgloon Formation. Clay from the Maldegem/Dongen Formation also belongs to category 2. Among the aquifers we find here the Holocene alluvial deposits from small rivers, Pleistocene aeolian sands (Boxtel/Gent Formation), gravels and sands from the river Meuse (alluvial plain and high terraces), as well as Neogene sands from the Oosterhout, Inden, Breda, Diest, Ville, Bolderberg, Berchem-Voort/Veldhoven Formations and Palaeogene units from the Eigenbilzen, Bilzen, Sint-Huibrechts-Hern/Tongeren and Brussel/Lede Formations.

The deviations found in this category may have multiple causes. For BXSCk1 for instance, the Dutch data probably take into account the existence of clay illuviation horizons in these deposits. Even though the data are consistent, the wide expert range for the Belgian BXz2 and BXz3 data are difficult

to explain. They are based on inversely modelled pumping tests. Data for STk1 are based on analogue units, hence the slight difference. SYk2 and SYk3 in fact show a good agreement for the Dutch and German model areas, however the expert range for the Dutch cases show a very low extreme minimum, which is based on air permeameter test results.
An interesting case is unit WAk1 (Weelde/Waalre Formation). The Belgian expert range stretches towards much lower values. It is regarded as expert range and not absolute range because the data is based on pumping tests. The Dutch expert range values are currently under investigation. The slight misfits for KIk1 and KIk2 are partially based on the fact that for some subareas analogue information was used. The very small expert range for the Belgian model area is based on only two values as quoted in the references (see Excel table) and is probably a severe underestimate of the full range. For more details on these two clay units we refer to the relevant worksheet in the Excel table. The relatively low absolute minimum for the Dutch KIk3 data is explained by the inclusion of small-scale permeameter test results from an analogue unit (Waalre Formation). The wide range for the German KIk4 data is due to the common practice of using a range of two orders of magnitude for aquitards.

For BRz1, the Belgian data show large ranges, because this unit incorporates many different formations (Diest and Bolderberg in the Roer Valley Graben, and Diest and Berchem in De Kempen).

In a few cases, a geological explanation may be put forward for the observed trends and fits-misfits. For instance, the higher German values for IEk1 may be due to the fact that this area is closer to the source (thus coarser material). Similarly, the slightly larger values for BRz1a in the Belgian model area can possibly be explained by the palaeogeographical situation, being closer to the hinterland (source area). The slightly larger Belgian VEVOc (Berchem/Voort) values can probably also be explained by the fact that this unit is sandier in the Belgian model area (coastal setting compared to marine conditions further north). Finally, the slightly larger Belgian VESOc values may be due to the fact that this unit is at shallower depth, less compacted and contains relatively coarse material compared to the Dutch setting.

Table 2 – Hydrogeological units, category 2. Aquitards are bold.

HLc	**SYk3**	**IEk1**	BRz3	TOz2
BXSCk1	**WAk1**	IEz2	BRz4	**MAc**
BXz2	MSz3	**IEk2**	VESOc	EZc
BXz3	**KIk1**	IEz3	VEVOc	**KOc**
BEz1	**KIk2**	**KLc**	RUz2	
STk1	**KIk3**	BRz1a	RUz3	
SYk2	**KIk4**	BRz1	**TOGOk1**	

Finally, units of category 3 are those that do not show any overlap for their expert ranges, and with various degrees of overlap of their absolute ranges. These units are listed in Table 3. Out of 10 units, 7 qualify as an aquitard: the Pleistocene fine-grained deposits of the Boxtel Formation, and overbank deposits from the Meuse. Most interestingly, the Rupelian Boom Clay is also featuring here, as well as the lignite layers from the Ville Formation. Among the aquifers we observe here sands and gravels from the Boxtel and Stramproy/Mol/Kieseloolite Formations and the sands from the Tielt/Dongen Formation.
The misfits in this category can be explained by several reasons. For the BXk1 and BXk2 units, the Belgian data are based on analogues of different genetic origin at a different location. For BXz4, the larger Belgian values are due to the fact that this unit includes a lot of gravel in the model area. In general, the BX Formation comprises a large range of sedimentary environments (aeolian, fluvial,

lacustrine, colluvial). For BEk1 and BEk2 again analogue data was used. The reason for the higher VIb1 and VIb2 values in the German model area is not clear and should receive attention.
The discrepancy for units RUBOk1 and TTc may be explained by the palaeogeographical situation. RUBOk1 represents a full marine setting in Belgium, while this most probably was not the case in the German model area (we note here that there are no data for the Netherlands). Similarly, the slightly larger values for unit TTc in the Belgian model area may also be due to the fact that it was situated in a more marginal setting.

Table 3 – Hydrogeological units, category 4. Aquitards are bold.

BXk1	BXz4	**BEk2**	**VIb2**	TTc
BXk2	**BEk1**	**VIb1**	**RUBOk1**	

4 HYDRAULIC CONDUCTIVITY OF FAULT ZONES – CASE STUDIES

4.1 Approach

Faults play an important role in flow and transport in regional groundwater systems (Bense et al. 2013; Lapperre et al. 2019). Faults can act as: i) barriers slowing down groundwater flow, ii) conduits speeding up groundwater flow, or iii) a combination of both (Bense et al. 2013; Walraevens et al. 2015; Batlle-Aguilar et al. 2017; Verbeeck et al. 2017; Oiro et al. 2018). Determining the flow and transport behaviour across these structures is challenging since they are rarely exposed on the surface and their hydraulic behaviour varies spatially and with depth (Ladevèze et al. 2018; Lapperre et al. 2019).
Two different approaches were adopted here to estimate the hydraulic conductivity of fault zones, based on two case studies. The case studies are the two pilot sites of the VoGERA project that are situated within the Roer Valley Graben: the Peel Boundary and Rauw Fault pilot sites (Zaadnoordijk et al., 2019).

Hydraulic connectivity across a fault near Veghel, which is part of the Peel Boundary fault zone, was assessed qualitatively using a detailed juxtaposition analysis. The existing 3D hydrogeological model of the area, created earlier in a H3O-project, was used as a starting point.

Hydraulic conductivity of the Rauw Fault was estimated using an extensive modelling exercise which in fact involves an update of the existing NAM model (Gedeon, 2008). The NAM model, or Neogene Aquifer Model, is the hydrogeological model that coincides with the Nete catchment in north-eastern Belgium. The update encompasses the conceptualization of faults as horizontal flow barriers in the model, as well as the inclusion of a new hydrostratigraphical scheme and the incorporation of additional piezometric calibration data.

4.2 Case study Peelrand Fault zone near Veghel

4.2.1 Introduction

This paragraph describes a pilot-study for a juxtaposition analysis of a fault near Veghel, which is part of the Peel boundary fault zone.
The area and fault of interest are located in the eastern part of the province of North-Brabant, the Netherlands, near the town of Veghel. This area is situated in the Roer Valley Graben. The fault of interest, hereinafter called the Veghel fault, is a normal fault and it is part of the north-eastern boundary fault zone of the graben (Figure 2) The study area includes a groundwater-protection and -extraction area (Figure 3). Petrel© software was used for building a local model and for the juxtaposition analysis itself.

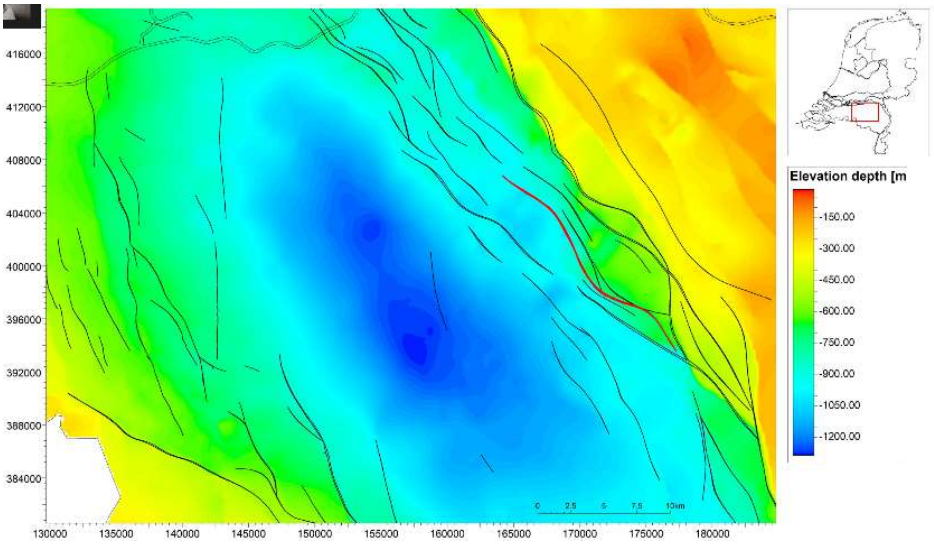

Figure 2 – The location of the Veghel fault (red) within the Peel Boundary fault zone. The base of the Breda Formation (NL)/Diest Formation (BE) is shown which reaches a depth of 1280 m BSL in the deepest part.

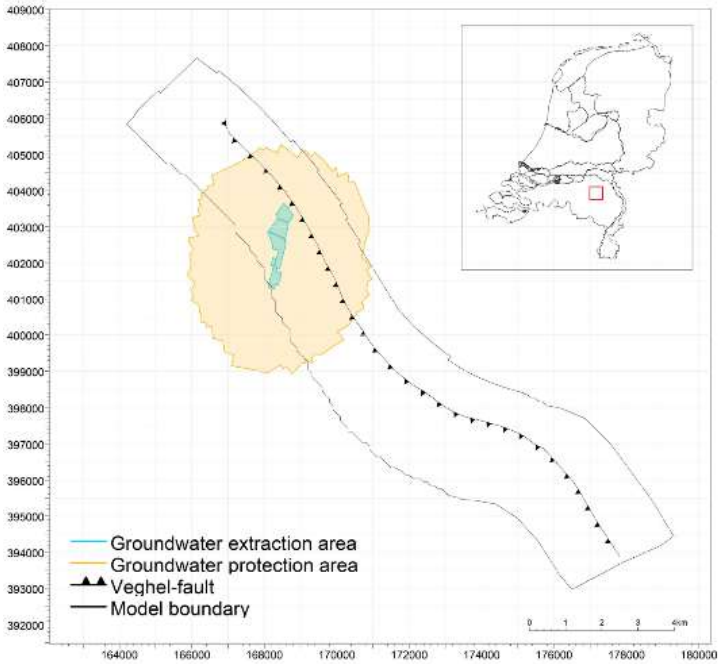

Figure 3 – Model area with groundwater protection and extraction areas.

4.2.2 Stratigraphy and fault-plane model

The fault plane and horizons were derived from the "*H3O- Roerdalslenk-Noordwest*" project. This is a hydrogeological model of the Palaeogene-Neogene interval of a section of the Roer Valley Graben area. From this project, 34 layers that are present within the study area were included (see Table 4).

It is common for these layers to have a certain sand-to-clay ratio (i.e. 90% sand, 10% clay) but for the sake of simplicity and the “proof-of-concept” nature of this exercise a binary approach was used and the layers were assumed to be 100% sand or 100% clay.

Table 4 – Stratigraphic layers included in the model, derived from the "H3O Roerdalslenk-Noordwest" project.

Analysis-code	Unit	Hydrogeological code	Lithology
1	Holocene	HLc	Sand
2	Boxtel sand 1	BXz2	Sand
3	Boxtel sand 2	BXz3	Sand
4	Boxtel sand 3	BXz4	Sand
5	Beegden sand 2	BEz2	Sand
6	Beegden sand 3	BEz3	Sand
7	Sterksel sand 1	STz1	Sand
8	*Sterksel clay 1*	*STk1*	*Clay*
9	Sterksel sand 2	STz2	Sand
10	*Stramproy clay 1*	*SYk1*	*Clay*
11	Stramproy sand 2	SYz2	Sand
12	Stramproy sand 3	SYz3	Sand
13	*Waalre clay 1*	*WAk1*	*Clay*
14	Peize sand 2	PZWAz2	Sand
15	*Waalre clay 2*	*WAk2*	*Clay*
16	Peize sand 3	PZWAz3	Sand
17	*Waalre clay 3*	*WAk3*	*Clay*
18	Peize sand 4	PZWAz4	Sand
19	Kieseloolite sand 1	KIz1	Sand
20	*Kieseloolite clay 1*	*KIk1*	*Clay*
21	Kieseloolite sand 2	KIz2	Sand
22	Kieseloolite sand 3	KIz3	Sand
23	Kieseloolite sand 4	KIz4	Sand
24	*Oosterhout clay 1*	*OOk1*	*Clay*
25	Oosterhout sand 2	OOz2	Sand
26	*Oosterhout complex*	*OOc*	*Clay*
27	Breda sand 1	BRz1	Sand
28	Breda sand 2	BRz2	Sand
29	Breda sand 3	BRz3	Sand
30	*Veldhoven*	*VEWIk1*	*Clay*
31	Voort	VEVOc	Sand
32	*Rupel*	*RUBOK1*	*Clay*
33	*Landen*	*HAc*	*Clay*
34	Heers	HSc	Sand

4.2.3 Method

4.2.3.1 Principles of juxtaposition analyses

The purpose of a juxtaposition analysis is to gain insight into possible lateral connections of different stratigraphic layers, or zones, at fault planes and the implications for groundwater flow based on the lithology of the layers involved. Connections of zones can be visualized with a matrix-scheme with zones in the footwall plotted on the Y-axis and zones in the hanging-wall plotted on the X-axis. Figure 4 and its accompanying matrix-scheme show a pre-deformation state in which each footwall-zone only connects to its hanging-wall equivalent. After deformation, zones in the footwall are juxtaposed to different zones in the hanging wall (Figure 5). When combined with lithological information, a juxtaposition analysis can be used to identify possible migration paths for groundwater flow (Figure 6).

With 34 zones a total of 595 different combinations of zone-to-zone contact are theoretically possible. The two lithologies in this study can result in three different combinations: sand-on-sand, clay-on-sand, clay-on-clay. On the fault plane the different combinations of zone-to-zone (Figure 12) and lithology-to-lithology contacts (Figure 13) can be visualized.

4.2.3.2 Clay smear

The horizontal permeability of a fault can be reduced significantly by clay-rich fault gouge. Clay-rich fault gouge can appear when clay-rich strata is “smeared” across the fault-plane during displacement of the fault (Figure 7). A thin, clay-rich barrier may thus be present in the fault zone, even at sand-on-sand contacts, hindering flow of groundwater or gas. This aspect was dealt with in the case study Rauw Fault near Mol, using a groundwater flow modelling approach (see section 4.3 and 4.3.5).

The possible presence of clay smear was not taken into account for the case study Peelrand Fault zone near Veghel. A thorough study, including clay smear, requires more detailed lithological information for each zone. This would also include simulations of clay-sand distributions within each zone.

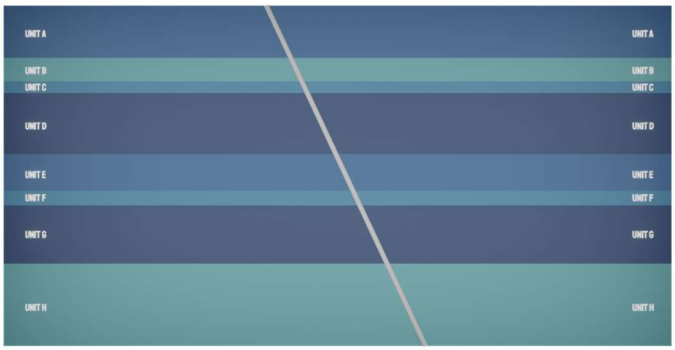

Footwall								
A								
B								
C								
D								
E								
F								
G								
H								
	A	B	C	D	E	F	G	H

Hanging-wall

Figure 4 – Pre-deformation situation with the future fault (grey). There are no lateral connections of zones to other zones as depicted by the matrix-scheme.

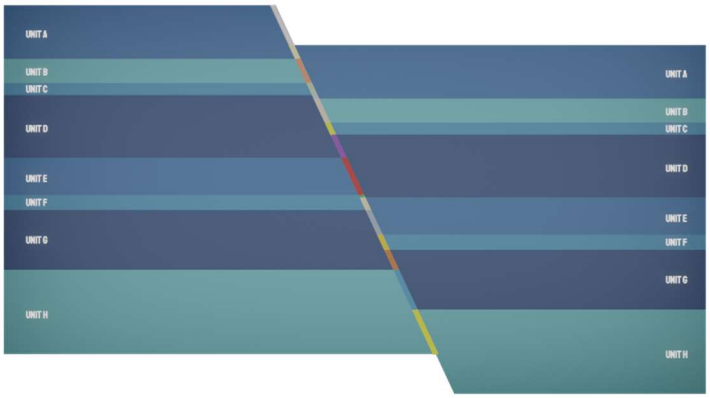

Footwall								
A								
B								
C								
D								
E								
F								
G								
H								
	A	B	C	D	E	F	G	H

Hanging-wall

Figure 5 – Post-deformation: the front-sides of the zones now connect to different zones. The matrix scheme now shows which zones are now juxtaposed, i.e. the hanging-wall side of unit A (to the right of the fault) is juxtaposed to the footwall-sides of units A, B, C and D (to the left of the fault).

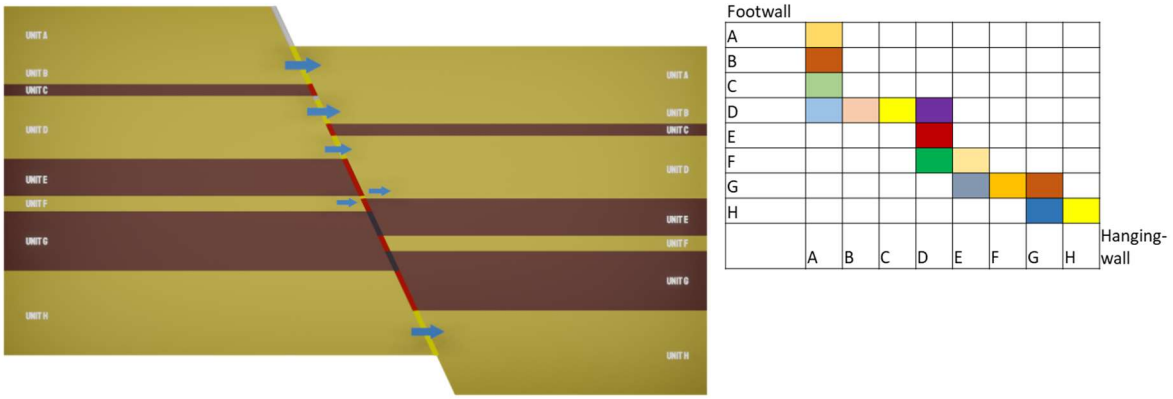

Figure 6 – Post-deformation: lithology. The juxtaposition results can be combined with lithological information in order to identify possible migration pathways for groundwater and/or gas.

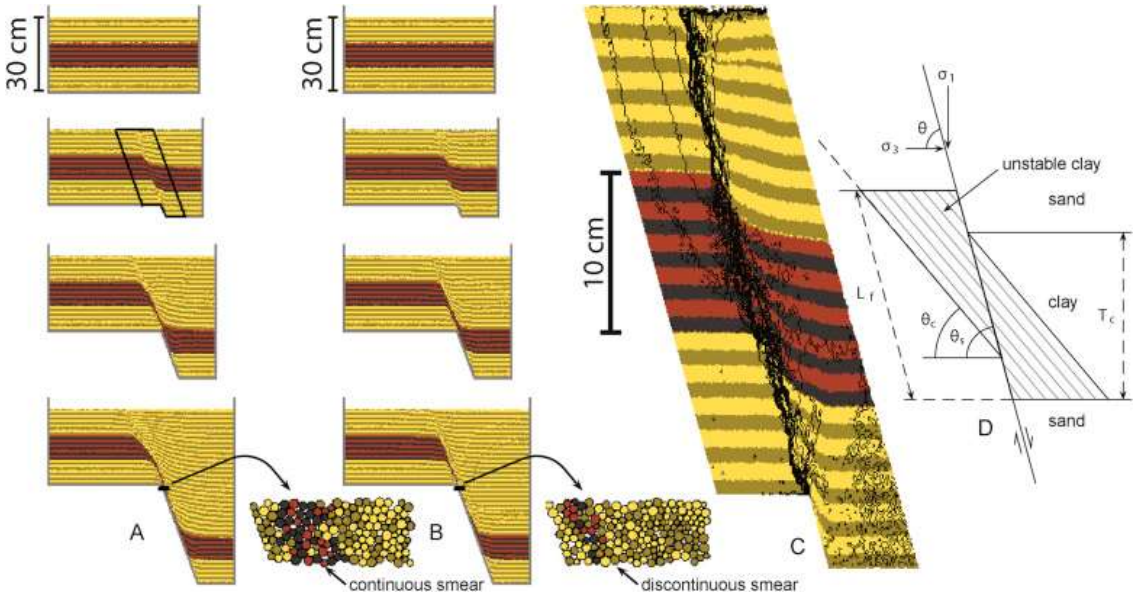

Figure 7 – An illustration of clay smear in a fault-zone. Situation B depicts a situation where the dark-coloured layer has the same properties as the surrounding sand layers. In situation A, the dark layer is weaker, resulting in transport of eroded material into the shear zone and thus continuous smear (Vrolijk et al., 2016).

4.2.3.3 3D pillar-grid voxel model

In order to run a juxtaposition analysis in Petrel©, the fault and the horizons have to be integrated into a voxel model. Petrel© offers a particular type of voxel model for this purpose, called a pillar-grid voxel model.

In contrast to regular voxel models, consisting of equally sized voxels, a pillar grid voxel model is characterized by irregularly sized and orientated voxels. The shape in the X- and Y-directions are

determined by the strike of the fault (Figure 8). The voxels are fitted around the fault plane (Figure 9). The benefit of this is that the fault plane does not cut through any voxels and there is no need for an additional method to assign cross-cut voxels to either the hanging wall or the footwall.
After fitting the voxel grid around the fault plane the horizons are added to the model. The thickness of each voxel is determined during this stage. Because there is only one layer of voxels for each zone, the height of each voxel is determined by the thickness of the zone it represents. For this pilot study with the binary approach to lithology, a single layer of voxels is sufficient. However, if necessary for intra-zone clay-sand distribution simulations, the zones can be subdivided into multiple layers of voxels. After the creation of the 34 zones (Figure 10) the dominant lithology can be assigned to each zone (Figure 11).

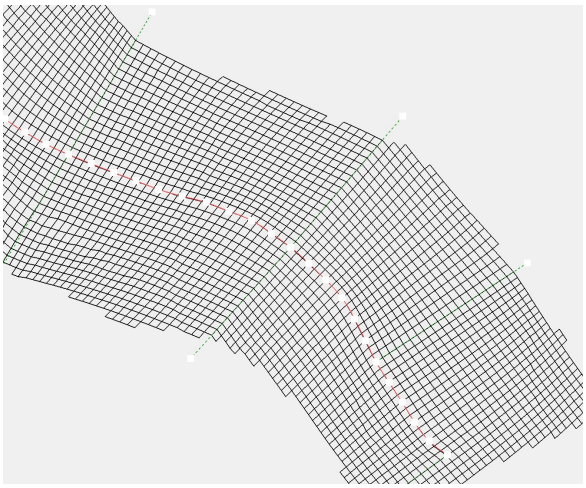

Figure 8 – Top view of the pillar grid voxel model, illustrating the "fitting of the voxels around the fault-plane (red-line).

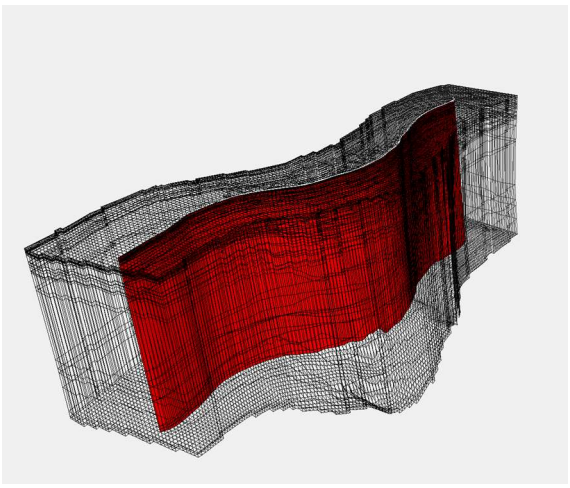

Figure 9 – 3D view of the pillar grid voxel model around the fault plane.

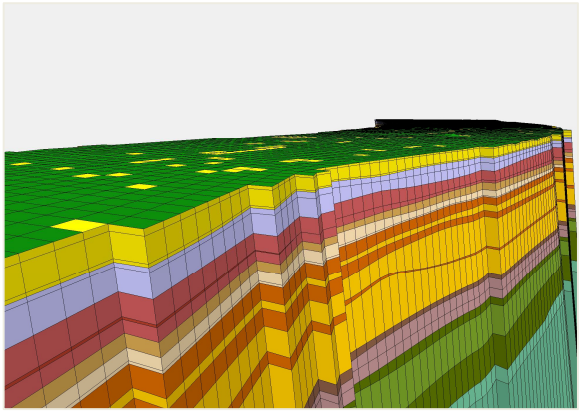

Figure 10 – 3D view of the top of pillar grid voxel model showing the stratigraphic zones.

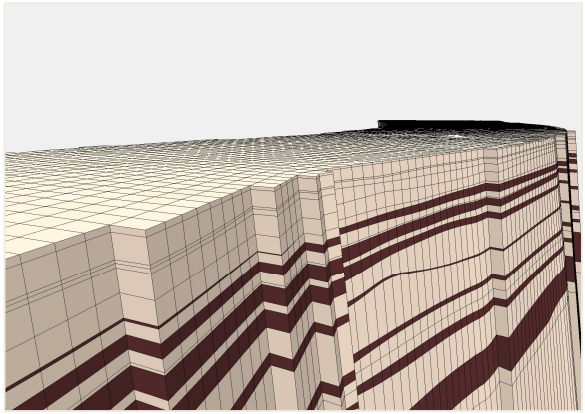

Figure 11– 3D view of the pillar grid voxel model, populated with the assigned lithologies.

4.2.4 *Results*

The juxtaposition analysis primarily results in visualizations of the zone-to-zone combinations, or juxtaposition zones, (Figure 12) and lithology-to-lithology (Figure 13) combinations along the fault plane. For the Veghel fault the juxtaposition analysis resulted in 177 juxtaposition zones. In order to reduce clutter and improve the readability of the fault-plane visualizations, juxtaposition zones can be turned on or off, for example to visualize juxtaposition zones within a certain interval with a particular lithology-to-lithology contact (Figure 12).

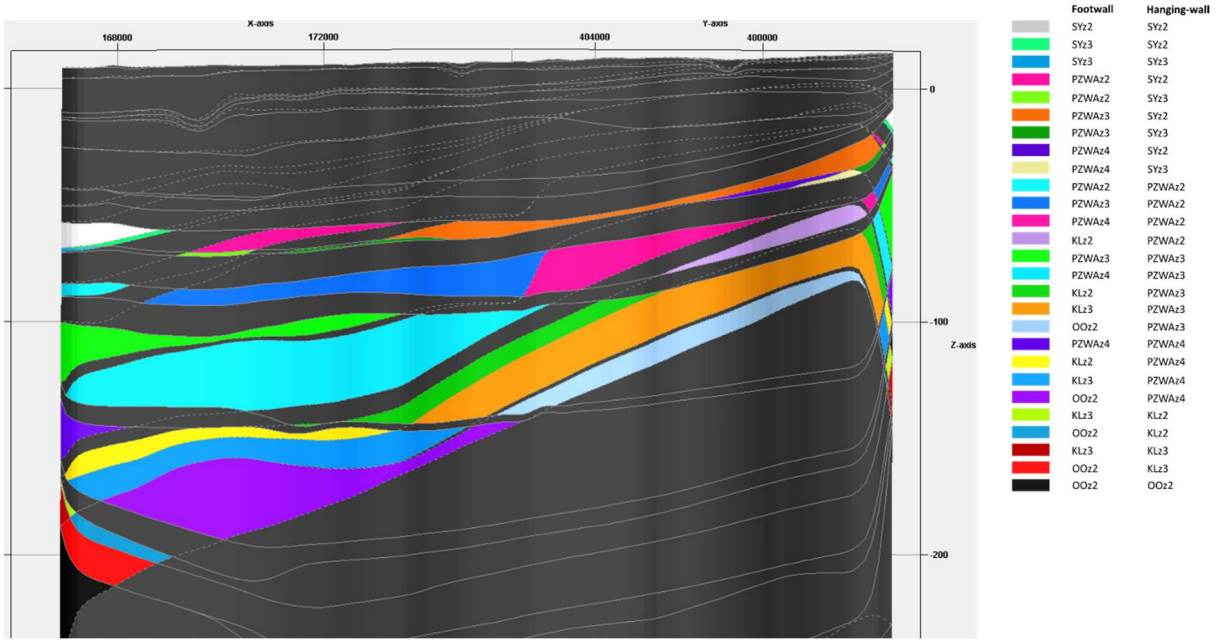

Figure 12 – Juxtaposition zones for sand-on-sand type contacts within the Stramproy-Oosterhout interval.

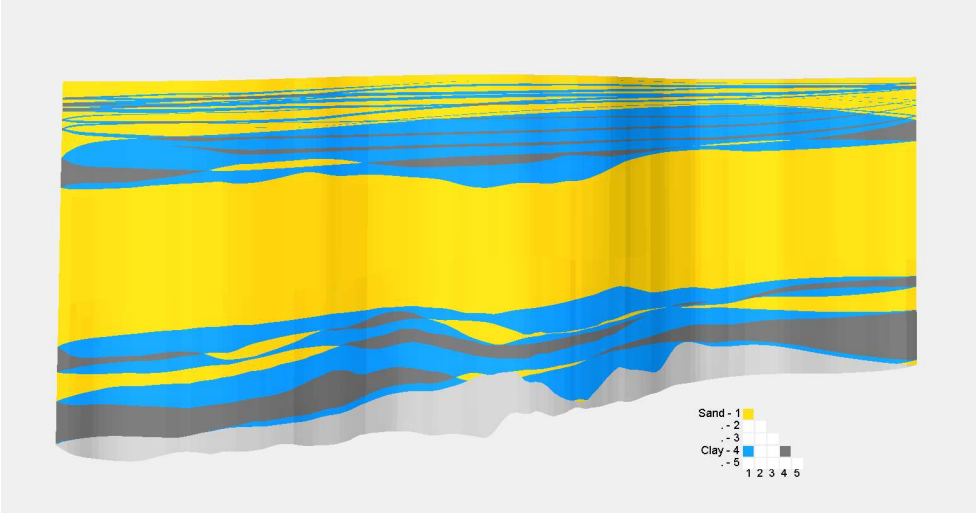

Figure 13 – 2D view of the fault plane for the entire interval. Colours correspond to types of contact. Yellow: sand-sand contact, blue: clay-sand contact, dark-grey: clay-clay contact, light-grey: Cenozoic strata-Mesozoic strata contact.

	X	Y	Depth	Fault face juxtaposed area	Veghel-breuk Totaal: k-layers side 1	Veghel-breuk Totaal: k-layers side 2	Facies Juxtaposi
1	175556.34	396912.10	15.36	0.00		2	
2	175569.11	396901.54	14.88	107.16	2	2	
3	175555.78	396911.54	14.29	37.00	2	3	
4	175568.26	396900.70	13.23	223.38	3	3	
5	175554.52	396910.29	11.89	105.63	3	4	
6	175566.79	396899.24	10.38	266.77	4	4	
7	175552.77	396908.55	8.54	185.50	4	5	
8	175564.73	396897.19	6.39	342.42	5	5	
9	175550.49	396906.28	4.16	203.10	5	6	
10	175561.79	396894.28	0.69	651.86	6	6	
11	175551.33	396899.46	-2.54	149.90	6	7	
12	175538.74	396908.43	-3.35	41.11	6	9	
13	175530.00	396914.55	-4.02	41.74	6	10	1
14	175587.15	396870.60	-3.79	52.61	7	7	
15	175574.15	396880.06	-4.46	43.79	7	9	
16	175542.88	396903.45	-5.27	140.42	7	10	1
17	175526.20	396915.18	-6.47	29.03	7	11	
18	175593.60	396864.37	-5.22	9.21	9	9	
19	175569.68	396881.99	-6.13	62.62	9	10	1
20	175533.05	396909.13	-7.31	49.81	9	11	
21	175583.14	396870.71	-7.19	101.25	10	10	
22	175546.17	396897.37	-9.09	325.28	10	11	1
23	175554.84	396887.39	-12.78	563.08	11	11	
24	175547.10	396890.41	-16.01	253.85	11	12	
25	175530.57	396900.71	-18.40	252.62	11	13	1
26	175583.53	396860.64	-18.32	48.43	12	12	
27	175544.52	396887.82	-20.89	289.66	12	13	1
28	175548.94	396881.54	-24.23	556.52	13	13	
29	175539.85	396885.24	-27.75	337.75	13	14	1

Figure 14 – Point data from the juxtaposition analysis.

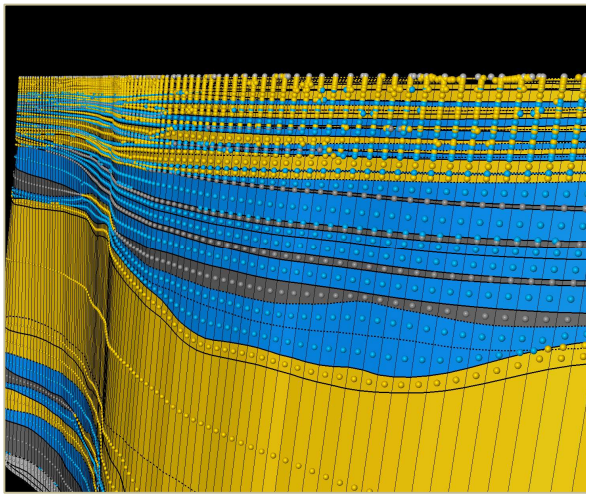

Figure 15 – Generated point at voxel-faces at the fault-plane

Points can be generated on each voxel-face at the fault plane (Figure 15). These points carry attributes with results from the juxtaposition analysis (Figure 14): the area of the voxel face at the fault plane in m^2, a numerical code for the zone on the footwall side (juxtaposition-code in Table 4), a numerical code for the zone on the hanging wall side (juxtaposition-code in Table 4), and a numerical code for the lithology-to-lithology contact type.
From the numerical data the different zone-to-zone combinations present can be derived as well as the total area in m^2 for each lithology-to-lithology contact type and subsequently be visualized in a matrix-scheme (Figure 16).
The ability to extract the results as shapefiles is currently not available within Petrel©.

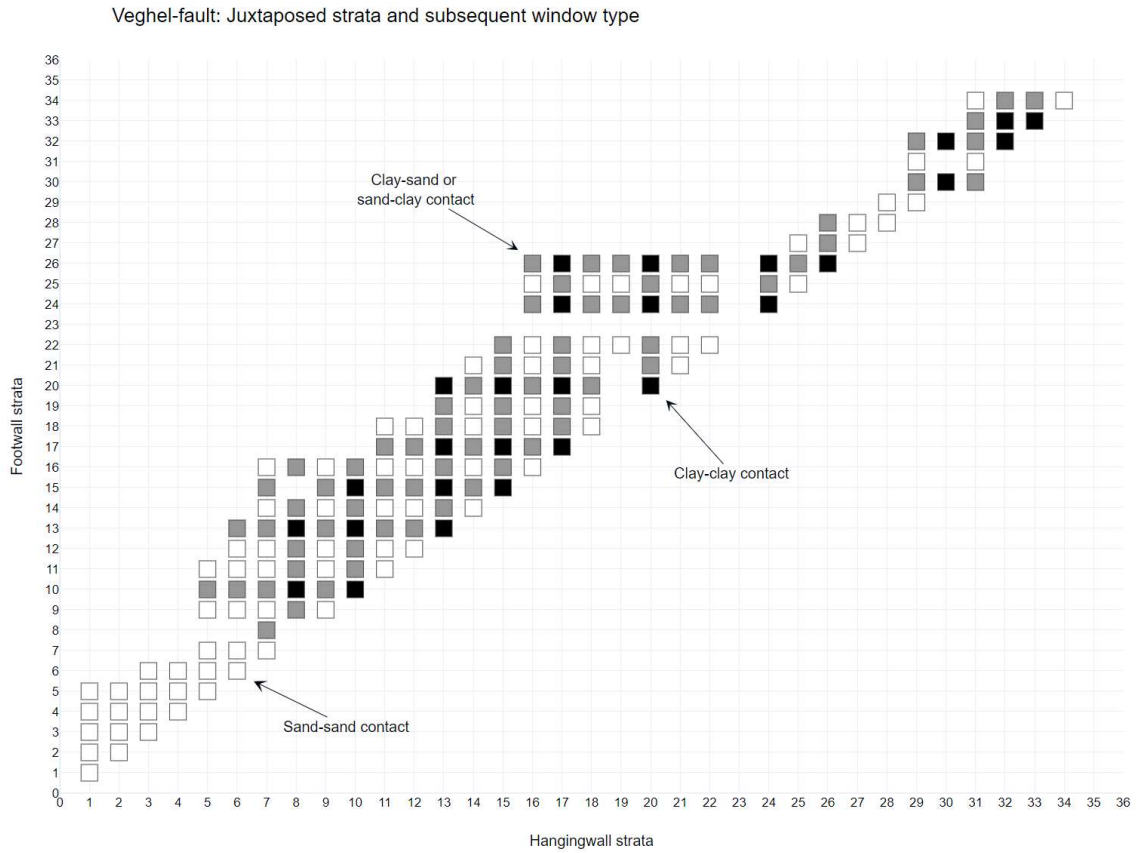

Figure 16 – Juxtaposition matrix-scheme for the Veghel fault. Colors correspond to the type of lithology-to-lithology contact. The numbers on the X- and Y-axis correspond to the juxtaposition codes in Table 4.

4.2.5 Fault characteristics

4.2.5.1 Displacement analysis

The pillar-grid voxel model also allows for an analysis of the displacement of the fault. The results of this analysis can be visualized on the fault plane and extracted, comparable to the juxtaposition analysis.

The results of the displacement analysis show that the majority of the displacement occurred in the centre of the fault plane (Figure 17). However, there is also a substantial amount of displacement on the left side and, in a lesser amount, on the right side of the fault plane. This can be explained by the evolution of the fault plane (see section 4.2.5.2 .

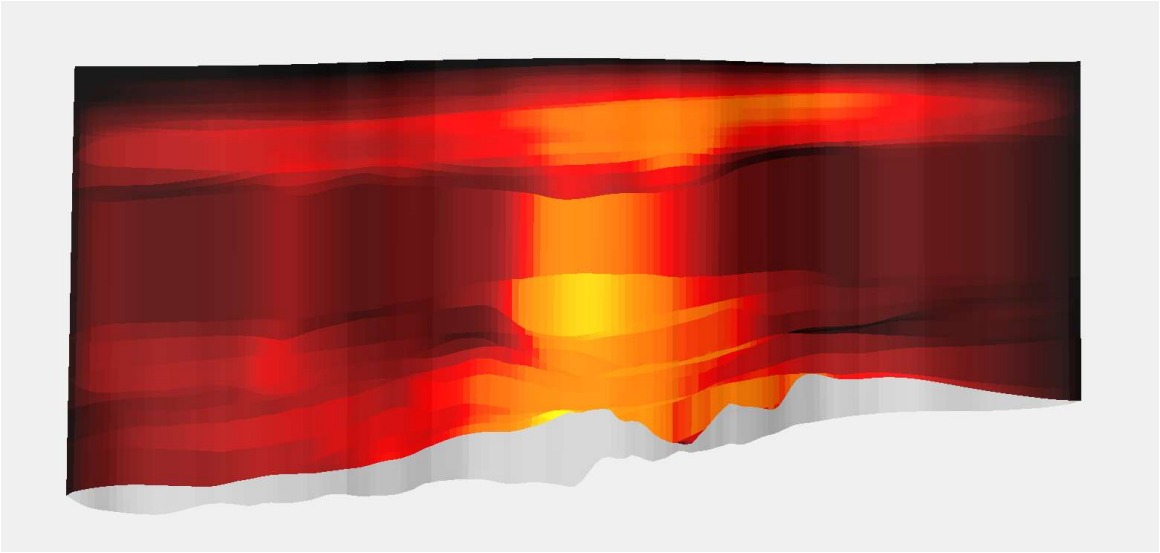

Figure 17 – 2D view of the fault plane with displacement values. Red = high displacement values, black = low displacement values.

4.2.5.2 Fault evolution

Large, regional faults do not originate in its present-day form instantaneously. They are the result of incremental growth of smaller faults that have eventually linked together. In the results of the displacement analysis we can identify two of these former, smaller faults or present-day fault segments.

These smaller faults have had their maximum amount of displacement in the centre of the fault-plane (Figure 18, t1). Over time, as displacement accumulated, the two faults planes grew in length (Figure 18, t2) until they eventually overlapped, creating a *relay ramp* between the two fault planes (Figure 18, t3). The creation of a relay ramp between two smaller faults is referred to as *soft linking*.

Further deformation and accumulation of strain can breach this relay ramp and subsequently *hard-link* these two faults together, with its centre between the centres of the former faults. The focus of additional displacement of the newly formed larger fault is at this new centre (Figure 18, t4).

Due to the elliptical shape of fault planes, a relay ramp can be breached at the centre depths of the fault segments and still be intact above and below the centre depths (Figure 20).

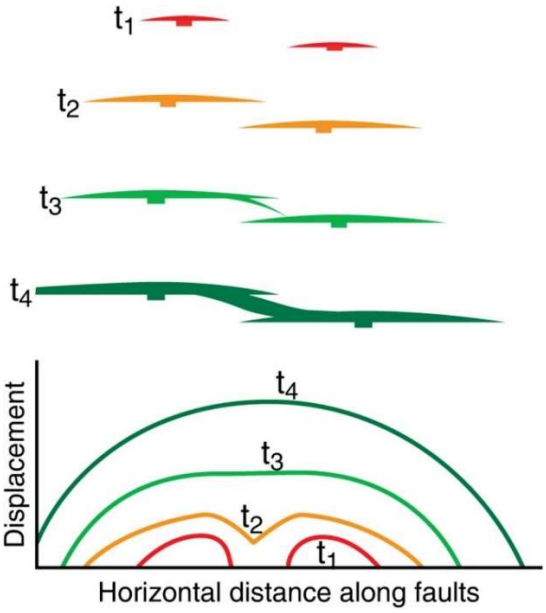

Figure 18 – Linking of two fault planes and the subsequent effect on the displacement graph over time (Fossen & Rotevatn, 2013).

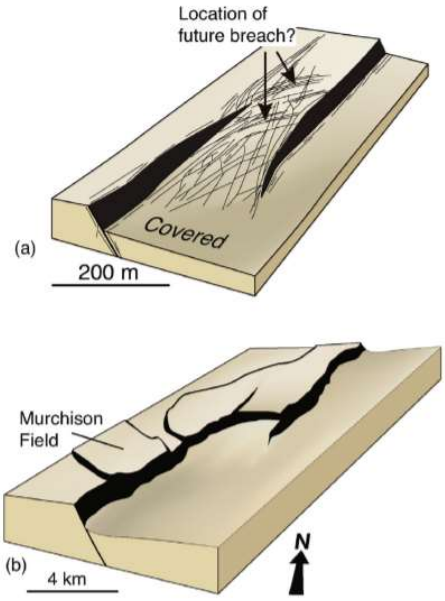

Figure 19 – Visualization of the relay ramp at t3 (top) and t4 (bottom) (Fossen & Rotevatn, 2013).

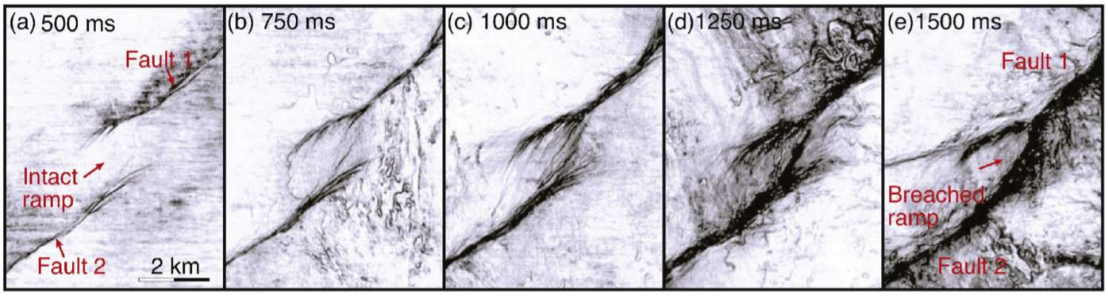

Figure 20 – Seismic data (variance time slices) showing two overlapping faults forming a relay ramp (a) that becomes breached at depth. At 1500 ms (two-way time) the ramp is completely breached (hard linked). From Fossen & Rotevatn (2013).

The evidence that evolved faults consist of fault-segments is also provided by the trace of an evolved fault. The lateral extension, overlapping and subsequent linking of fault segments will cause a curve in the fault trace of an evolved fault (fault trace at t4, Figure 18). The Veghel fault also shows this typical curved feature (Figure 2).
In the case of the Veghel fault it is unknown if the relay ramp is fully breached and the two fault segments are hard linked. The Veghel fault plane is based on 2D seismic data. At the location of the relay ramp the fault has been interpreted on three seismic lines, spaced roughly 1500 meters apart. Therefore, the interpretation for the Veghel fault-plane is not detailed enough to make any statements about the state of the relay ramp. 3D seismic data is required for an interpretation that would be detailed enough for the study of the relay ramp.

4.2.5.3 Implications for groundwater flow

Relay ramps are structurally complex due to the large amount of smaller fractures with varying orientations. This is irrespective of whether the fault segments are hard- or soft-linked. These areas of fault-linkage play an important role in groundwater dynamics around faults, even in mature and advanced faults, due to *relay-enhanced fault permeability*.

A damaged but intact relay ramp (soft-linking) may increase lateral flow of fluid, or bed-parallel flow, due to the increased fracture density. A breached relay ramp (hard-linking) of fault segments reduces this lateral flow due to the occurrence of low-permeable deformation bands. However, the fractured damage zone may still offer a conduit for vertical migration of fluids. Figure 21 illustrates the vertical migration of fluids along the fault surface in the context of a sealing fault with an intact relay ramp.

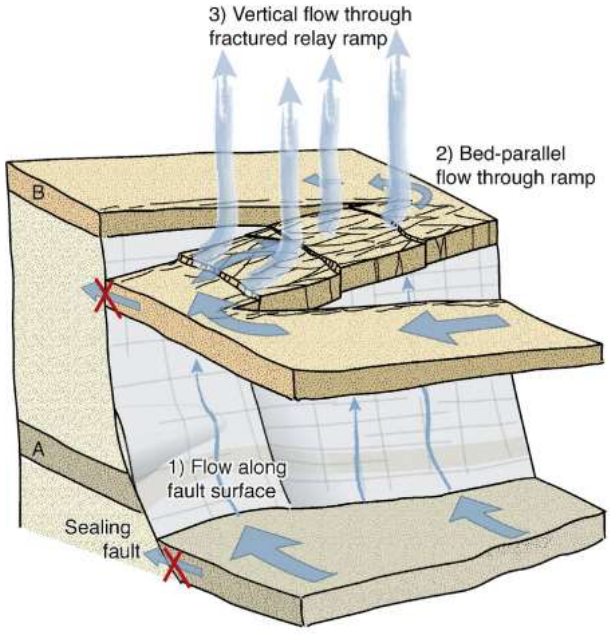

Figure 21 – Fractured structure of an intact relay ramp showing vertical flow through the damage zone. From Fossen & Rotevatn (2013).

4.3 Case study Rauw Fault near Mol

4.3.1 Introduction

4.3.1.1 General

For the Neogene aquifer in Flanders, groundwater flow and solute transport models were developed in the frameworks of safety and feasibility studies for the underlying Boom Clay Formation as potential host rock for geological disposal of radioactive waste, and the category A surface disposal project (Mallants 2010; ONDRAF/NIRAS 2010; Cool et al. 2013). However, the simulated fluxes and transport parameters of these models are still subject to large uncertainties, as they are typically constrained by hydraulic heads only, and their current conceptualization does not differentiate the fault zones from the undisturbed aquifer materials (Gedeon, 2008). The goal then of this work is to produce an update of the Neogene aquifer model (NAM) including the conceptualization of relevant faults as horizontal flow barriers. Ultimately, the modelling exercise will give quantitative insight into the hydraulic properties of normal faults in the Neogene.

4.3.1.2 The Neogene aquifer

The Neogene aquifer in the Nete catchment is located in the Campine area, in the northeast of Flanders (Figure 22), and considered to be the most important groundwater reservoir in the region (Coetsiers and Walraevens 2006). The area is characterized by a very low relief with altitudes ranging from 5 to 70 meters (m TAW, Tweede Algemene Waterpassing) and the hydrography is oriented in an east-to-west drainage system that belongs to the Scheldt river basin. The Neogene sediments dip towards the north-northeast with a gentle slope of about 1-2% with some disturbances towards the west by different faults. Quaternary deposits with various textures and thicknesses overlie the Neogene units and constitute the upper few meters of the aquifer system. The hydrostratigraphical units that subcrop below the younger Quaternary deposits are composed of lower Pleistocene and Pliocene sediments (Figure 23). The lower Pleistocene and upper Pliocene consist of the clayey Weelde Formation (which corresponds with the upper WA units), and the sandy Malle (PZWA, partially), Merksplas (PZWA/MS, partially), Mol (SY/KI) and Lillo (MS/OO) Formations, resting on the Miocene mixed clayey-sandy Kasterlee Formation (KLc) which was deposited in shallow-marine to estuarine conditions. It is underlain by the Diest Sands (BR), which in turn overlay the late Oligocene and lower Miocene Voort (VE) and Berchem (VE) Sands. The Boom Clay (RU), an Oligocene marine sediment, forms the lower boundary of the system. Similarly to the overlaying formations, it dips towards the east-northeast with an increasing thickness. In this work, the combined Quaternary deposits, Pleistocene, upper and lower Pliocene aquifers together with the Oligocene and lower Miocene Aquifer System are referred to as the 'Neogene Aquifer'. Notwithstanding their lithological differences, Patyn et al. (1989) concluded from hydrogeological observations that these sediments behave as a single aquifer.

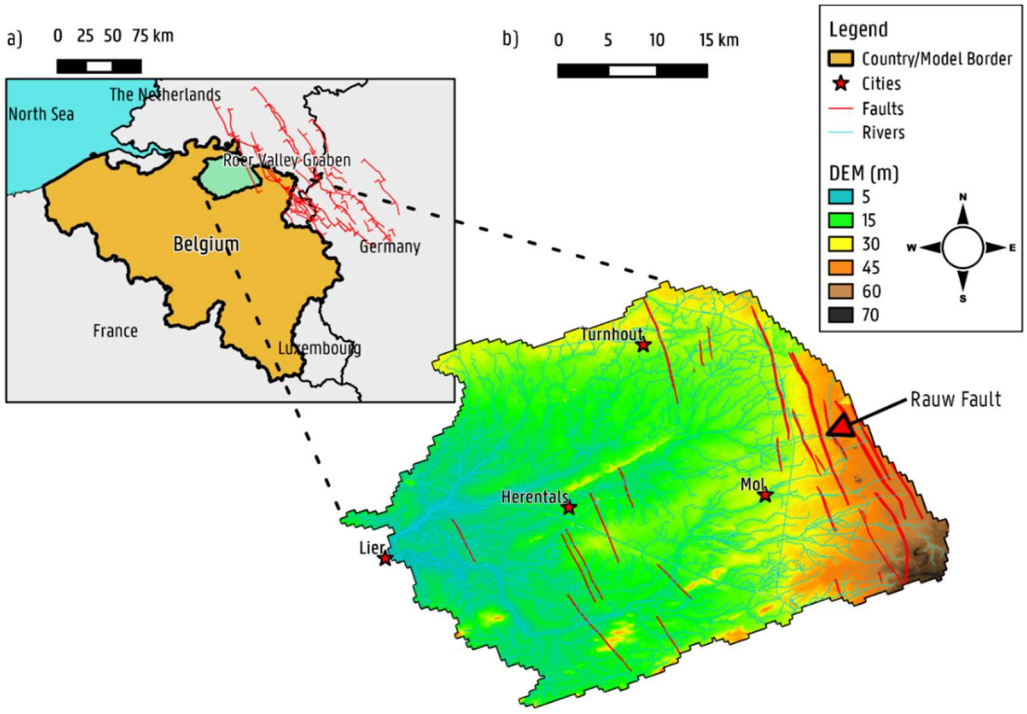

Figure 22 – Geographical location of a) Belgium within Europe, b) the surface elevation of the study area within the Nete catchment.

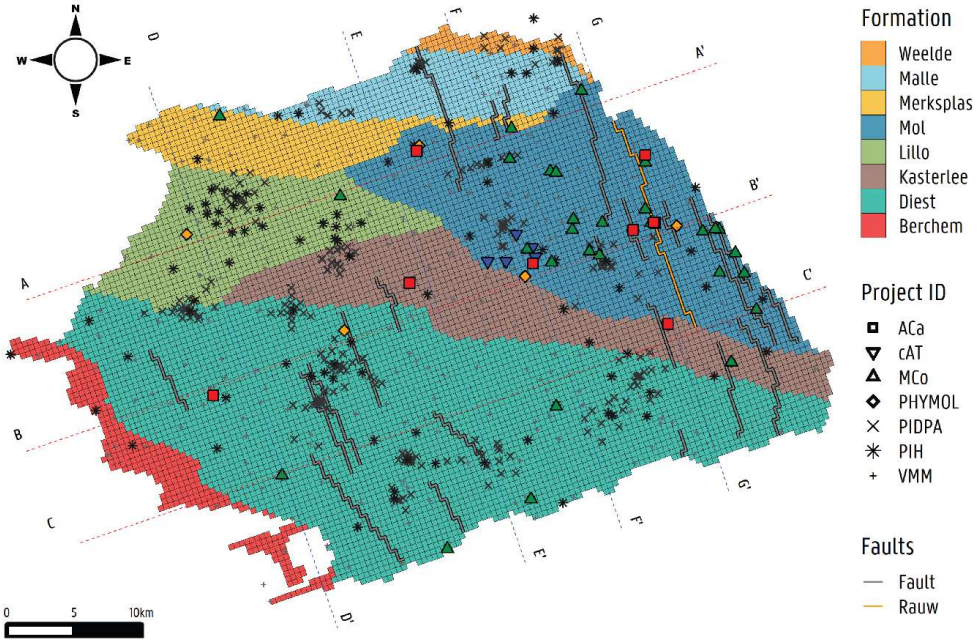

Figure 23 – Subcrop map of the Neogene aquifer formations in the Nete catchment as discretized in the second layer of the numerical model. It indicates faults (emphasis on the Rauw fault), cross sections, observation, sampling and measurement points.

4.3.1.3 The Rauw fault

In the eastern part of the Nete catchment faults occur formed as a consequence of the development of the Roer Valley Graben, the north-western branch of the Rhine graben (Verbeeck et al. 2017). The most important of these faults outside the proper Roer Valley Graben and in terms of Cenozoic offset, is the Rauw fault which is proven to have been active during the Pleistocene (Verbeeck et al. 2017). The Rauw fault was active and caused a displacement of >7 meters during the Quaternary. While the offset increases with depth it does not have a clear surface expression. The Rauw fault consists of two separate branches, around 700 m apart, for which the movement of one has stopped earlier and the most recent one has taken over the activity (informally called the Rauw-1 fault; Verbeeck et al. 2017). The latter is the one which is routinely called 'the Rauw fault' throughout this study. The observed hydraulic gradient across the fault zone appears significant, with head differences of ca. 1.7m over a horizontal distance of around 60 meters as observed at the ON-MOL-2 site (Figure 24).

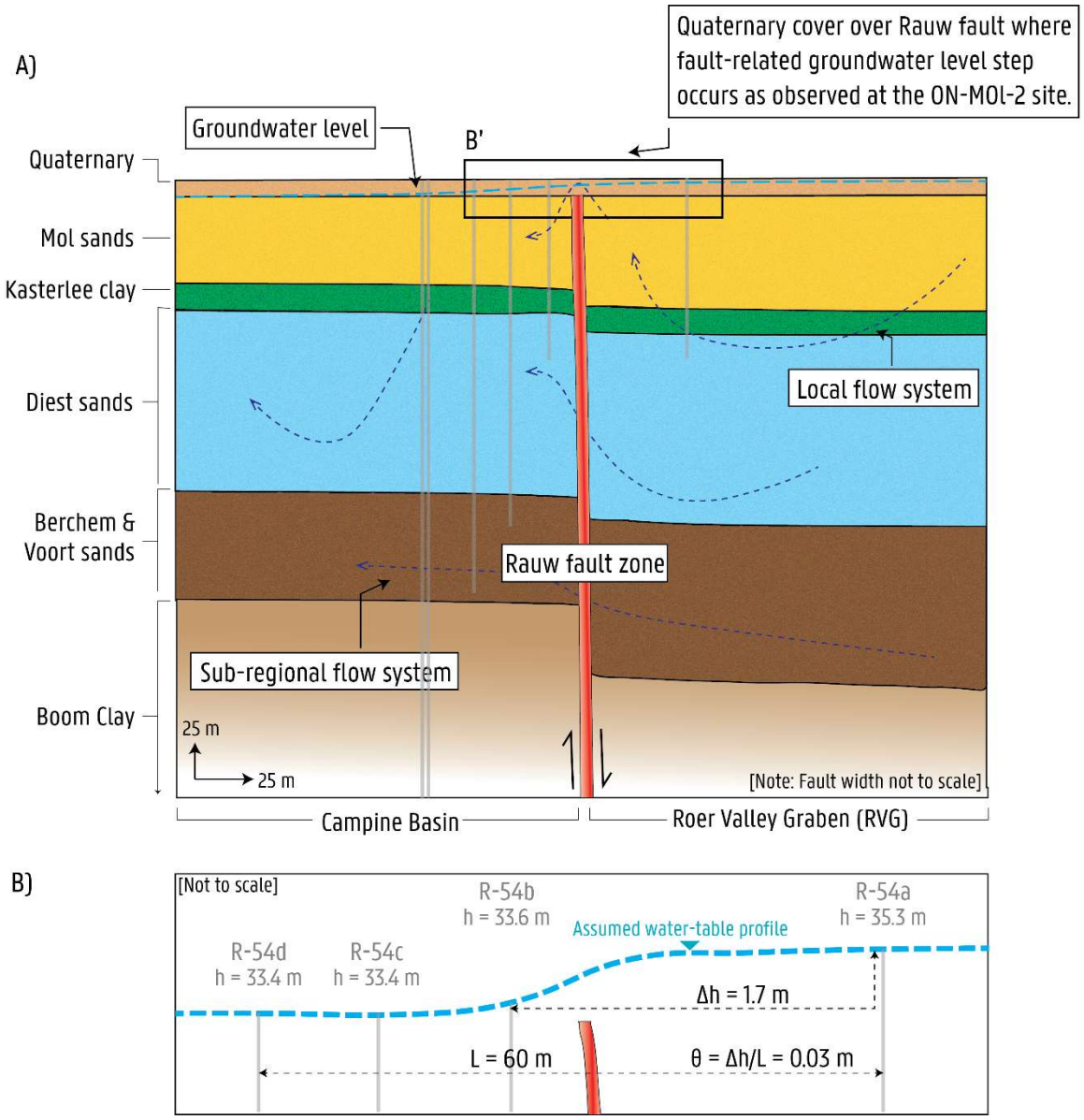

Figure 24 – Conceptual model of the Rauw fault zone at the ON-MOL-2 site.

4.3.1.4 The Neogene aquifer model (NAM)

For the current work, the Neogene aquifer model (NAM), a steady-state groundwater flow model constructed by Gedeon (2008), has been updated and used for simulations. The original NAM model by Gedeon (2008) has a lateral boundary that coincides with the catchment boundaries of the Kleine and Grote Nete rivers. The top boundary is put at the ground surface elevation whilst the bottom boundary to the top of the Boom clay formation (Figure 25). The Neogene aquifer becomes thicker in north-eastern direction, from the southwestern corner where Boom clay is present at the ground surface. The groundwater flow in the Neogene aquifer is driven mainly by surface hydrological features, i.e. recharge and river leakage inflows, and outflows from abstraction wells and river outflow assuming that it is laterally isolated (Gedeon 2008). It is assumed to be in dynamic equilibrium, with no long-term trends in groundwater flow, which allows for a steady-state simulation (Gedeon 2008).

In the model update, the Hydrologic Unit Flow (HUF) package (Anderman and Hill 2000) is implemented in the NAM model. The HUF package allows to define explicitly the vertical geometry of the hydrogeological system, independent of the defined numerical model layers. With its use, numerical instability is avoided where very thin to very thick cells would be used by following the standard approach (i.e. model layers corresponding to hydrostratigraphic units), while the downside is that sharp boundaries between contrasting material properties are attenuated by weighted averaging of the hydraulic conductivity values. The thickness of the modelling domain ranges from several meters in the south-west to more than 400 m in the north-east.

4.3.2 Model modifications and conceptualization of faults

4.3.2.1 Structure

The total thickness of the original model domain is discretized in 16 vertical layers with varying thickness (Gedeon 2008). In the new model this was modified increasing the number to 49 vertical layers, and similarly to Gedeon (2008) thinning out closer to the surface to ensure smaller modelling cells close to surface hydrological features were groundwater gradients are the highest. However, the model maintains homogeneous layer thickness (10 m) from -50 m ASL and deeper to ensure a good resolution in the deeper parts of the aquifer. The modelled area was kept from the original model, discretized into a regular model grid of 96 rows and 146 columns resulting in cells with dimensions of 400 m × 400 m.

The original model assumed 7 hydrostratigraphic units: Kempen, Pliocene, Kasterlee Clay, Diest, Berchem, Voort and Boom Clay (Gedeon 2008). The subdivision was made in accordance with the subregional model from Meyus (1998). In the new model, this was modified following the latest hydrostratigraphic 3D model (H3D) model by Deckers et al. (2019). The hydrostratigraphic formations included in the H3D model were included in the new version of the NAM model assuming 10 hydrostratigraphic units: the informal Kempen unit (younger Quaternary layers), Weelde, Malle, Merksplas, Mol, Lillo, Kasterlee Clay, Diest, Berchem and the Boom Aquitard. A schematization of the hydrostratigraphic units and the model domain are shown in Figure 25. Additionally, the faults included in the H3D model were also included in the new version of the NAM model. A total of 23 faults was simulated with the horizontal flow barrier (HFB) package (Harbaugh 2005) starting from the top of the second numerical layer (from 12 to 18 meters depth) to the bottom of the modelled domain, given that the fault does not present a clear surface expression (Verbeeck et al. 2017). However, being a buried-fault relatively close to the surface (< 5 meters), an alternative model scenario with the fault starting at the top of the model domain is tested as performed by Marshall et al. (2020).

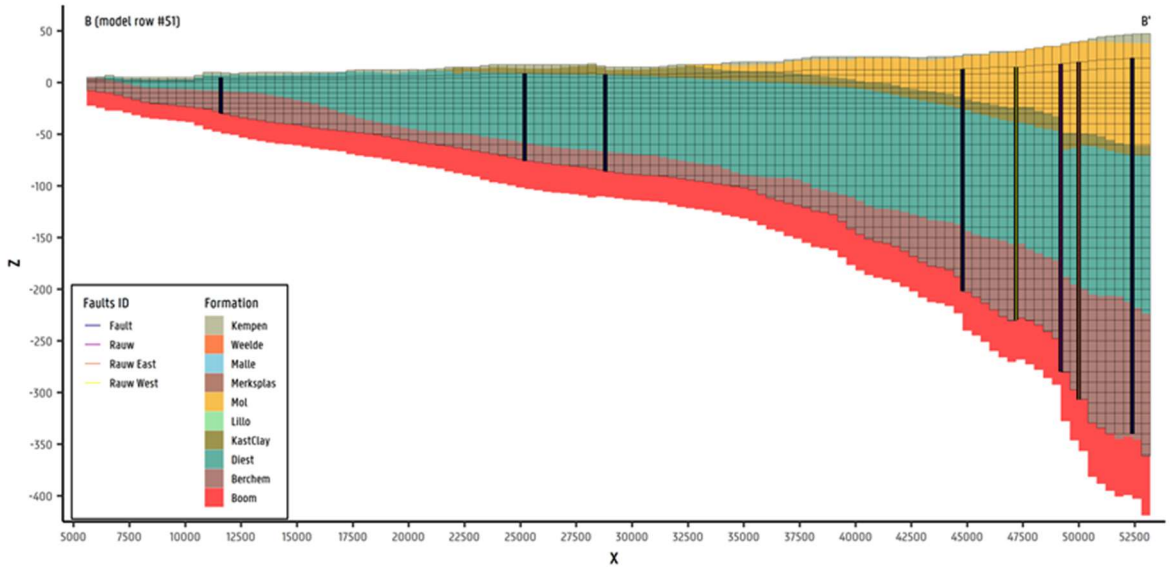

Figure 25 – Cross section on model row 51 (cross-section B-B' in Figure 23) showing the model grid, hydrostratigraphic formations and faults as modelled.

4.3.2.2 Hydrological stresses

The river, lake and canal network was defined in the original NAM by Gedeon (2008) using the river (RIV) package (Harbaugh 2005). Rogiers (2015) improved the model by implementing the MODFLOW drain (DRN) package (Harbaugh 2005). The conductance set for the boundaries was taken from the values used by Gedeon (2008), being 5m²/d/m² for lakes, 20 m²/d/m for rivers, 10^{-7}m²/d/m² for the Albert canal and 10^{-2}m²/d/m for small canals. Next, groundwater abstractions were included, and range from a few m³/d to more than 300 m³/d. In the original NAM model, recharge rate was applied regionally, divided into 4 recharge zones. The zonation was based on the infiltration capacity of the soil, depending on the permeability of the aquifer layer and/or the thickness (Gedeon 2008). For the current work, a spatially distributed recharge was applied with values obtained from DiCiacca (2020). A scaling factor (a multiplier layer) was used during the model inversion for the calibration of the recharge values. The initial? groundwater level used in this calculation was obtained from the initial heads of the calibrated original groundwater model (Gedeon, 2008). The average value for the distributed recharge is 269 mm/y.

4.3.2.3 Hydraulic head observations

The original NAM model uses 111 hydraulic-head observation points, distributed mainly in the area close to the Mol site in the Nete catchment with filters located in the Neogene aquifer (above the Boom clay). These observations come from the regional and local piezometric networks maintained by SCK CEN (Gedeon, 2008). Gedeon (2008) mentions the lack of observations in several areas across the model domain which influences the model results. For this reason, observations from the Databank Ondergrond Vlaanderen (DOV) are included now. A total of 1283 averaged hydraulic head observation values were added to the observations from the original model and are being used for steady-state flow model inversion.

4.3.2.4 Parameters and Model Calibration

The update of the hydrostratigraphic units has brought several changes in comparison with the original model, for which the previous parameter values were used for initial model run tests, as shown in Table 5. Additionally, faults as HFB were each included as an individual model parameter called hydraulic characteristic Hydchr (d^{-1}). Several model tests were performed to determine a suitable value for the hydraulic characteristic, starting by using the values of the adjacent formations, then reducing these values, to end up defining a homogeneous value for each HFB (these are shown as 'initial' value in Table 5). The results of these tests were evaluated while performing parameter optimization. The hydraulic characteristic Hydchr is equal to the horizontal hydraulic conductivity Kh(m/d) of the fault, assuming a fault zone of w = 1 m wide, given the formula Hydchr = Kh/w.

From the beginning of the modelling exercise, several fault conceptualizations were tested including fully penetrating faults, non-homogenous faults (determining the hydraulic characteristics from the adjacent formations will lead to spatially distributed hydraulic characteristic values if the fault cuts through different formations), and with varying hydraulic characteristics (varying width of the fault zone).). However, given that the fault's dip causes a horizontal offset of around 50 to 250 meters (spatially dependent) over the vertical domain from the surface to the top of the Boom clay, and the groundwater flow model cells are 400 m x 400 m, the faults were assumed to be vertical in all tests (displacement < model cell dimensions). The simulated barriers are of a constant thickness (based on the hydraulic characteristic (Harbaugh,2005)), linear, vertical, and with homogeneous hydraulic properties. Offset of stratigraphic layers or changes in topography across the barriers were not considered given that they strictly have to follow the boundaries of a numerical model cell.

Automatic parameter optimization is used as technique for model inversion. Several algorithms were used for global model optimization such as the Standard Particle Swarm Optimization (spso11) (Knight et al. 2012; Zambrano-Bigiarini and Rojas 2013; Zambrano-Bigiarini et al. 2013), and Differential Evolution (Mullen et al. 2011). Dimensionless scaled sensitivities (DSS) can be used to compare the importance of different observations to the estimation of a single parameter and to compare the importance of different parameters to the calculation of a single simulated value (Vandersteen et al., 2011). The DSS is used to calculate the composite scaled sensitivities (CSS) for determining the most sensitive parameters.

4.3.2.5 Particle tracking

Backward particle tracking was performed using MODPATH 7 (Pollock 2016). MODPATH is a particle-tracking model that simulates advective transport, designed to work with the flow output from MODFLOW (Pollock 2015). Here we use it to determine the main flow patterns across the HFB at different depths and test the potential for the faults to act as horizontal barriers or vertical conduits.

4.3.3 Groundwater flow model results

Overall the hydraulic head decreases according to the topography from the eastern side in the highest topographic area of the modelling domain, to the western side of the domain with a total difference of around 65 meters of head, following the discharge direction of the hydraulic features (i.e. rivers, canals). The model performance of the original NAM model by Gedeon (2008) had a root-mean squared error (RMSE) of 2.08 meters accounting for a total head loss of 34.43 meters. With the new modifications made to the NAM model, the RMSE has been lowered to 0.70 meters but now accounting for a head loss of 46.54 meters, covering to a larger extent the modelling domain.

Figure 26 shows the composite scaled sensitivity (CSS) values for all modelled parameters, where the parameter for the Rauw fault ('HFB_RAUW') presents the highest CSS value among the HFB parameter group. The absolute dimensionless scaled sensitivity (DSS) for only the HFB group of parameters is shown in Figure 27. This figure indicates a higher sensitivity of the Rauw fault parameter as compared to the rest of the HFB defined parameters. Additionally, it shows the total number of observations (above the bar) that are being influenced by it.

Table 5 – Overview of initial and final parameters for the updated version of the NAM model. Kh = horizontal hydraulic conductivity, Va = vertical anisotropy, Avg. = average, Coeff. = coefficient, Hydchr = hydraulic characteristic.

Model Parameter	Original Model	Updated Model	Initial	Final	Value
Kempen	x	x	23	78.1	Kh (m/d)
Weelde	-	x	5	5	Kh (m/d)
Malle	-	x	5	5	Kh (m/d)
Merksplas	-	x	5	1.2	Kh (m/d)
Lillo	-	x	5	10.4	Kh (m/d)
Mol	-	x	5	15.1	Kh (m/d)
Kasterlee Clay	x	x	1	1	Kh (m/d)
Kasterlee	x	x	3225	100	Va
Diest	x	x	5	7.3	Kh (m/d)
Berchem-Voort	x	x	0.5	0.5	Kh (m/d)
Recharge	-	x	268	269	Avg. (mm/y)
Canals	x	x	1	1	Coeff.
Rivers	x	x	1000	39.7	Coeff.
Drains	-	x	-	5000	Coeff.
Lake	x	x	10000	10000	Coeff.
Rauw Fault	-	x	0.01	8.69e-04	Hydchr (d^{-1})
Rauw Fault (East)	-	x	0.01	6.60e-02	Hydchr (d^{-1})
Rauw Fault (West)	-	x	0.01	0.01	Hydchr (d^{-1})
Poppel Fault	-	x	0.01	5.35e-03	Hydchr (d^{-1})
089 Fault	-	x	0.01	9.77e-02	Hydchr (d^{-1})
100 Fault	-	x	0.01	1.03e-02	Hydchr (d^{-1})
112 Fault	-	x	0.01	5.56e-01	Hydchr (d^{-1})
Other Faults (16)	-	x	0.01	0.01	Hydchr (d^{-1})

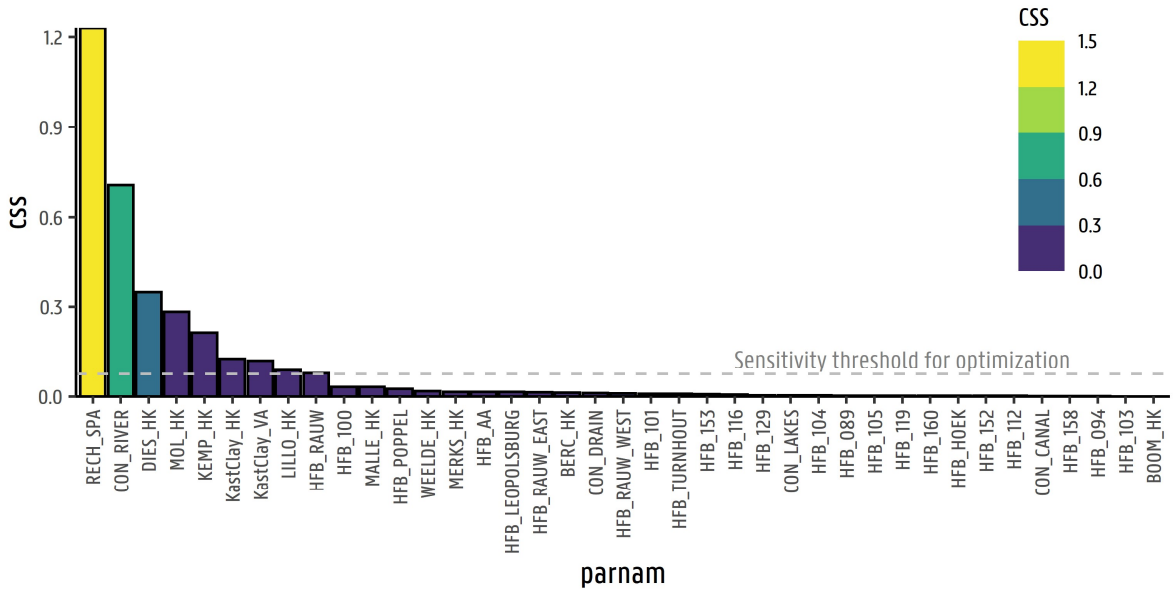

Figure 26 – Sensitivity analysis results for all model parameters. Recharge and river conductance show the highest CSS, followed by hydraulic conductivity of several major hydrogeological units. The parameter for the Rauw fault ('HFB_RAUW') presents the highest CSS value among the HFB parameter group (the fault parameter group).

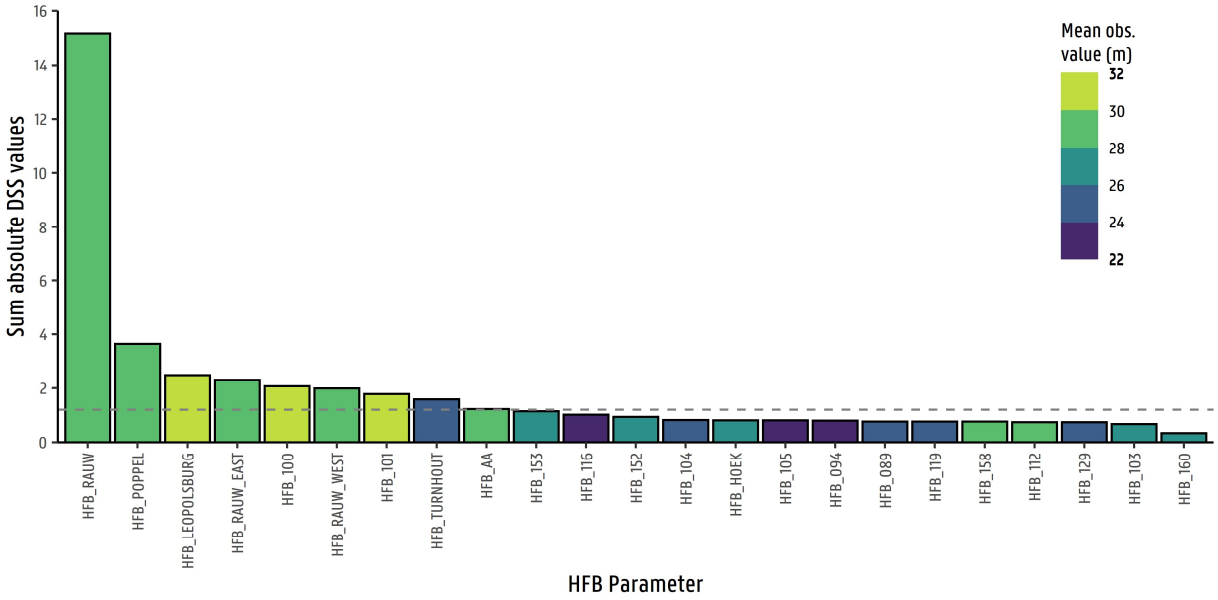

Figure 27 – Absolute DSS values for each HFB parameter. A higher level of magnitude of sensitivity of the Rauw fault parameter in relation to the rest of the HFB defined parameters can be seen. The total number of observations (above the bar) that are being influenced by the fault are shown above the bar.

Figure 28 shows the differences in hydraulic head between two models: the model with optimized parameters (including HFB), and the model with optimized parameters but

deactivating the HFB. The simulated heads between the model with HFB activated minus the model with HFB deactivated are ca. 1.5 m higher in altitude to the east of the Rauw fault. This difference in head indicates also the observed hydraulic head values on both sides of the Rauw fault. At the ON-MOL-2 site, piezometers R-54a (eastern) and R-54b,c,d,e (western) are separated by around 60 meters in the horizontal distance, with a piezometric head difference of around 1.7 meters (Figure 24). This value largely corresponds to the current modelling results indicating that this is in fact a fault-related groundwater level step, however, being a buried fault (without surface expression) it is not driven by topographic offsets but mainly by a combination of fault hydraulic properties and local groundwater circulation.

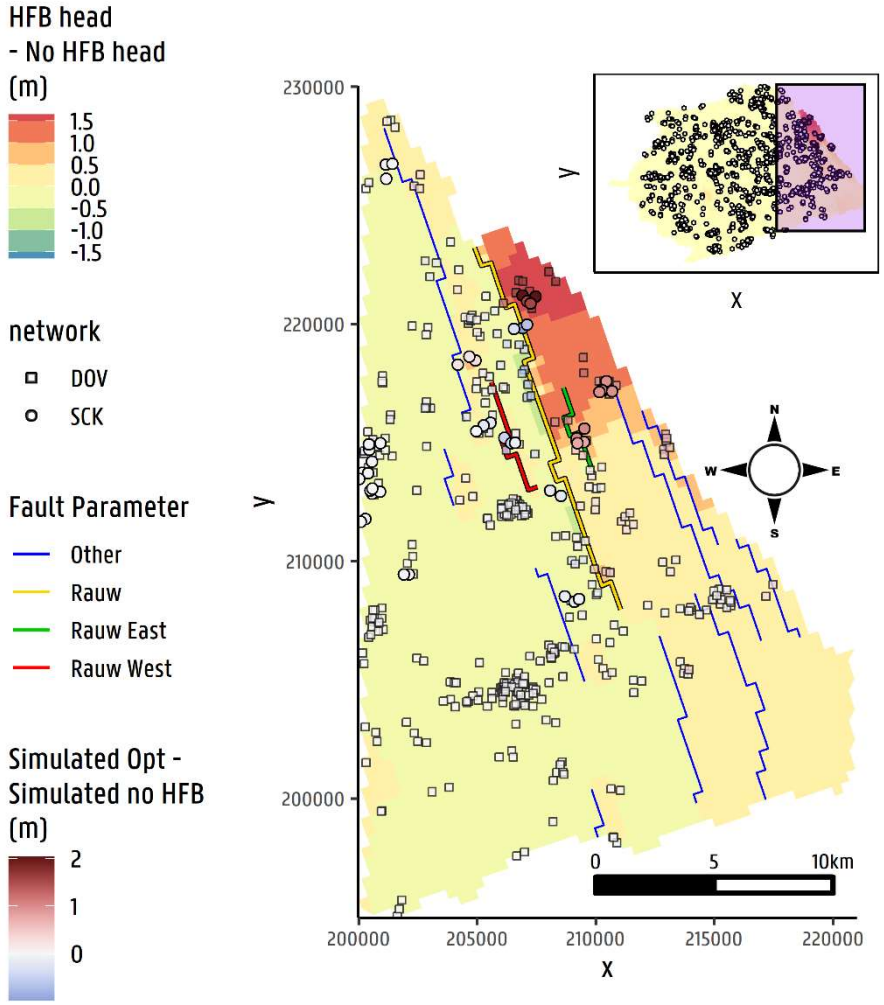

Figure 28 – Hydraulic head distribution over the Rauw fault zone. The colour map shows the difference in simulated head between the model with HFB activated minus the model without activated HFB. The higher heads from the model with HFB to the east of the fault are in accordance with the observed step in groundwater head (ca. 1.7 m higher to the east of the fault, see Figure 24). The coloured observation points of the piezometric networks show the same information.

A forward particle tracking model run was performed to observe the advective travel flow paths from a location at the eastern side of the Rauw fault at several depths along the entire vertical

model domain, as shown in Figure 29. Particles located in the Diest and younger formations travel in a downward direction crossing through the easternmost fault. When arriving in the block between that fault and the Rauw fault they start to travel upwards and along the fault due to the difference in hydraulic conductivity (lower across the fault) versus the formation they are located in. Particles that begin in the upper parts of the aquifer flow above HFB_RAUW then travel downwards once they are at the western side of it; others flow through it and then continue their travel downwards similarly. Afterwards, particles begin traveling upwards most likely following the natural local groundwater system circulation being driven by the surface water networks, since there is no indication of other faults having a clear effect on the groundwater flow pattern. On the other hand, the flow of particles located in the Berchem formation does not appear to be strongly influenced by the Rauw fault, or any other fault, flowing close to the Boom Clay to be later discharged vertically in a more downstream location. The overall flow pattern is indicative that the Neogene aquifer consists of several local flow systems conforming the general regional system.

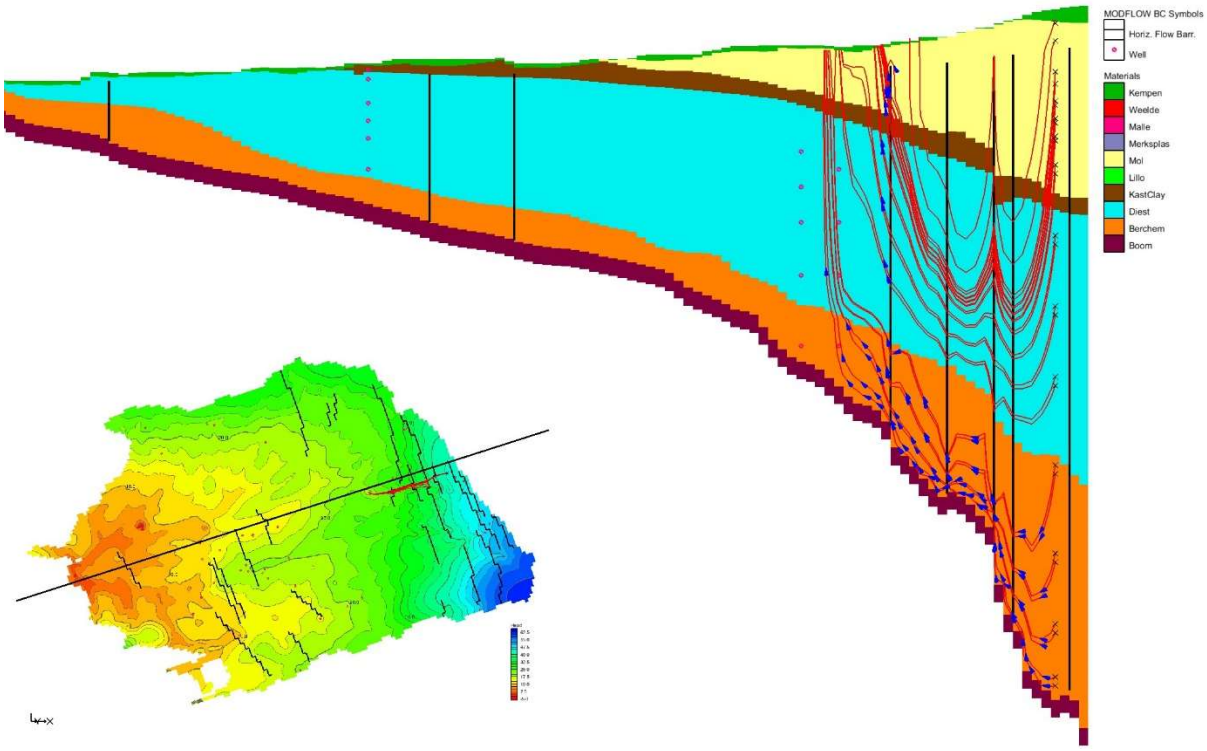

Figure 29 – Forward particle tracking using MODPATH. See text for detailed explanation.

4.3.4 Dealing with conceptual uncertainties

The current results from the groundwater flow model rely on the conceptual model consideration that the Rauw fault is a) a buried fault, b) a fault where groundwater flows upwards vertically along the fault to a larger degree than horizontally and downgradient, c) that groundwater is overflowing above the fault and then flowing downgradient, d) that this is creating a groundwater level step (head difference, see Figure 28), and e) that it is not fully-penetrating entire the entire model domain. The fault is conceptualized/introduced in the updated model starting from the second numerical model layer, at around ~15 meters below the ground surface (varies along the fault, depth determined at the ON-MOL-2 site), and

extending to the bottom of the model, cross-cutting all underlying hydrogeological formations. The depth to the top of the fault following this conceptualization represents about 3% of the total vertical discretization of the model (470.1 meters). In reality the top of the fault is buried around ~1 meter or less (as observed at the ON-MOL-2 site; Verbeeck et al., 2017) below the ground surface (0.21% of the total depth).

The scenario where the fault is fully penetrating the whole vertical model domain was developed to investigate the changes in hydraulic parameters and how these influence the currently produced flow fields. A similar calibration procedure was followed for the fully penetrating fault scenario as for the buried fault. The RMSE value of the fully penetrating fault is lower than the one from the buried fault by 0.01 meters. When comparing the head observations in the range between 25 m to 45 m (observations in the surroundings of the Rauw fault), the difference in the RMSE is only 0.001 meters. The hydraulic characteristic of the Rauw fault parameter increased by a factor of 2.88 in relation to the previous optimal value (Table 5). This would result in increased flow across the Rauw fault, mostly taking place in the Diest Formation, but diminishing the upwards vertical flow magnitude closer to the surface. The Kempen and Merksplas Kh values also increased. This in combination with the increase in conductivity of the Rauw fault conductivity, would allow more groundwater to flow across the Rauw fault from east to west reducing the upwards flow component. .
In reality, the geometry of faults is much more complex, as discussed by Verbeeck et al. (2017). As they may act as conduits, barriers or complex hybrid conduit-barrier systems, a low-permeability fault core can be surrounded by a higher-permeability "damage zone" in a more local scale (Caine et al. 1996; Bense and Person 2006; Bense et al. 2013). The results from testing a variation in the conceptual structure of the Rauw fault shows us that structural/conceptual design uncertainty can be a considerable source of uncertainty, which is often neglected/overlooked (Refsgaard et al. 2012; Lin and Beck 2012).

4.3.5 The hydraulic characteristic of the Rauw fault: conclusion

The hydraulic characteristic of the Rauw fault, expressed as Hydchr = Kh/w, and other adjacent faults in the Nete catchment, is shown in Table 5. The simulated value is 8.69e-04 d^{-1}, which is the lowest value of all the investigated faults. As shown above, a different conceptualization of the fault results in a Hydchr value which is 2.88 times higher, i.e. 2.50e-3d^{-1}. Combining both values leads to a working value of 1e-3d^{-1}. Not only proves the Rauw fault to be the most impermeable for horizontal flow, its HFB parameter also shows to be the most sensitive of all fault parameters (Figure 27).

The hydraulic characteristic of the Rauw fault can fully explain the observed groundwater head difference at the ON-Mol-2 site (Figure 24) and the upward vertical flow upstream of the fault (Figure 29). Clearly, the other faults do not show such distinct pattern, neither in groundwater head distribution up- and downstream of the fault (Figure 28), nor in the flow pattern.

The conversion of the hydraulic characteristic Hydchr to Kh is dependent on the conceptualization of relevant fault zone thickness. For an assumed width of 1 m, the Kh equals Hydchr in m/d. However, assessing the thickness of the affected zone on each side of the fault is not straightforward in loose sandy sediment. Verbeeck et al. (2017) observed in a thin-section of the fault a 1 mm thick clay-rich band with intact fault-parallel clay orientation and colour banding, without deformation of clay-coated sand grains. If we accept this band to be the hydraulically relevant thickness of the fault, the intrinsic Kh of the Rauw fault, as represented by

this clay-rich band, would be as low as ca. 1e-6 m/d. However, it has to be noted that not only clay smearing may contribute to modifications of the permeability. Once a hydraulic barrier is formed, organic matter may accumulate upstream of it due to lateral (ground)water flow, thereby further decreasing the permeability. In addition, modifications of the sedimentary fabric (sorting) may also influence the hydraulic properties near a fault (Bense et al., 2013).

The observed head difference of ca. 1.7 m is in general smaller than the one observed along the Grote Brogel fault, a neotectonic feature of the Roer Valley Graben situated a few km to the east of the Rauw fault (Deckers et al., 2018). The highest head difference observed is more than 12 m, but at locations where the fault is branching, individual head steps tend to be smaller, reaching those of the Rauw fault. The large head differences over the Grote Brogel fault can partially be explained by the larger topographical gradient between the hanging wall and footwall blocks.

5 CONCLUSION AND RECOMMENDATIONS

5.1 Conclusions

Not surprisingly, the metadata analysis of K-values for aquifers and aquitards shows that the availability of data on hydraulic conductivity decreases with depth.
For some of the hydrogeological units no data are available at all, for example for unit HAc, or for specific subareas. It is striking to note that data are lacking for important aquitards such as the Boom Clay in the Dutch part of the Roer Valley Graben and the lignite layers of the Ville Formation in the Dutch and Belgian part of the project area. Although data reliability presented in this study is a first assessment only, it shows that the reliability of available hydraulic conductivity data decreases with depth.

Of the 59 hydrogeological units for which hydraulic conductivity data are available in more than one country:

- 18 units show a very good agreement for K values between the various subareas. These units are all aquifers and dominated by relatively pure quartz sand, coarse to fine, with various degrees of gravel. They are mostly deposited in a fluvial-estuarine setting, while some units refer to a shallow marine environment.
- 32 units show a good agreement for K values between the various subareas, in the sense that their expert ranges at least partially overlap. However, for some subareas either the expert and/or absolute minimum or maximum shows a significant offset and/or the full range is much smaller or larger. Around 47% of these units (15 out of 32) are aquitards.
- 10 do not show any overlap for their expert ranges, and with various degrees of overlap of their absolute ranges. Out of 10 units, 7 qualify as an aquitard.

The juxtaposition and displacement analysis of a fault near Veghel, which is part of the Peel Boundary Fault zone, provide a better 3D insight in areas where hydraulic connectivity across the fault plane is expected to occur. However, 3D seismic data is required for an interpretation that would be detailed enough for the study of the relay ramp, areas of fault-linkage that play an important role in groundwater dynamics around faults.

The nature of groundwater dynamics around faults that act as horizontal flow barriers was assessed through exhaustive numerical modelling of groundwater flow along the Rauw Fault near Mol. The results of this exercise show how the flow pattern can be deflected in an upward direction, and fully explain observations of abrupt groundwater head gradients across the fault. The modelling exercise leads to an estimate of the hydraulic characteristic of the fault, which, in combination with the width of the barrier zone, leads to a value for hydraulic conductivity of the fault. Another way of characterising hydraulic properties of fault zones is demonstrated for the Peel Boundary Fault near Veghel, using a detailed juxtaposition analysis.

5.2 Recommendations

Information on hydrogeological units that are at greater depth in the central part of the Roer Valley Graben, is sometimes available in neighbouring countries where these units are exposed or at a shallow depth. This offers good opportunities for a joint elaboration and analyses of

(hydro)geological data, especially for the important aquifers and aquitards. We therefore would recommend starting a follow-up project focusing on a small number of these aquifers and aquitards.

In this study the ranges in hydraulic conductivity in the different H3O subareas were analysed visually. To make the interpretation more robust we would recommend a statistical analysis on the metadata.

We have demonstrated that advanced techniques can be used to characterise groundwater flow dynamics near faults. For a follow-up project we would recommend the use of both techniques on a single fault to determine groundwater fluxes across faults. Ultimately, a database with hydraulic properties of the most important Roer Valley Graben faults may be established.

In order to assess the hydraulic characteristics of a fault, monitoring wells on both sides and at close range of the fault, with screens in all important aquifers, are required. In the Roer Valley Graben such monitoring sites are lacking. We therefor hardly recommend installing pairs of monitoring wells along the major fault zones in the Roer Valley Graben, in particular along the faults that border the graben. This would enable a better estimate of the influx of groundwater across the fault zone and thus of the water balance of the Roer Valley Graben.

6 REFERENCES

Anderman, E.R., Hill, M.C., 2000. Modflow-2000, the U.S. geological survey modular ground-water model — documentation of the hydrogeologic-unit flow (huf) package. USGS: Open File Report 00-342 96.

Batlle-Aguilar, J., Banks, E.W., Batelaan, O. et al., 2017. Groundwater residence time and aquifer recharge in multilayered, semi-confined and faulted aquifer systems using environmental tracers. Journal of Hydrology 546:150–165. https://doi.org/10.1016/j.jhydrol.2016.12.036.

Bense, V.F., Gleeson, T., Loveless, S.E. et al., 2013. Fault zone hydrogeology. Earth-Science Reviews 127:171–192. https://doi.org/10.1016/j.earscirev.2013.09.008.

Bear, J., 1972. Dynamics of Fluids in Porous Media. Elsevier, New York.

Bense, V.F., Person, M.A., 2006. Faults as conduit-barrier systems to fluid flow in siliciclastic sedimentary aquifers. Water Resources Research 42: https://doi.org/10.1029/2005wr004480

Caine, J.S., Evans, J.P., Forster, C.B., 1996. Fault zone architecture and permeability structure. Geology 24:1025. https://doi.org/10.1130/0091-7613(1996)024<1025:fzaaps>2.3.co;2

Buma, J.T., Reindersma, R., 2021. Resources of groundwater, harmonized at Cross-Border and Pan-European Scale, Deliverable 3.4: Harmonisation of volumes, water balances and recharge and discharge fluxes. Horizon 2020 GeoERA RESOURCE project, Technical Report D3.4, WP3.

Coetsiers, M., Walraevens, K., 2006. Chemical characterization of the Neogene Aquifer, Belgium. Hydrogeology Journal 14: 1556–1568. https://doi.org/10.1007/s10040-006-0053-0

Cool, W., Vermariën, E., Wacquier, W., Perko, J., 2013. The long-term safety and performance analyses of the surface disposal facility for the Belgian category a waste at Dessel. Proceedings of the 15th International Conference on Environmental Remediation and Radioactive Waste Management - ICEM2013-9628.

Deckers, J., Van Noten, K., Schiltz, M., Lecocq, T., Vanneste, K., 2018. Integrated study on the topographic and shallow subsurface expression of the Grote Brogel Fault at the boundary of the Roer Valley Graben, Belgium. Tectonophysics 722: 486-506. https://doi.org/10.1016/j.tecto.2017.11.019

Deckers, J., De Koninck, R., Bos, S., et al., 2019. Geologisch (g3dv3) en hydrogeologisch (h3d) 3D-lagenmodel van Vlaanderen. Studie uitgevoerd in opdracht van: Vlaams planbureau voor omgeving (departement omgeving) en vlaamse milieumaatschappij., Vlaamse Milieumaatschappij.

DiCiacca, A., 2020. Spatially distributed recharge and groundwater – surface water interactions in groundwater models: from the field to the catchment scale. PhD thesis, KU Leuven.

Domenico, P.A., Schwartz, F.W., 1997. Physical and Chemical Hydrogeology, 2nd Edition. Wiley.

Fossen, H., Rotevatn, A., 2013. Fault linkage and relay structures in extensional settings—A review. Earth-Science Reviews. 154: 14 -28. https://doi.org/10.1016/j.earscirev.2015.11.014

Gedeon, M., 2008. Neogene Aquifer Model. Institute for Environment, Health, Safety, Belgian Nuclear Research Centre (SCKCEN), Boeretang 200, 2400 Mol, Belgium.

Harbaugh, A.W., 2005. MODFLOW-2005, The U.S. Geological Survey Ground-water Model, Ground-water Flow Process. USGS: Techniques and Methods 6-A16 1–253. https://doi.org/https://doi.org/10.3133/tm6A16

Knight, N., Sousa, P., Barrett, J.L., Atran, S., 2012. Standard Particle Swarm Optimization. hal-00764996

Ladevèze, P., Rivard, C., Lavoie, D. et al., 2018. Fault and natural fracture control on upward fluid migration: Insights from a shale gas play in the st. Lawrence platform, Canada. Hydrogeology Journal 27: 121–143. https://doi.org/10.1007/s10040-018-1856-5

Lapperre, R.E., Kasse, C., Bense, V.F. et al., 2019. An overview of fault zone permeabilities and groundwater level steps in the Roer Valley Rift System. Netherlands Journal of Geosciences 98: e5. https://doi.org/10.1017/njg.2019.4

Lin, Z., Beck, M.B., 2012. Accounting for structural error and uncertainty in a model: An approach based on model parameters as stochastic processes. Environmental Modelling & Software 27-28: 97–111. https://doi.org/10.1016/j.envsoft.2011.08.015

Mallants, D., 2010. A long-term solution for Belgian category A waste: SCK CEN provides scientific input for the surface disposal facility in Dessel. Mol.

Marshall, S.K., Cook, P.G., Konikow, L.F. et al., 2020. Conjoint use of hydraulic head and groundwater age data to detect hydrogeologic barriers. Hydrogeology Journal 28: 1003–1019. https://doi.org/10.1007/s10040-019-02095-9

Meyus, Y., 1998. Sub-regional simulation of the water flow in the Neogene aquifer at the Mol site. SCK CEN, Mol, R-3251.

Mullen, K., Ardia, D., Gil, D. et al., 2011. DEoptim: AnRPackage for global optimization by differential evolution. Journal of Statistical Software 40: 1-26. https://doi.org/10.18637/jss.v040.i06

Oiro, S., Comte, J.C., Soulsby, C., Walraevens, K., 2018. Using stable water isotopes to identify spatio-temporal controls on groundwater recharge in two contrasting East African aquifer systems. Hydrological Sciences Journal 63: 862–877. https://doi.org/10.1080/02626667.2018.1459625

ONDRAF/NIRAS, 2010. The cAt project in Dessel: A long-term solution for Belgian category a waste.

Patyn, J., Ledoux, E., Bonne, A., 1989. Geohydrological research in relation to radioactive waste disposal in an argillaceous formation. Journal of Hydrology 109: 267–285. https://doi.org/10.1016/0022-1694(89)90019-X

Pollock, D.W., 2016. User guide for MODPATH version 7A particle-tracking model for MODFLOW.

Pollock, D.W. 2015. Extending the MODPATH algorithm to rectangular unstructured grids. Groundwater 54: 121–125. https://doi.org/10.1111/gwat.12328

Refsgaard, J.C., Christensen, S., Sonnenborg, T.O. et al. 2012. Review of strategies for handling geological uncertainty in groundwater flow and transport modeling. Advances in Water Resources 36: 36–50. https://doi.org/10.1016/j.advwatres.2011.04.006

Rogiers, B., 2015. Groundwater flow and solute transport modelling from within R: The RMODFLOW and RMT3DMS packages. In: MODFLOW and more 2015: Modeling a complex world. SCK-CEN, Golden, Colorado.

Rushton, K.R., Redshaw, S.C., 1979. Seepage and groundwater flow: Numerical analysis by analogue and digital methods. New York, John Wiley and Sons.

Vandersteen, K., Gedeon, M., Rogiers, B., 2011. Transient model of the confined aquifers below the Boom Clay: 2011 update. External Report SCK CEN-ER-199. Mol, Belgium.

Vandersteen, K., Gedeon, M., Leterme, B., 2013. Hydrogeology of North-East Belgium. External Report SCK CEN-ER-136. Mol, Belgium.

Verbeeck, K., Wouters, L., Vanneste, K. et al., 2017. Episodic activity of a dormant fault in tectonically stable Europe: The Rauw fault (NE Belgium). Tectonophysics 699: 146–163. https://doi.org/10.1016/j.tecto.2017.01.023

Vrolijk, P., Urai, J., Kettermann, M., 2016. Clay smear: Review of mechanisms and applications. Journal of Structural Geology 86: 95-152. https://doi.org/10.1016/j.jsg.2015.09.006

Walraevens, K., Mjemah, I.C., Mtoni, Y., Van Camp, M., 2015. Sources of salinity and urban pollution in the Quaternary sand aquifers of Dar es Salaam, Tanzania. Journal of African Earth Sciences 102: 149–165. https://doi.org/10.1016/j.jafrearsci.2014.11.003

Zaadnoordijk, W., Szalkai, A. , Beerten, K., Mallin Martin, D., Ward, R., , Bowes, M., Newell, A., Smedley, P., Broers, H.P., Slenter, C., Loveless, S., 2019. Deliverable D3.1 Technical report on evidence for potential pathways for groundwater contamination from subsurface energy activities and investigation/data collection plan. Horizon 2020 GeoERA VoGERA project, Technical Report 1, WP3.

Zambrano-Bigiarini, M., Clerc, M., Rojas, R., 2013. Standard particle swarm optimisation 2011 at CEC-2013: A baseline for future PSO improvements. In: 2013 IEEE congress on evolutionary computation. IEEE.

Zambrano-Bigiarini, M., Rojas, R., 2013. A model-independent particle swarm optimisation software for model calibration. Environmental Modelling & Software 43: 5–25. https://doi.org/10.1016/j.envsoft.2013.01.004

APPENDIX 1

Excel workbook

APPENDIX 2

Pdf file with fact sheets per model unit

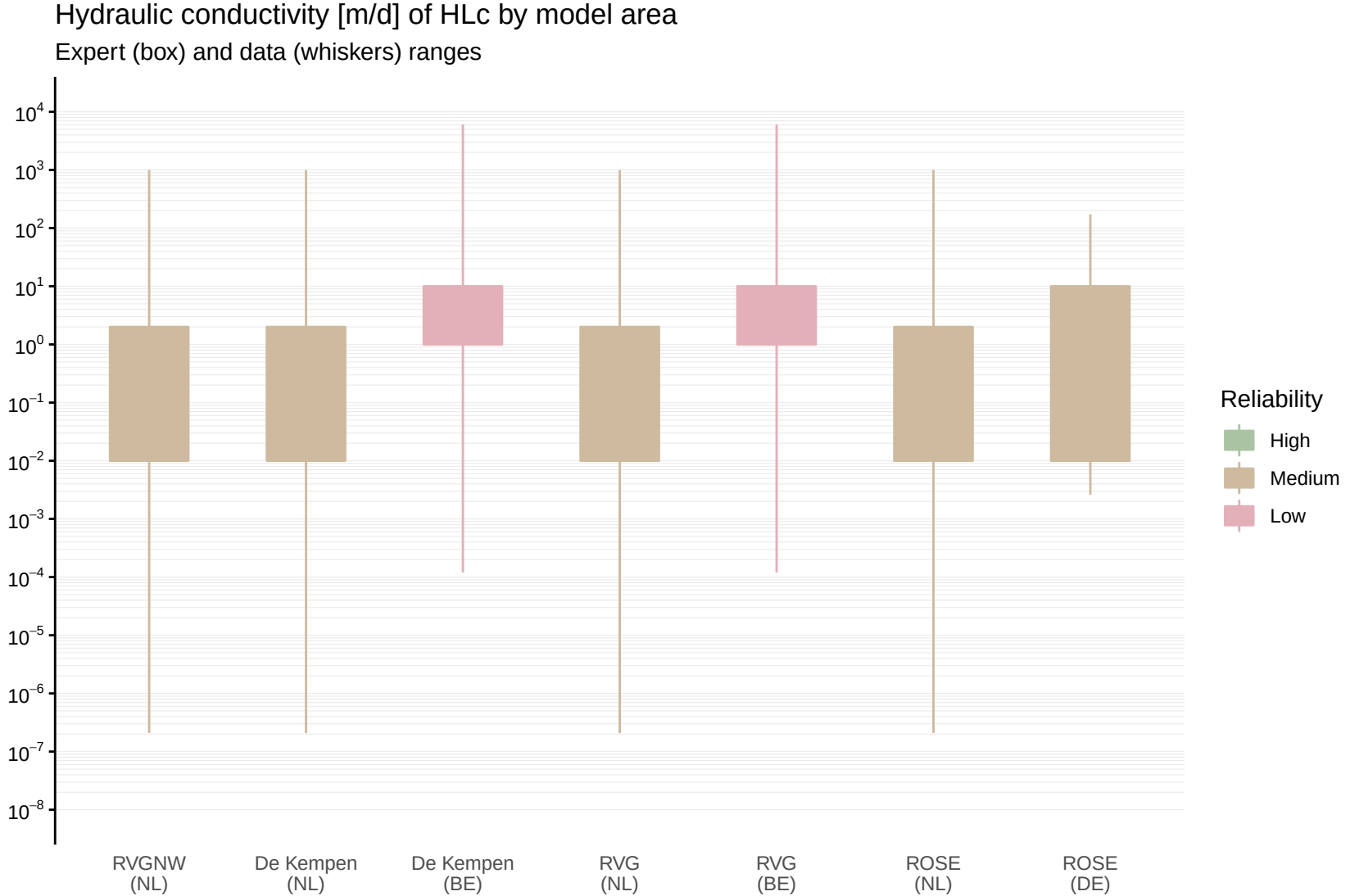
Hydraulic conductivity [m/d] of HLc by model area
Expert (box) and data (whiskers) ranges
10^{4}
10^{3}
10^{2}
10^{1}
10^{0}
10^{-1}
10^{-2}
10^{-3}
10^{-4}
10^{-5}
10^{-6}
10^{-7}
10^{-8}
RVGNW (NL)
De Kempen (NL)
De Kempen (BE)
RVG (NL)
RVG (BE)
ROSE (NL)
ROSE (DE)
Reliability
High
Medium
Low

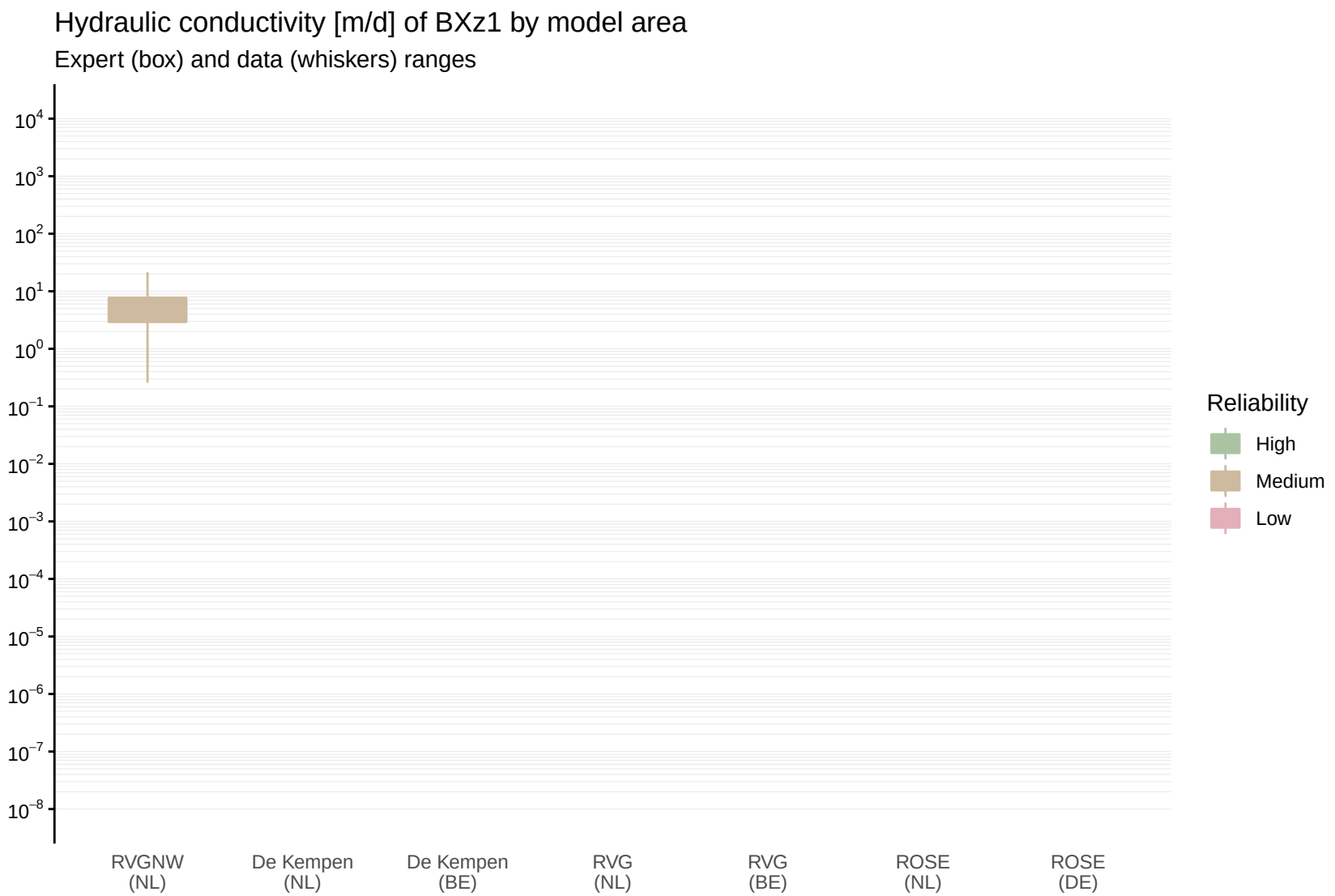
Hydraulic conductivity [m/d] of BXz1 by model area
Expert (box) and data (whiskers) ranges
10^{4}
10^{3}
10^{2}
10^{1}
10^{0}
10^{-1}
10^{-2}
10^{-3}
10^{-4}
10^{-5}
10^{-6}
10^{-7}
10^{-8}
RVGNW (NL)
De Kempen (NL)
De Kempen (BE)
RVG (NL)
RVG (BE)
ROSE (NL)
ROSE (DE)
Reliability
High
Medium
Low

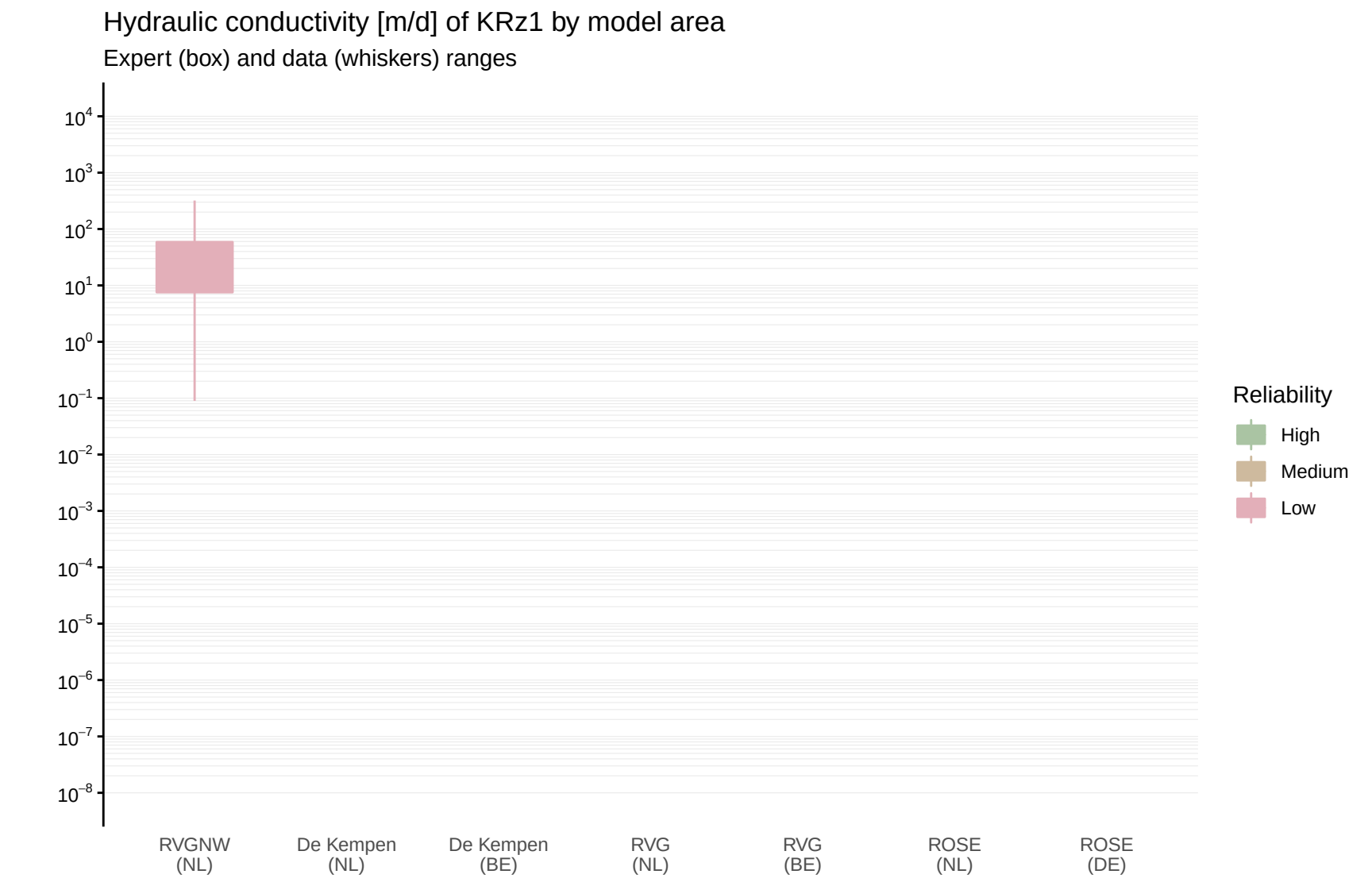
Hydraulic conductivity [m/d] of KRz1 by model area
Expert (box) and data (whiskers) ranges
10^{4}
10^{3}
10^{2}
10^{1}
10^{0}
10^{-1}
10^{-2}
10^{-3}
10^{-4}
10^{-5}
10^{-6}
10^{-7}
10^{-8}
RVGNW (NL)
De Kempen (NL)
De Kempen (BE)
RVG (NL)
RVG (BE)
ROSE (NL)
ROSE (DE)
Reliability
High
Medium
Low

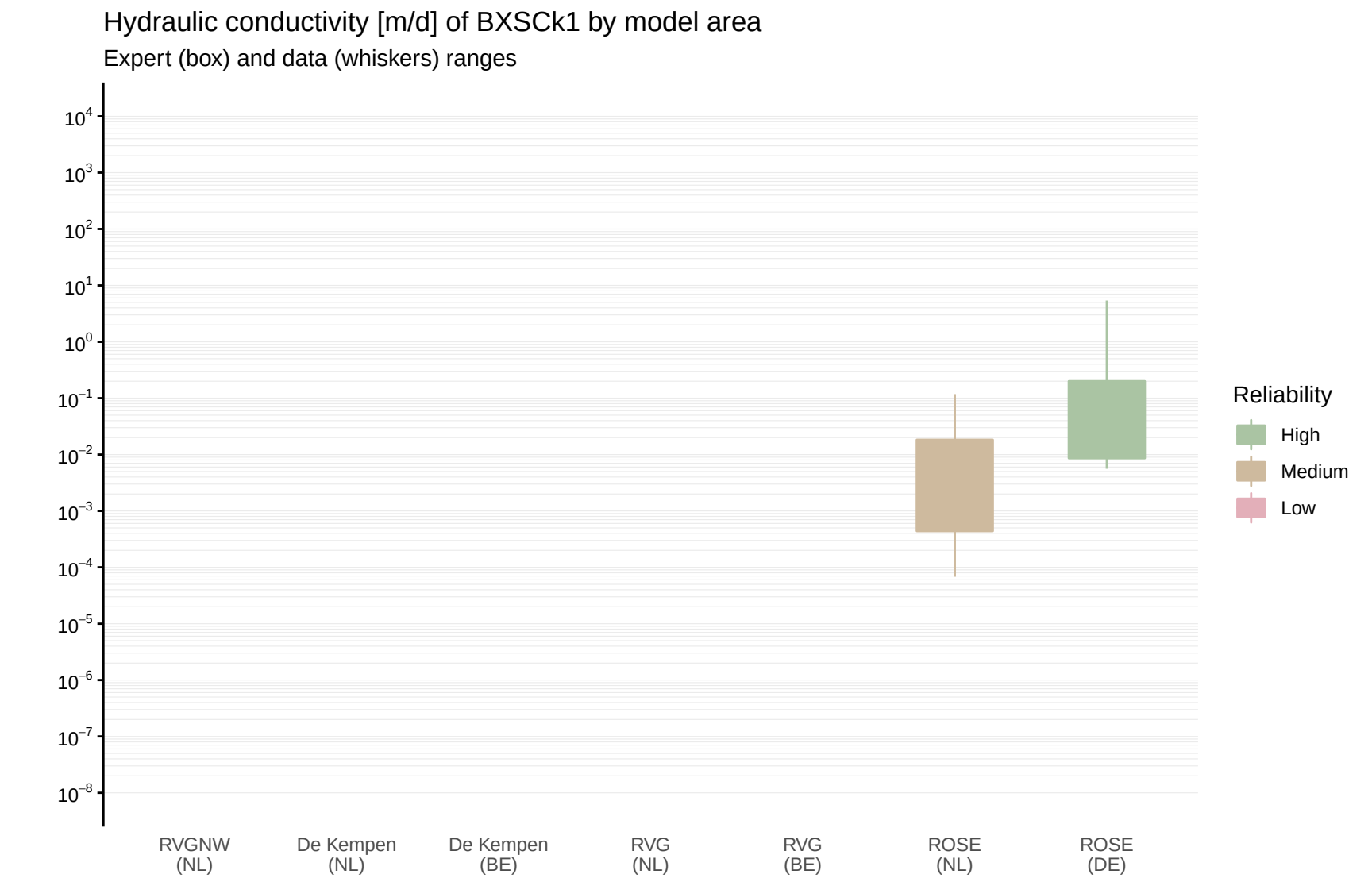
Hydraulic conductivity [m/d] of BXSCk1 by model area
Expert (box) and data (whiskers) ranges
10^{4}
10^{3}
10^{2}
10^{1}
10^{0}
10^{-1}
10^{-2}
10^{-3}
10^{-4}
10^{-5}
10^{-6}
10^{-7}
10^{-8}
RVGNW (NL)
De Kempen (NL)
De Kempen (BE)
RVG (NL)
RVG (BE)
ROSE (NL)
ROSE (DE)
Reliability
High
Medium
Low

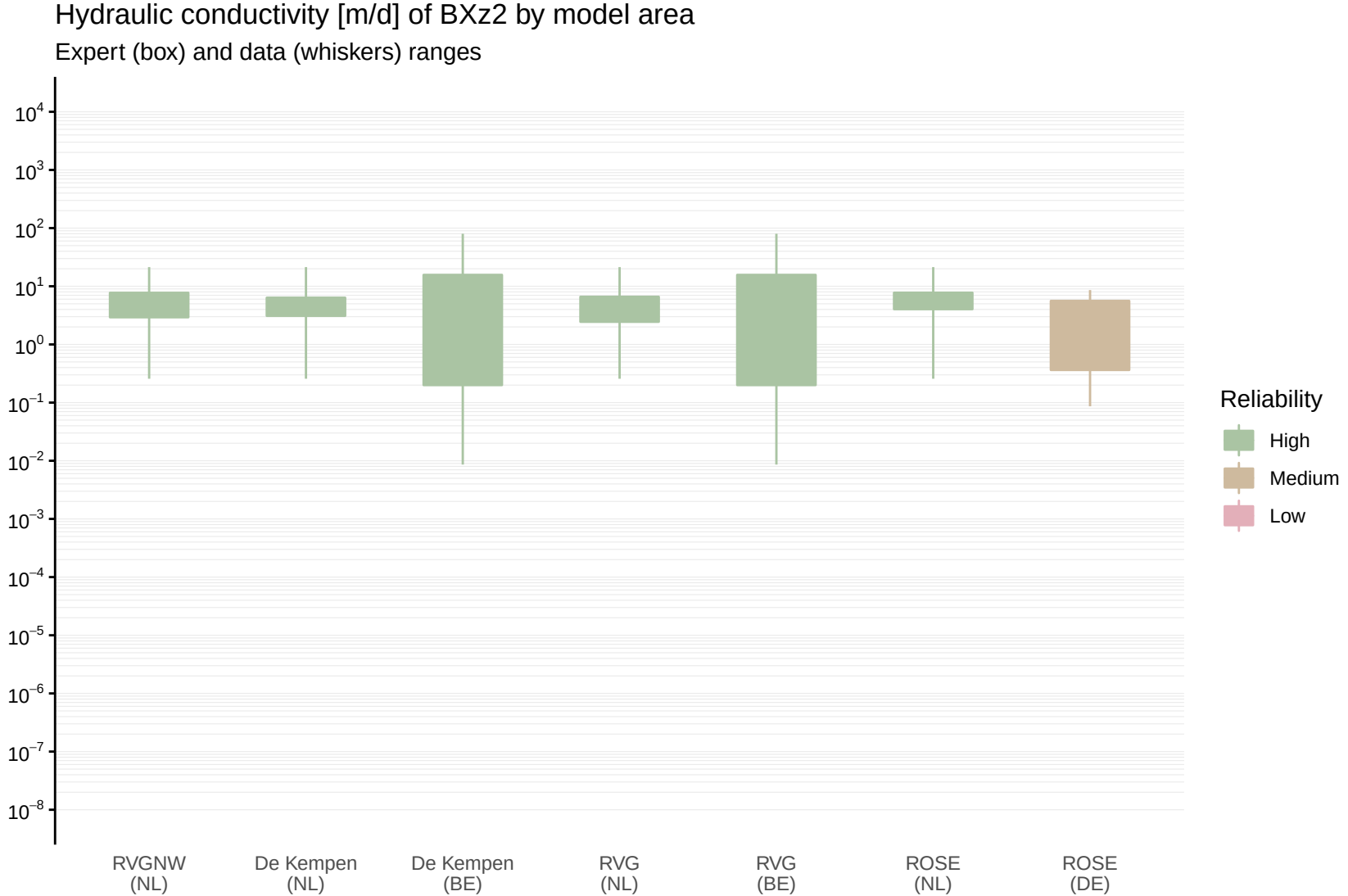
Hydraulic conductivity [m/d] of BXz2 by model area
Expert (box) and data (whiskers) ranges
10^{4}
10^{3}
10^{2}
10^{1}
10^{0}
10^{-1}
10^{-2}
10^{-3}
10^{-4}
10^{-5}
10^{-6}
10^{-7}
10^{-8}
RVGNW (NL)
De Kempen (NL)
De Kempen (BE)
RVG (NL)
RVG (BE)
ROSE (NL)
ROSE (DE)
Reliability
High
Medium
Low

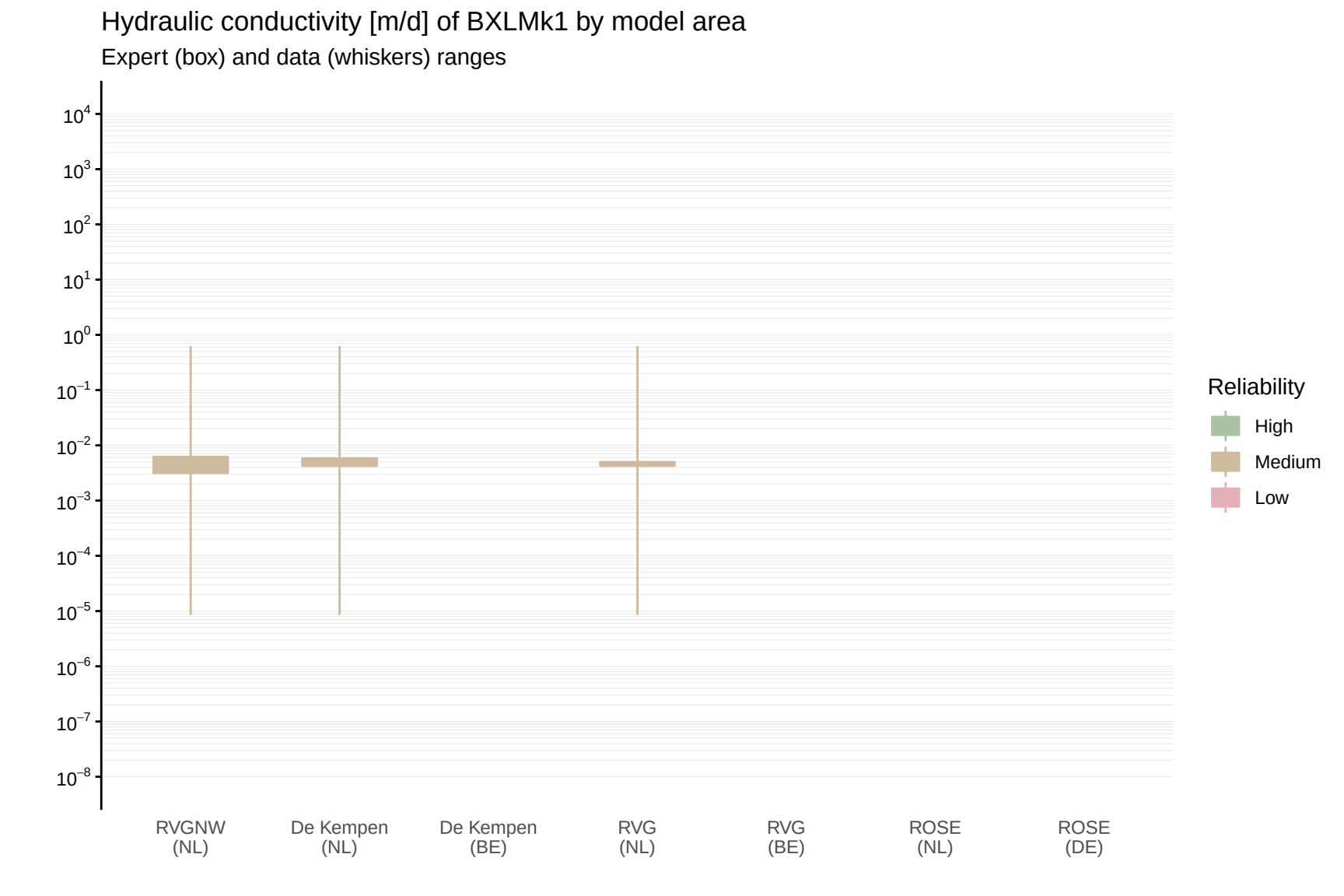
Hydraulic conductivity [m/d] of BXLMk1 by model area
Expert (box) and data (whiskers) ranges
10^{4}
10^{3}
10^{2}
10^{1}
10^{0}
10^{-1}
10^{-2}
10^{-3}
10^{-4}
10^{-5}
10^{-6}
10^{-7}
10^{-8}
RVGNW (NL)
De Kempen (NL)
De Kempen (BE)
RVG (NL)
RVG (BE)
ROSE (NL)
ROSE (DE)
Reliability
High
Medium
Low

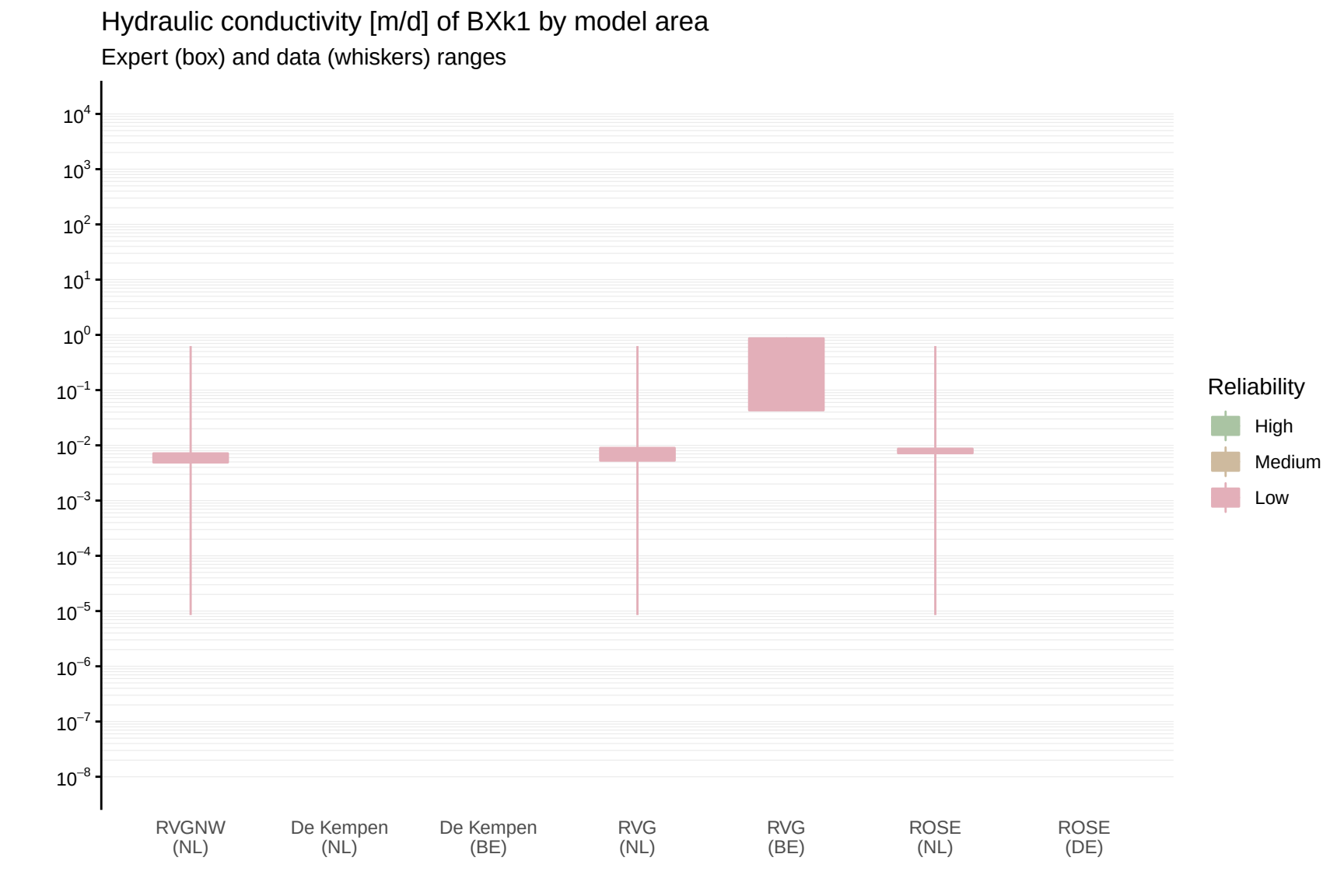
Hydraulic conductivity [m/d] of BXk1 by model area
Expert (box) and data (whiskers) ranges
10^{4}
10^{3}
10^{2}
10^{1}
10^{0}
10^{-1}
10^{-2}
10^{-3}
10^{-4}
10^{-5}
10^{-6}
10^{-7}
10^{-8}
RVGNW (NL)
De Kempen (NL)
De Kempen (BE)
RVG (NL)
RVG (BE)
ROSE (NL)
ROSE (DE)
Reliability
High
Medium
Low

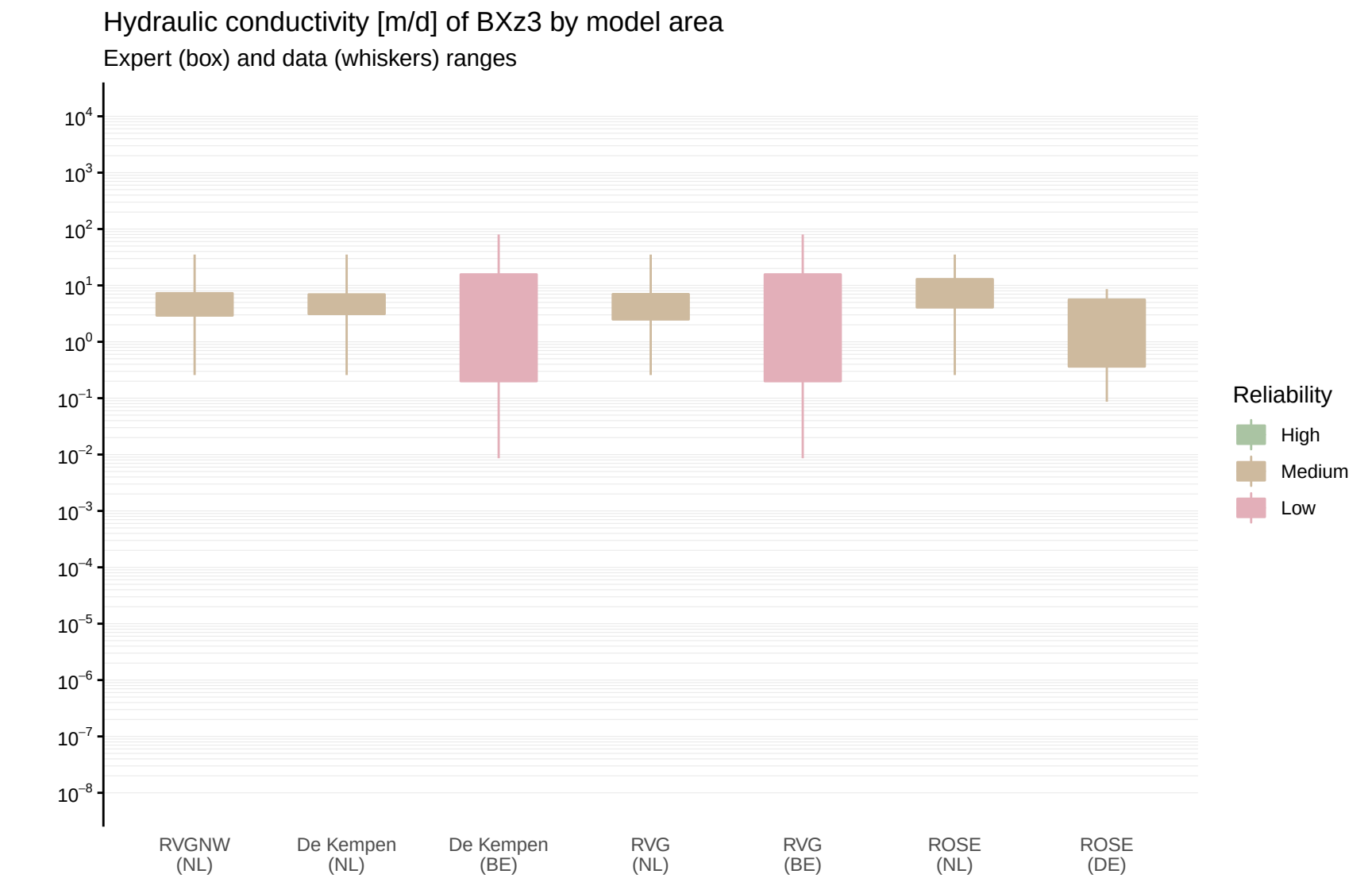
Hydraulic conductivity [m/d] of BXz3 by model area
Expert (box) and data (whiskers) ranges
10^{4}
10^{3}
10^{2}
10^{1}
10^{0}
10^{-1}
10^{-2}
10^{-3}
10^{-4}
10^{-5}
10^{-6}
10^{-7}
10^{-8}
RVGNW (NL)
De Kempen (NL)
De Kempen (BE)
RVG (NL)
RVG (BE)
ROSE (NL)
ROSE (DE)
Reliability
High
Medium
Low

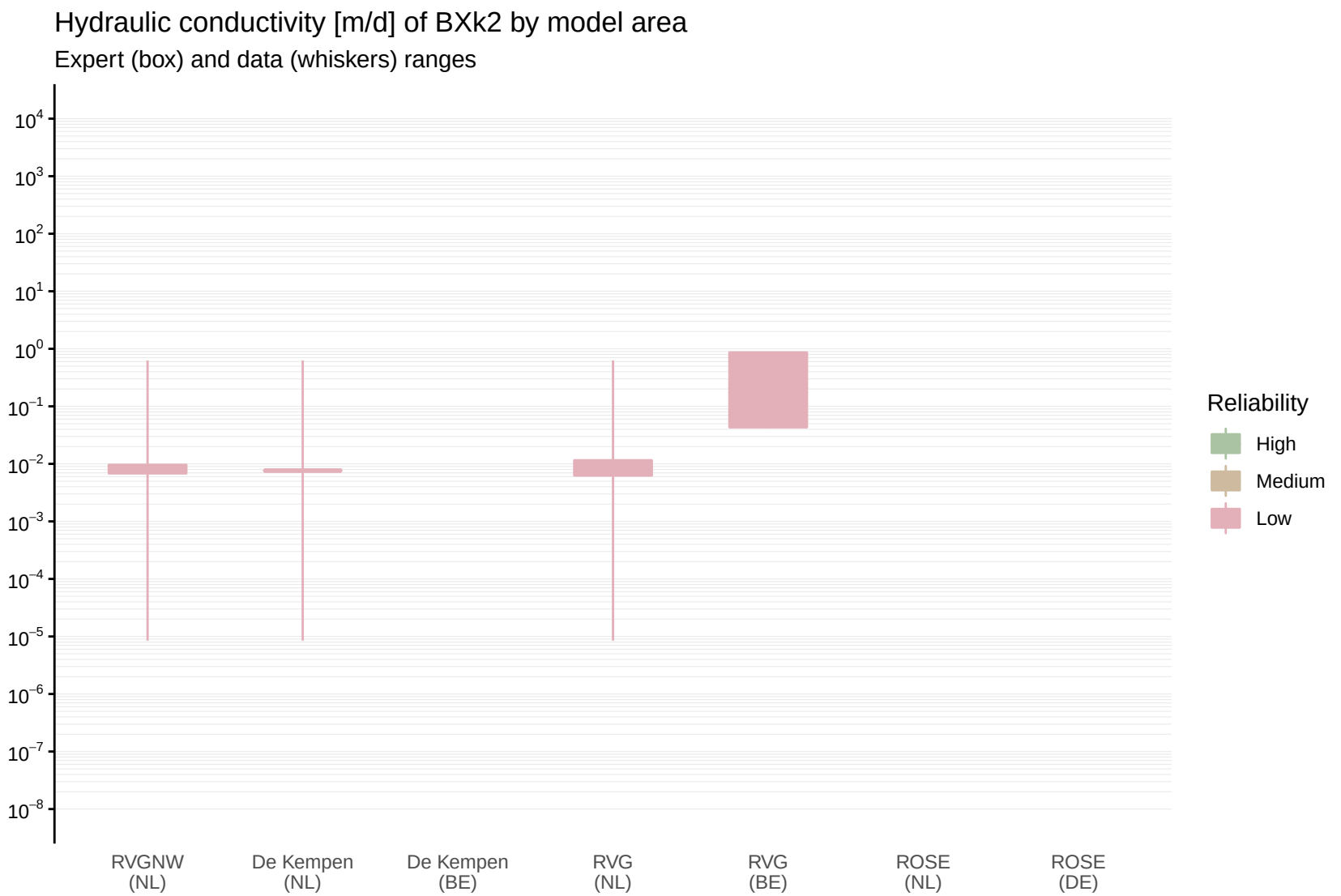
Hydraulic conductivity [m/d] of BXk2 by model area
Expert (box) and data (whiskers) ranges
10^{4}
10^{3}
10^{2}
10^{1}
10^{0}
10^{-1}
10^{-2}
10^{-3}
10^{-4}
10^{-5}
10^{-6}
10^{-7}
10^{-8}
RVGNW (NL)
De Kempen (NL)
De Kempen (BE)
RVG (NL)
RVG (BE)
ROSE (NL)
ROSE (DE)
Reliability
High
Medium
Low

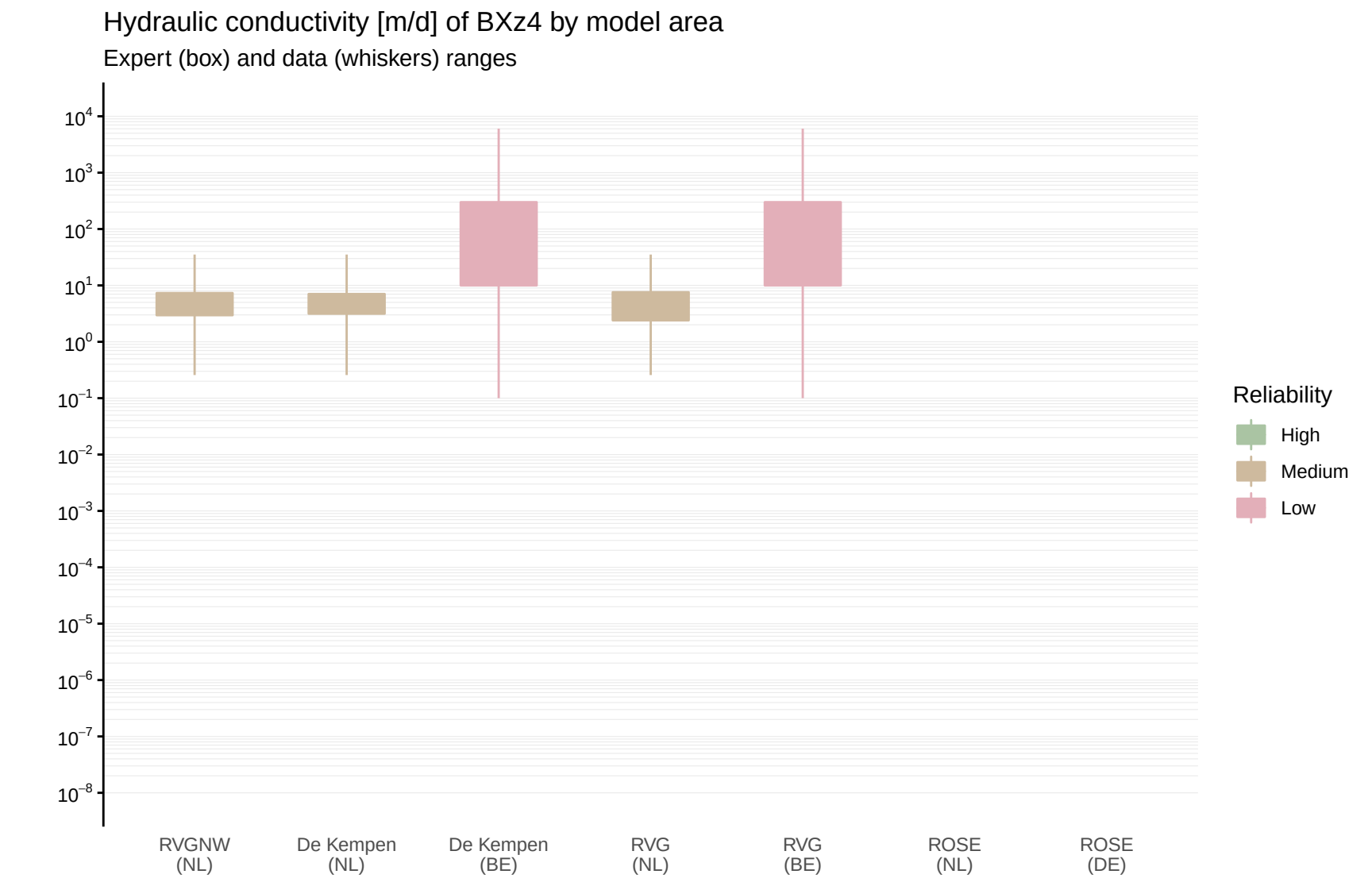
Hydraulic conductivity [m/d] of BXz4 by model area
Expert (box) and data (whiskers) ranges
10^{4}
10^{3}
10^{2}
10^{1}
10^{0}
10^{-1}
10^{-2}
10^{-3}
10^{-4}
10^{-5}
10^{-6}
10^{-7}
10^{-8}
RVGNW (NL)
De Kempen (NL)
De Kempen (BE)
RVG (NL)
RVG (BE)
ROSE (NL)
ROSE (DE)
Reliability
High
Medium
Low

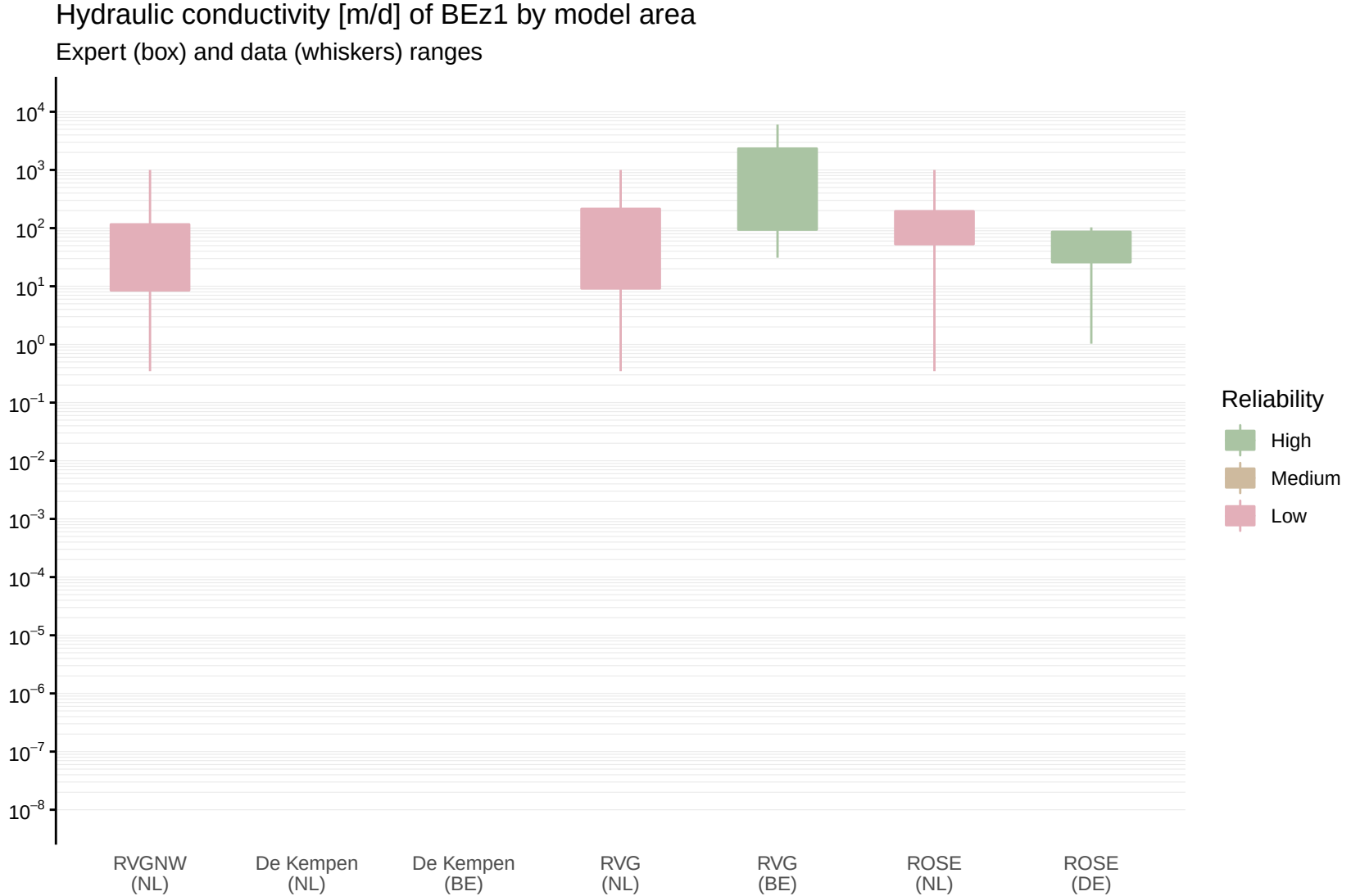
Hydraulic conductivity [m/d] of BEz1 by model area
Expert (box) and data (whiskers) ranges
10^{4}
10^{3}
10^{2}
10^{1}
10^{0}
10^{-1}
10^{-2}
10^{-3}
10^{-4}
10^{-5}
10^{-6}
10^{-7}
10^{-8}
RVGNW (NL)
De Kempen (NL)
De Kempen (BE)
RVG (NL)
RVG (BE)
ROSE (NL)
ROSE (DE)
Reliability
High
Medium
Low

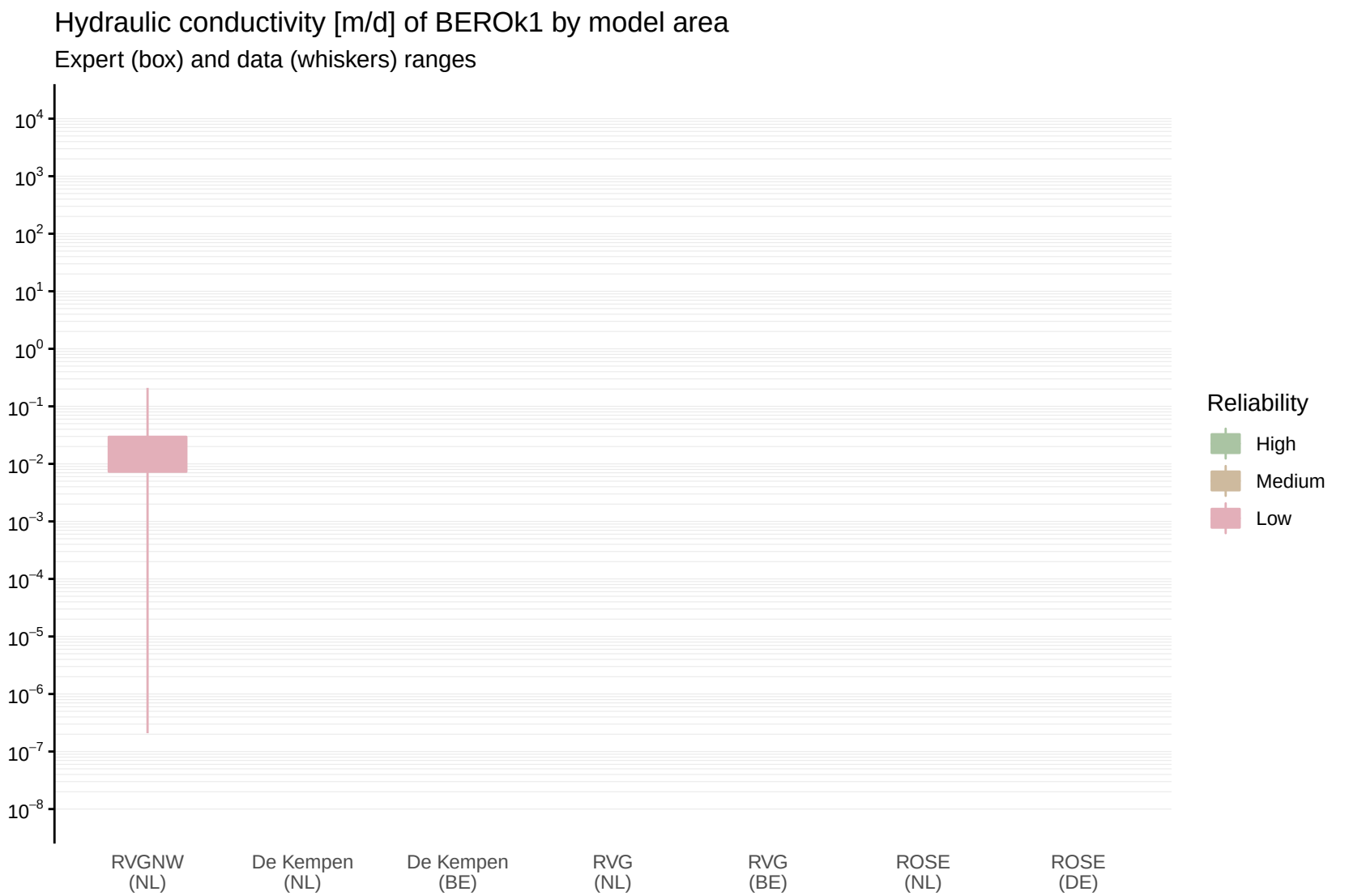
Hydraulic conductivity [m/d] of BEROk1 by model area
Expert (box) and data (whiskers) ranges
10^{4}
10^{3}
10^{2}
10^{1}
10^{0}
10^{-1}
10^{-2}
10^{-3}
10^{-4}
10^{-5}
10^{-6}
10^{-7}
10^{-8}
RVGNW (NL)
De Kempen (NL)
De Kempen (BE)
RVG (NL)
RVG (BE)
ROSE (NL)
ROSE (DE)
Reliability
High
Medium
Low

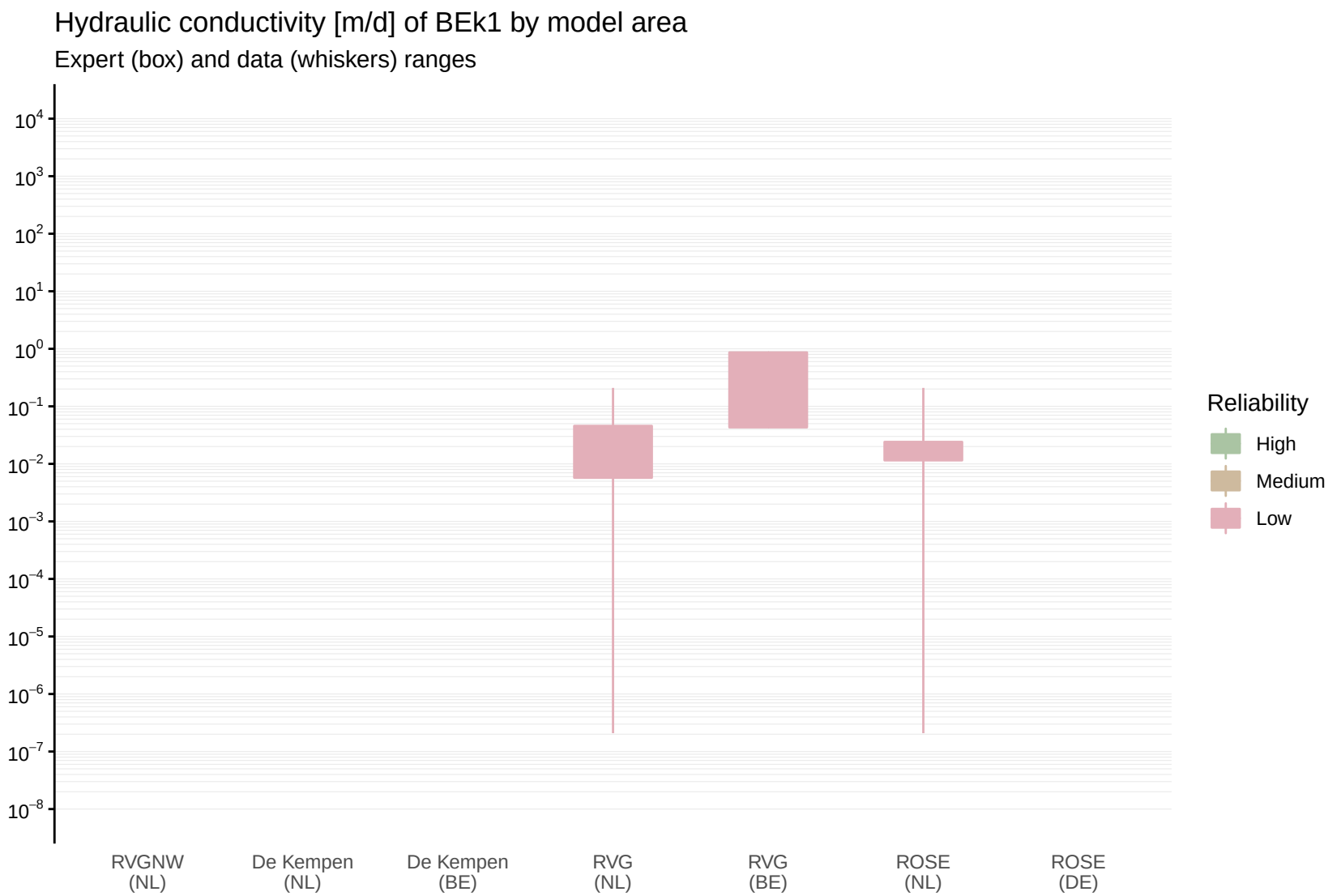
Hydraulic conductivity [m/d] of BEk1 by model area
Expert (box) and data (whiskers) ranges
10^{4}
10^{3}
10^{2}
10^{1}
10^{0}
10^{-1}
10^{-2}
10^{-3}
10^{-4}
10^{-5}
10^{-6}
10^{-7}
10^{-8}
RVGNW (NL)
De Kempen (NL)
De Kempen (BE)
RVG (NL)
RVG (BE)
ROSE (NL)
ROSE (DE)
Reliability
High
Medium
Low

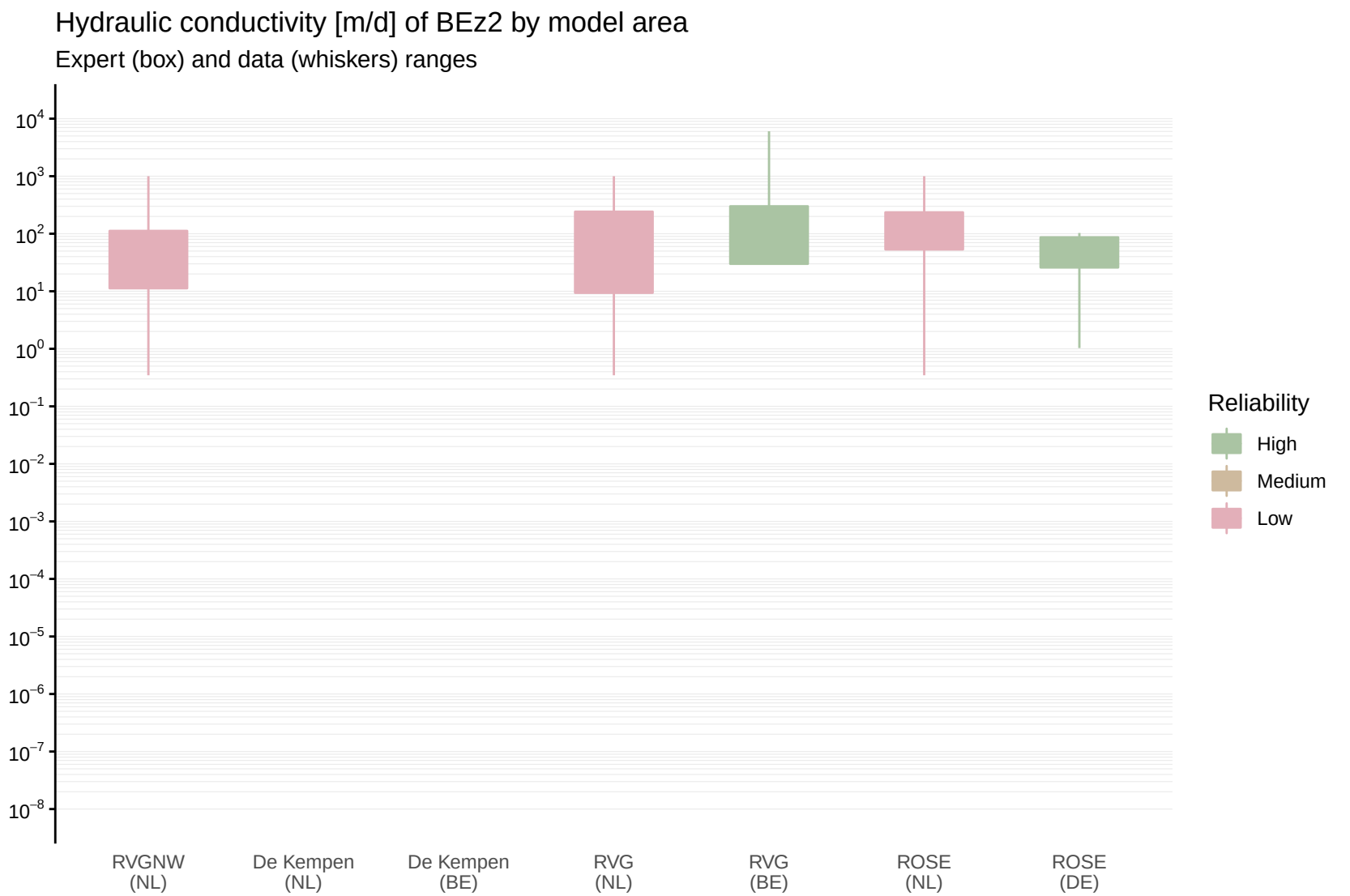
Hydraulic conductivity [m/d] of BEz2 by model area
Expert (box) and data (whiskers) ranges
10^{4}
10^{3}
10^{2}
10^{1}
10^{0}
10^{-1}
10^{-2}
10^{-3}
10^{-4}
10^{-5}
10^{-6}
10^{-7}
10^{-8}
RVGNW (NL)
De Kempen (NL)
De Kempen (BE)
RVG (NL)
RVG (BE)
ROSE (NL)
ROSE (DE)
Reliability
High
Medium
Low

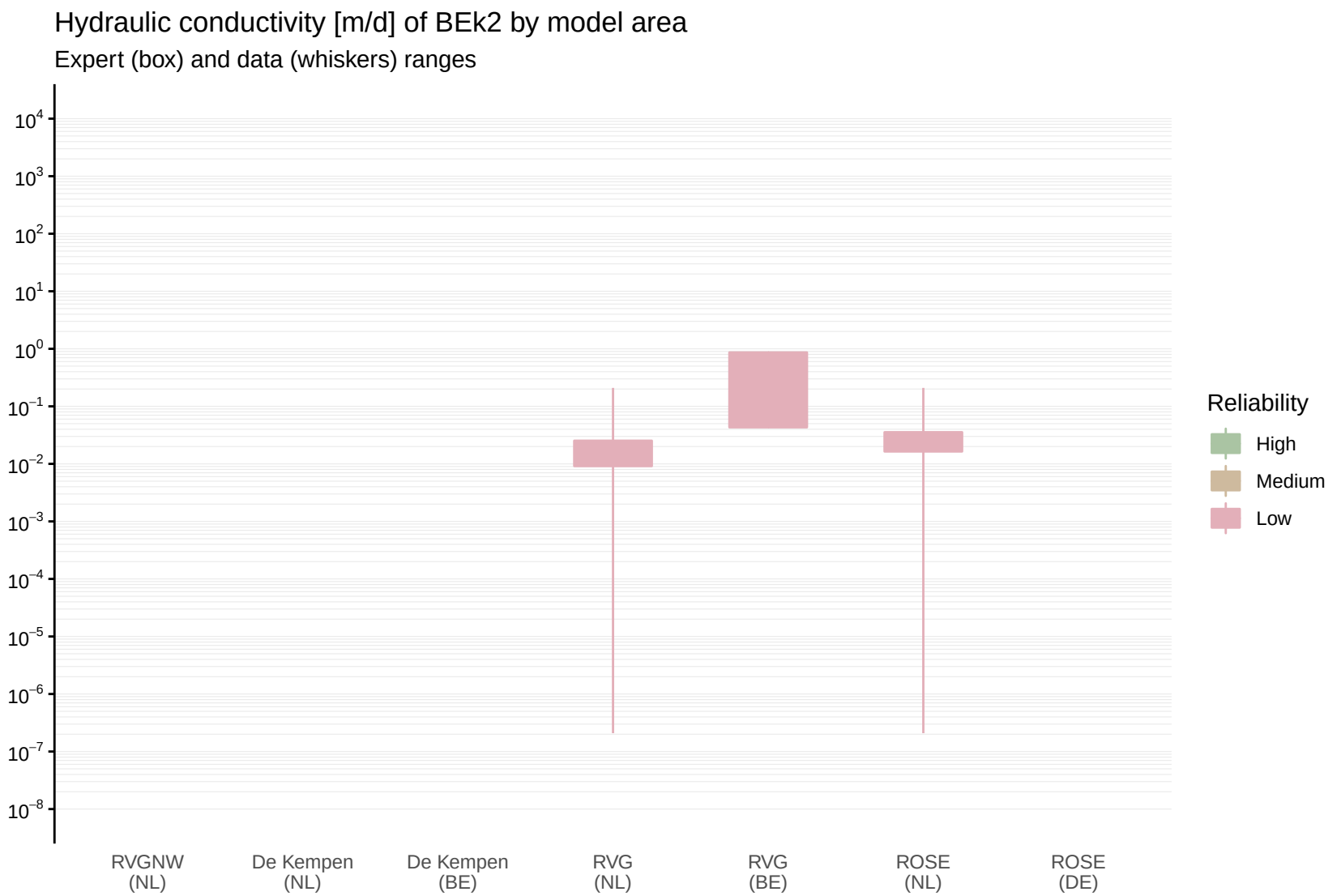
Hydraulic conductivity [m/d] of BEk2 by model area
Expert (box) and data (whiskers) ranges
10^{4}
10^{3}
10^{2}
10^{1}
10^{0}
10^{-1}
10^{-2}
10^{-3}
10^{-4}
10^{-5}
10^{-6}
10^{-7}
10^{-8}
RVGNW (NL)
De Kempen (NL)
De Kempen (BE)
RVG (NL)
RVG (BE)
ROSE (NL)
ROSE (DE)
Reliability
High
Medium
Low

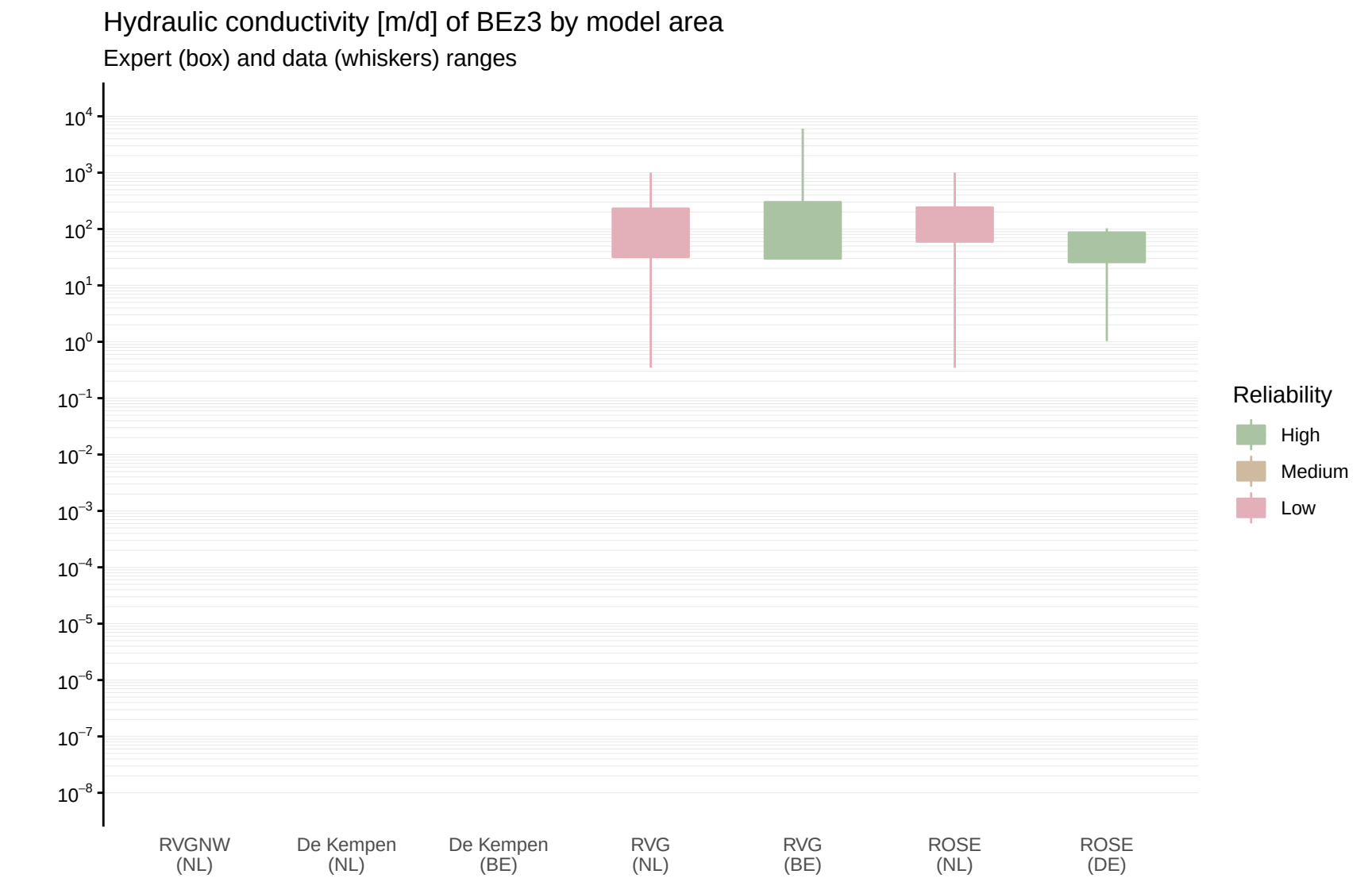
Hydraulic conductivity [m/d] of BEz3 by model area
Expert (box) and data (whiskers) ranges
10^{4}
10^{3}
10^{2}
10^{1}
10^{0}
10^{-1}
10^{-2}
10^{-3}
10^{-4}
10^{-5}
10^{-6}
10^{-7}
10^{-8}
RVGNW (NL)
De Kempen (NL)
De Kempen (BE)
RVG (NL)
RVG (BE)
ROSE (NL)
ROSE (DE)
Reliability
High
Medium
Low

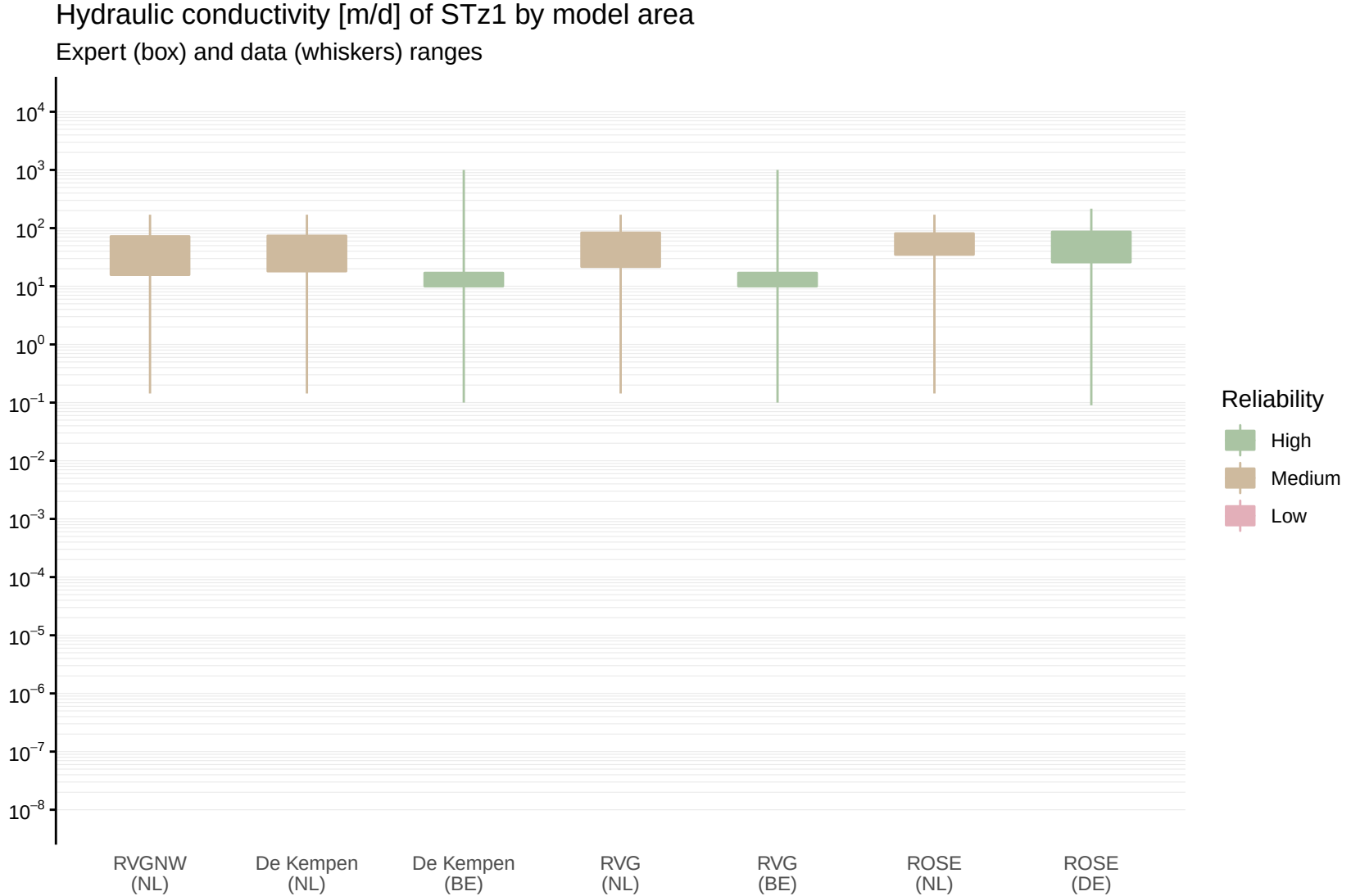
Hydraulic conductivity [m/d] of STz1 by model area
Expert (box) and data (whiskers) ranges
10^{4}
10^{3}
10^{2}
10^{1}
10^{0}
10^{-1}
10^{-2}
10^{-3}
10^{-4}
10^{-5}
10^{-6}
10^{-7}
10^{-8}
RVGNW (NL)
De Kempen (NL)
De Kempen (BE)
RVG (NL)
RVG (BE)
ROSE (NL)
ROSE (DE)
Reliability
High
Medium
Low

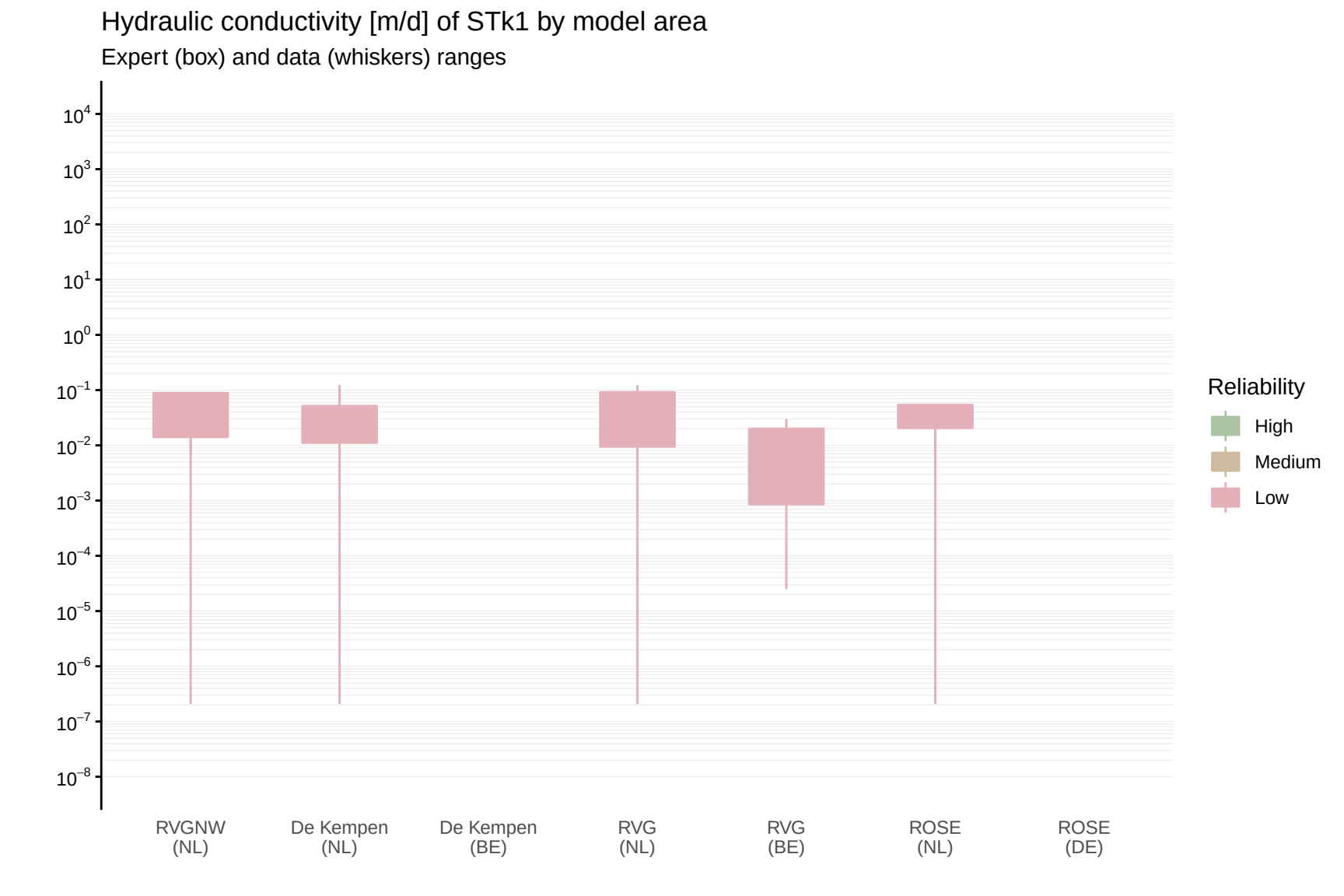
Hydraulic conductivity [m/d] of STk1 by model area
Expert (box) and data (whiskers) ranges
10^{4}
10^{3}
10^{2}
10^{1}
10^{0}
10^{-1}
10^{-2}
10^{-3}
10^{-4}
10^{-5}
10^{-6}
10^{-7}
10^{-8}
RVGNW (NL)
De Kempen (NL)
De Kempen (BE)
RVG (NL)
RVG (BE)
ROSE (NL)
ROSE (DE)
Reliability
High
Medium
Low

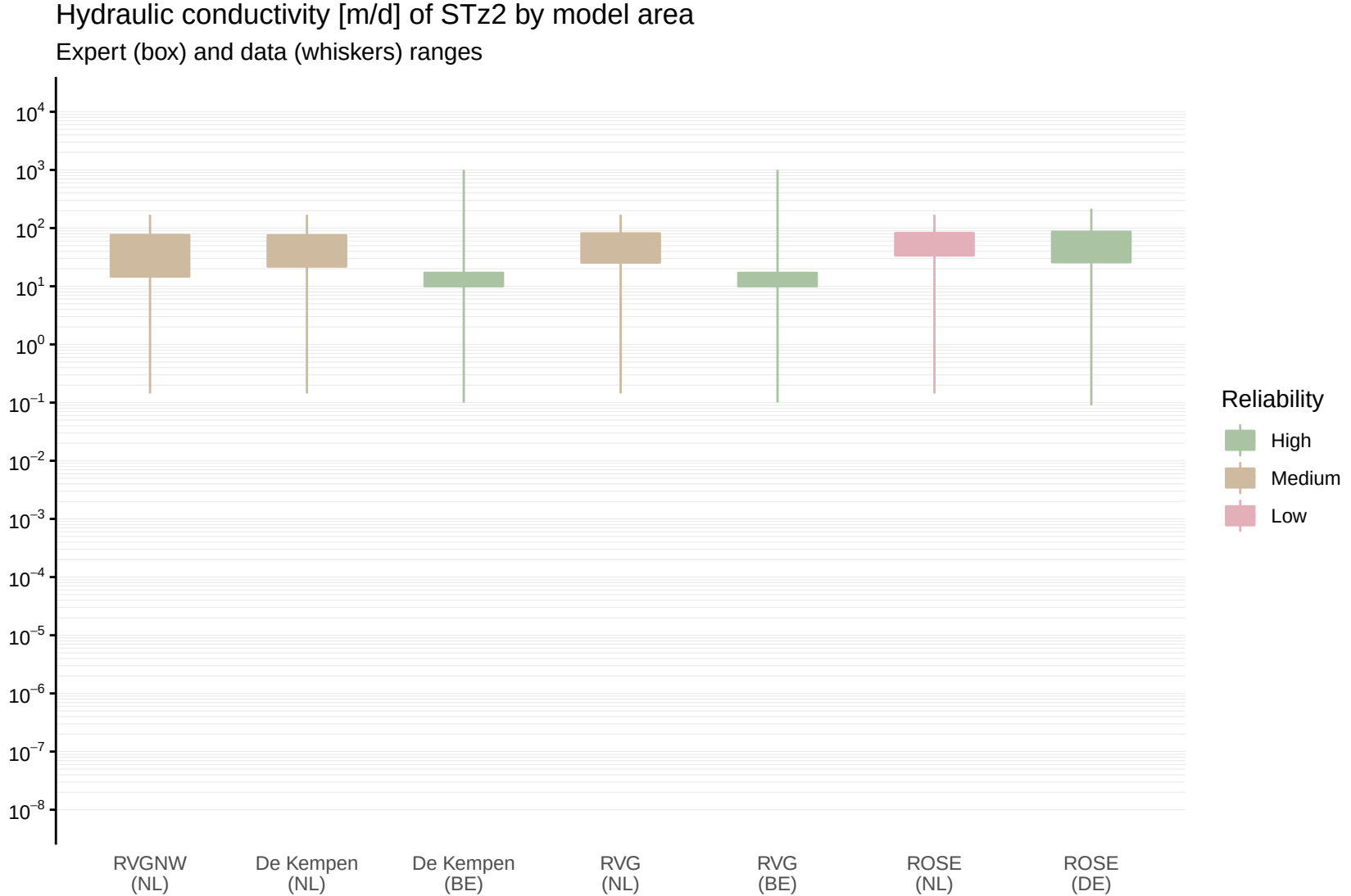
Hydraulic conductivity [m/d] of STz2 by model area
Expert (box) and data (whiskers) ranges
10^{4}
10^{3}
10^{2}
10^{1}
10^{0}
10^{-1}
10^{-2}
10^{-3}
10^{-4}
10^{-5}
10^{-6}
10^{-7}
10^{-8}
RVGNW (NL)
De Kempen (NL)
De Kempen (BE)
RVG (NL)
RVG (BE)
ROSE (NL)
ROSE (DE)
Reliability
High
Medium
Low

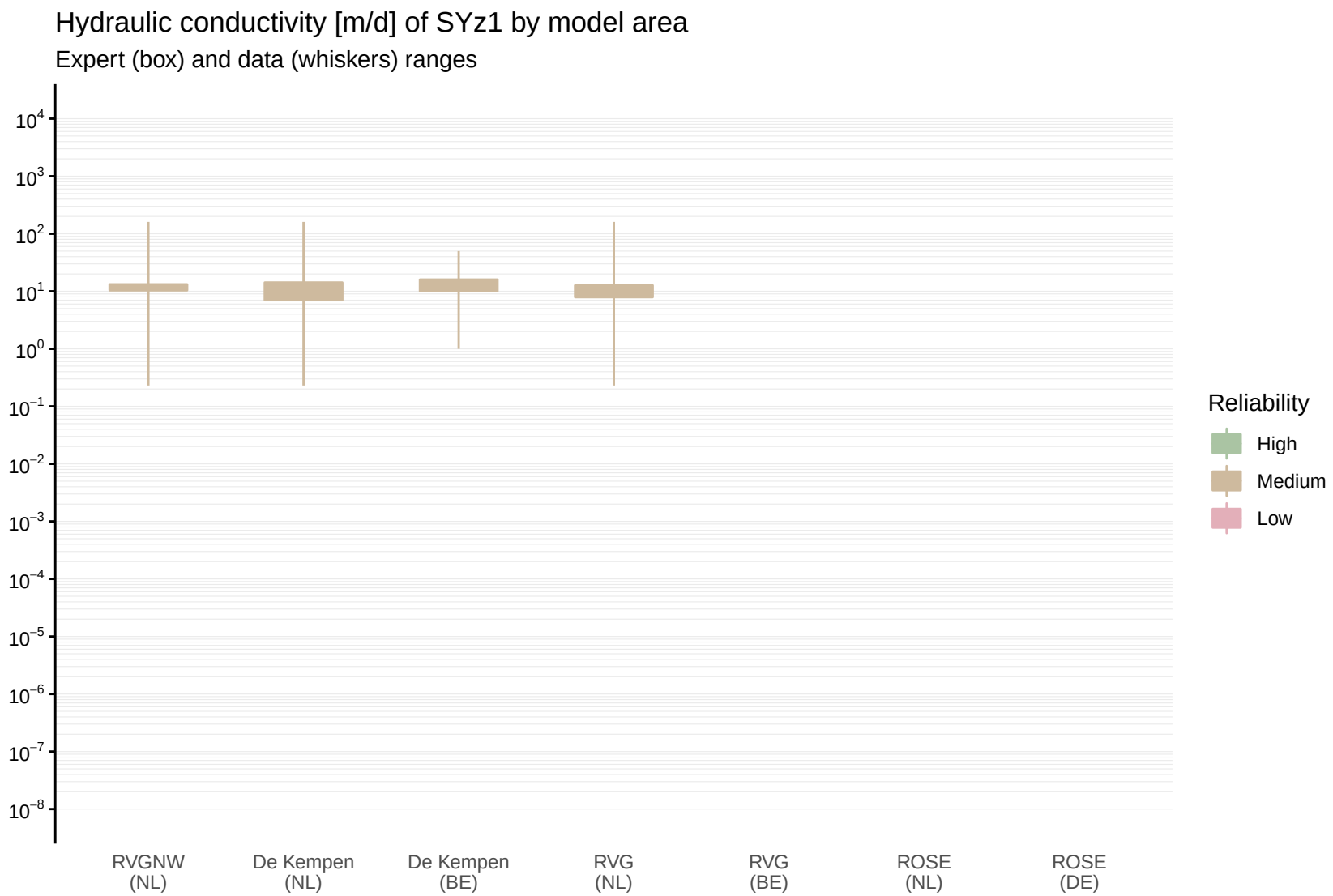
Hydraulic conductivity [m/d] of SYz1 by model area
Expert (box) and data (whiskers) ranges
10^{4}
10^{3}
10^{2}
10^{1}
10^{0}
10^{-1}
10^{-2}
10^{-3}
10^{-4}
10^{-5}
10^{-6}
10^{-7}
10^{-8}
RVGNW (NL)
De Kempen (NL)
De Kempen (BE)
RVG (NL)
RVG (BE)
ROSE (NL)
ROSE (DE)
Reliability
High
Medium
Low

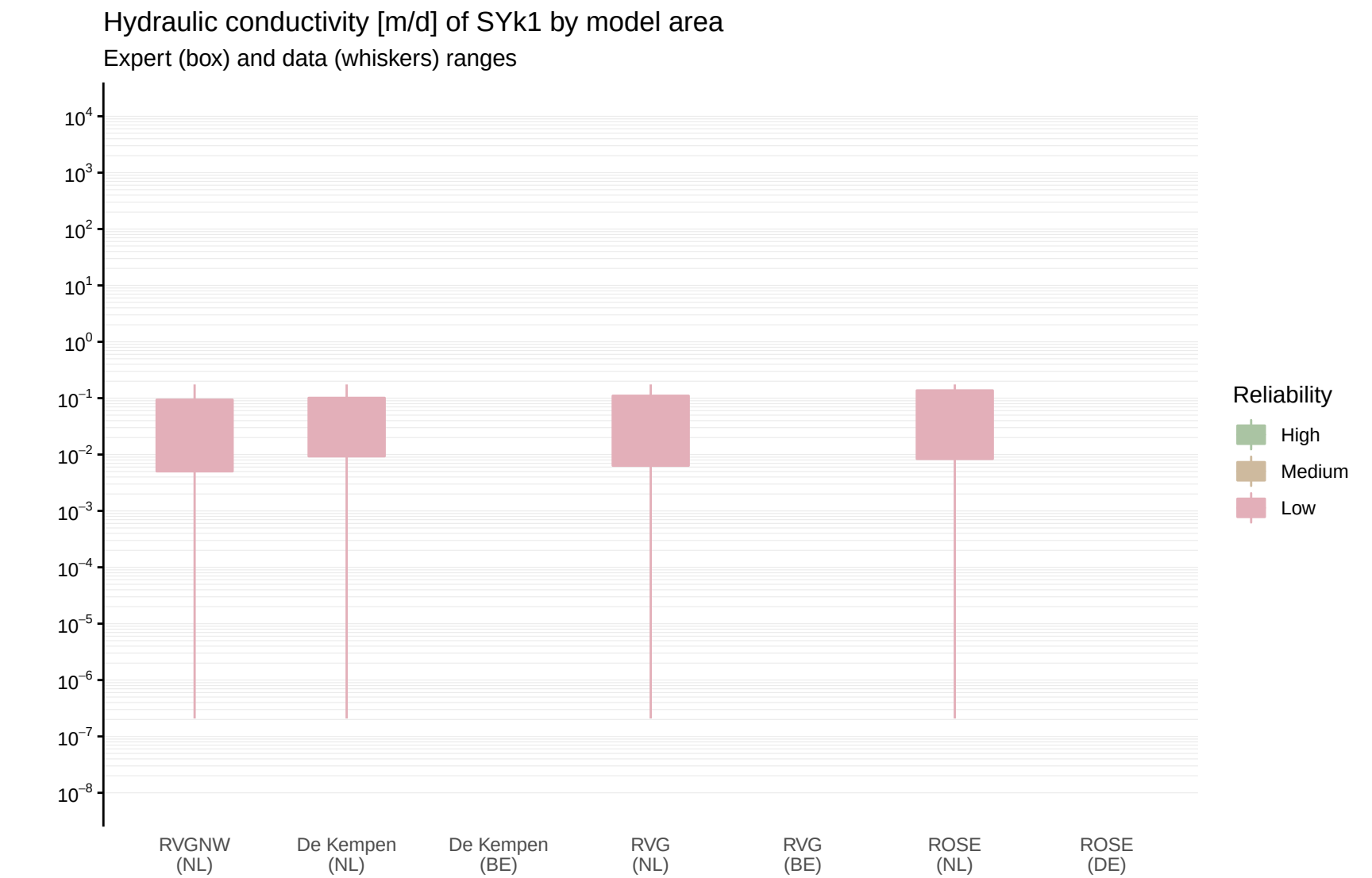
Hydraulic conductivity [m/d] of SYk1 by model area
Expert (box) and data (whiskers) ranges
10^{4}
10^{3}
10^{2}
10^{1}
10^{0}
10^{-1}
10^{-2}
10^{-3}
10^{-4}
10^{-5}
10^{-6}
10^{-7}
10^{-8}
RVGNW (NL)
De Kempen (NL)
De Kempen (BE)
RVG (NL)
RVG (BE)
ROSE (NL)
ROSE (DE)
Reliability
High
Medium
Low

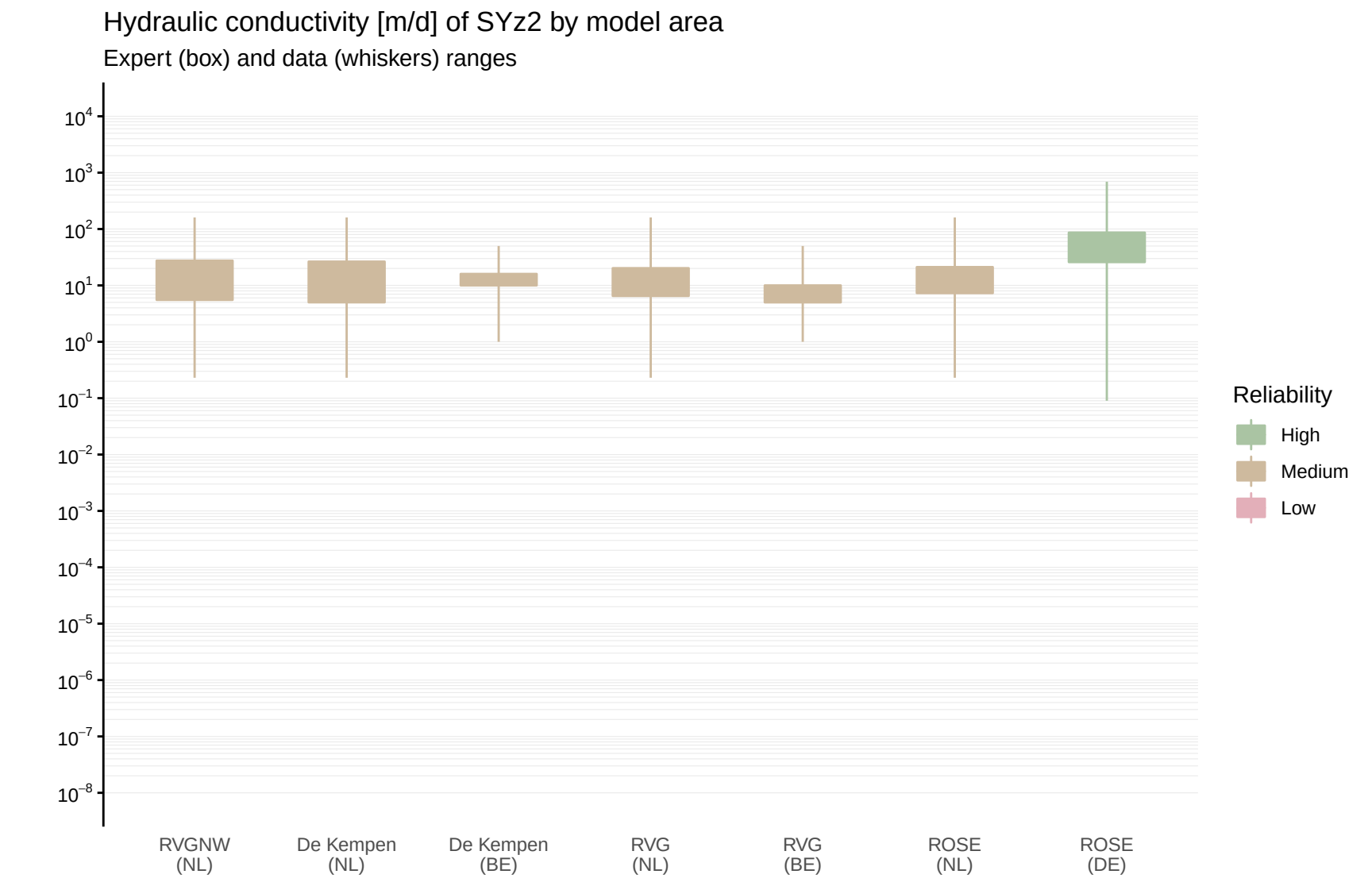
Hydraulic conductivity [m/d] of SYz2 by model area
Expert (box) and data (whiskers) ranges
10^{4}
10^{3}
10^{2}
10^{1}
10^{0}
10^{-1}
10^{-2}
10^{-3}
10^{-4}
10^{-5}
10^{-6}
10^{-7}
10^{-8}
RVGNW (NL)
De Kempen (NL)
De Kempen (BE)
RVG (NL)
RVG (BE)
ROSE (NL)
ROSE (DE)
Reliability
High
Medium
Low

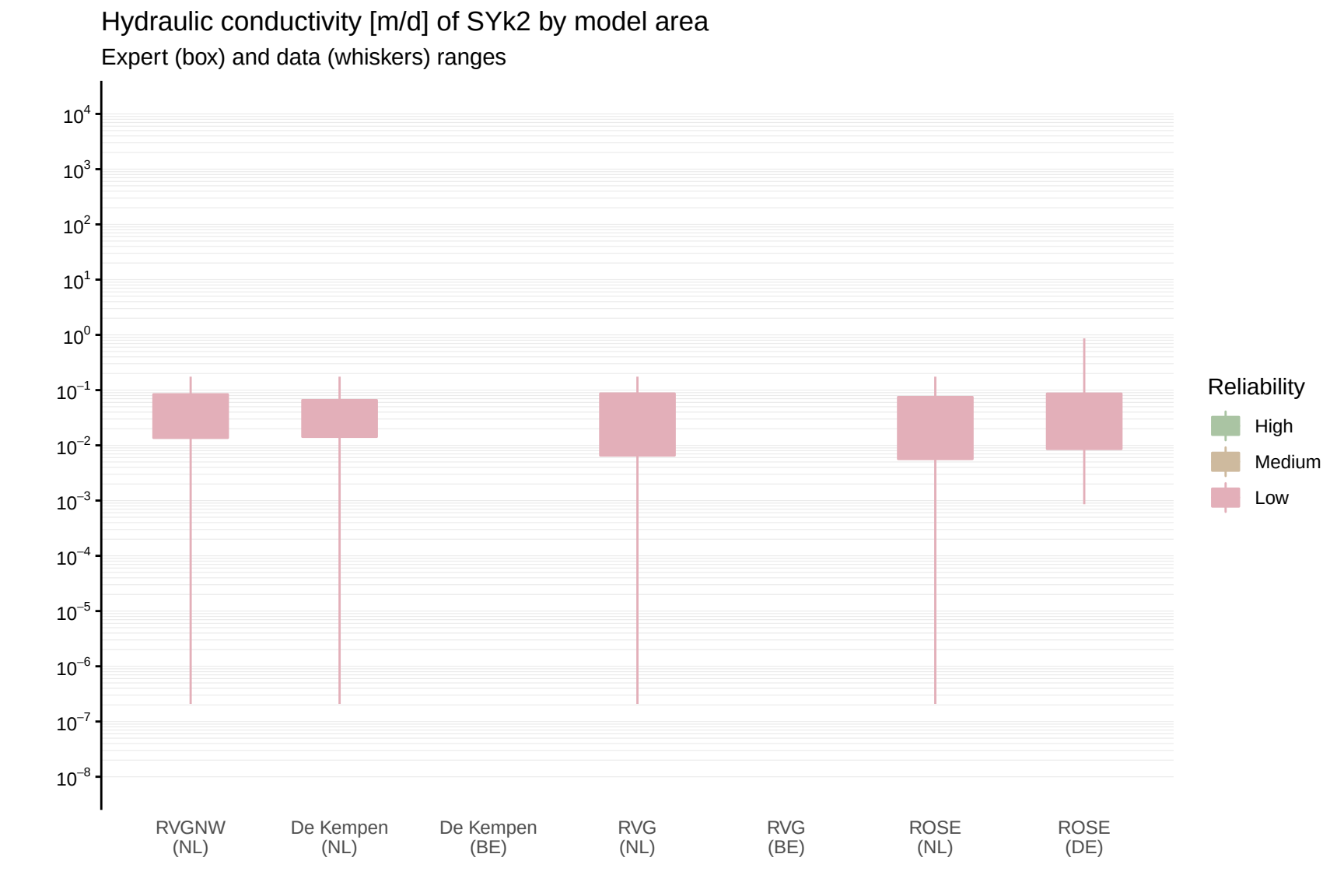
Hydraulic conductivity [m/d] of SYk2 by model area
Expert (box) and data (whiskers) ranges
10^{4}
10^{3}
10^{2}
10^{1}
10^{0}
10^{-1}
10^{-2}
10^{-3}
10^{-4}
10^{-5}
10^{-6}
10^{-7}
10^{-8}
RVGNW (NL)
De Kempen (NL)
De Kempen (BE)
RVG (NL)
RVG (BE)
ROSE (NL)
ROSE (DE)
Reliability
High
Medium
Low

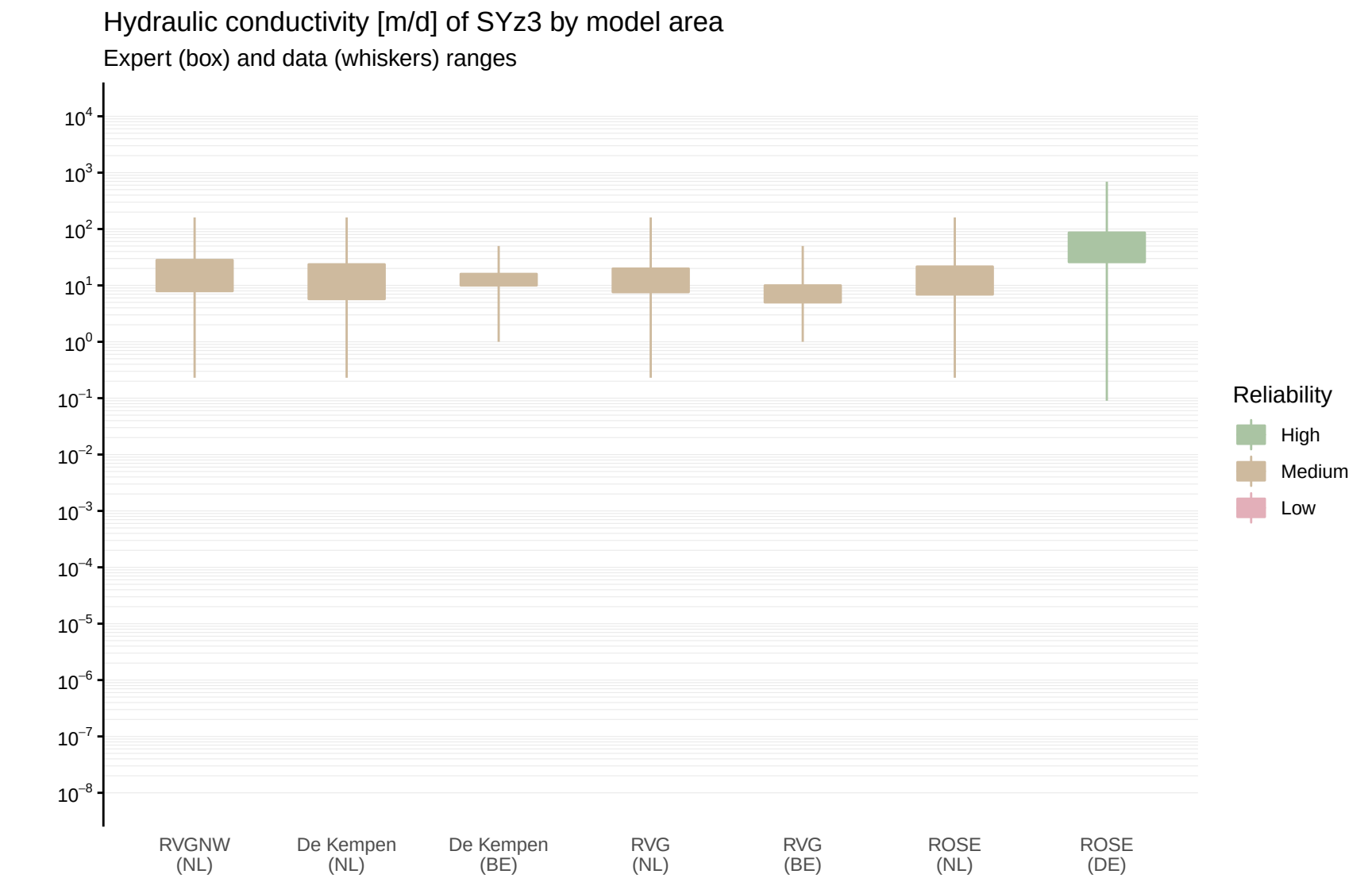
Hydraulic conductivity [m/d] of SYz3 by model area
Expert (box) and data (whiskers) ranges
10^{4}
10^{3}
10^{2}
10^{1}
10^{0}
10^{-1}
10^{-2}
10^{-3}
10^{-4}
10^{-5}
10^{-6}
10^{-7}
10^{-8}
RVGNW (NL)
De Kempen (NL)
De Kempen (BE)
RVG (NL)
RVG (BE)
ROSE (NL)
ROSE (DE)
Reliability
High
Medium
Low

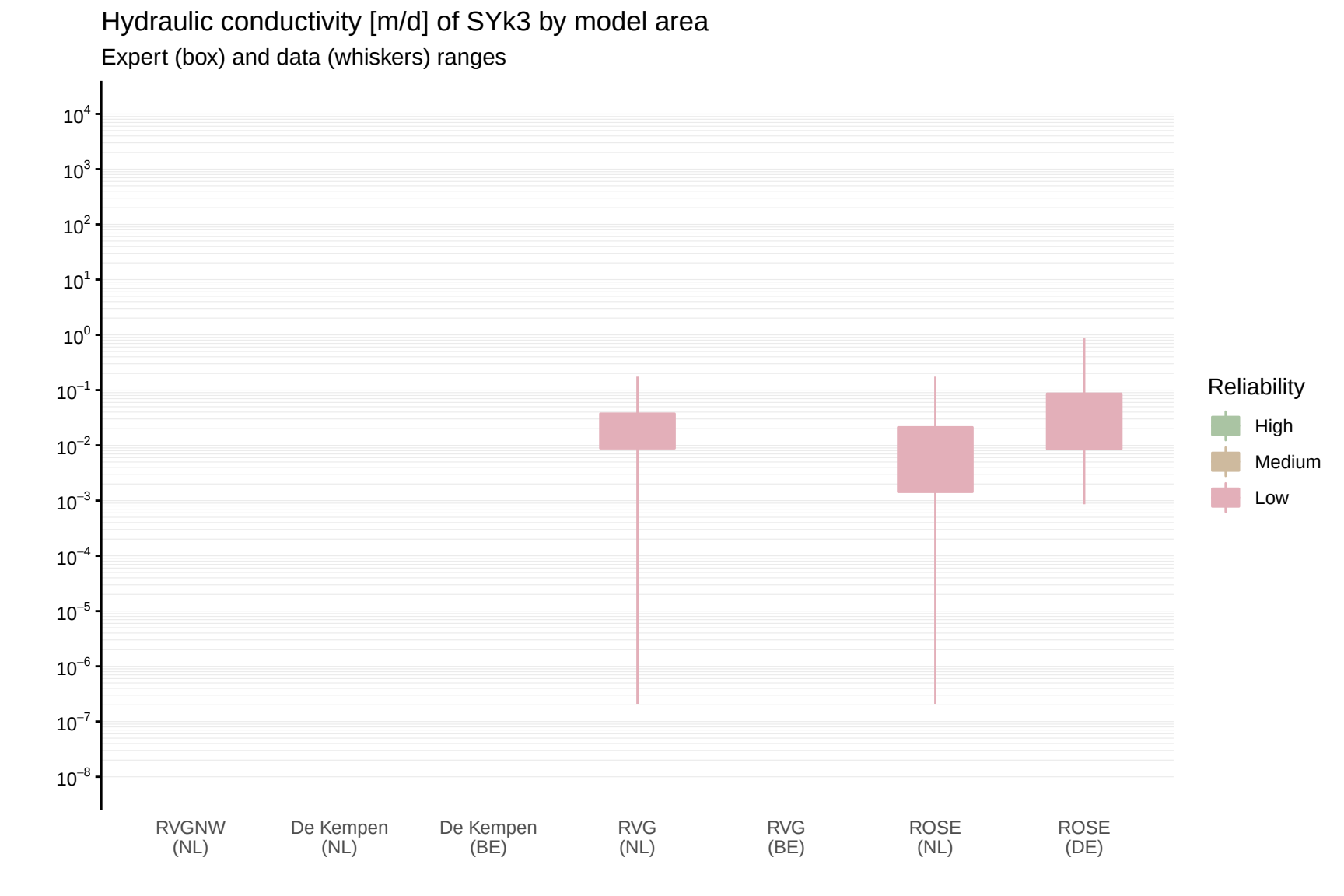
Hydraulic conductivity [m/d] of SYk3 by model area
Expert (box) and data (whiskers) ranges
10^{4}
10^{3}
10^{2}
10^{1}
10^{0}
10^{-1}
10^{-2}
10^{-3}
10^{-4}
10^{-5}
10^{-6}
10^{-7}
10^{-8}
RVGNW (NL)
De Kempen (NL)
De Kempen (BE)
RVG (NL)
RVG (BE)
ROSE (NL)
ROSE (DE)
Reliability
High
Medium
Low

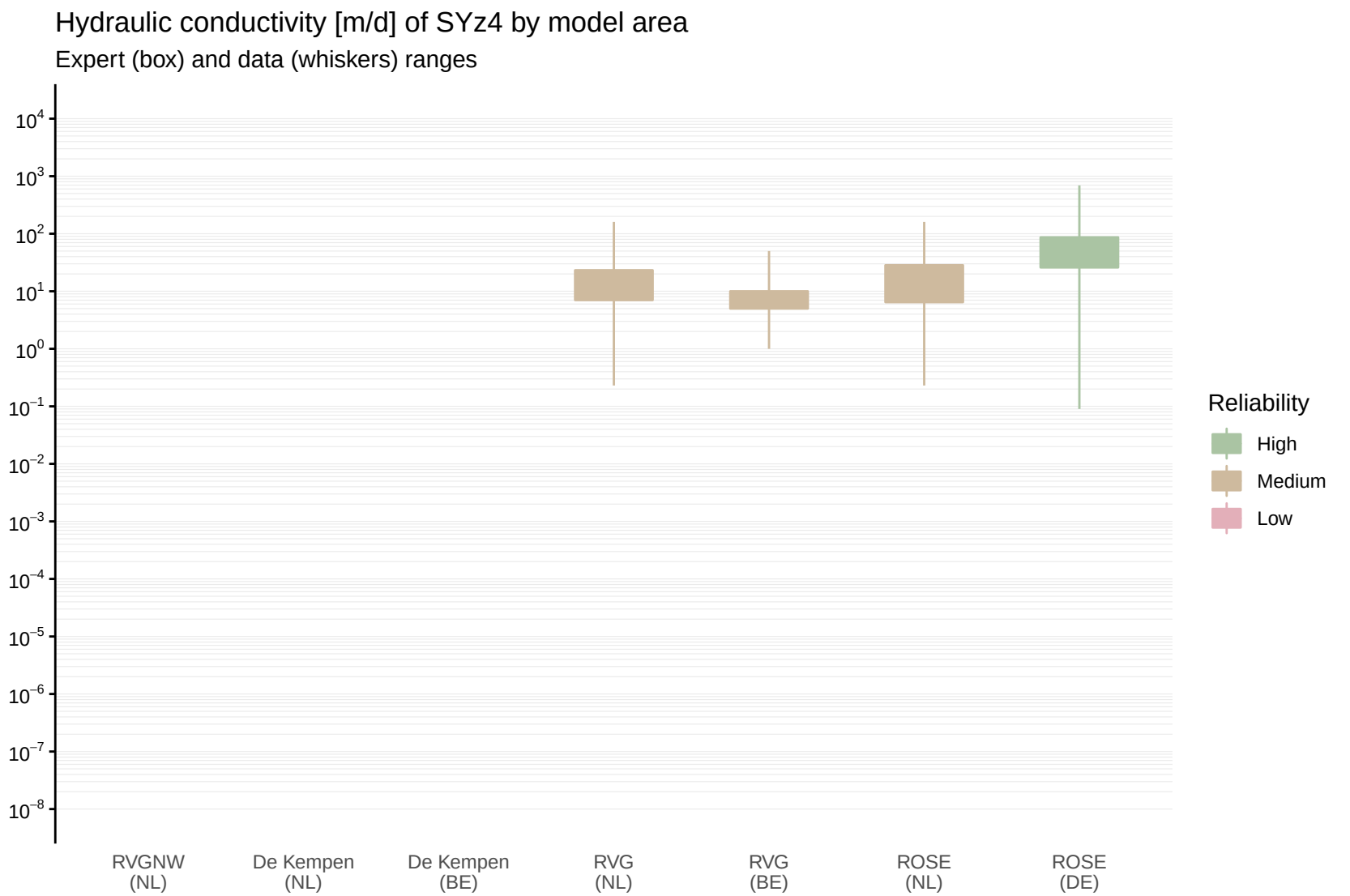
Hydraulic conductivity [m/d] of SYz4 by model area
Expert (box) and data (whiskers) ranges
10^{4}
10^{3}
10^{2}
10^{1}
10^{0}
10^{-1}
10^{-2}
10^{-3}
10^{-4}
10^{-5}
10^{-6}
10^{-7}
10^{-8}
RVGNW (NL)
De Kempen (NL)
De Kempen (BE)
RVG (NL)
RVG (BE)
ROSE (NL)
ROSE (DE)
Reliability
High
Medium
Low

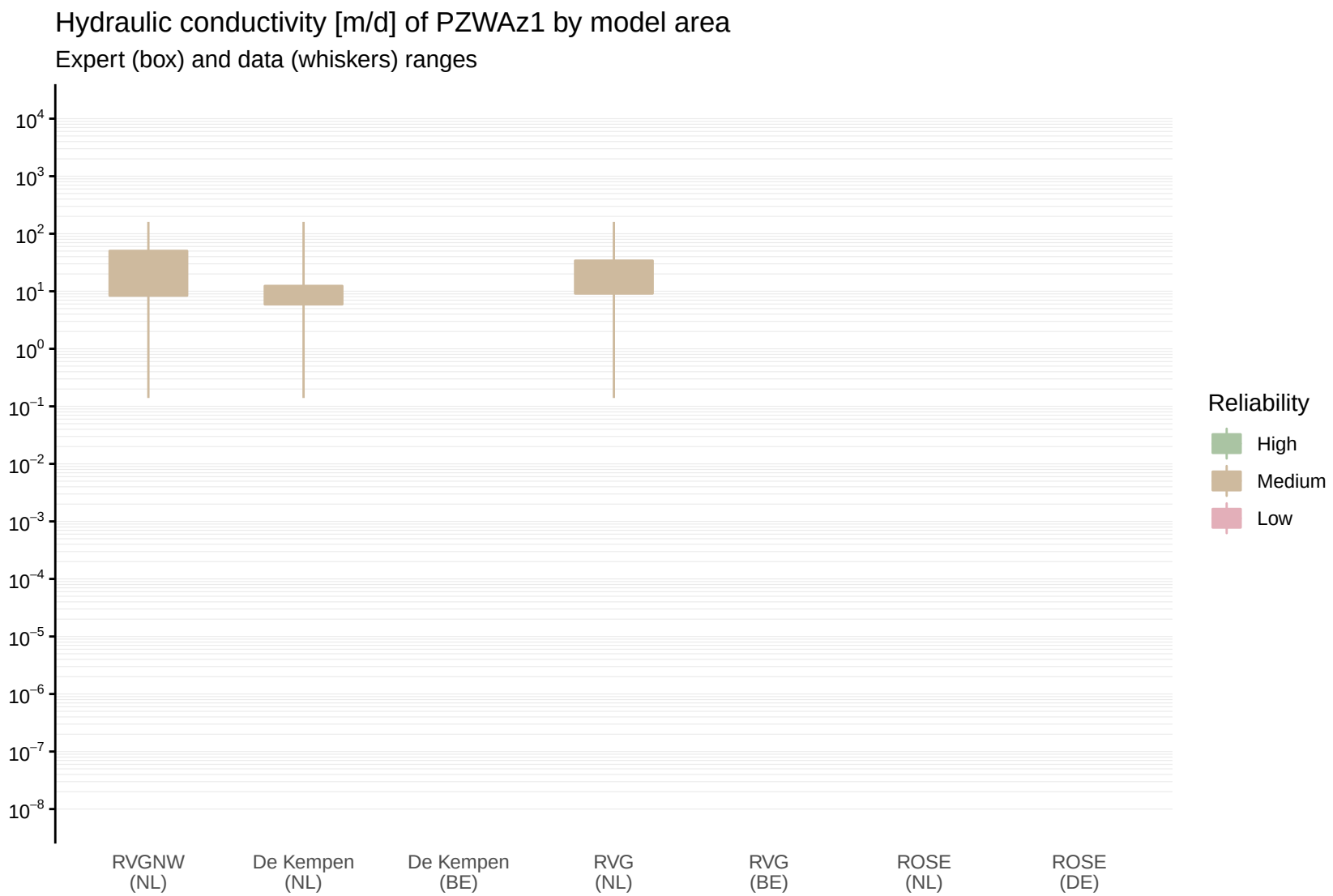
Hydraulic conductivity [m/d] of PZWAz1 by model area
Expert (box) and data (whiskers) ranges
10^{4}
10^{3}
10^{2}
10^{1}
10^{0}
10^{-1}
10^{-2}
10^{-3}
10^{-4}
10^{-5}
10^{-6}
10^{-7}
10^{-8}
RVGNW (NL)
De Kempen (NL)
De Kempen (BE)
RVG (NL)
RVG (BE)
ROSE (NL)
ROSE (DE)
Reliability
High
Medium
Low

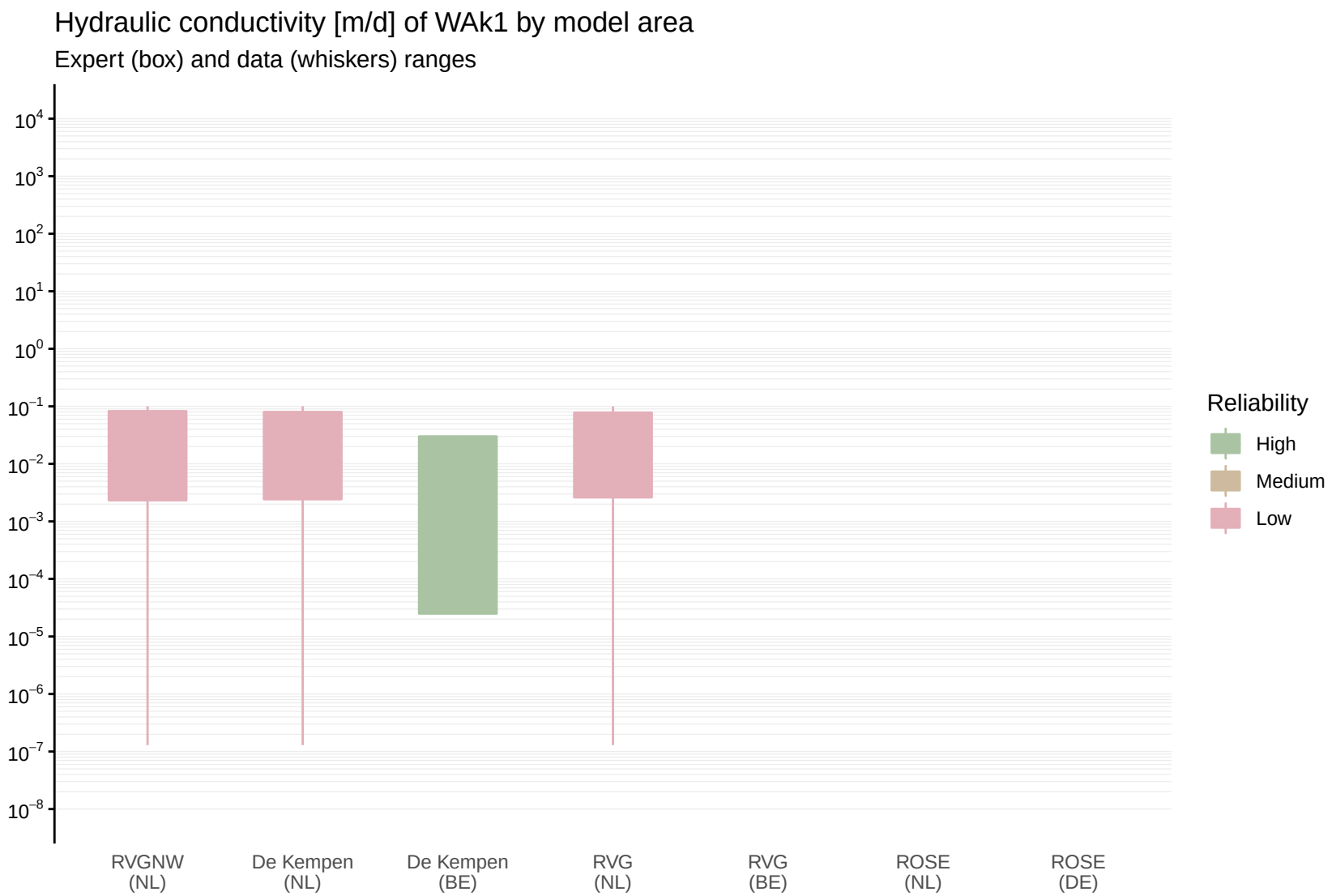
Hydraulic conductivity [m/d] of WAk1 by model area
Expert (box) and data (whiskers) ranges
10^{4}
10^{3}
10^{2}
10^{1}
10^{0}
10^{-1}
10^{-2}
10^{-3}
10^{-4}
10^{-5}
10^{-6}
10^{-7}
10^{-8}
RVGNW (NL)
De Kempen (NL)
De Kempen (BE)
RVG (NL)
RVG (BE)
ROSE (NL)
ROSE (DE)
Reliability
High
Medium
Low

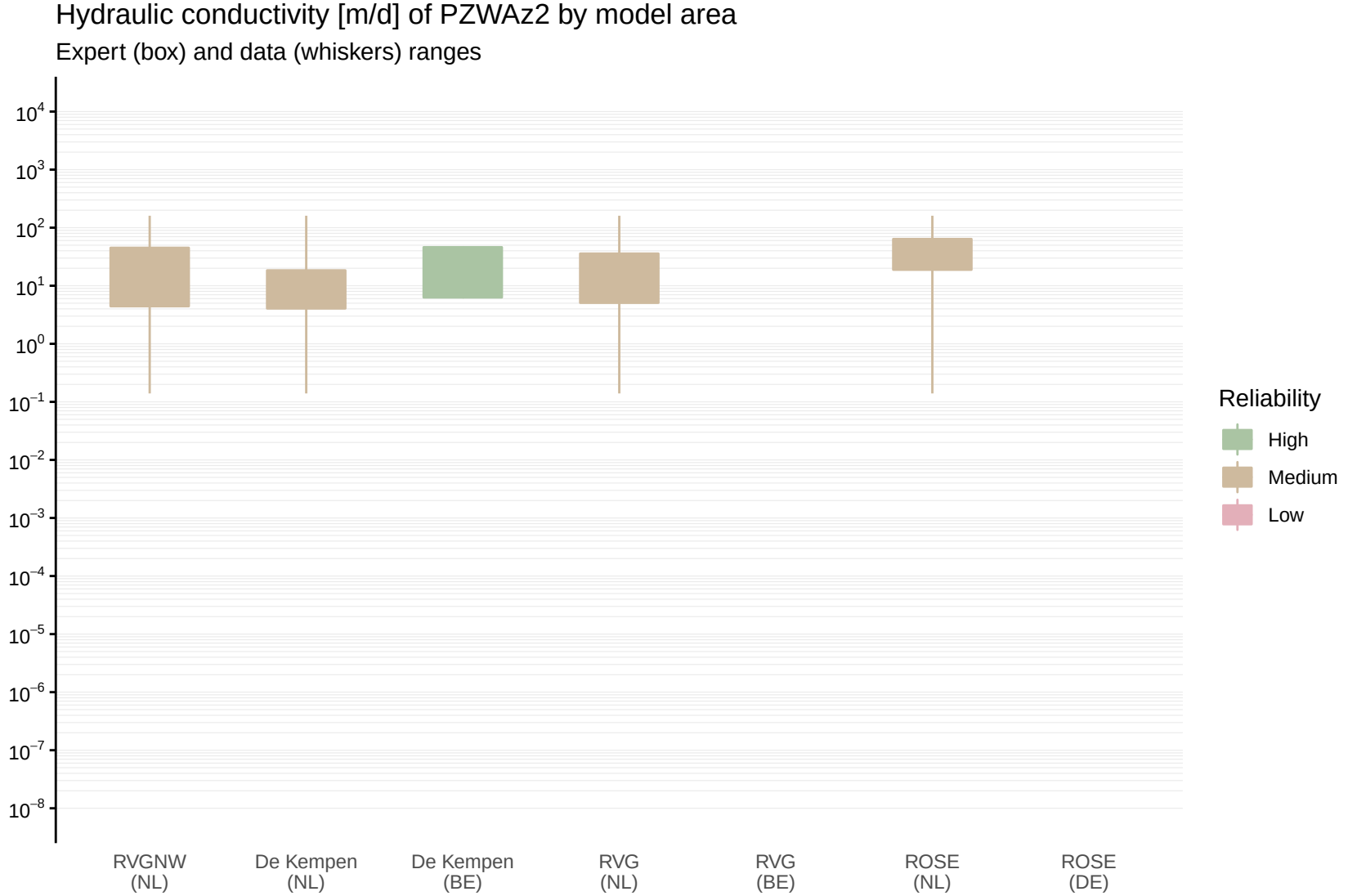
Hydraulic conductivity [m/d] of PZWAz2 by model area
Expert (box) and data (whiskers) ranges
10^{4}
10^{3}
10^{2}
10^{1}
10^{0}
10^{-1}
10^{-2}
10^{-3}
10^{-4}
10^{-5}
10^{-6}
10^{-7}
10^{-8}
RVGNW (NL)
De Kempen (NL)
De Kempen (BE)
RVG (NL)
RVG (BE)
ROSE (NL)
ROSE (DE)
Reliability
High
Medium
Low

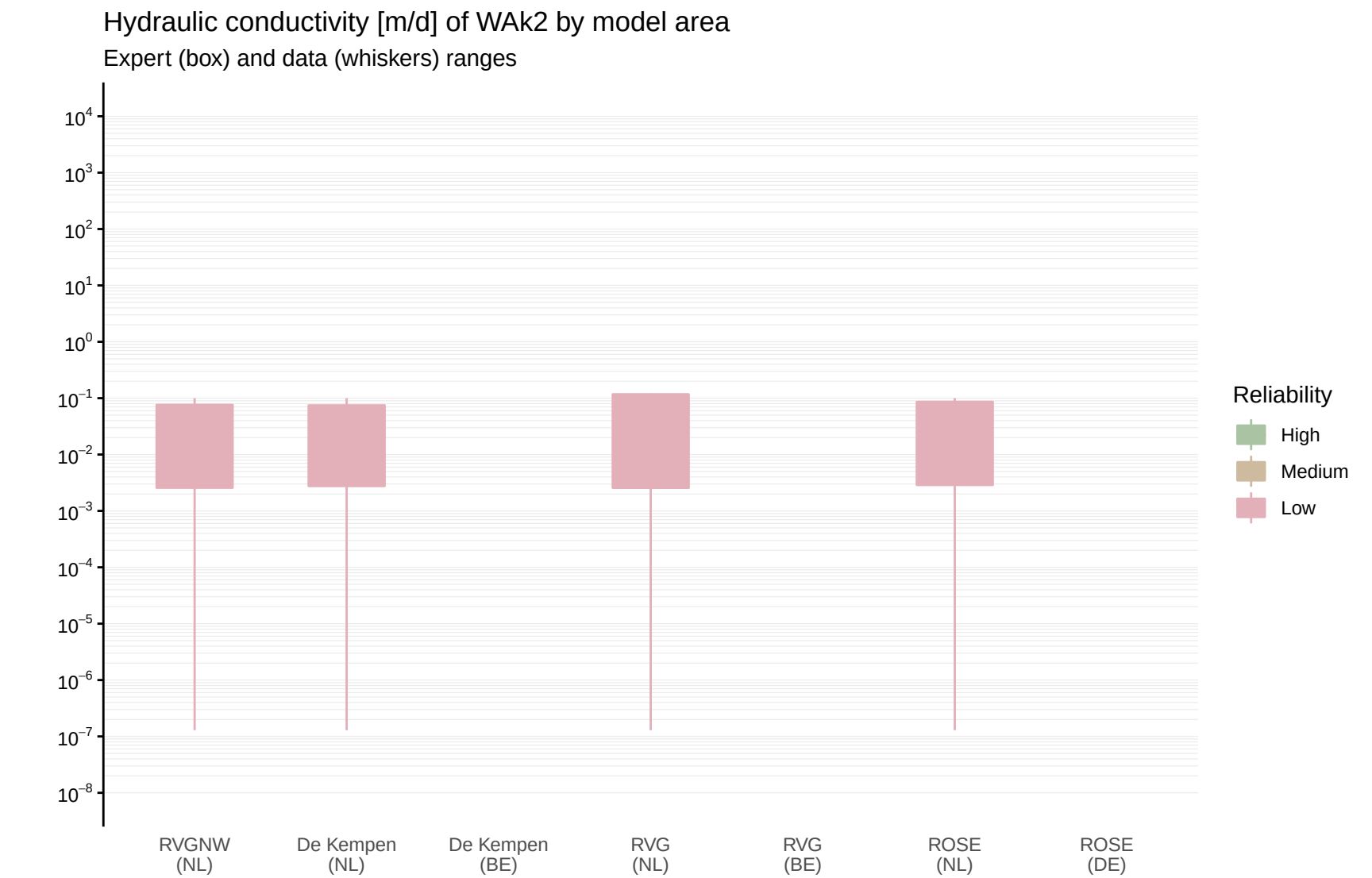
Hydraulic conductivity [m/d] of WAk2 by model area
Expert (box) and data (whiskers) ranges
10^{4}
10^{3}
10^{2}
10^{1}
10^{0}
10^{-1}
10^{-2}
10^{-3}
10^{-4}
10^{-5}
10^{-6}
10^{-7}
10^{-8}
RVGNW (NL)
De Kempen (NL)
De Kempen (BE)
RVG (NL)
RVG (BE)
ROSE (NL)
ROSE (DE)
Reliability
High
Medium
Low

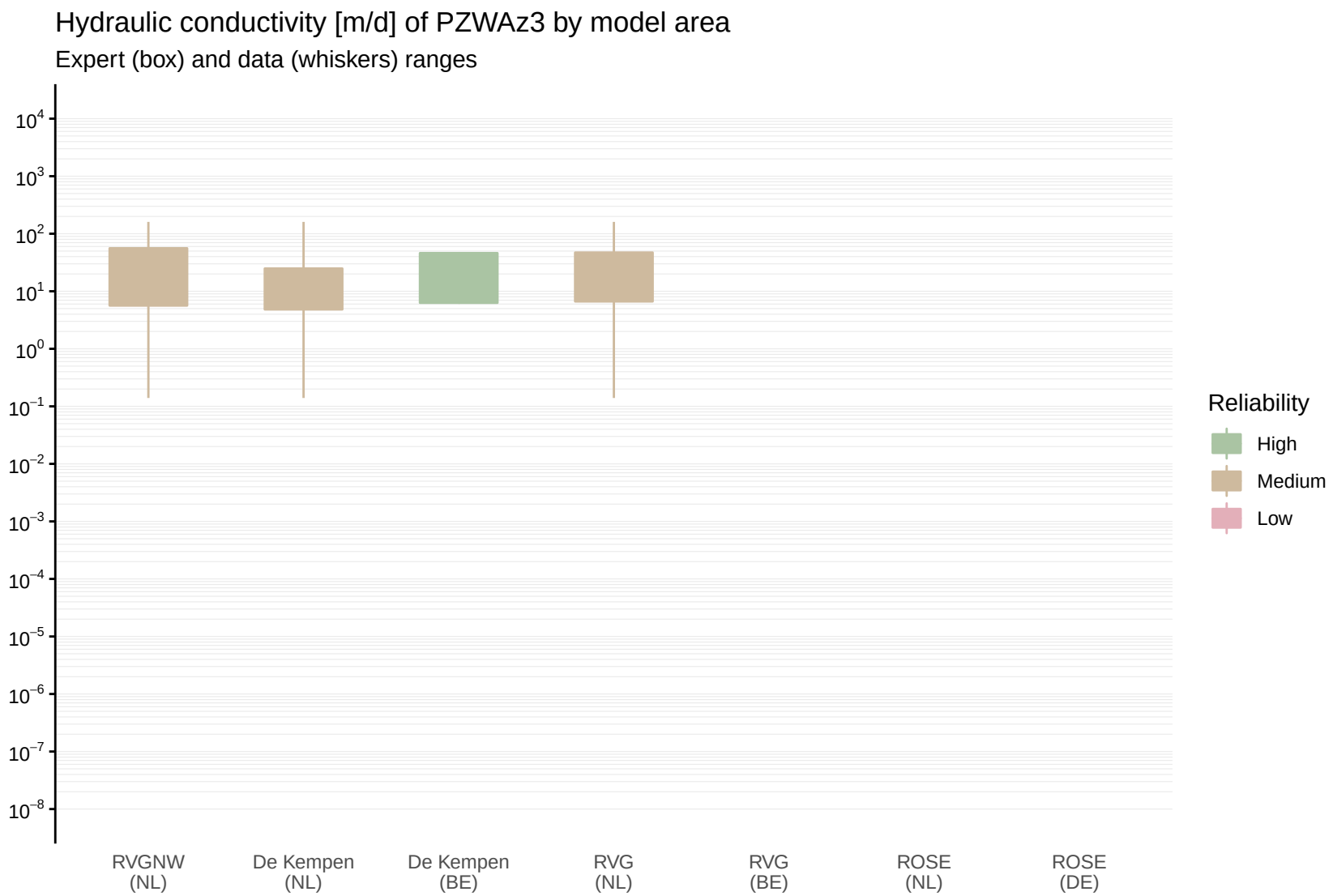
Hydraulic conductivity [m/d] of PZWAz3 by model area
Expert (box) and data (whiskers) ranges
10^{4}
10^{3}
10^{2}
10^{1}
10^{0}
10^{-1}
10^{-2}
10^{-3}
10^{-4}
10^{-5}
10^{-6}
10^{-7}
10^{-8}
RVGNW (NL)
De Kempen (NL)
De Kempen (BE)
RVG (NL)
RVG (BE)
ROSE (NL)
ROSE (DE)
Reliability
High
Medium
Low

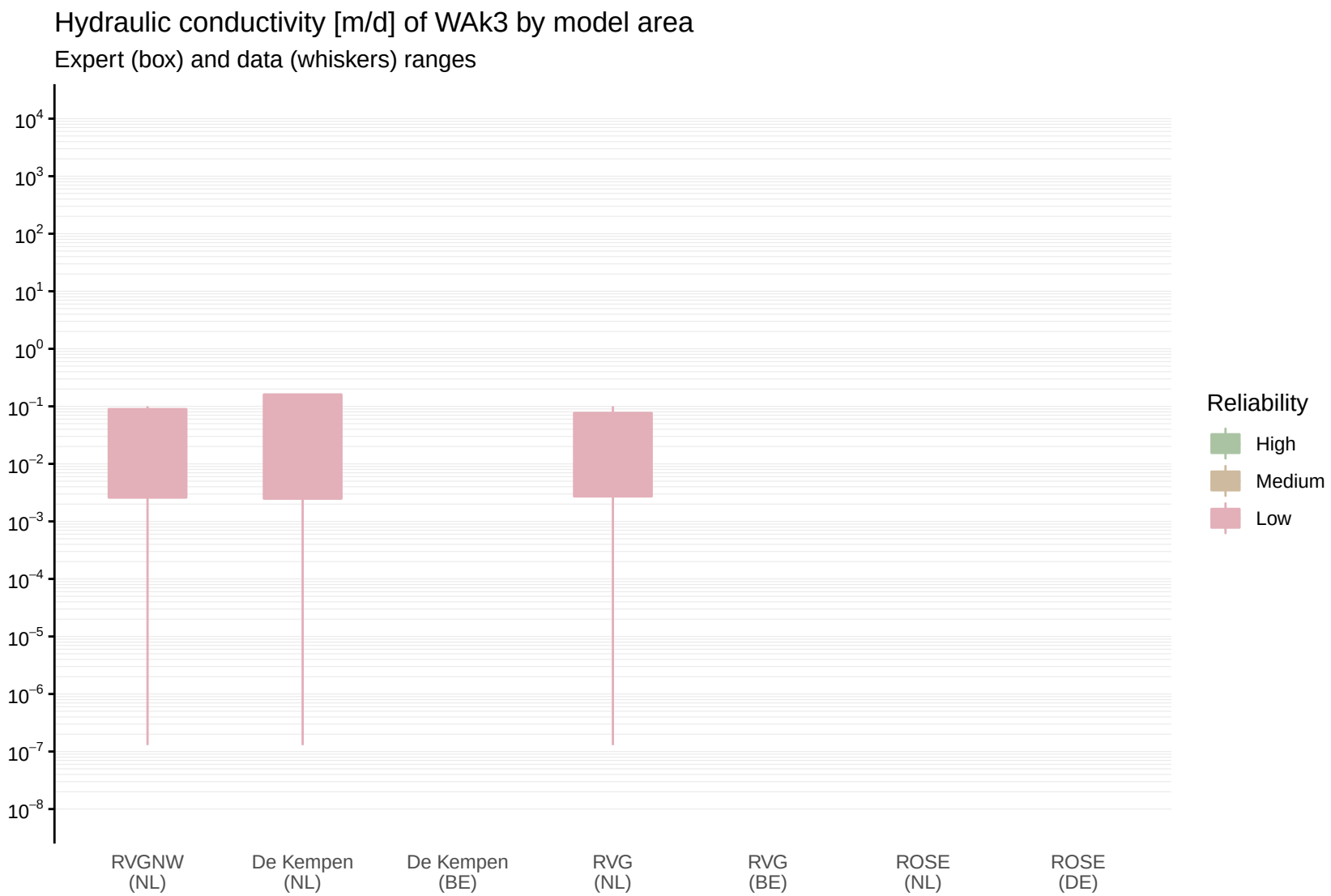
Hydraulic conductivity [m/d] of WAk3 by model area
Expert (box) and data (whiskers) ranges
10^{4}
10^{3}
10^{2}
10^{1}
10^{0}
10^{-1}
10^{-2}
10^{-3}
10^{-4}
10^{-5}
10^{-6}
10^{-7}
10^{-8}
RVGNW (NL)
De Kempen (NL)
De Kempen (BE)
RVG (NL)
RVG (BE)
ROSE (NL)
ROSE (DE)
Reliability
High
Medium
Low

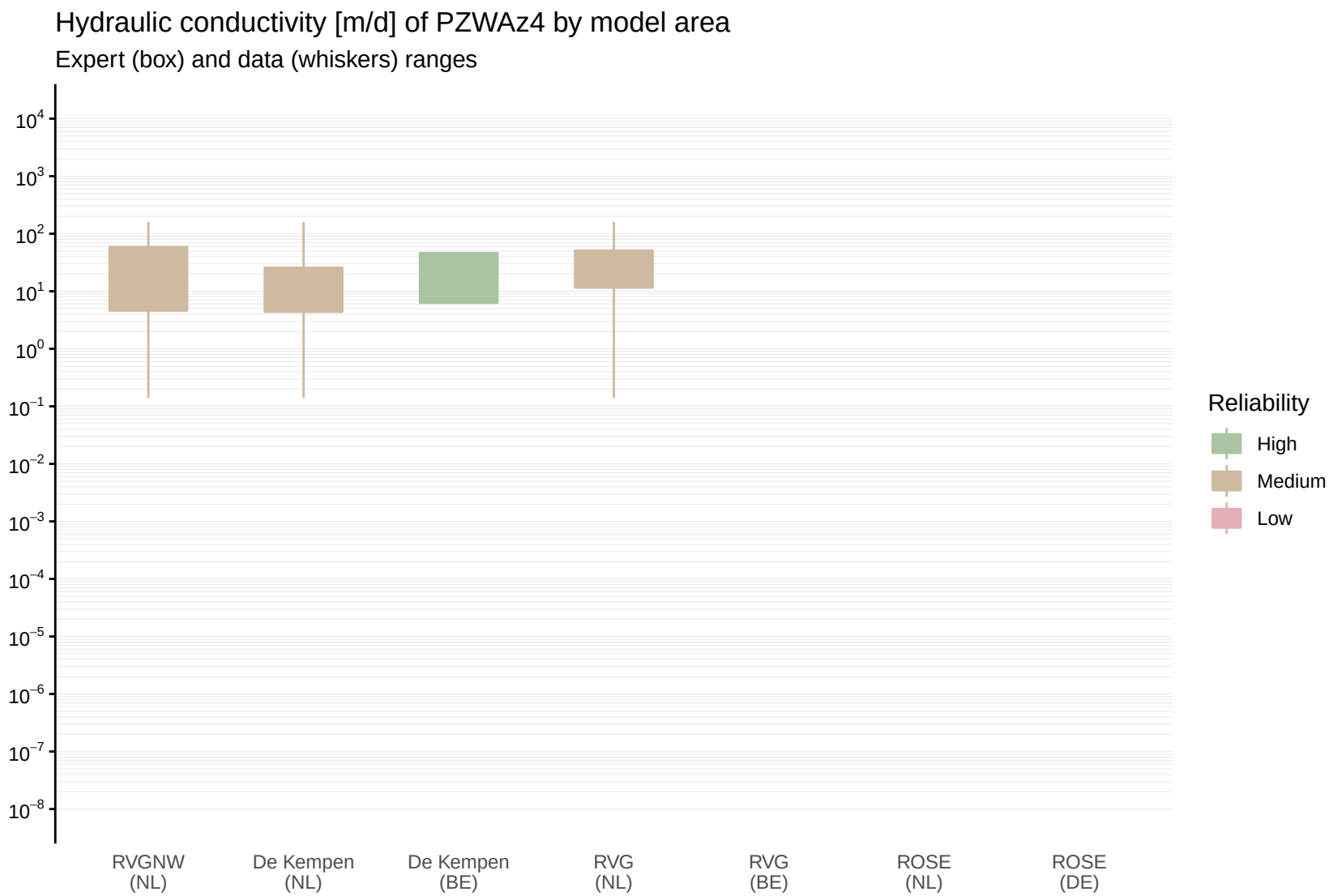
Hydraulic conductivity [m/d] of PZWAz4 by model area
Expert (box) and data (whiskers) ranges
10^{4}
10^{3}
10^{2}
10^{1}
10^{0}
10^{-1}
10^{-2}
10^{-3}
10^{-4}
10^{-5}
10^{-6}
10^{-7}
10^{-8}
RVGNW (NL)
De Kempen (NL)
De Kempen (BE)
RVG (NL)
RVG (BE)
ROSE (NL)
ROSE (DE)
Reliability
High
Medium
Low

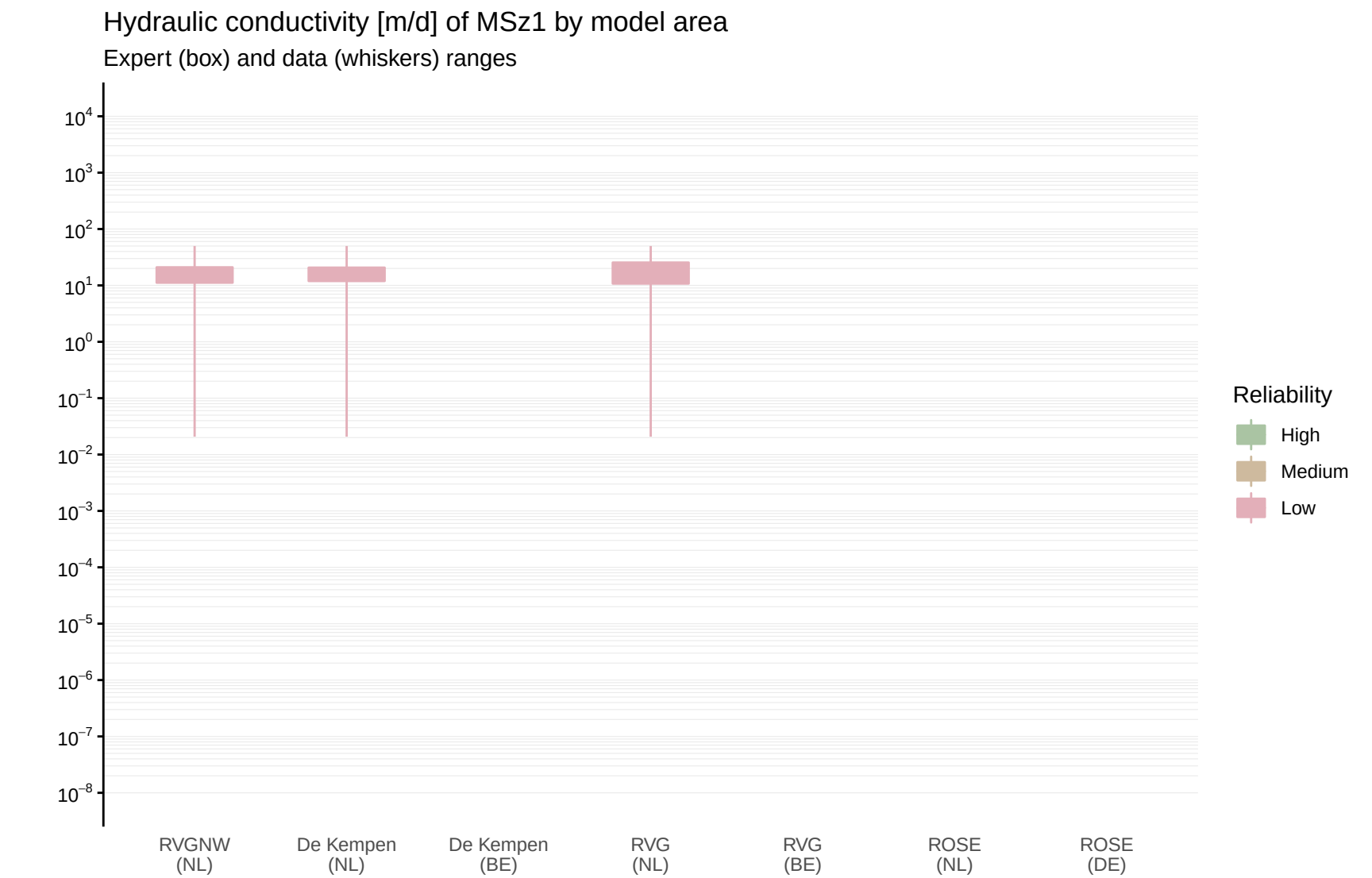
Hydraulic conductivity [m/d] of MSz1 by model area
Expert (box) and data (whiskers) ranges
10^{4}
10^{3}
10^{2}
10^{1}
10^{0}
10^{-1}
10^{-2}
10^{-3}
10^{-4}
10^{-5}
10^{-6}
10^{-7}
10^{-8}
RVGNW (NL)
De Kempen (NL)
De Kempen (BE)
RVG (NL)
RVG (BE)
ROSE (NL)
ROSE (DE)
Reliability
High
Medium
Low

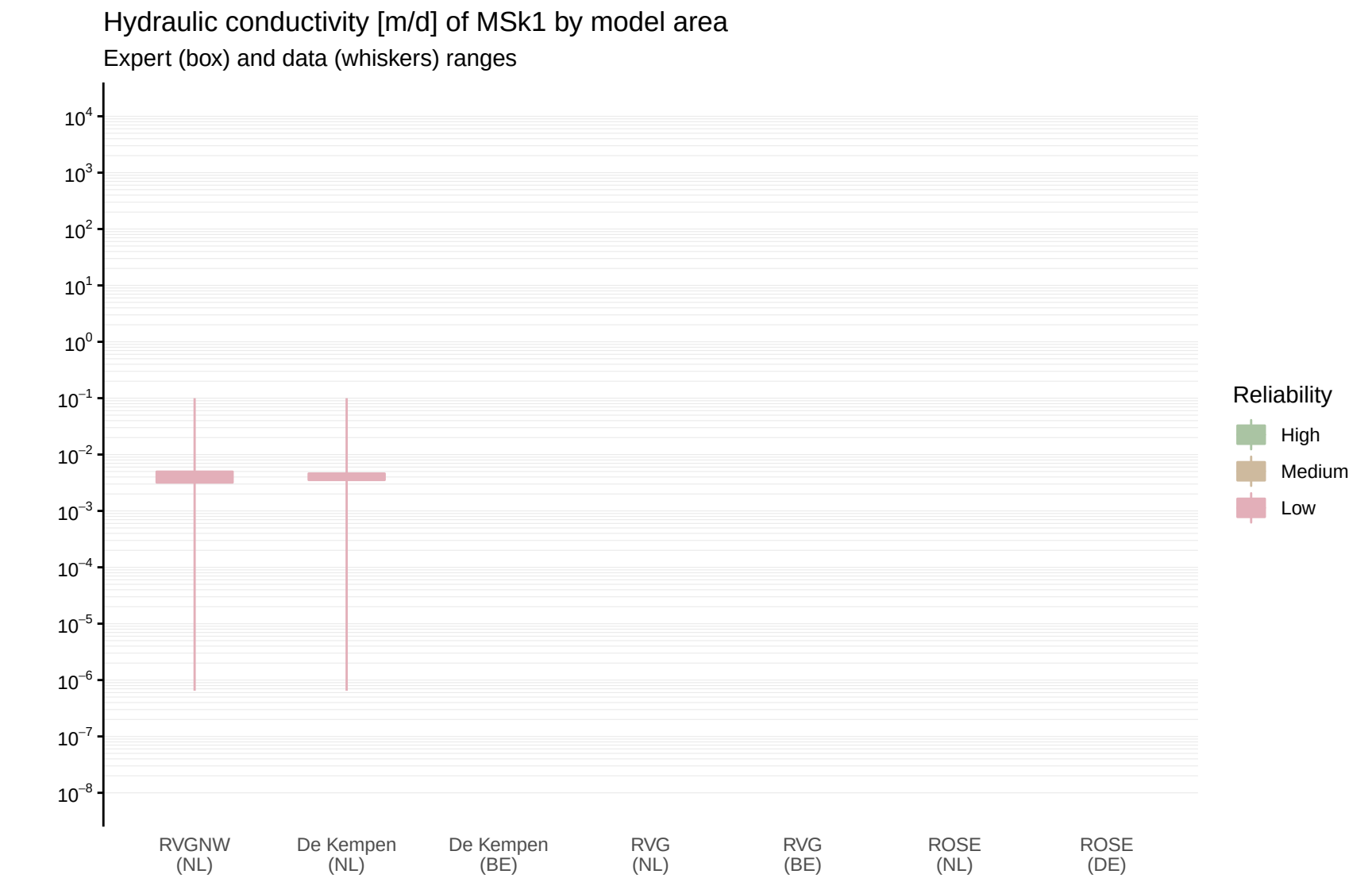
Hydraulic conductivity [m/d] of MSk1 by model area
Expert (box) and data (whiskers) ranges
10^{4}
10^{3}
10^{2}
10^{1}
10^{0}
10^{-1}
10^{-2}
10^{-3}
10^{-4}
10^{-5}
10^{-6}
10^{-7}
10^{-8}
RVGNW (NL)
De Kempen (NL)
De Kempen (BE)
RVG (NL)
RVG (BE)
ROSE (NL)
ROSE (DE)
Reliability
High
Medium
Low

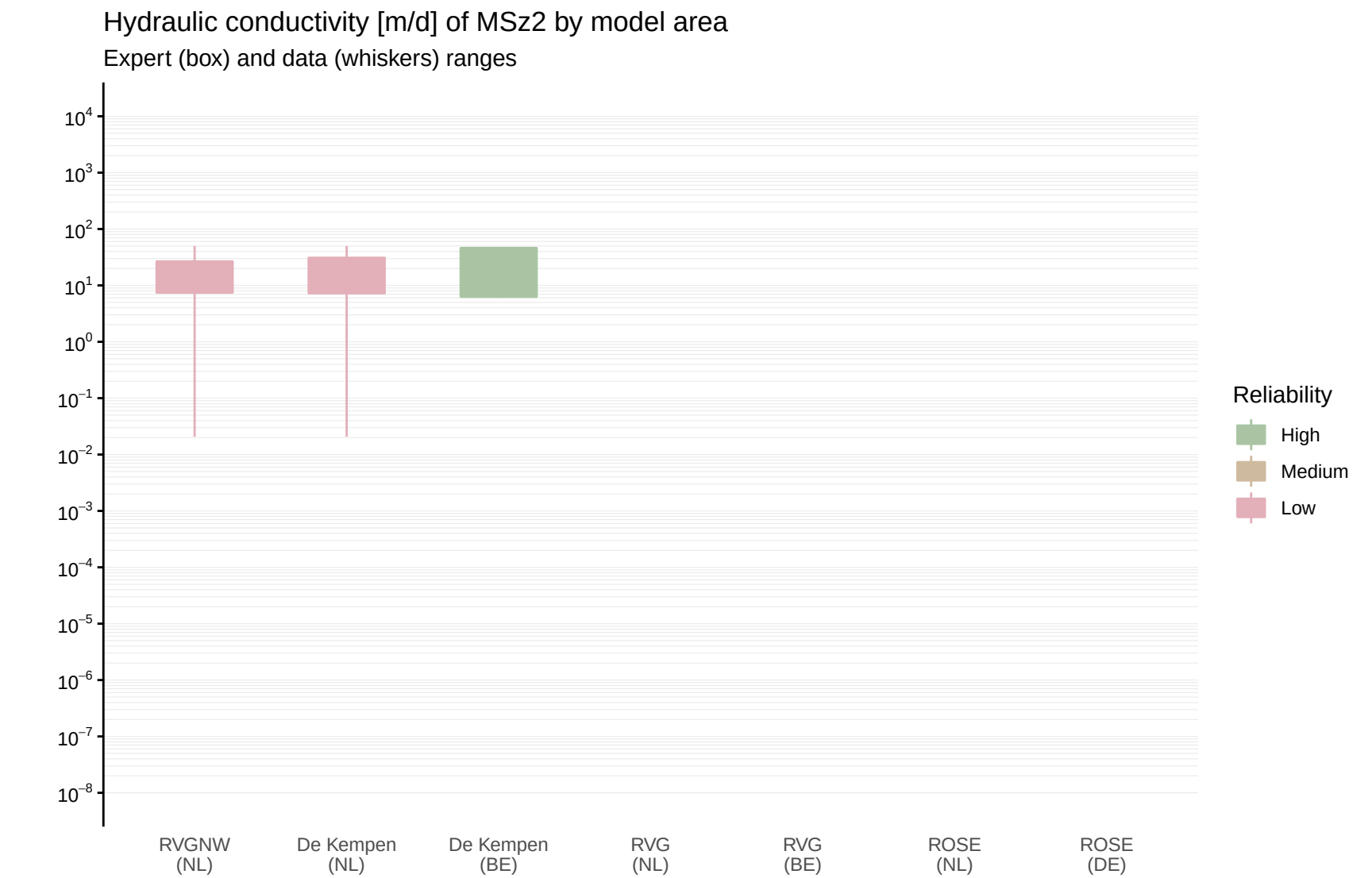
Hydraulic conductivity [m/d] of MSz2 by model area
Expert (box) and data (whiskers) ranges
10^{4}
10^{3}
10^{2}
10^{1}
10^{0}
10^{-1}
10^{-2}
10^{-3}
10^{-4}
10^{-5}
10^{-6}
10^{-7}
10^{-8}
RVGNW (NL)
De Kempen (NL)
De Kempen (BE)
RVG (NL)
RVG (BE)
ROSE (NL)
ROSE (DE)
Reliability
High
Medium
Low

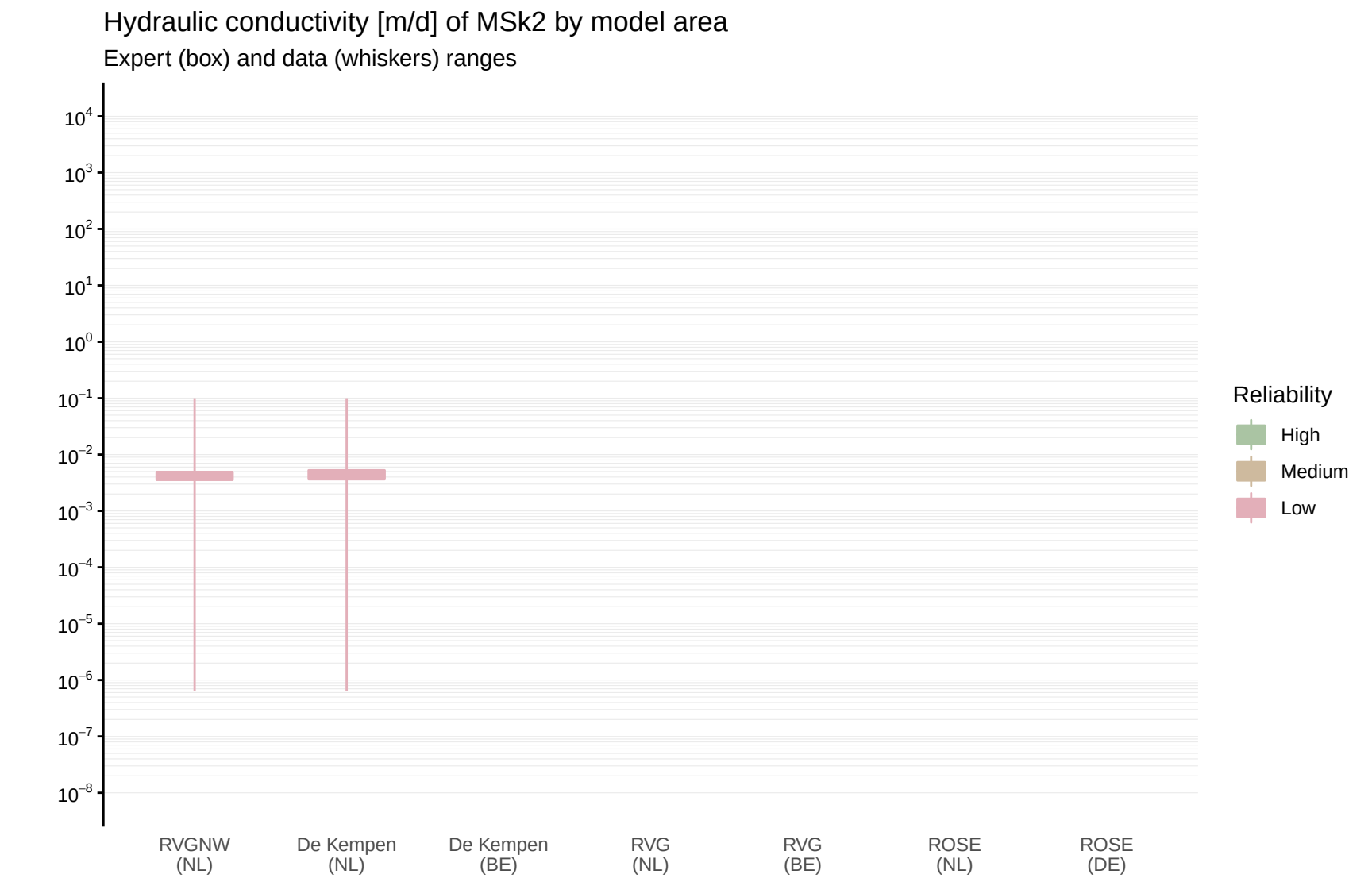
Hydraulic conductivity [m/d] of MSk2 by model area
Expert (box) and data (whiskers) ranges
10^{4}
10^{3}
10^{2}
10^{1}
10^{0}
10^{-1}
10^{-2}
10^{-3}
10^{-4}
10^{-5}
10^{-6}
10^{-7}
10^{-8}
RVGNW (NL)
De Kempen (NL)
De Kempen (BE)
RVG (NL)
RVG (BE)
ROSE (NL)
ROSE (DE)
Reliability
High
Medium
Low

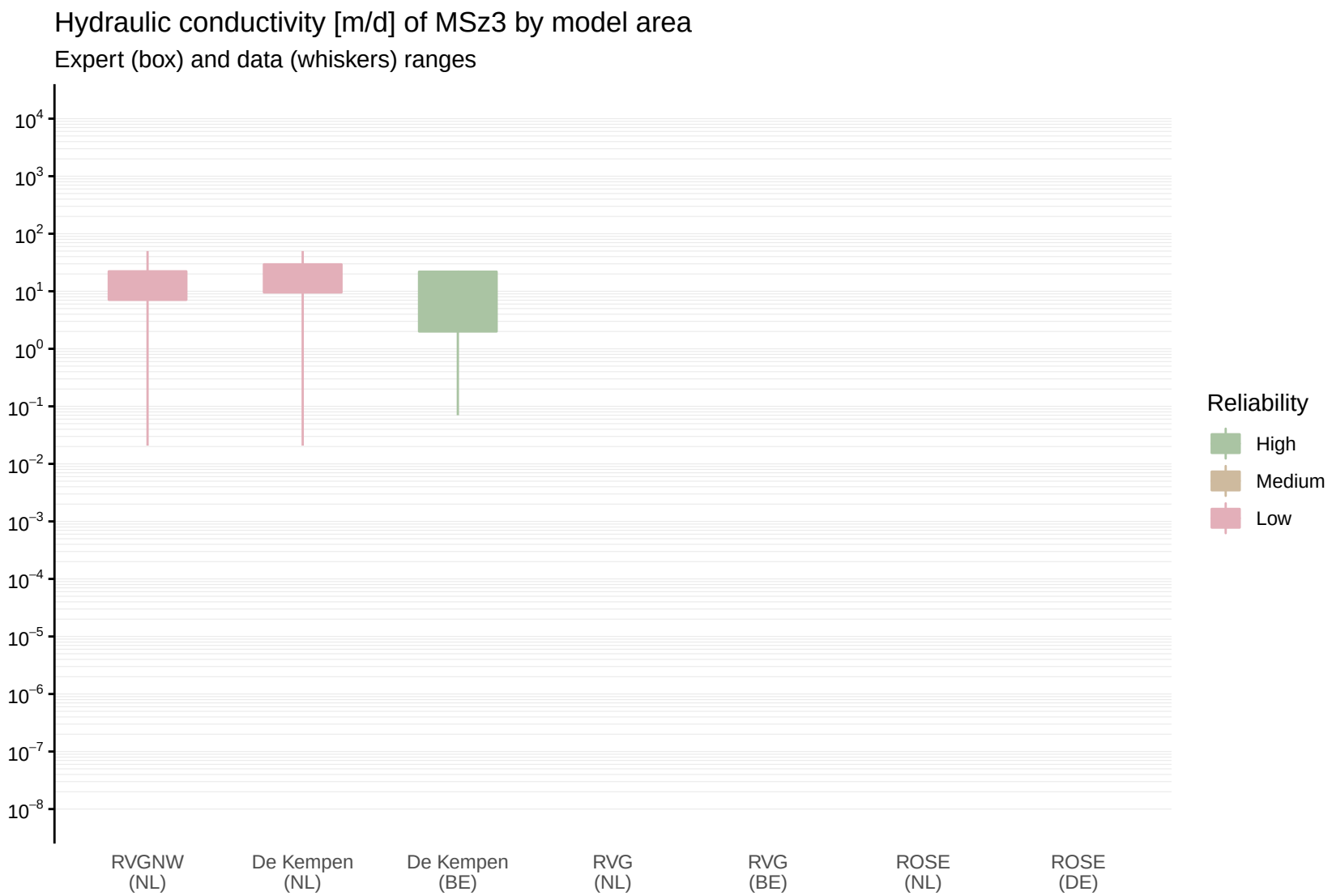
Hydraulic conductivity [m/d] of MSz3 by model area
Expert (box) and data (whiskers) ranges
10^{4}
10^{3}
10^{2}
10^{1}
10^{0}
10^{-1}
10^{-2}
10^{-3}
10^{-4}
10^{-5}
10^{-6}
10^{-7}
10^{-8}
RVGNW (NL)
De Kempen (NL)
De Kempen (BE)
RVG (NL)
RVG (BE)
ROSE (NL)
ROSE (DE)
Reliability
High
Medium
Low

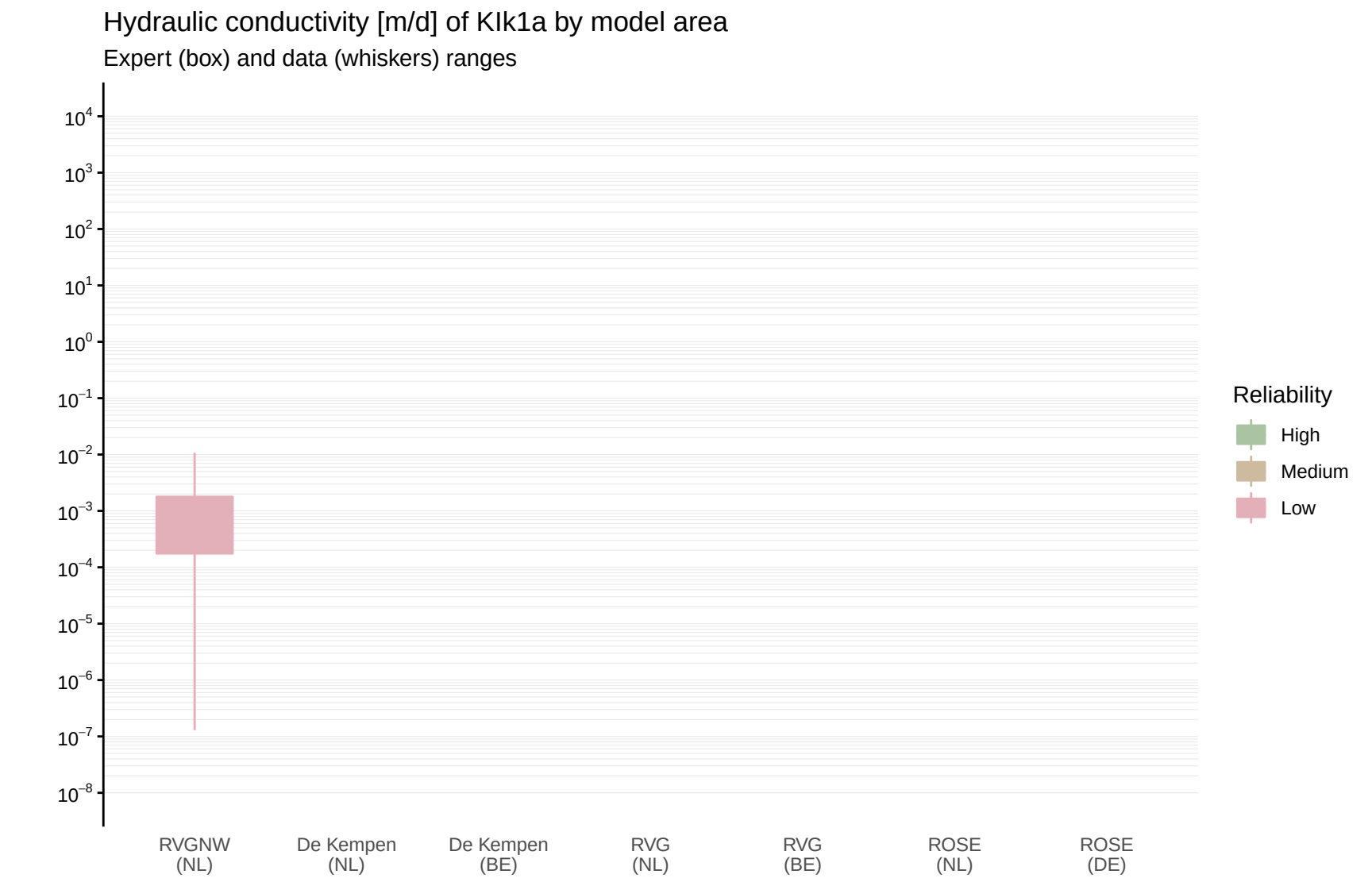
Hydraulic conductivity [m/d] of KIk1a by model area
Expert (box) and data (whiskers) ranges
10^{4}
10^{3}
10^{2}
10^{1}
10^{0}
10^{-1}
10^{-2}
10^{-3}
10^{-4}
10^{-5}
10^{-6}
10^{-7}
10^{-8}
RVGNW (NL)
De Kempen (NL)
De Kempen (BE)
RVG (NL)
RVG (BE)
ROSE (NL)
ROSE (DE)
Reliability
High
Medium
Low

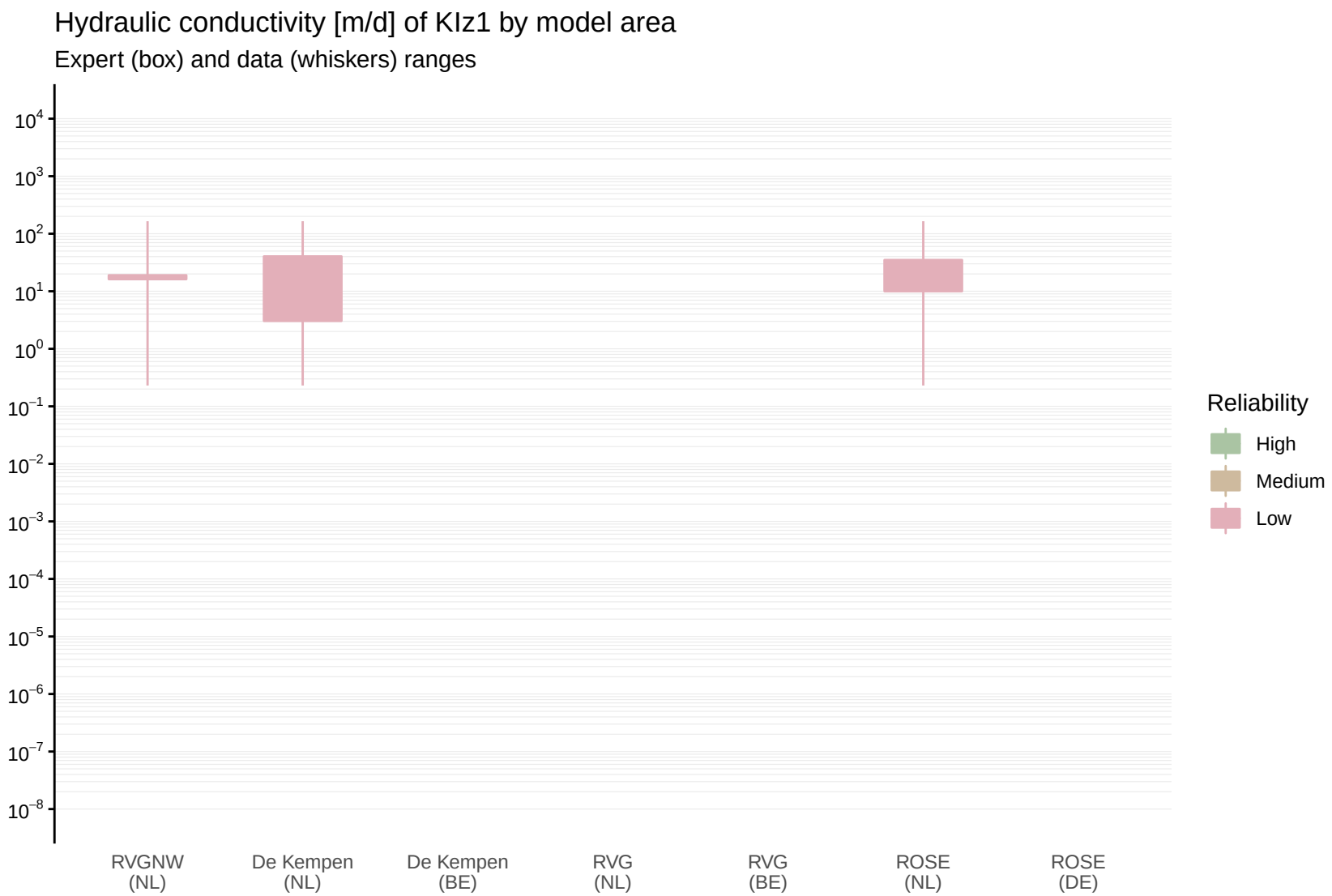
Hydraulic conductivity [m/d] of KIz1 by model area
Expert (box) and data (whiskers) ranges
10^{4}
10^{3}
10^{2}
10^{1}
10^{0}
10^{-1}
10^{-2}
10^{-3}
10^{-4}
10^{-5}
10^{-6}
10^{-7}
10^{-8}
RVGNW (NL)
De Kempen (NL)
De Kempen (BE)
RVG (NL)
RVG (BE)
ROSE (NL)
ROSE (DE)
Reliability
High
Medium
Low

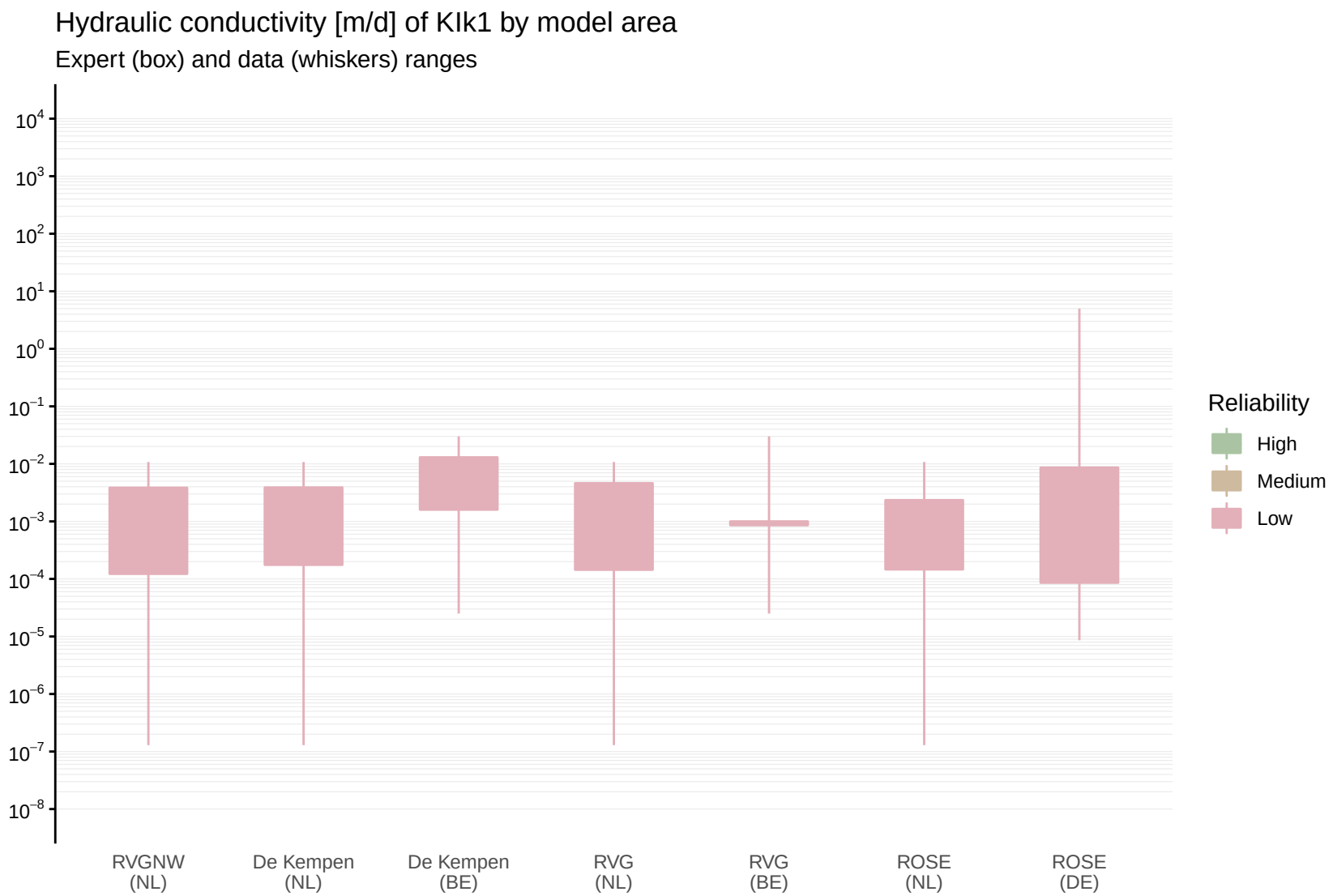
Hydraulic conductivity [m/d] of KIk1 by model area
Expert (box) and data (whiskers) ranges
10^{4}
10^{3}
10^{2}
10^{1}
10^{0}
10^{-1}
10^{-2}
10^{-3}
10^{-4}
10^{-5}
10^{-6}
10^{-7}
10^{-8}
RVGNW (NL)
De Kempen (NL)
De Kempen (BE)
RVG (NL)
RVG (BE)
ROSE (NL)
ROSE (DE)
Reliability
High
Medium
Low

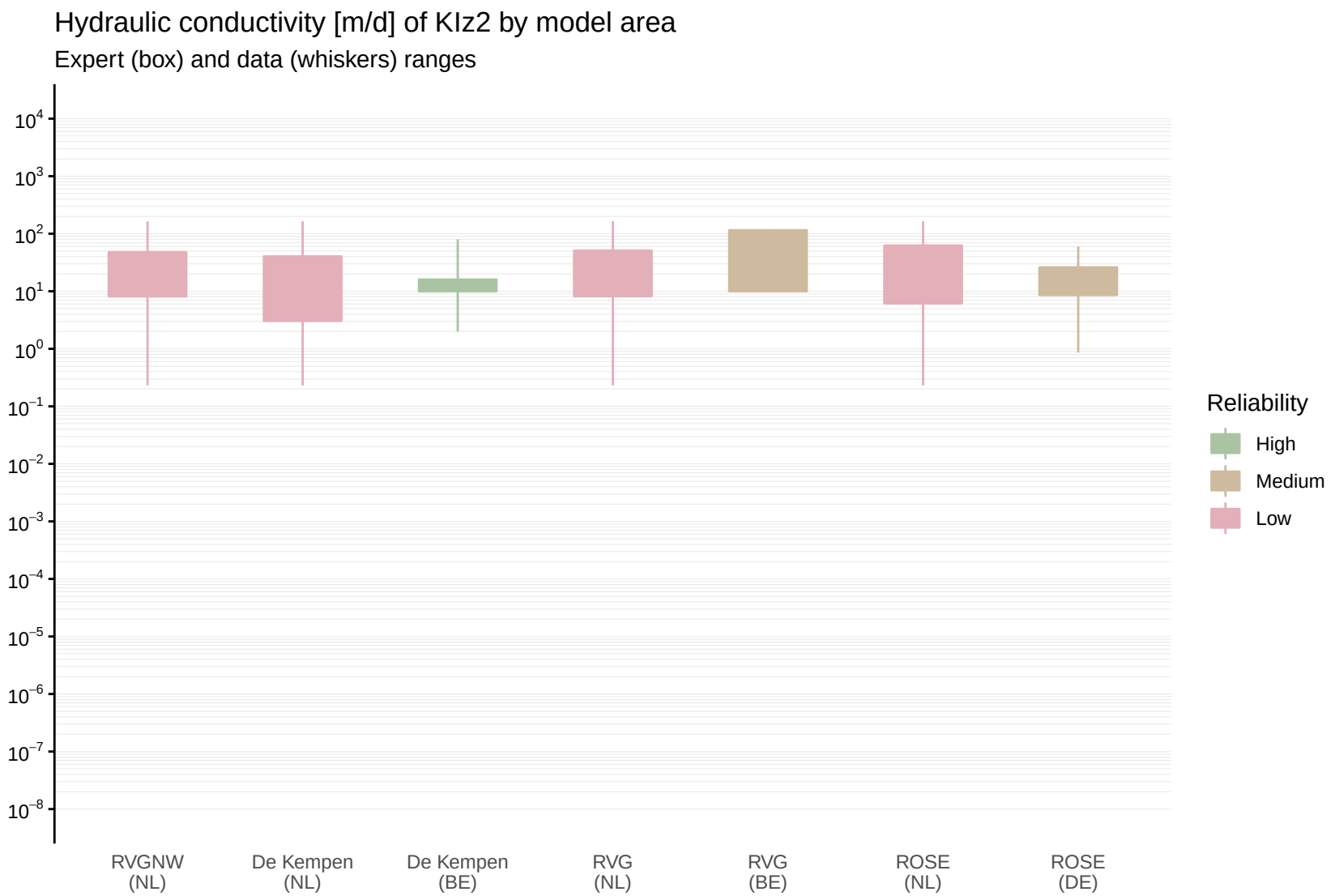
Hydraulic conductivity [m/d] of KIz2 by model area
Expert (box) and data (whiskers) ranges
10^{4}
10^{3}
10^{2}
10^{1}
10^{0}
10^{-1}
10^{-2}
10^{-3}
10^{-4}
10^{-5}
10^{-6}
10^{-7}
10^{-8}
RVGNW (NL)
De Kempen (NL)
De Kempen (BE)
RVG (NL)
RVG (BE)
ROSE (NL)
ROSE (DE)
Reliability
High
Medium
Low

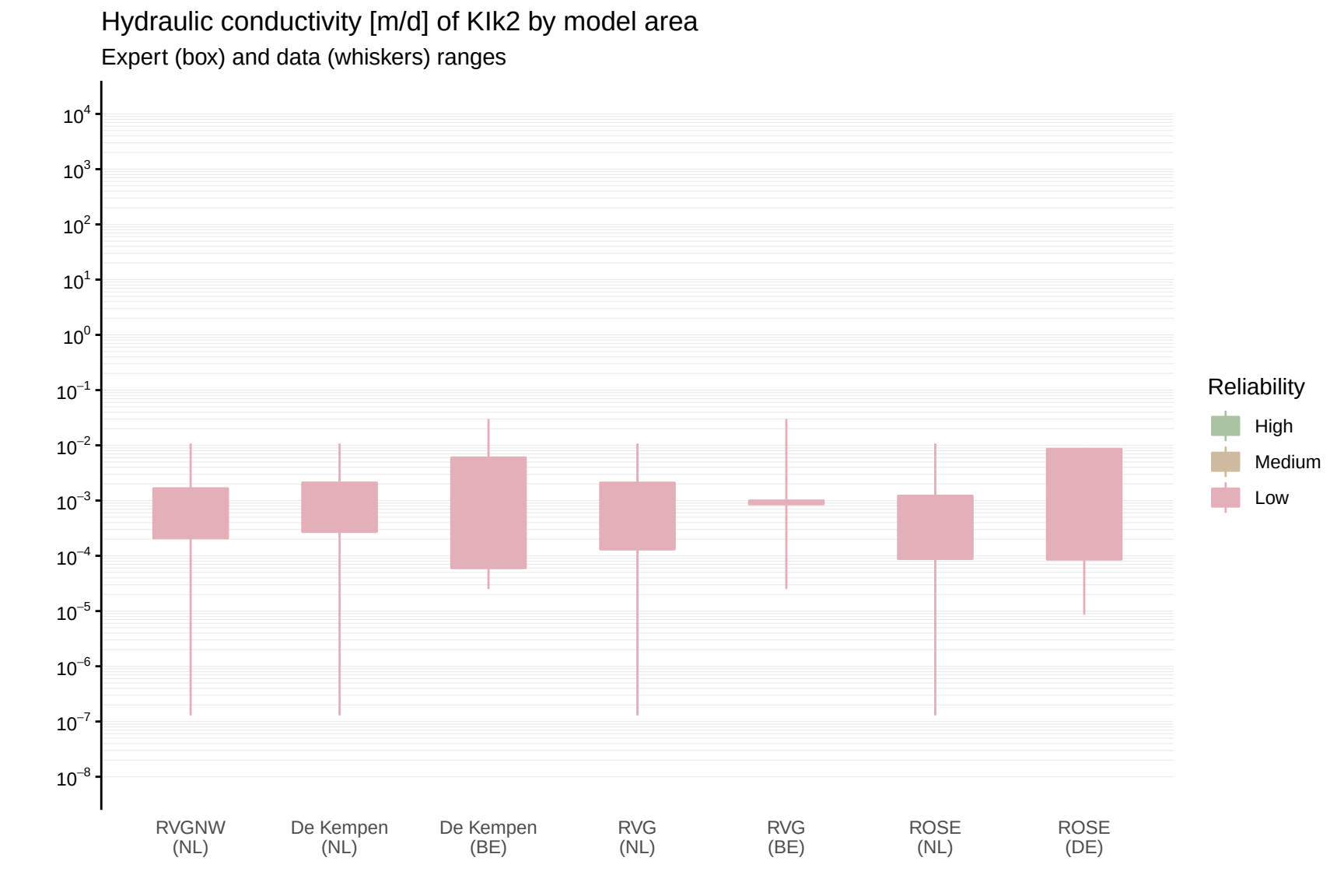
Hydraulic conductivity [m/d] of KIk2 by model area
Expert (box) and data (whiskers) ranges
10^{4}
10^{3}
10^{2}
10^{1}
10^{0}
10^{-1}
10^{-2}
10^{-3}
10^{-4}
10^{-5}
10^{-6}
10^{-7}
10^{-8}
RVGNW (NL)
De Kempen (NL)
De Kempen (BE)
RVG (NL)
RVG (BE)
ROSE (NL)
ROSE (DE)
Reliability
High
Medium
Low

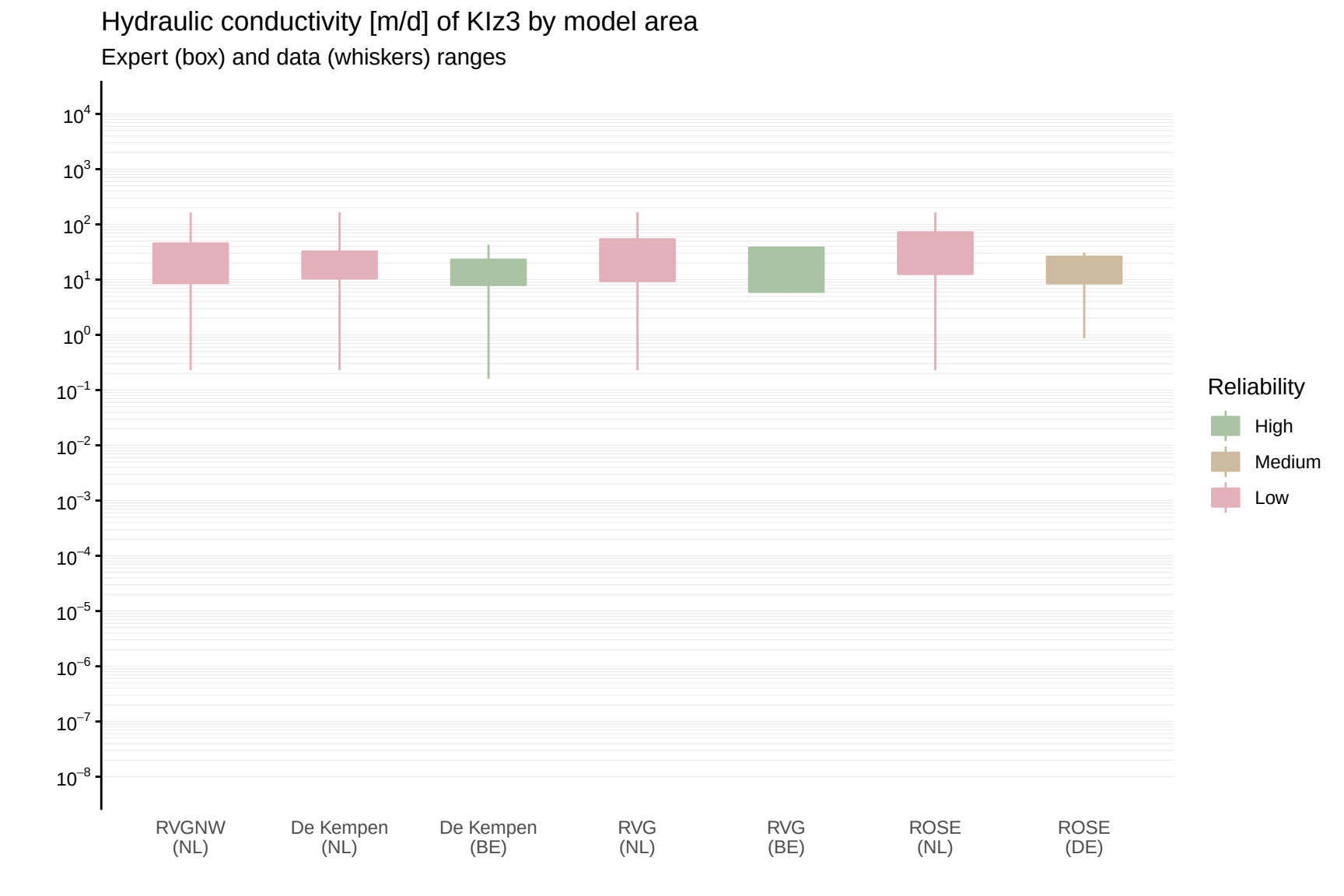
Hydraulic conductivity [m/d] of KIz3 by model area
Expert (box) and data (whiskers) ranges
10^{4}
10^{3}
10^{2}
10^{1}
10^{0}
10^{-1}
10^{-2}
10^{-3}
10^{-4}
10^{-5}
10^{-6}
10^{-7}
10^{-8}
RVGNW (NL)
De Kempen (NL)
De Kempen (BE)
RVG (NL)
RVG (BE)
ROSE (NL)
ROSE (DE)
Reliability
High
Medium
Low

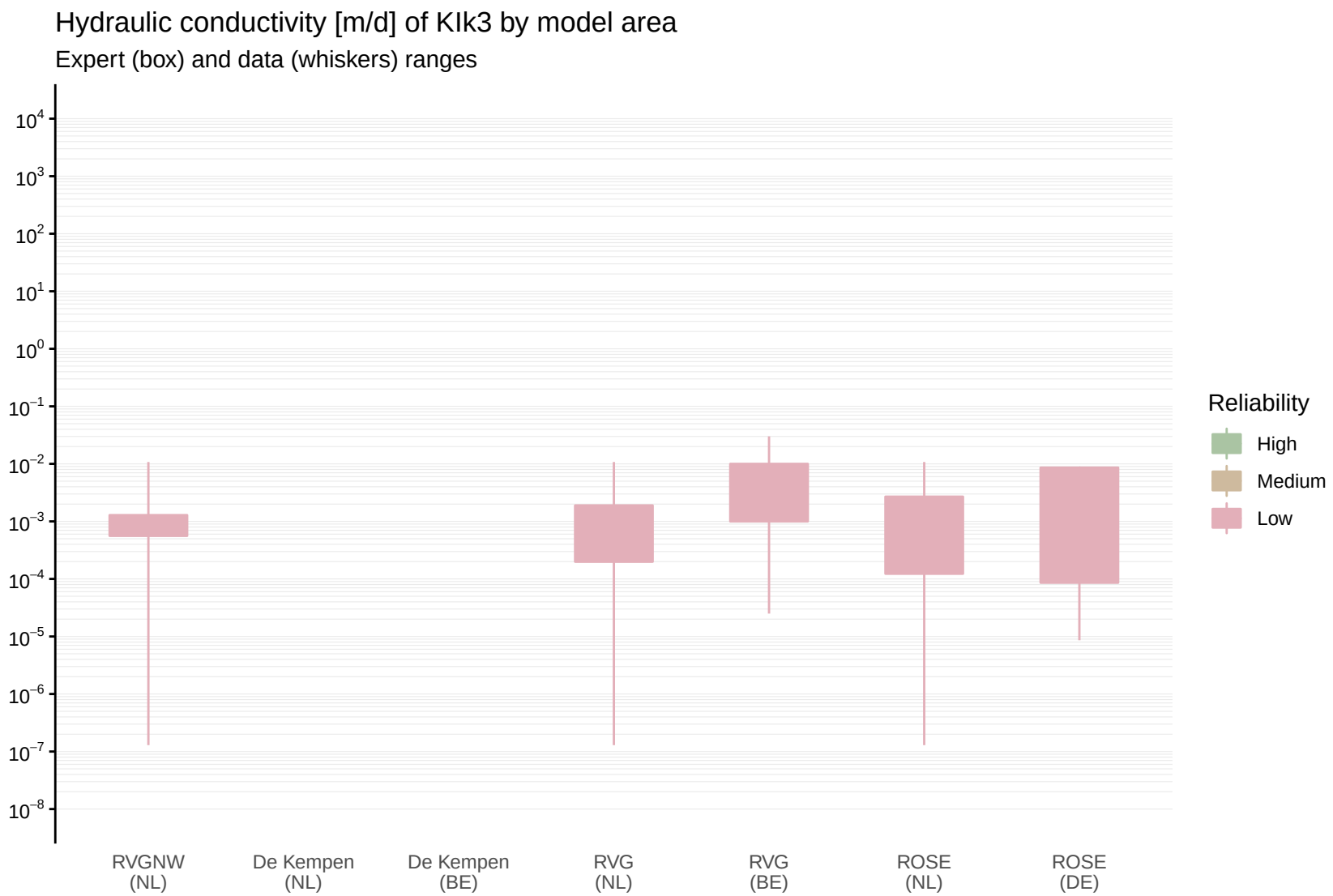
Hydraulic conductivity [m/d] of KIk3 by model area
Expert (box) and data (whiskers) ranges
10^{4}
10^{3}
10^{2}
10^{1}
10^{0}
10^{-1}
10^{-2}
10^{-3}
10^{-4}
10^{-5}
10^{-6}
10^{-7}
10^{-8}
RVGNW (NL)
De Kempen (NL)
De Kempen (BE)
RVG (NL)
RVG (BE)
ROSE (NL)
ROSE (DE)
Reliability
High
Medium
Low

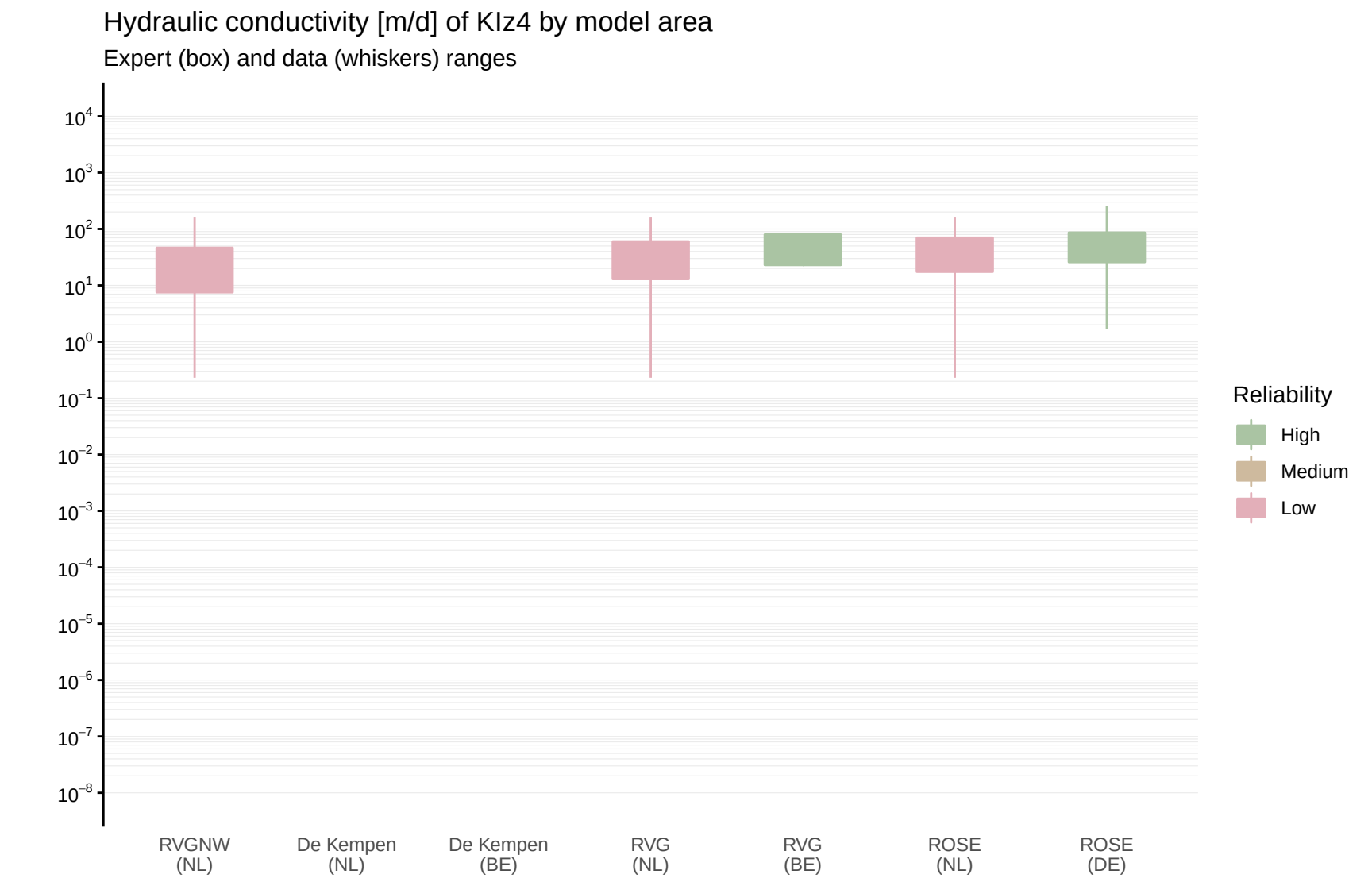
Hydraulic conductivity [m/d] of KIz4 by model area
Expert (box) and data (whiskers) ranges
10^{4}
10^{3}
10^{2}
10^{1}
10^{0}
10^{-1}
10^{-2}
10^{-3}
10^{-4}
10^{-5}
10^{-6}
10^{-7}
10^{-8}
RVGNW (NL)
De Kempen (NL)
De Kempen (BE)
RVG (NL)
RVG (BE)
ROSE (NL)
ROSE (DE)
Reliability
High
Medium
Low

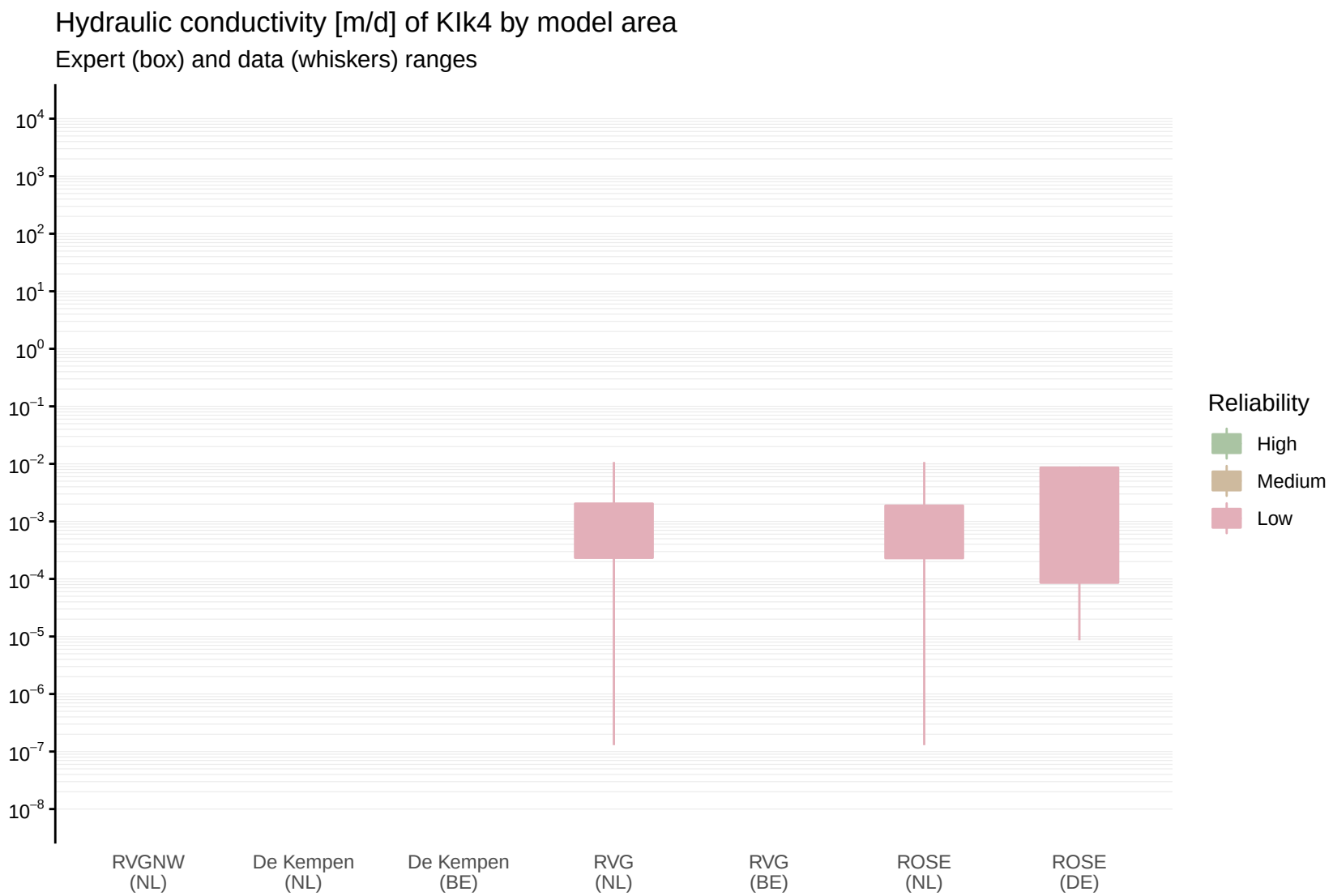
Hydraulic conductivity [m/d] of KIk4 by model area
Expert (box) and data (whiskers) ranges
10^{4}
10^{3}
10^{2}
10^{1}
10^{0}
10^{-1}
10^{-2}
10^{-3}
10^{-4}
10^{-5}
10^{-6}
10^{-7}
10^{-8}
RVGNW (NL)
De Kempen (NL)
De Kempen (BE)
RVG (NL)
RVG (BE)
ROSE (NL)
ROSE (DE)
Reliability
High
Medium
Low

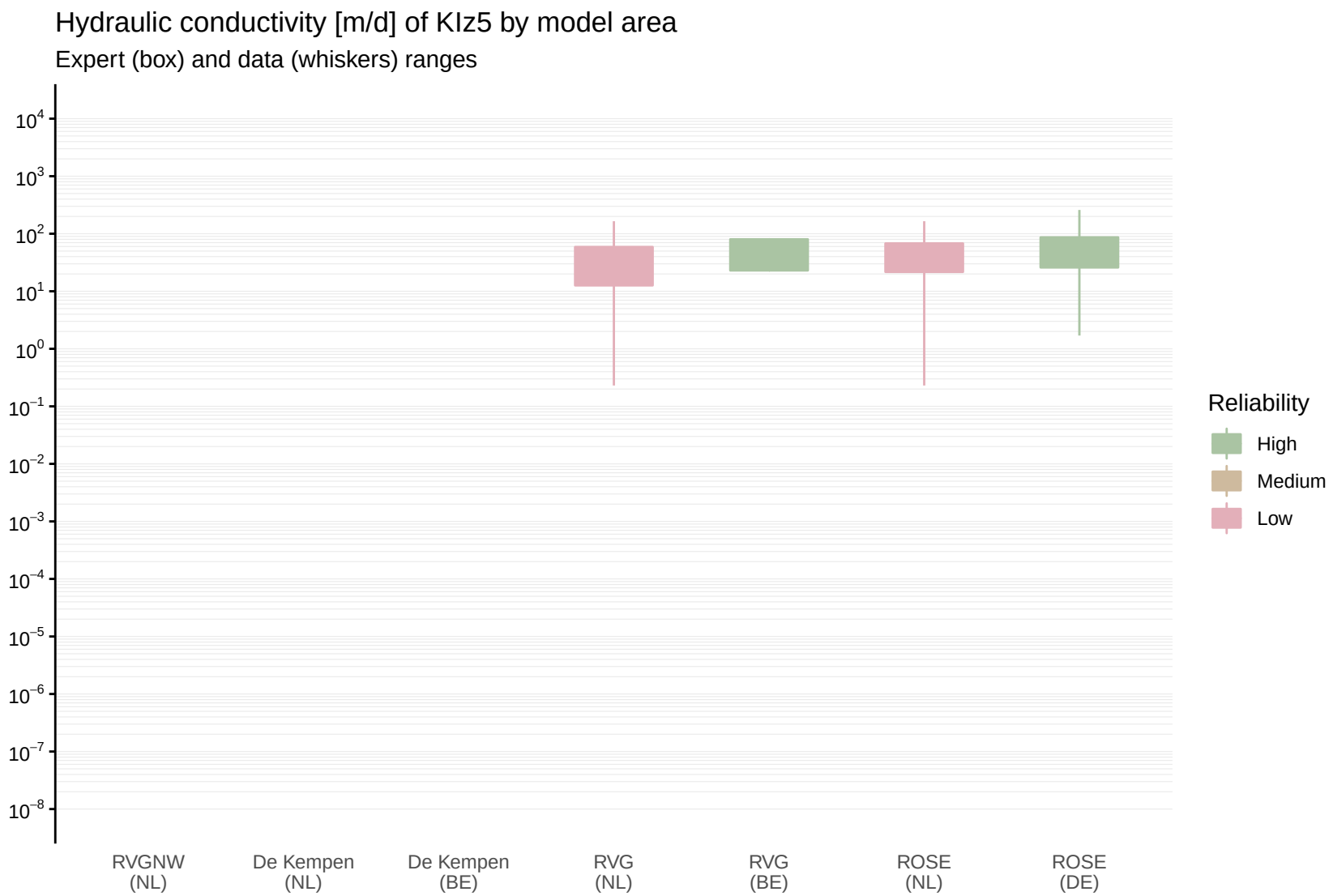
Hydraulic conductivity [m/d] of KIz5 by model area
Expert (box) and data (whiskers) ranges
10^{4}
10^{3}
10^{2}
10^{1}
10^{0}
10^{-1}
10^{-2}
10^{-3}
10^{-4}
10^{-5}
10^{-6}
10^{-7}
10^{-8}
RVGNW (NL)
De Kempen (NL)
De Kempen (BE)
RVG (NL)
RVG (BE)
ROSE (NL)
ROSE (DE)
Reliability
High
Medium
Low

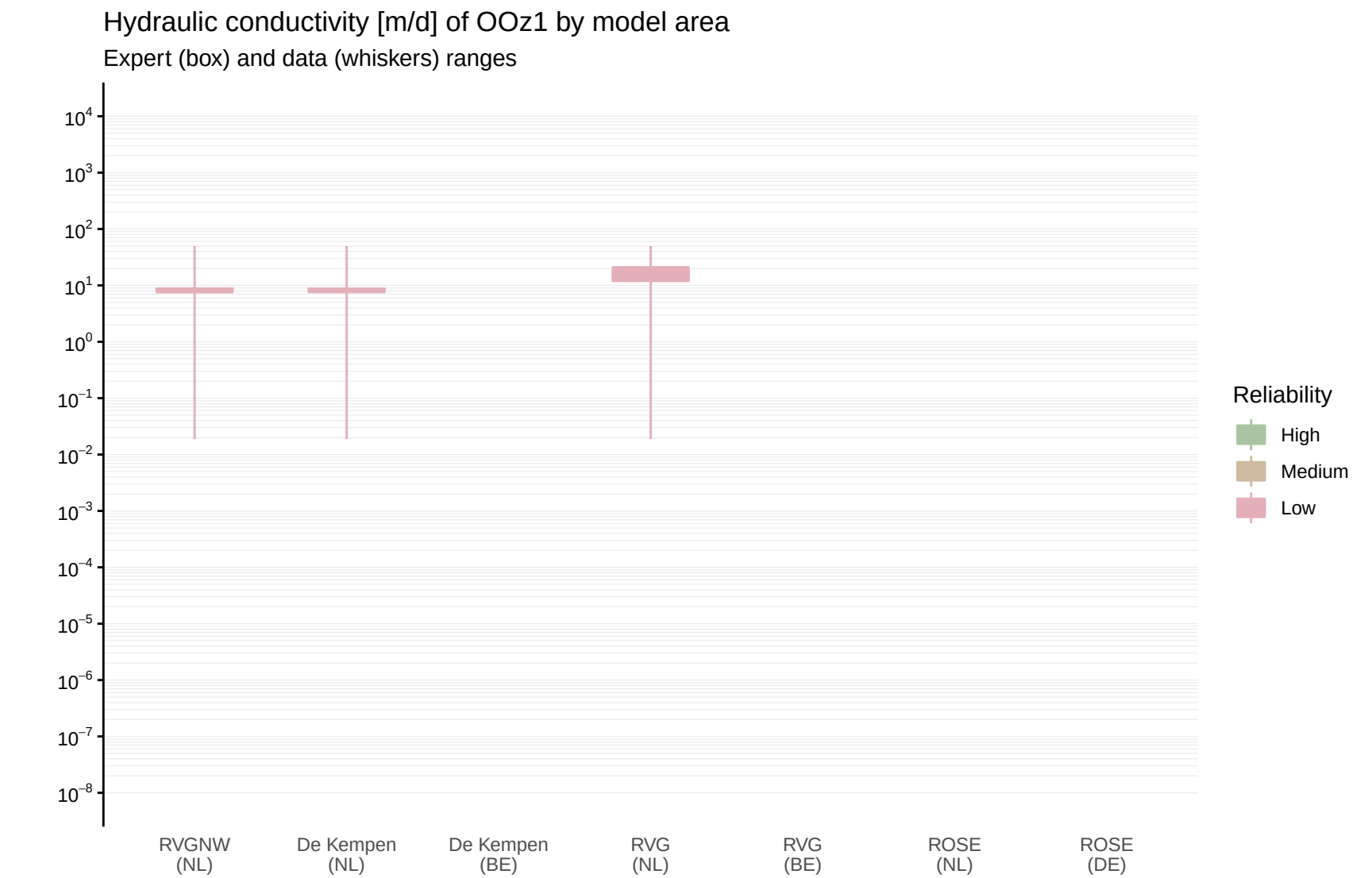
Hydraulic conductivity [m/d] of OOz1 by model area
Expert (box) and data (whiskers) ranges
10^{4}
10^{3}
10^{2}
10^{1}
10^{0}
10^{-1}
10^{-2}
10^{-3}
10^{-4}
10^{-5}
10^{-6}
10^{-7}
10^{-8}
RVGNW (NL)
De Kempen (NL)
De Kempen (BE)
RVG (NL)
RVG (BE)
ROSE (NL)
ROSE (DE)
Reliability
High
Medium
Low

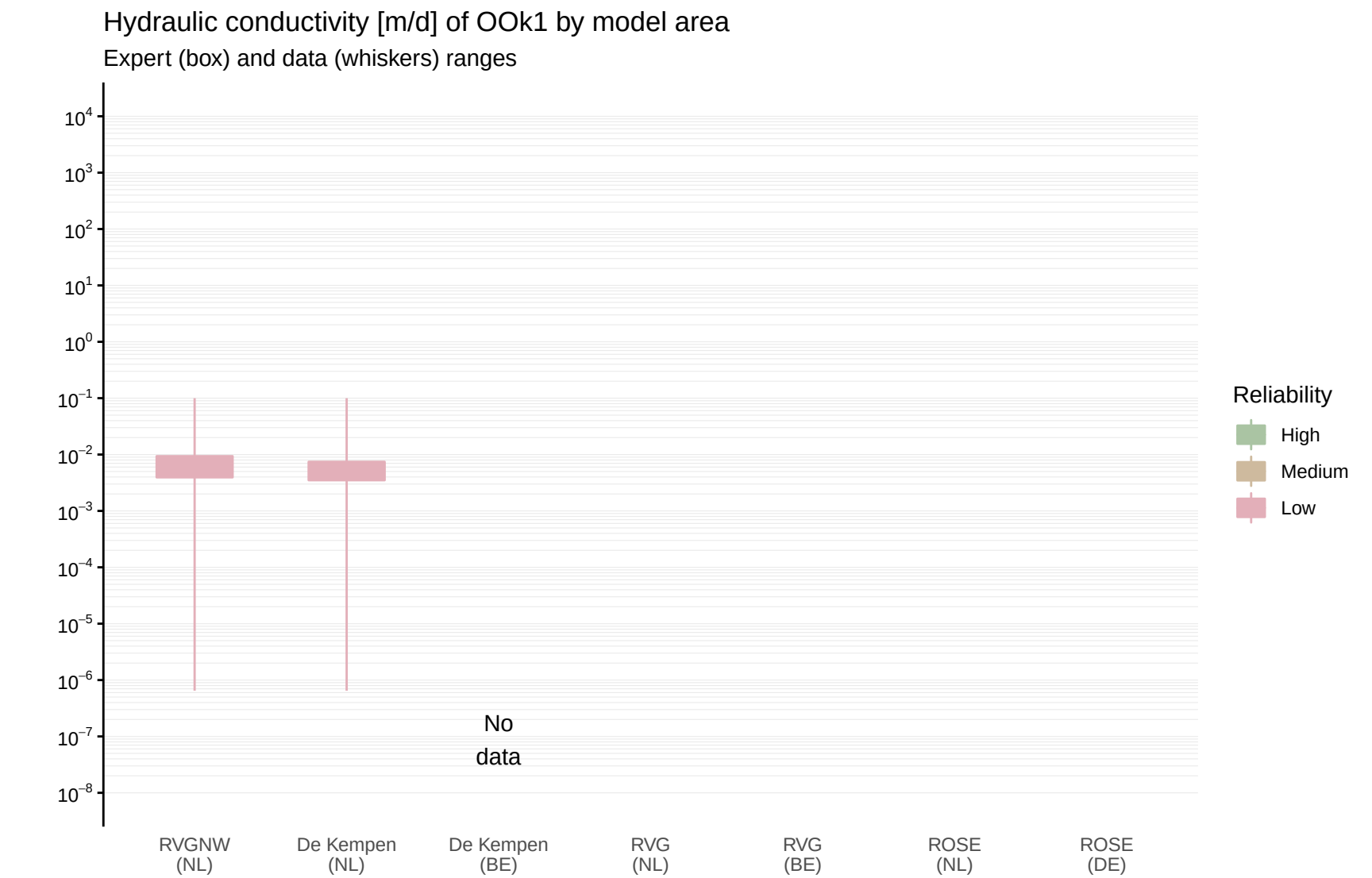
Hydraulic conductivity [m/d] of OOk1 by model area
Expert (box) and data (whiskers) ranges
10^{4}
10^{3}
10^{2}
10^{1}
10^{0}
10^{-1}
10^{-2}
10^{-3}
10^{-4}
10^{-5}
10^{-6}
10^{-7}
10^{-8}
No data
RVGNW (NL)
De Kempen (NL)
De Kempen (BE)
RVG (NL)
RVG (BE)
ROSE (NL)
ROSE (DE)
Reliability
High
Medium
Low

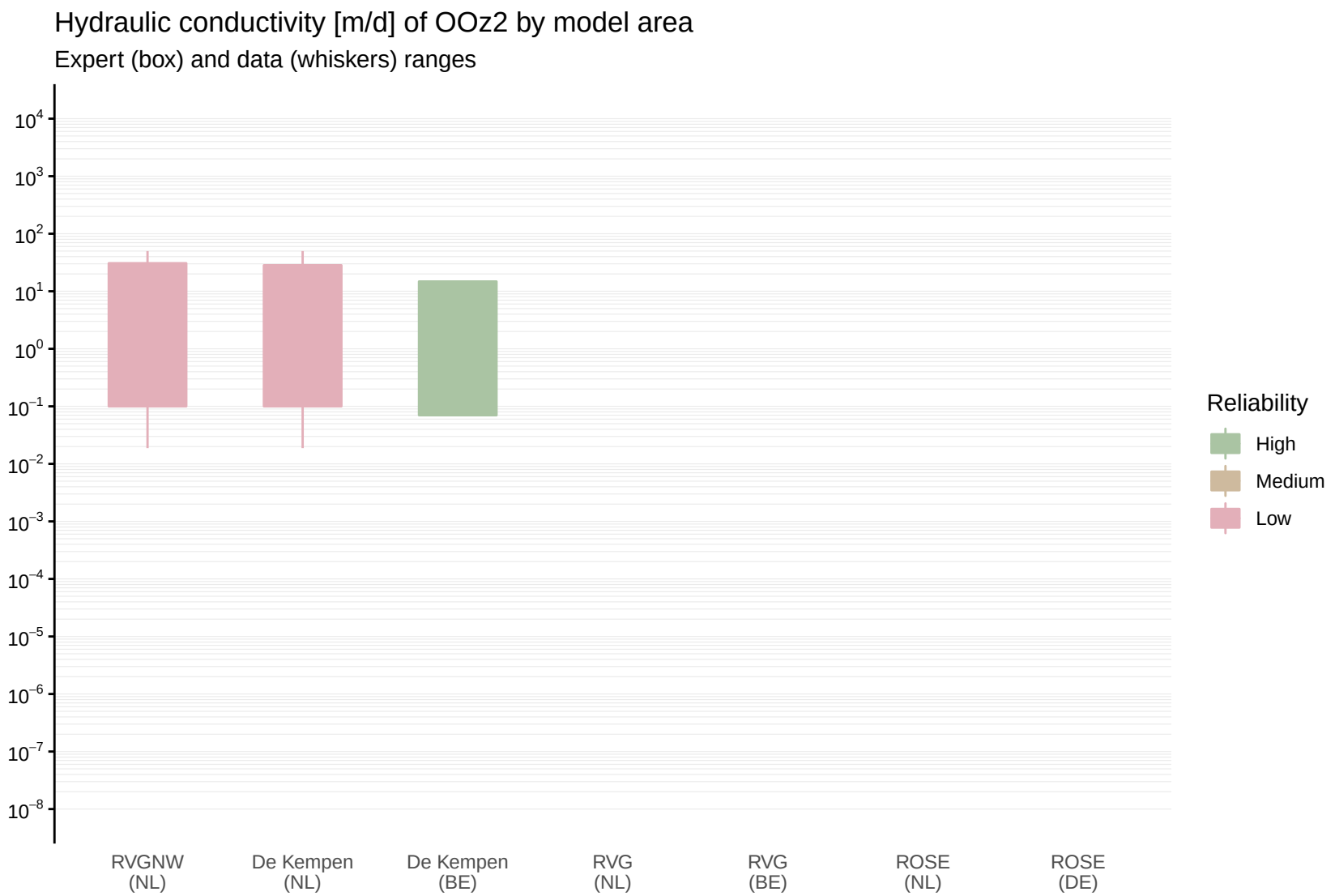
Hydraulic conductivity [m/d] of OOz2 by model area
Expert (box) and data (whiskers) ranges
10^{4}
10^{3}
10^{2}
10^{1}
10^{0}
10^{-1}
10^{-2}
10^{-3}
10^{-4}
10^{-5}
10^{-6}
10^{-7}
10^{-8}
RVGNW (NL)
De Kempen (NL)
De Kempen (BE)
RVG (NL)
RVG (BE)
ROSE (NL)
ROSE (DE)
Reliability
High
Medium
Low

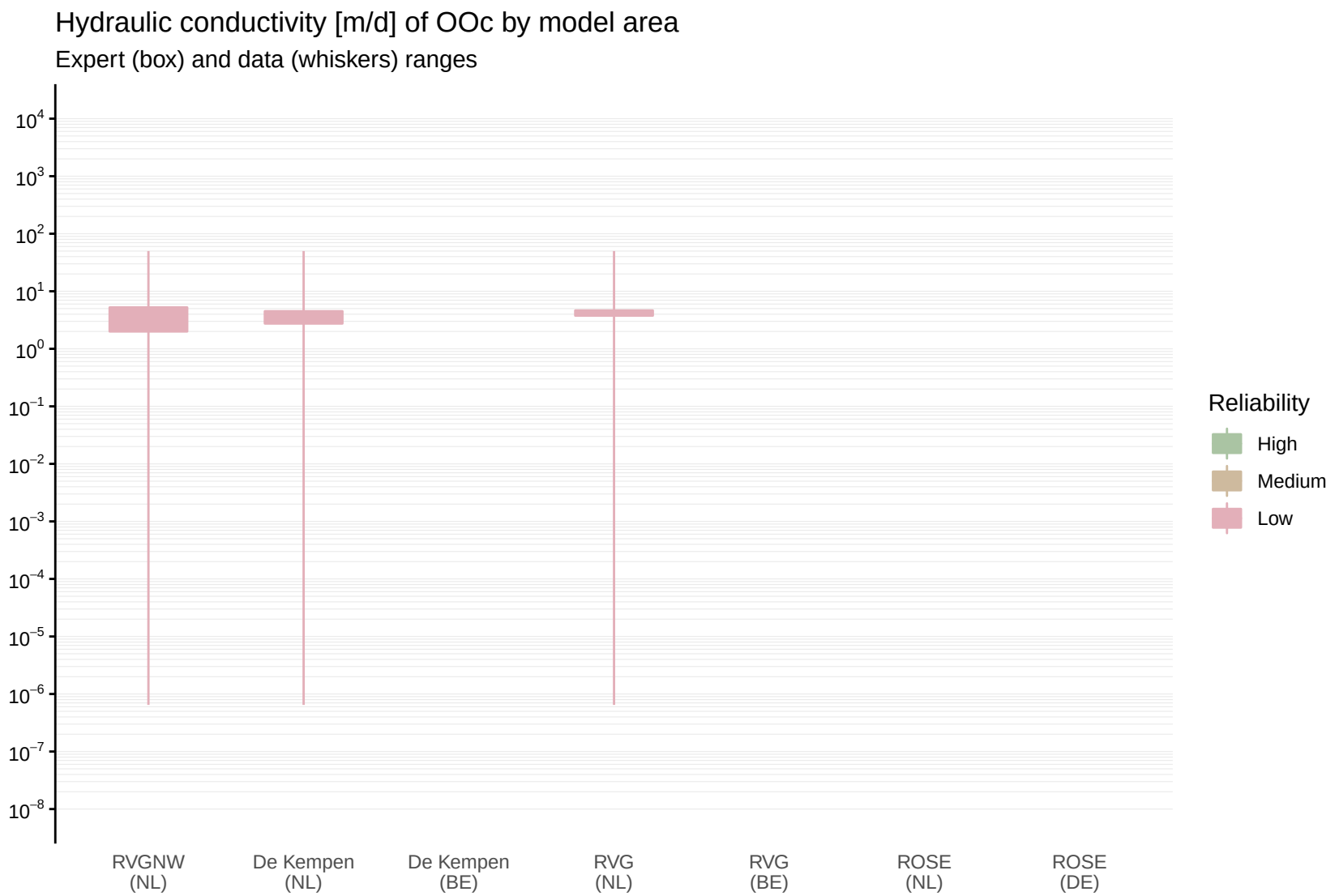
Hydraulic conductivity [m/d] of OOc by model area
Expert (box) and data (whiskers) ranges
10^{4}
10^{3}
10^{2}
10^{1}
10^{0}
10^{-1}
10^{-2}
10^{-3}
10^{-4}
10^{-5}
10^{-6}
10^{-7}
10^{-8}
RVGNW (NL)
De Kempen (NL)
De Kempen (BE)
RVG (NL)
RVG (BE)
ROSE (NL)
ROSE (DE)
Reliability
High
Medium
Low

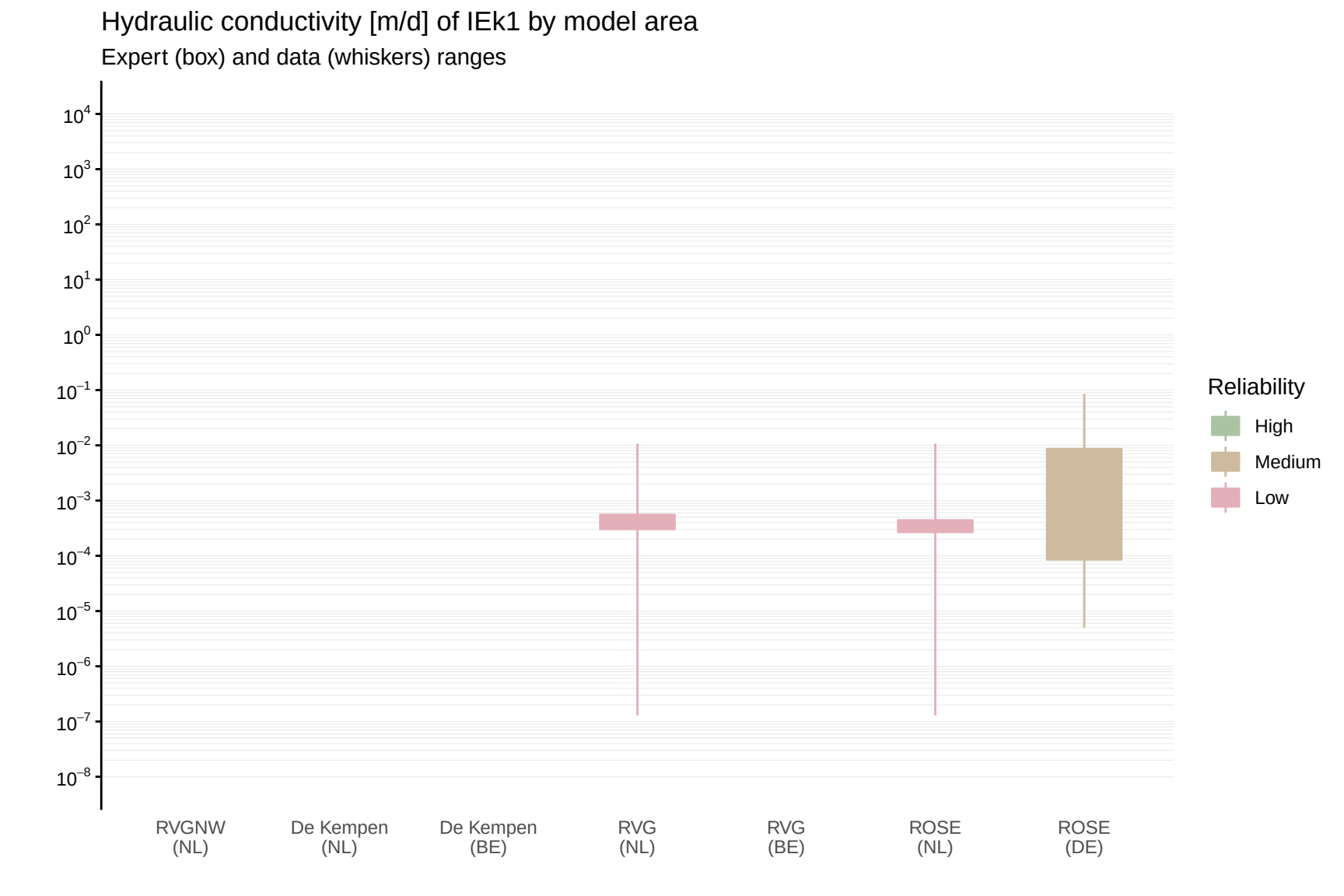
Hydraulic conductivity [m/d] of IEk1 by model area
Expert (box) and data (whiskers) ranges
10^{4}
10^{3}
10^{2}
10^{1}
10^{0}
10^{-1}
10^{-2}
10^{-3}
10^{-4}
10^{-5}
10^{-6}
10^{-7}
10^{-8}
RVGNW (NL)
De Kempen (NL)
De Kempen (BE)
RVG (NL)
RVG (BE)
ROSE (NL)
ROSE (DE)
Reliability
High
Medium
Low

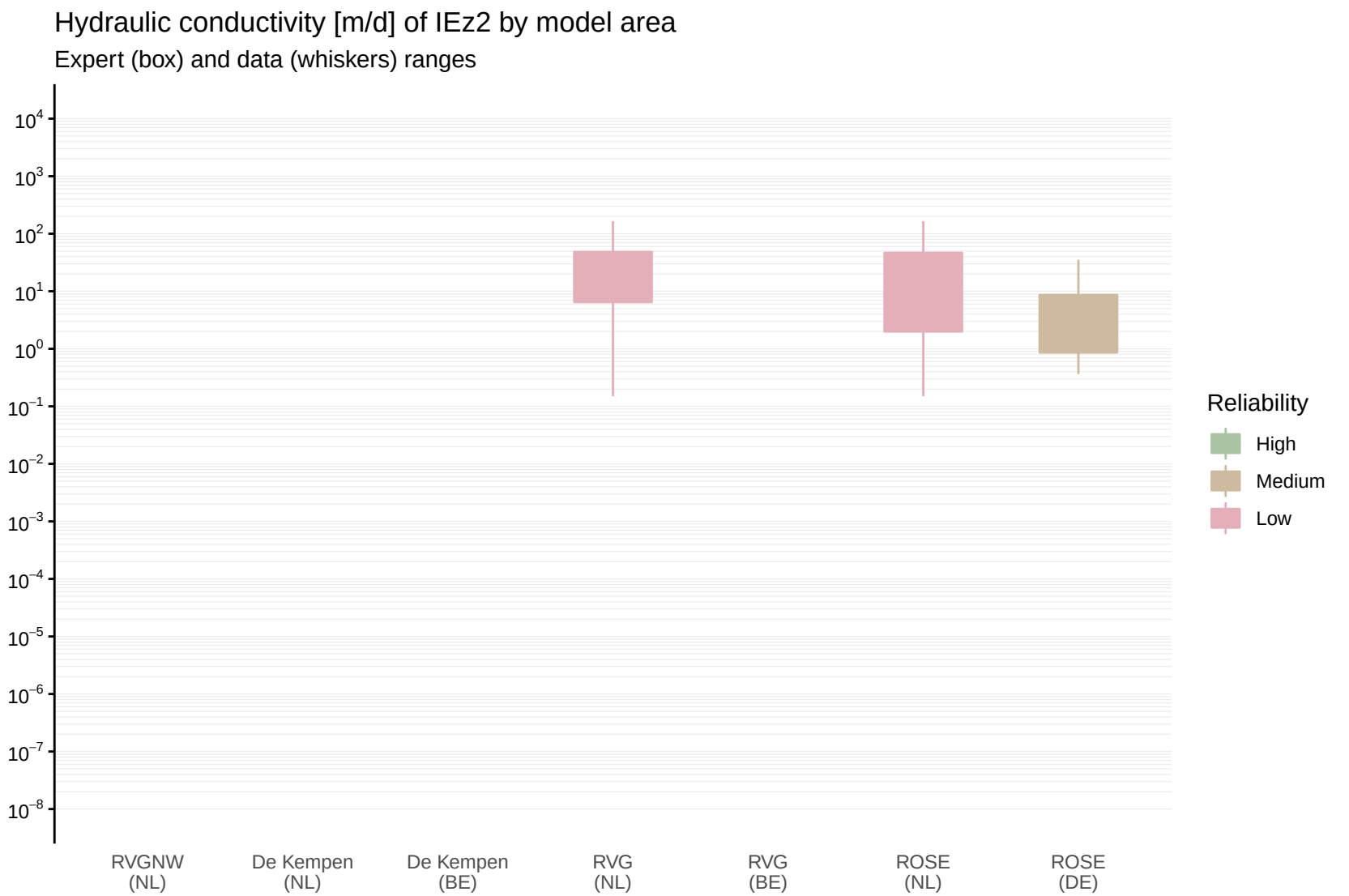
Hydraulic conductivity [m/d] of IEz2 by model area
Expert (box) and data (whiskers) ranges
10^{4}
10^{3}
10^{2}
10^{1}
10^{0}
10^{-1}
10^{-2}
10^{-3}
10^{-4}
10^{-5}
10^{-6}
10^{-7}
10^{-8}
RVGNW (NL)
De Kempen (NL)
De Kempen (BE)
RVG (NL)
RVG (BE)
ROSE (NL)
ROSE (DE)
Reliability
High
Medium
Low

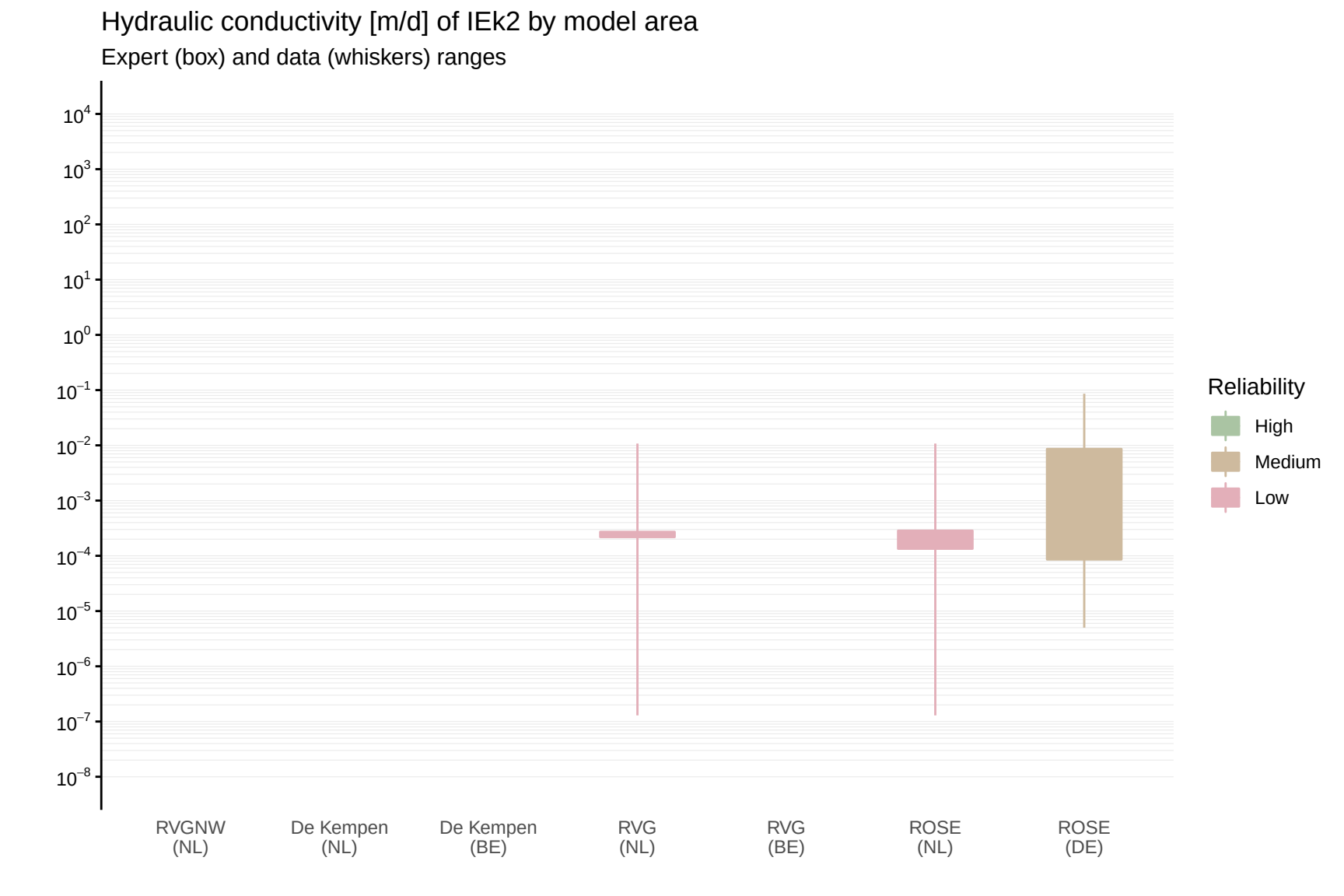
Hydraulic conductivity [m/d] of IEk2 by model area
Expert (box) and data (whiskers) ranges
10^{4}
10^{3}
10^{2}
10^{1}
10^{0}
10^{-1}
10^{-2}
10^{-3}
10^{-4}
10^{-5}
10^{-6}
10^{-7}
10^{-8}
RVGNW (NL)
De Kempen (NL)
De Kempen (BE)
RVG (NL)
RVG (BE)
ROSE (NL)
ROSE (DE)
Reliability
High
Medium
Low

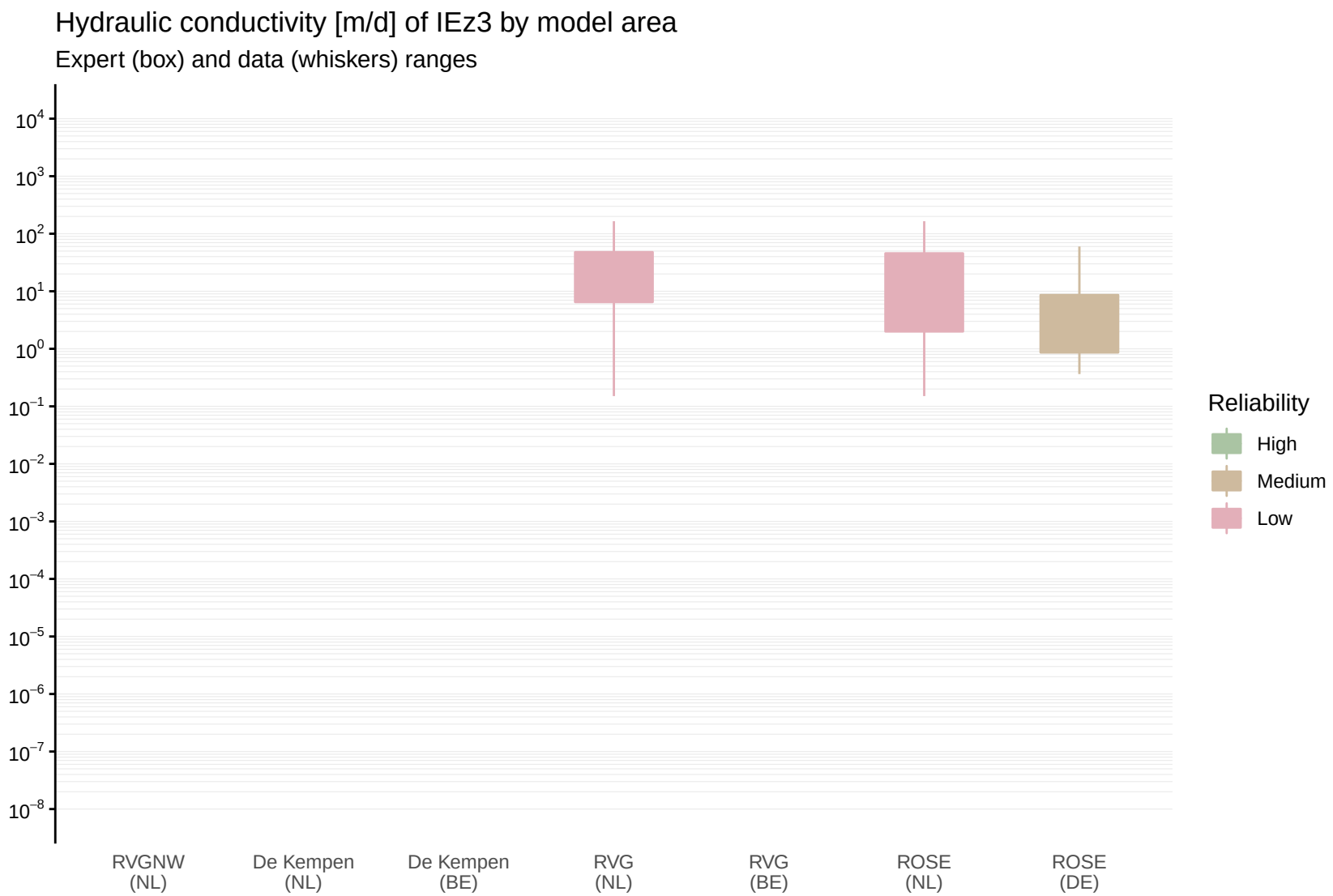
Hydraulic conductivity [m/d] of IEz3 by model area
Expert (box) and data (whiskers) ranges
10^{4}
10^{3}
10^{2}
10^{1}
10^{0}
10^{-1}
10^{-2}
10^{-3}
10^{-4}
10^{-5}
10^{-6}
10^{-7}
10^{-8}
RVGNW (NL)
De Kempen (NL)
De Kempen (BE)
RVG (NL)
RVG (BE)
ROSE (NL)
ROSE (DE)
Reliability
High
Medium
Low

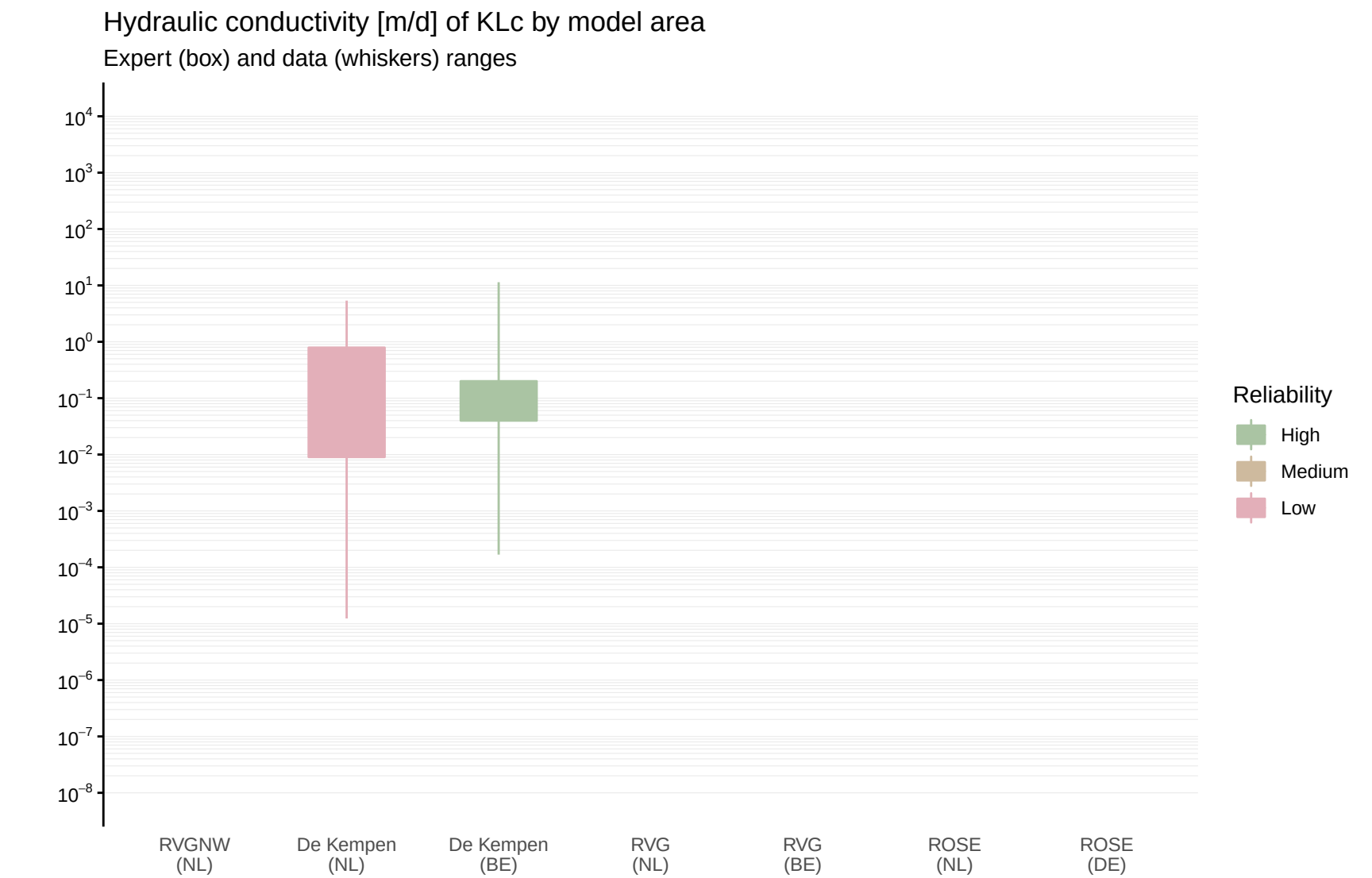
Hydraulic conductivity [m/d] of KLc by model area
Expert (box) and data (whiskers) ranges
10^{4}
10^{3}
10^{2}
10^{1}
10^{0}
10^{-1}
10^{-2}
10^{-3}
10^{-4}
10^{-5}
10^{-6}
10^{-7}
10^{-8}
RVGNW (NL)
De Kempen (NL)
De Kempen (BE)
RVG (NL)
RVG (BE)
ROSE (NL)
ROSE (DE)
Reliability
High
Medium
Low

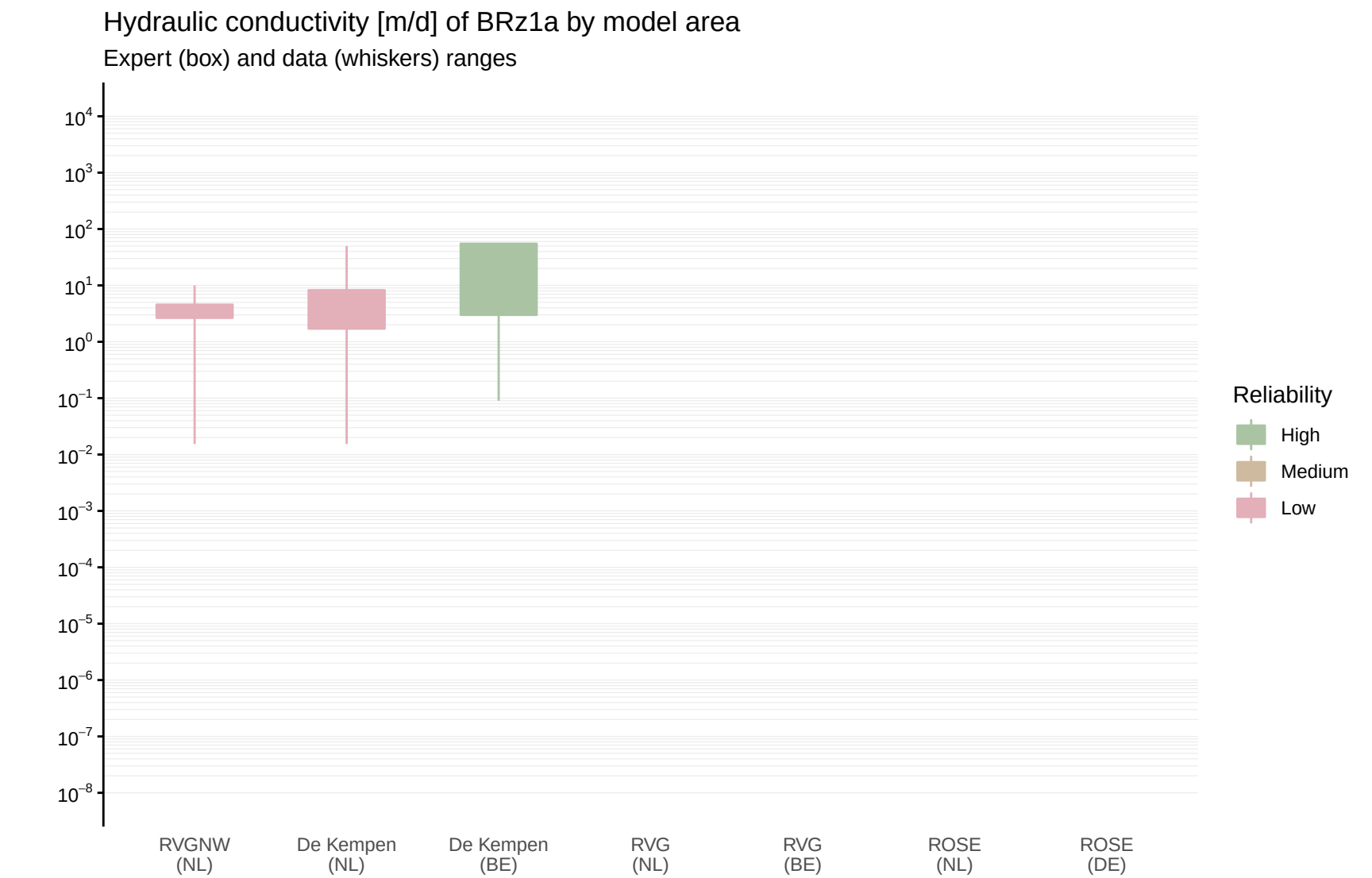
Hydraulic conductivity [m/d] of BRz1a by model area
Expert (box) and data (whiskers) ranges
10^{4}
10^{3}
10^{2}
10^{1}
10^{0}
10^{-1}
10^{-2}
10^{-3}
10^{-4}
10^{-5}
10^{-6}
10^{-7}
10^{-8}
RVGNW (NL)
De Kempen (NL)
De Kempen (BE)
RVG (NL)
RVG (BE)
ROSE (NL)
ROSE (DE)
Reliability
High
Medium
Low

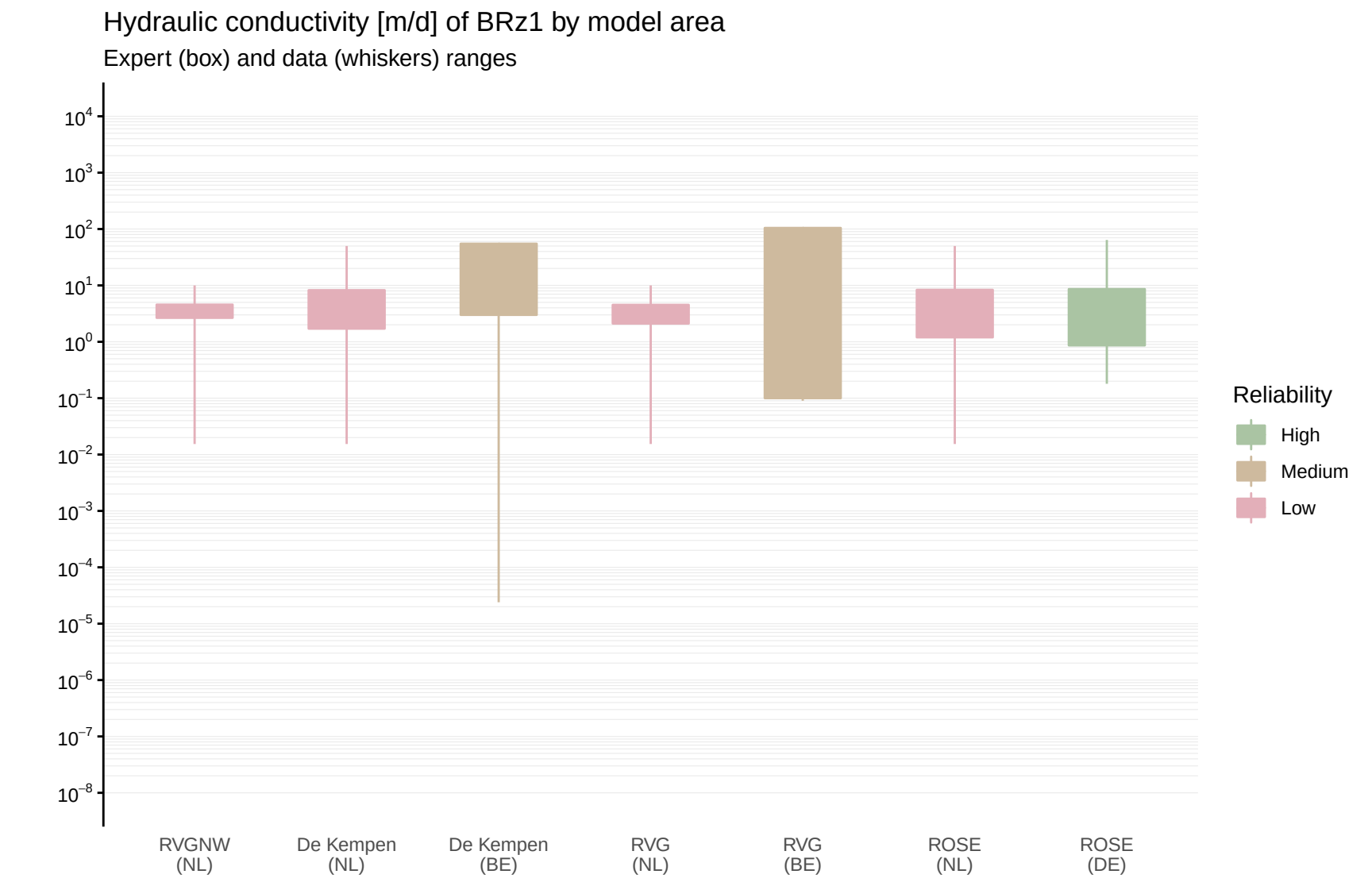
Hydraulic conductivity [m/d] of BRz1 by model area
Expert (box) and data (whiskers) ranges
10^{4}
10^{3}
10^{2}
10^{1}
10^{0}
10^{-1}
10^{-2}
10^{-3}
10^{-4}
10^{-5}
10^{-6}
10^{-7}
10^{-8}
RVGNW (NL)
De Kempen (NL)
De Kempen (BE)
RVG (NL)
RVG (BE)
ROSE (NL)
ROSE (DE)
Reliability
High
Medium
Low

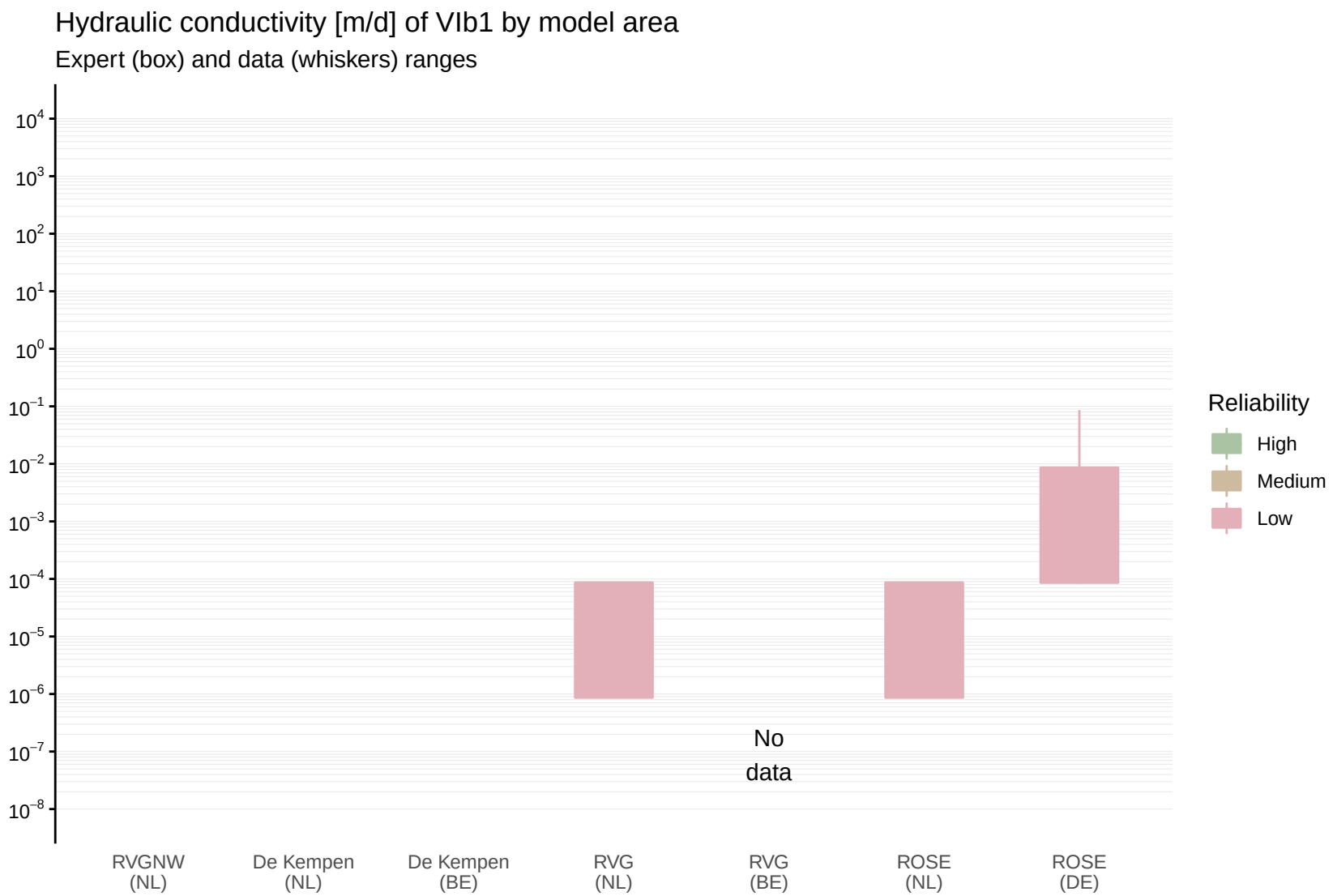
Hydraulic conductivity [m/d] of VIb1 by model area
Expert (box) and data (whiskers) ranges
10^{4}
10^{3}
10^{2}
10^{1}
10^{0}
10^{-1}
10^{-2}
10^{-3}
10^{-4}
10^{-5}
10^{-6}
10^{-7}
10^{-8}
No
data
RVGNW
(NL)
De Kempen
(NL)
De Kempen
(BE)
RVG
(NL)
RVG
(BE)
ROSE
(NL)
ROSE
(DE)
Reliability
High
Medium
Low

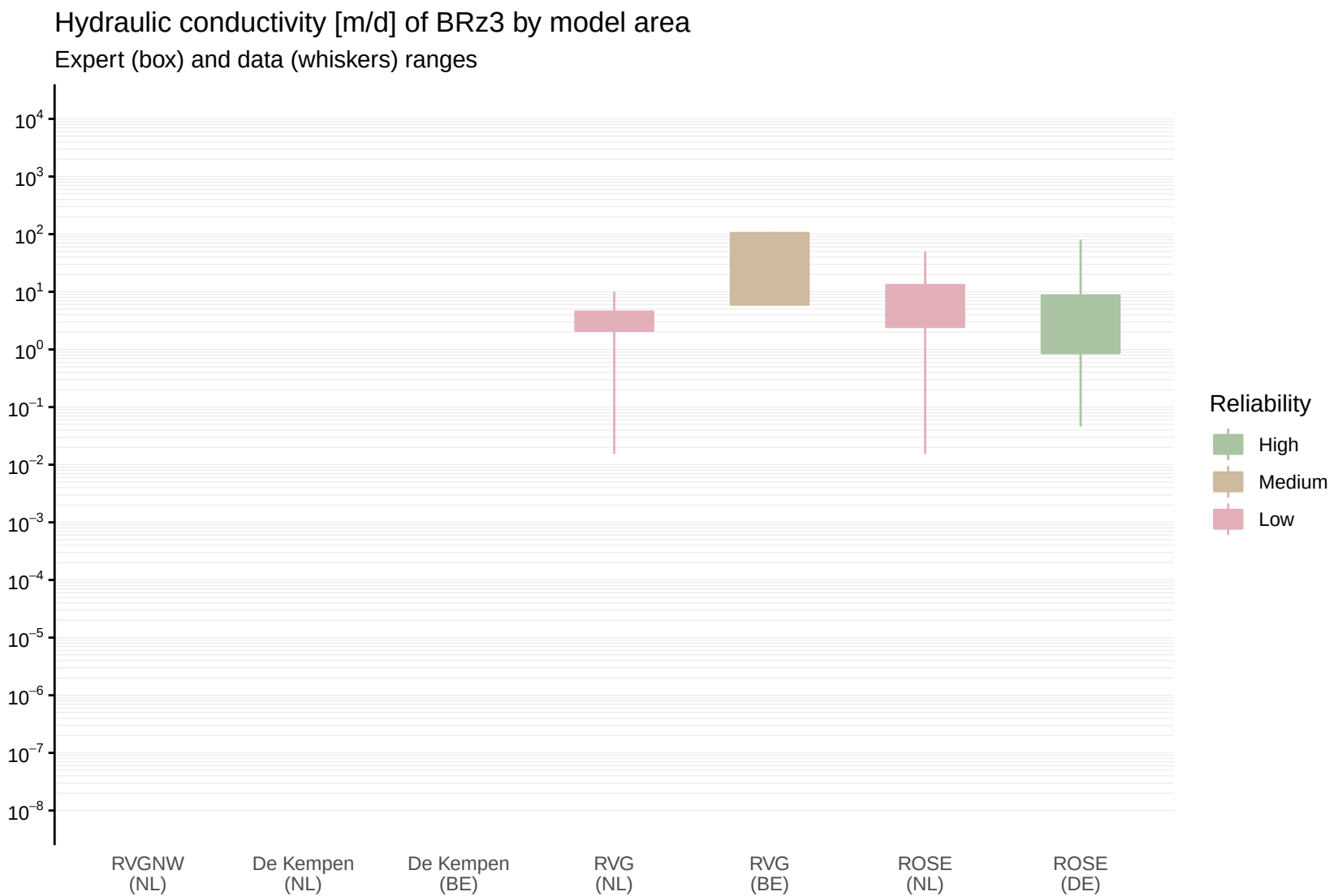
Hydraulic conductivity [m/d] of BRz3 by model area
Expert (box) and data (whiskers) ranges
10^{4}
10^{3}
10^{2}
10^{1}
10^{0}
10^{-1}
10^{-2}
10^{-3}
10^{-4}
10^{-5}
10^{-6}
10^{-7}
10^{-8}
RVGNW (NL)
De Kempen (NL)
De Kempen (BE)
RVG (NL)
RVG (BE)
ROSE (NL)
ROSE (DE)
Reliability
High
Medium
Low

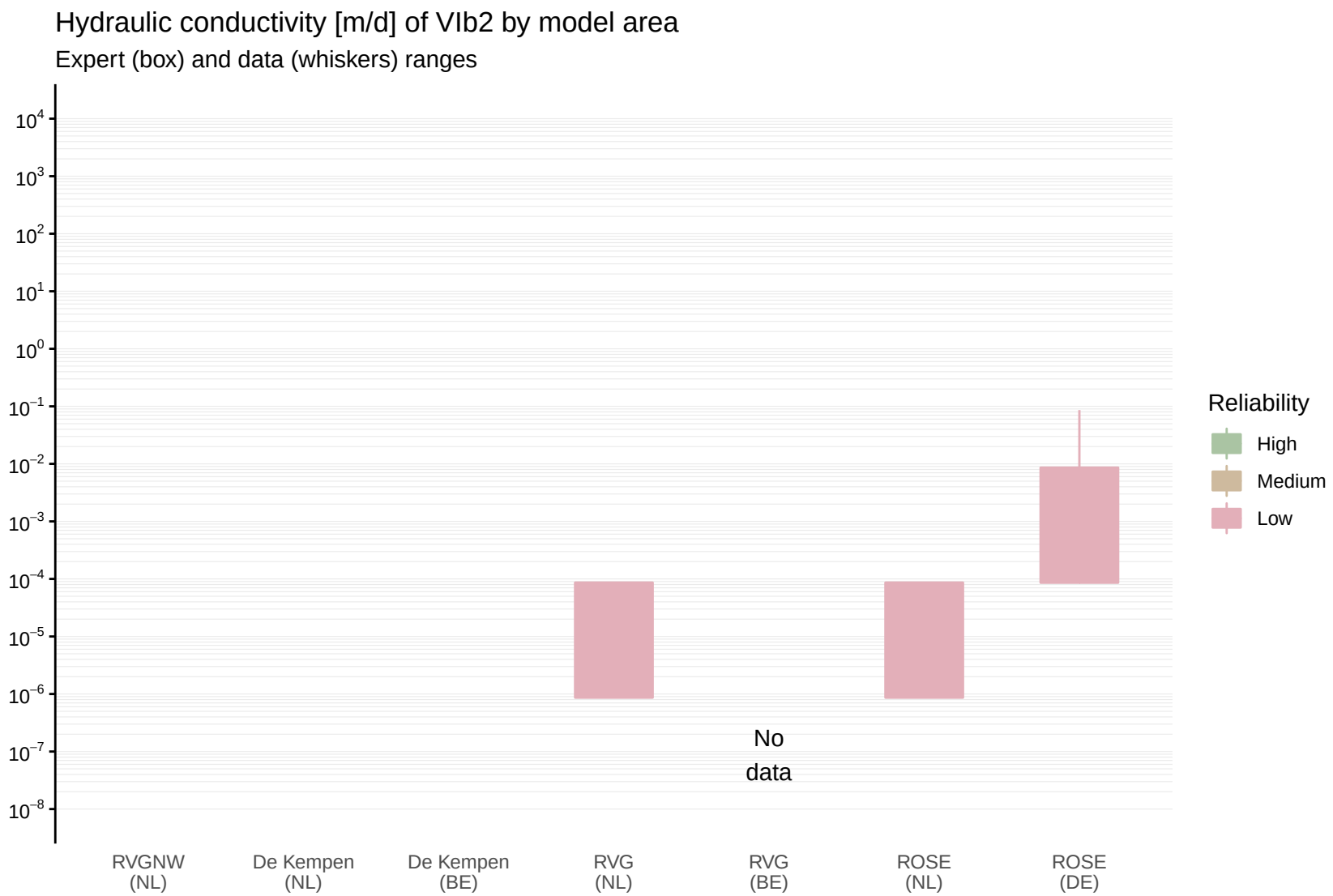
Hydraulic conductivity [m/d] of VIb2 by model area
Expert (box) and data (whiskers) ranges
10^{4}
10^{3}
10^{2}
10^{1}
10^{0}
10^{-1}
10^{-2}
10^{-3}
10^{-4}
10^{-5}
10^{-6}
10^{-7}
10^{-8}
No
data
RVGNW
(NL)
De Kempen
(NL)
De Kempen
(BE)
RVG
(NL)
RVG
(BE)
ROSE
(NL)
ROSE
(DE)
Reliability
High
Medium
Low

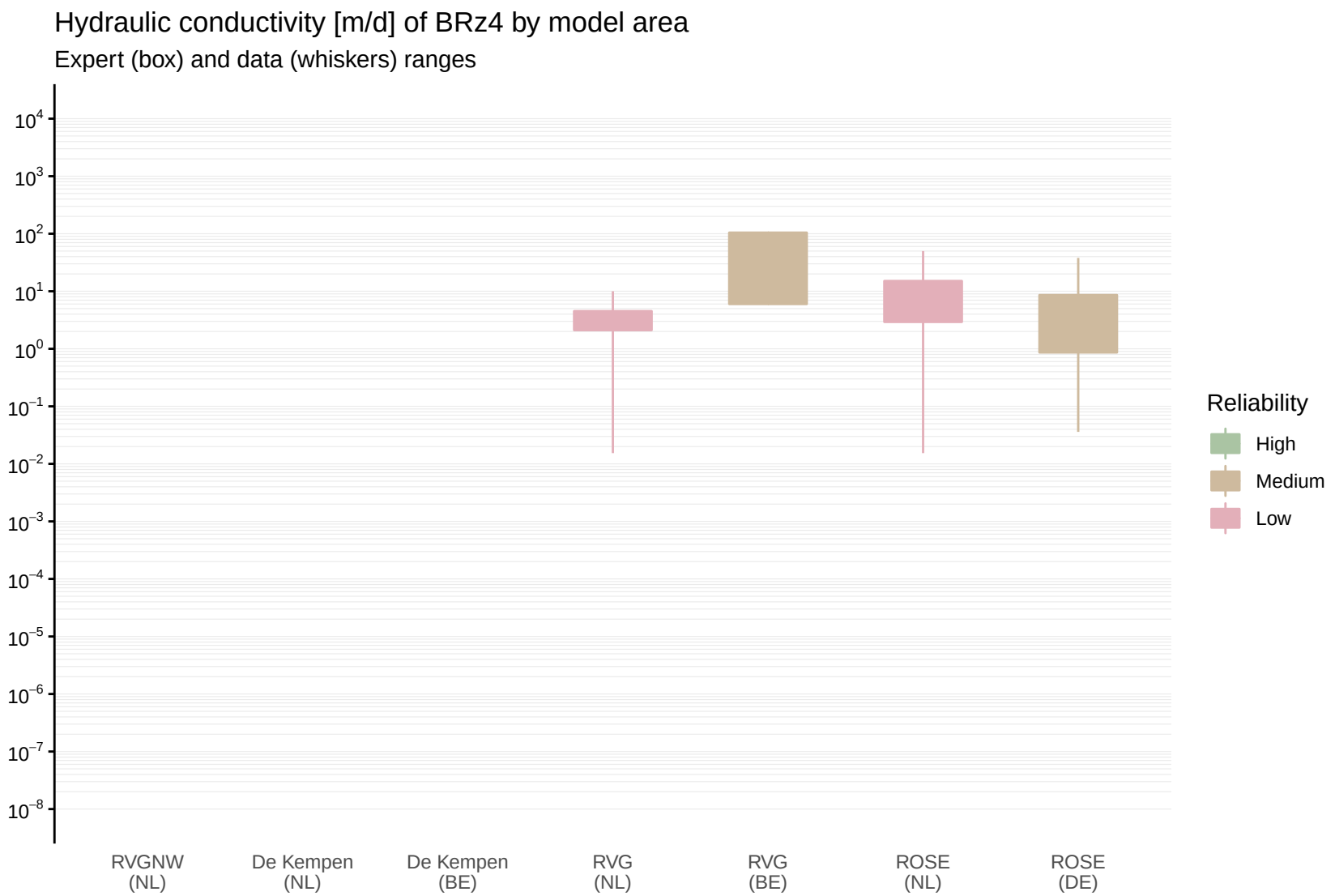
Hydraulic conductivity [m/d] of BRz4 by model area
Expert (box) and data (whiskers) ranges
10^{4}
10^{3}
10^{2}
10^{1}
10^{0}
10^{-1}
10^{-2}
10^{-3}
10^{-4}
10^{-5}
10^{-6}
10^{-7}
10^{-8}
RVGNW (NL)
De Kempen (NL)
De Kempen (BE)
RVG (NL)
RVG (BE)
ROSE (NL)
ROSE (DE)
Reliability
High
Medium
Low

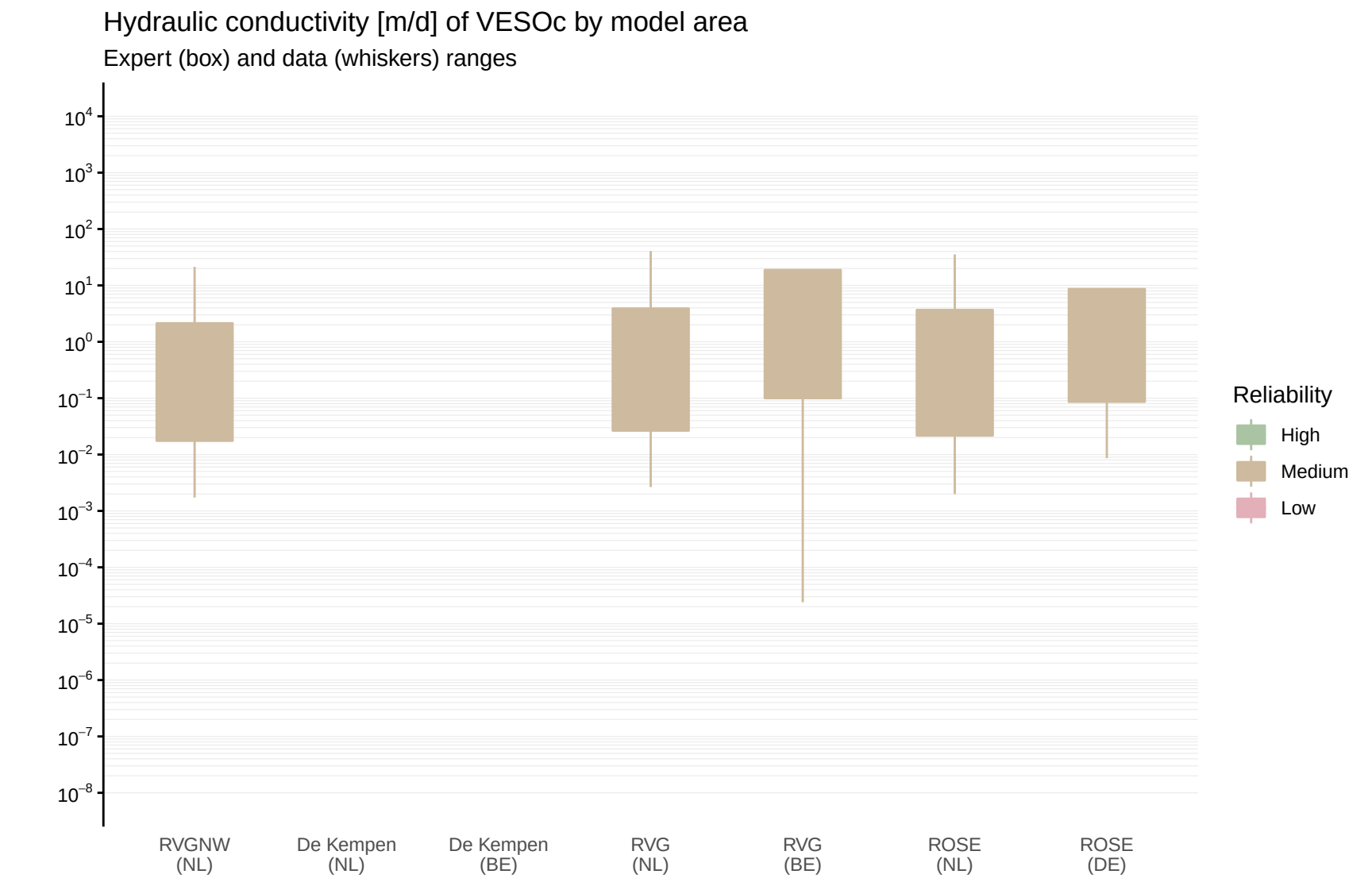
Hydraulic conductivity [m/d] of VESOc by model area
Expert (box) and data (whiskers) ranges
10^{4}
10^{3}
10^{2}
10^{1}
10^{0}
10^{-1}
10^{-2}
10^{-3}
10^{-4}
10^{-5}
10^{-6}
10^{-7}
10^{-8}
RVGNW (NL)
De Kempen (NL)
De Kempen (BE)
RVG (NL)
RVG (BE)
ROSE (NL)
ROSE (DE)
Reliability
High
Medium
Low

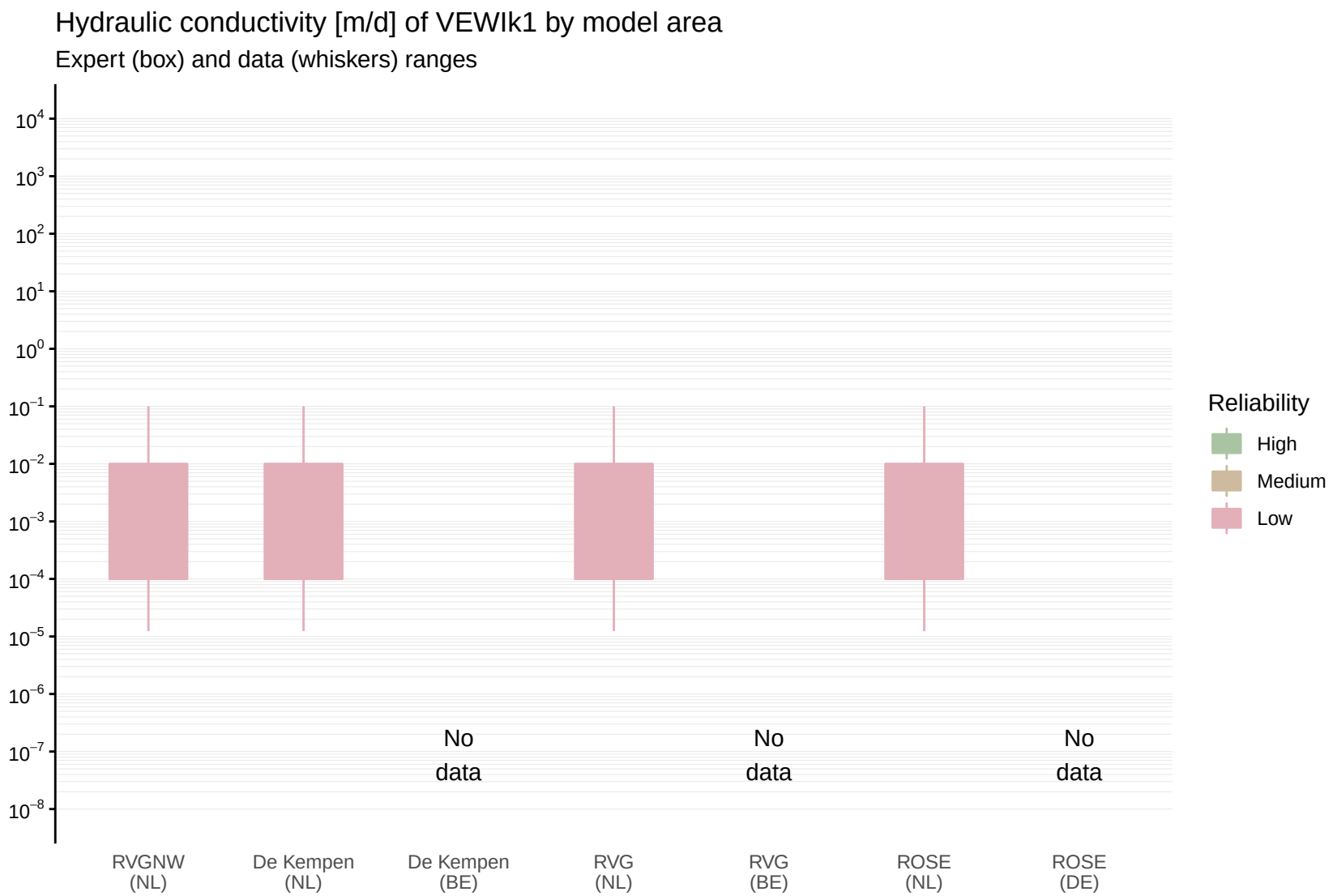
Hydraulic conductivity [m/d] of VEWIk1 by model area
Expert (box) and data (whiskers) ranges
10^{4}
10^{3}
10^{2}
10^{1}
10^{0}
10^{-1}
10^{-2}
10^{-3}
10^{-4}
10^{-5}
10^{-6}
10^{-7}
10^{-8}
No data
No data
No data
RVGNW (NL)
De Kempen (NL)
De Kempen (BE)
RVG (NL)
RVG (BE)
ROSE (NL)
ROSE (DE)
Reliability
High
Medium
Low

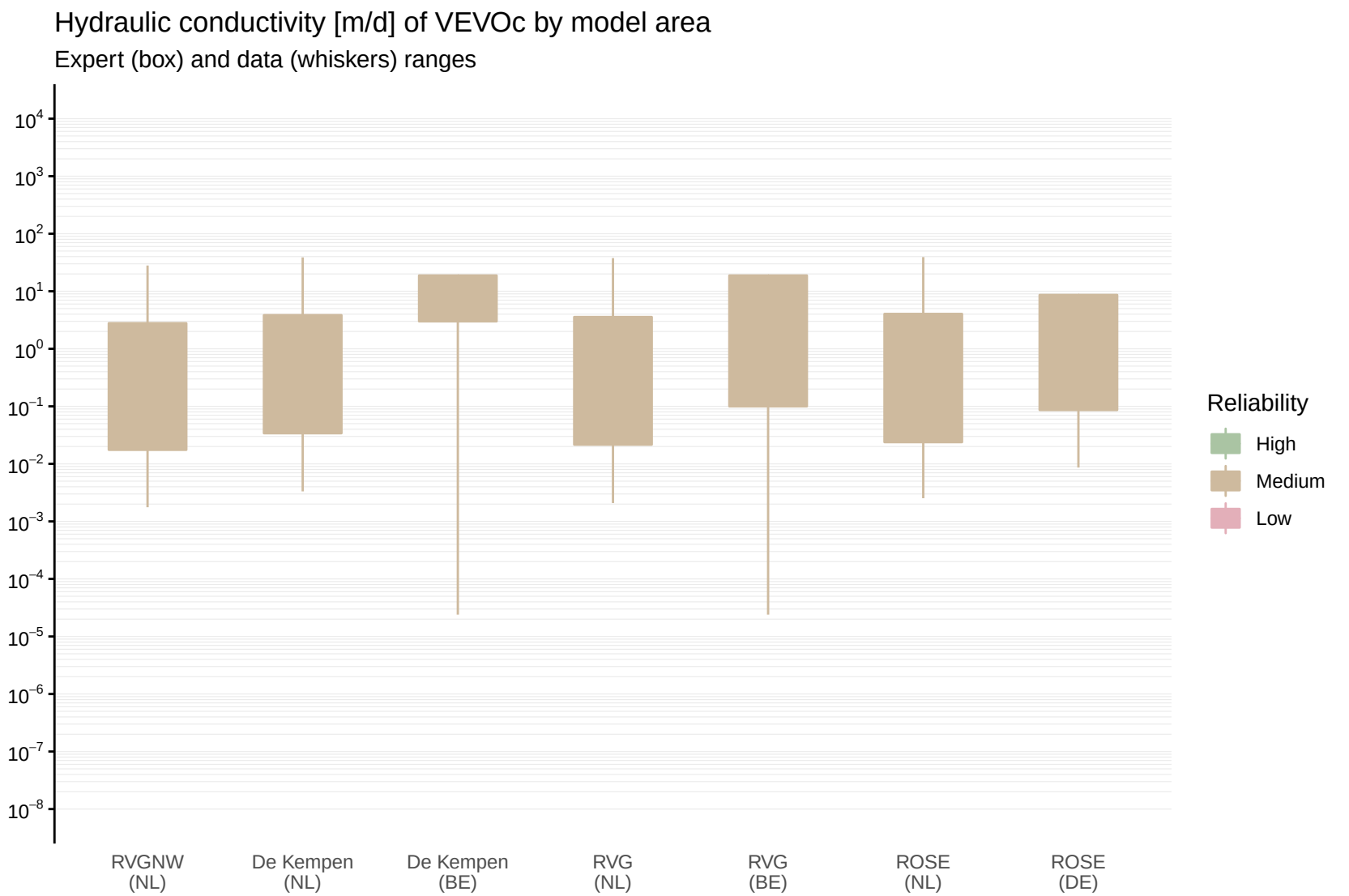
Hydraulic conductivity [m/d] of VEVOc by model area
Expert (box) and data (whiskers) ranges
10^{4}
10^{3}
10^{2}
10^{1}
10^{0}
10^{-1}
10^{-2}
10^{-3}
10^{-4}
10^{-5}
10^{-6}
10^{-7}
10^{-8}
RVGNW (NL)
De Kempen (NL)
De Kempen (BE)
RVG (NL)
RVG (BE)
ROSE (NL)
ROSE (DE)
Reliability
High
Medium
Low

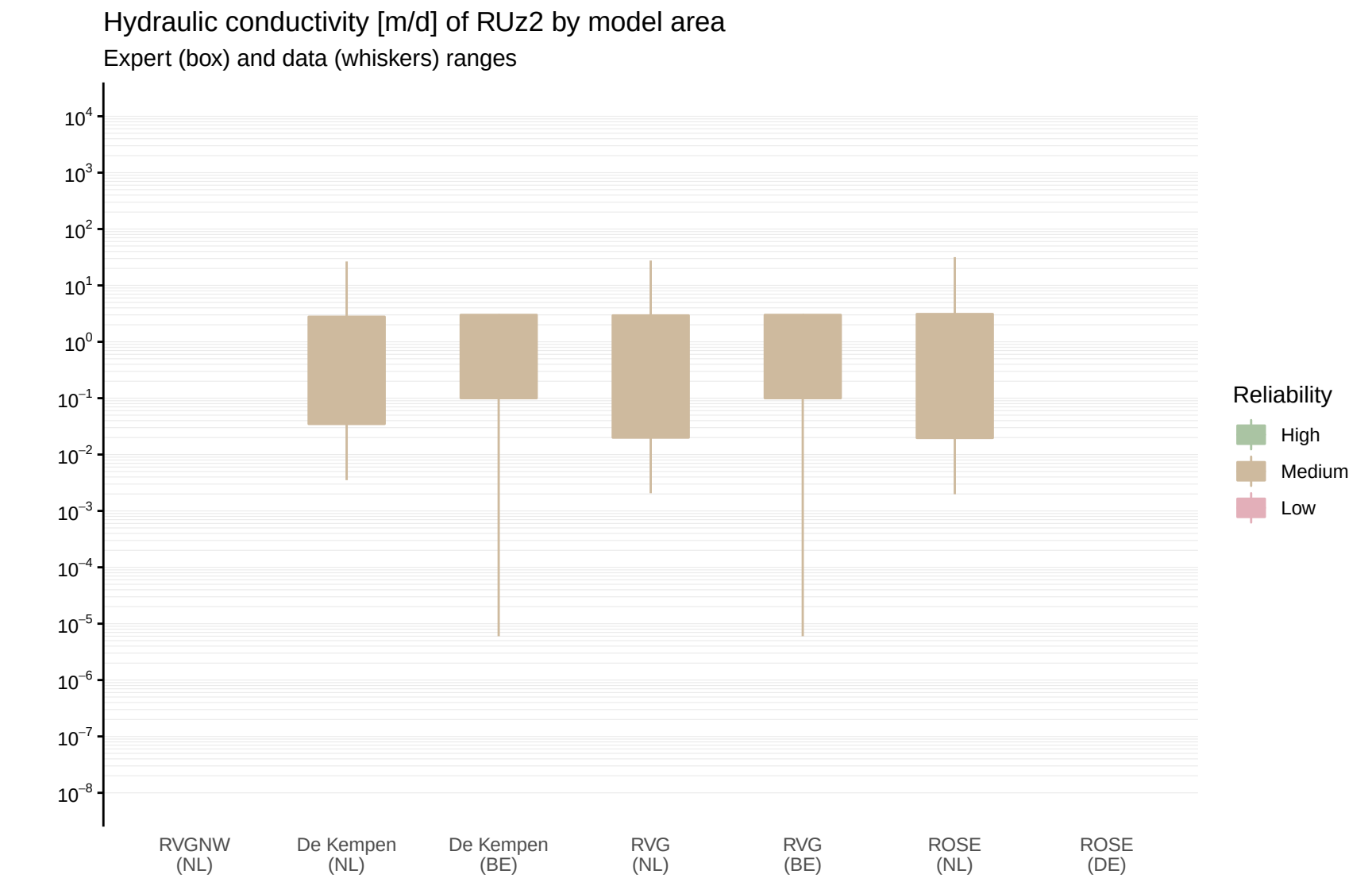
Hydraulic conductivity [m/d] of RUz2 by model area
Expert (box) and data (whiskers) ranges
10^{4}
10^{3}
10^{2}
10^{1}
10^{0}
10^{-1}
10^{-2}
10^{-3}
10^{-4}
10^{-5}
10^{-6}
10^{-7}
10^{-8}
RVGNW (NL)
De Kempen (NL)
De Kempen (BE)
RVG (NL)
RVG (BE)
ROSE (NL)
ROSE (DE)
Reliability
High
Medium
Low

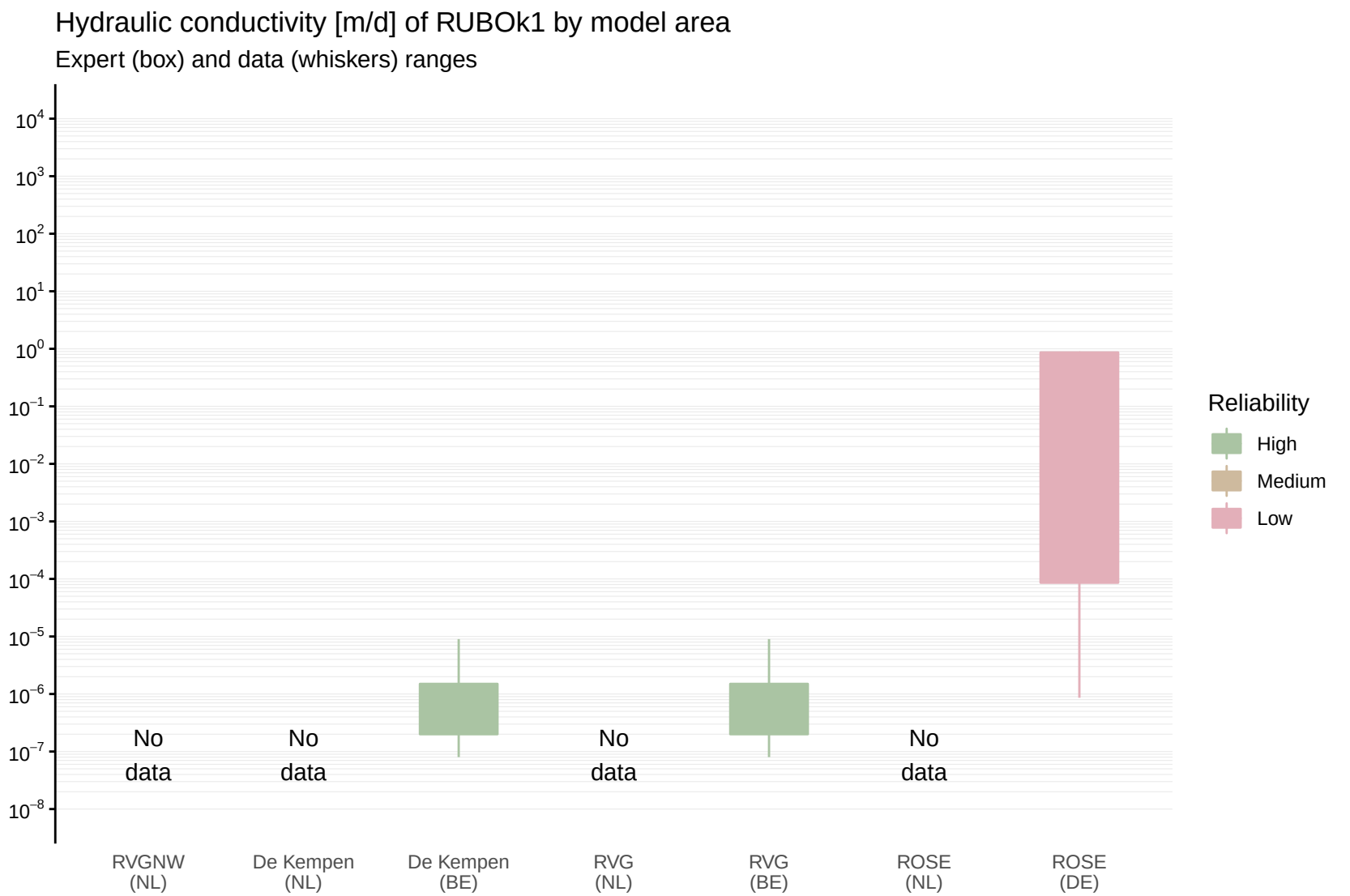
Hydraulic conductivity [m/d] of RUBOk1 by model area
Expert (box) and data (whiskers) ranges
10^{4}
10^{3}
10^{2}
10^{1}
10^{0}
10^{-1}
10^{-2}
10^{-3}
10^{-4}
10^{-5}
10^{-6}
10^{-7}
10^{-8}
No data
No data
No data
No data
RVGNW (NL)
De Kempen (NL)
De Kempen (BE)
RVG (NL)
RVG (BE)
ROSE (NL)
ROSE (DE)
Reliability
High
Medium
Low

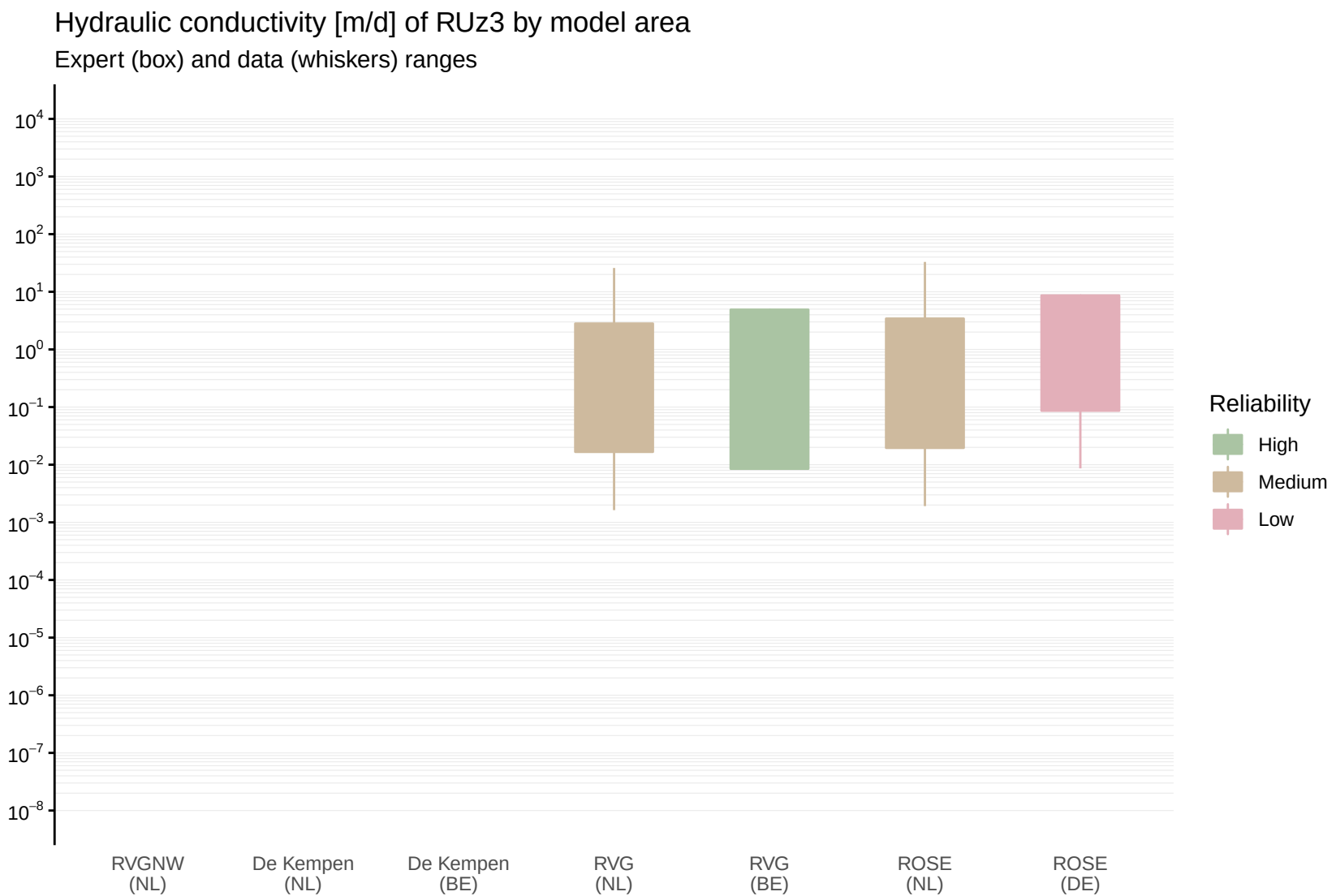
Hydraulic conductivity [m/d] of RUz3 by model area
Expert (box) and data (whiskers) ranges
10^{4}
10^{3}
10^{2}
10^{1}
10^{0}
10^{-1}
10^{-2}
10^{-3}
10^{-4}
10^{-5}
10^{-6}
10^{-7}
10^{-8}
RVGNW (NL)
De Kempen (NL)
De Kempen (BE)
RVG (NL)
RVG (BE)
ROSE (NL)
ROSE (DE)
Reliability
High
Medium
Low

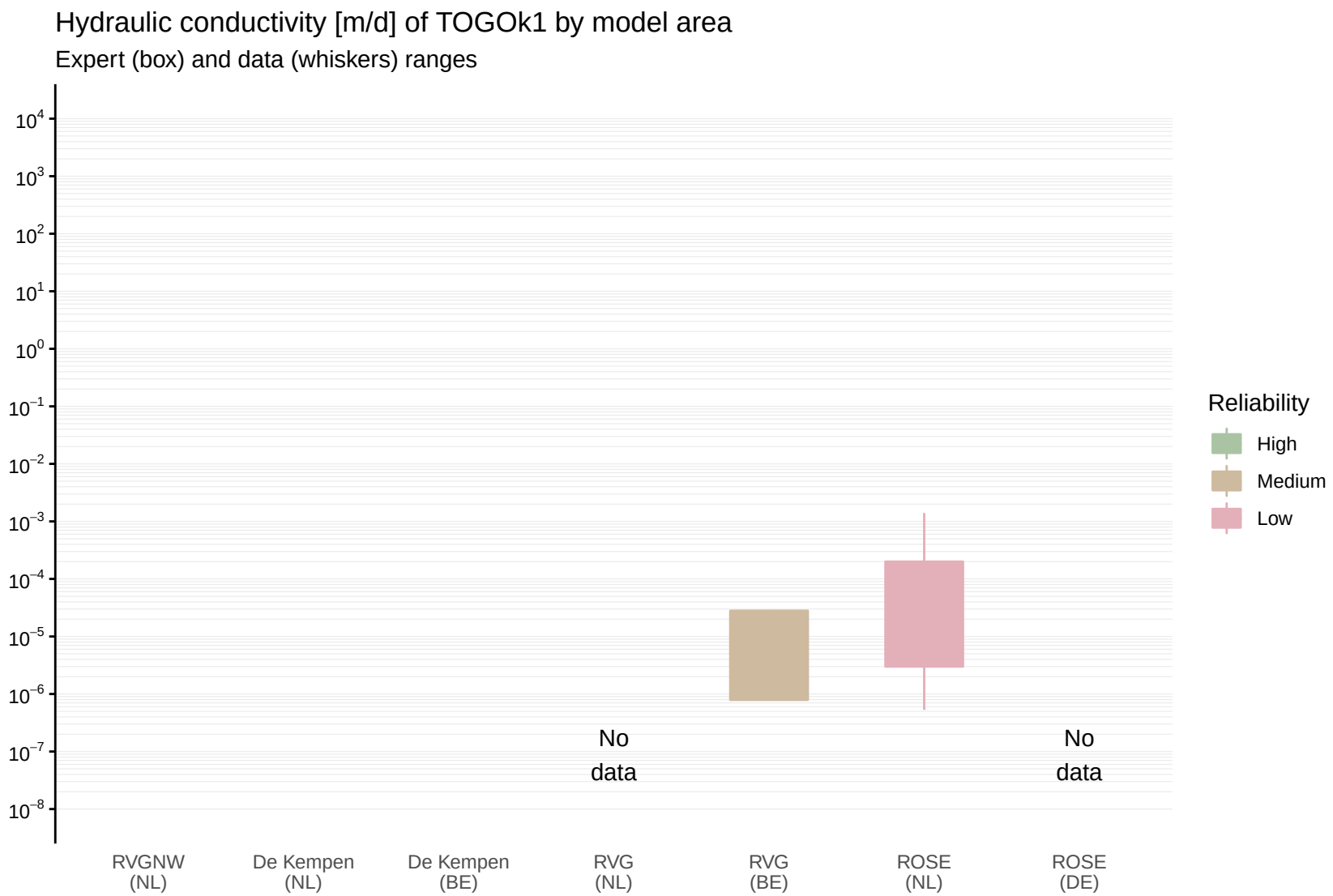
Hydraulic conductivity [m/d] of TOGOk1 by model area
Expert (box) and data (whiskers) ranges
10^{4}
10^{3}
10^{2}
10^{1}
10^{0}
10^{-1}
10^{-2}
10^{-3}
10^{-4}
10^{-5}
10^{-6}
10^{-7}
10^{-8}
No data
No data
RVGNW (NL)
De Kempen (NL)
De Kempen (BE)
RVG (NL)
RVG (BE)
ROSE (NL)
ROSE (DE)
Reliability
High
Medium
Low

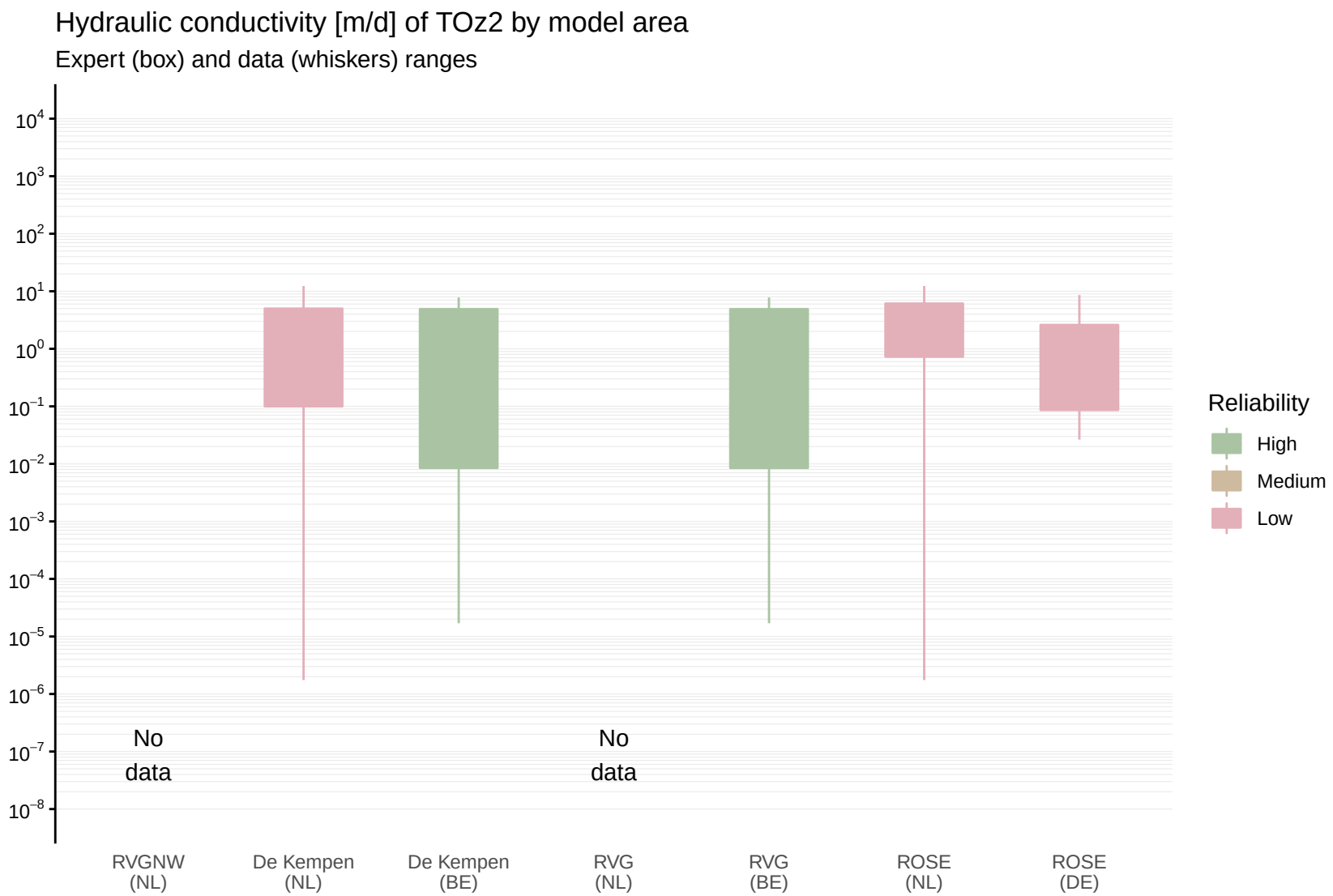
Hydraulic conductivity [m/d] of TOz2 by model area
Expert (box) and data (whiskers) ranges
10^{4}
10^{3}
10^{2}
10^{1}
10^{0}
10^{-1}
10^{-2}
10^{-3}
10^{-4}
10^{-5}
10^{-6}
10^{-7}
10^{-8}
No data
No data
RVGNW (NL)
De Kempen (NL)
De Kempen (BE)
RVG (NL)
RVG (BE)
ROSE (NL)
ROSE (DE)
Reliability
High
Medium
Low

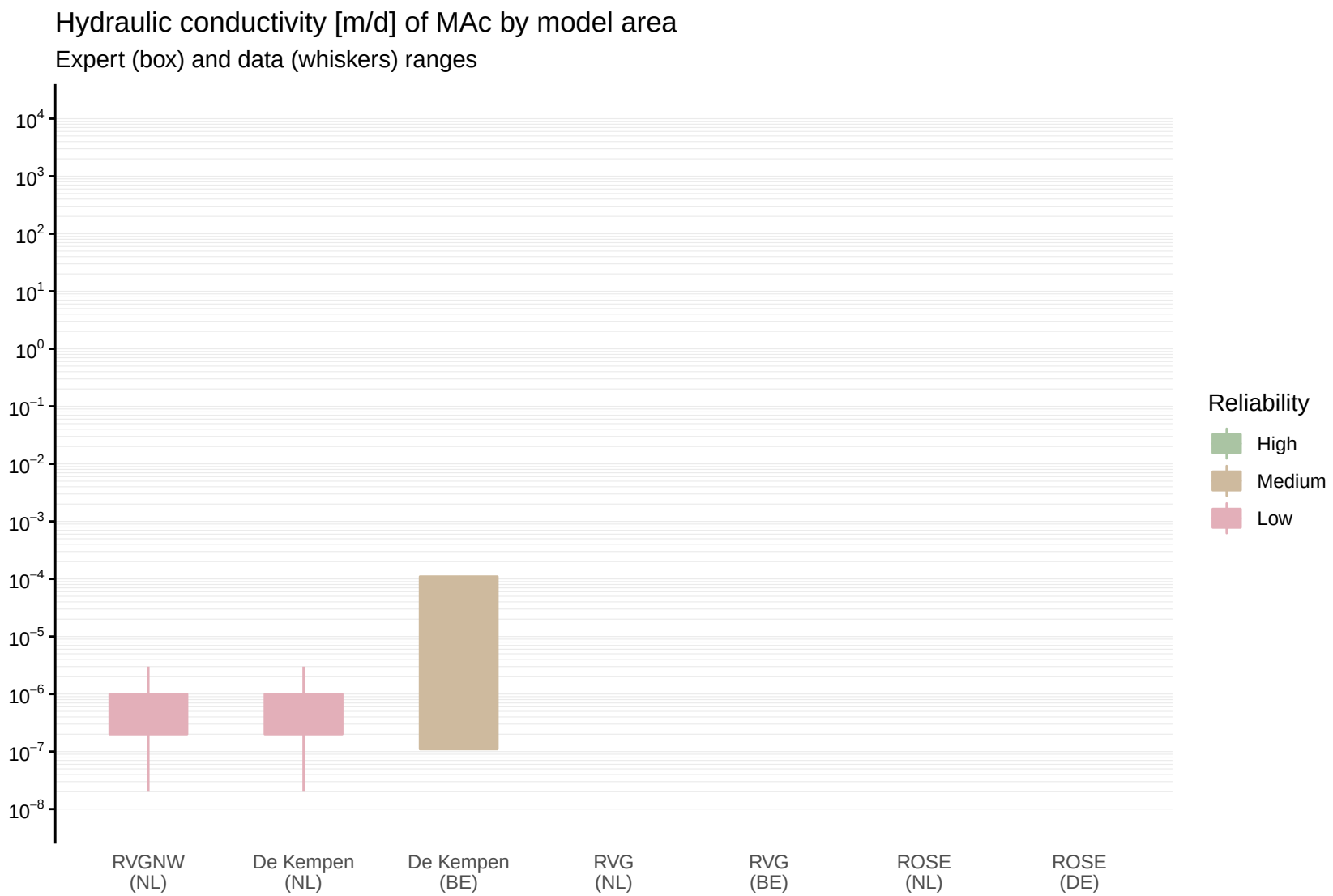
Hydraulic conductivity [m/d] of MAc by model area
Expert (box) and data (whiskers) ranges
10^{4}
10^{3}
10^{2}
10^{1}
10^{0}
10^{-1}
10^{-2}
10^{-3}
10^{-4}
10^{-5}
10^{-6}
10^{-7}
10^{-8}
RVGNW (NL)
De Kempen (NL)
De Kempen (BE)
RVG (NL)
RVG (BE)
ROSE (NL)
ROSE (DE)
Reliability
High
Medium
Low

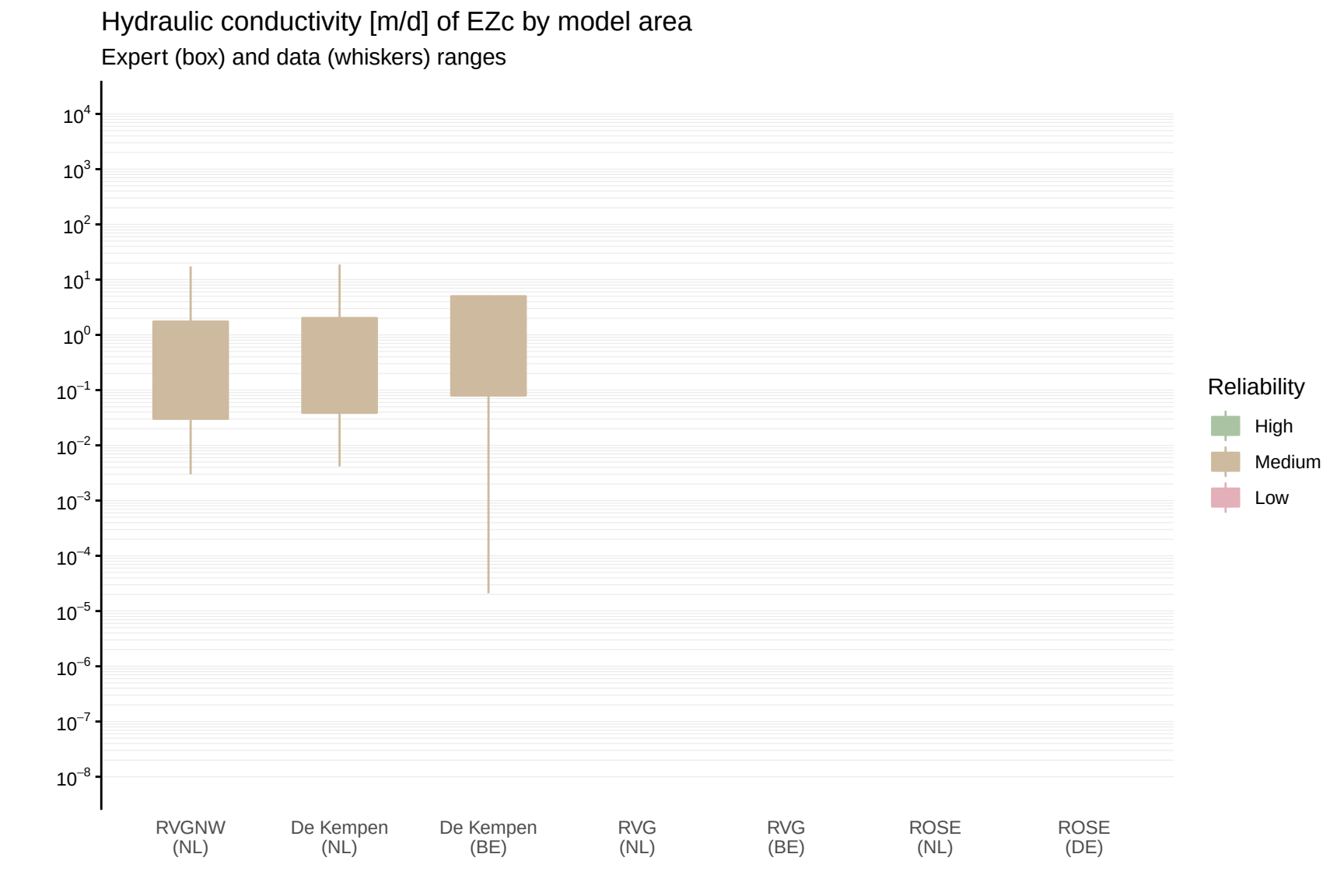
Hydraulic conductivity [m/d] of EZc by model area
Expert (box) and data (whiskers) ranges
10^{4}
10^{3}
10^{2}
10^{1}
10^{0}
10^{-1}
10^{-2}
10^{-3}
10^{-4}
10^{-5}
10^{-6}
10^{-7}
10^{-8}
RVGNW (NL)
De Kempen (NL)
De Kempen (BE)
RVG (NL)
RVG (BE)
ROSE (NL)
ROSE (DE)
Reliability
High
Medium
Low

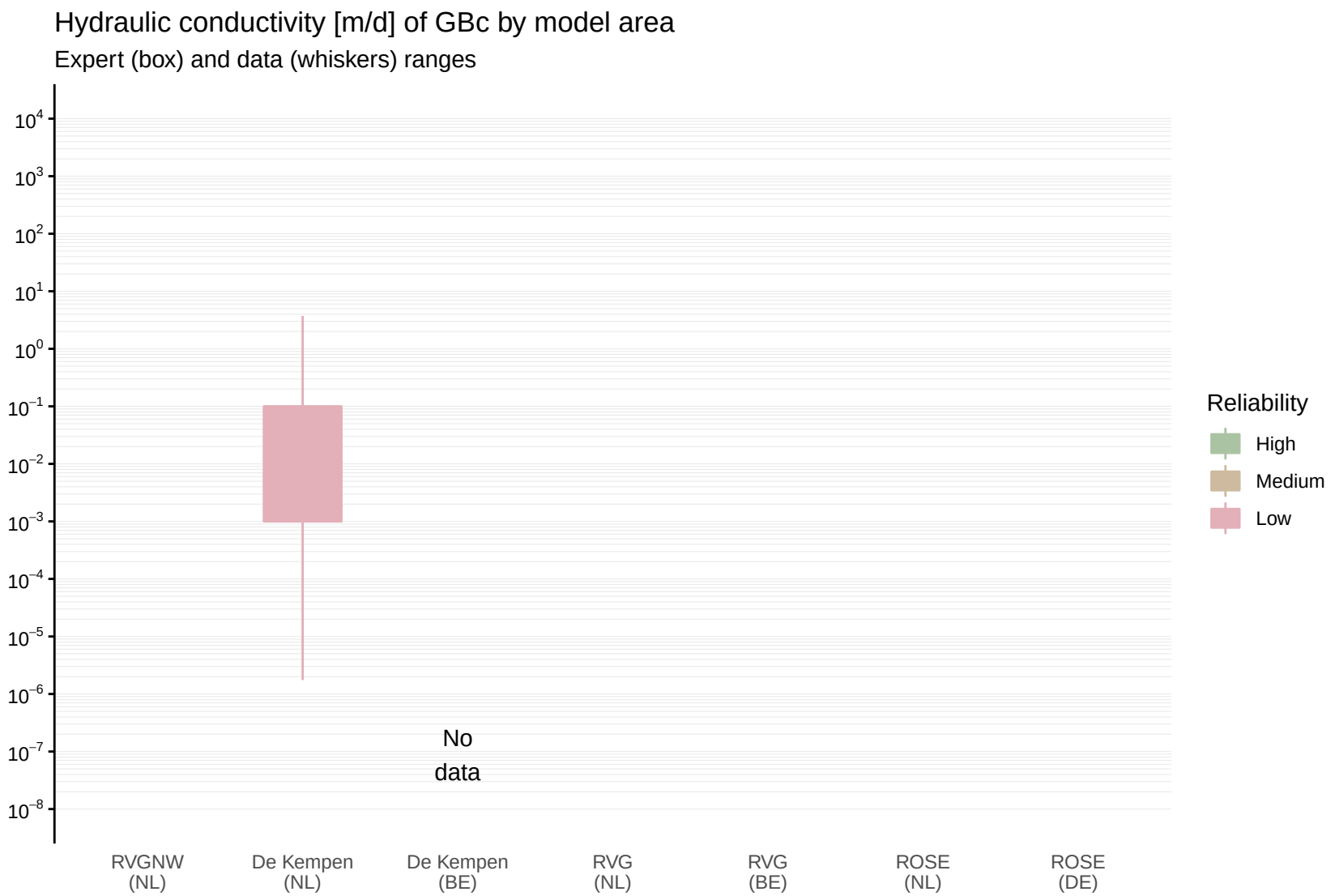
Hydraulic conductivity [m/d] of GBc by model area
Expert (box) and data (whiskers) ranges
10^{4}
10^{3}
10^{2}
10^{1}
10^{0}
10^{-1}
10^{-2}
10^{-3}
10^{-4}
10^{-5}
10^{-6}
10^{-7}
10^{-8}
No data
RVGNW (NL)
De Kempen (NL)
De Kempen (BE)
RVG (NL)
RVG (BE)
ROSE (NL)
ROSE (DE)
Reliability
High
Medium
Low

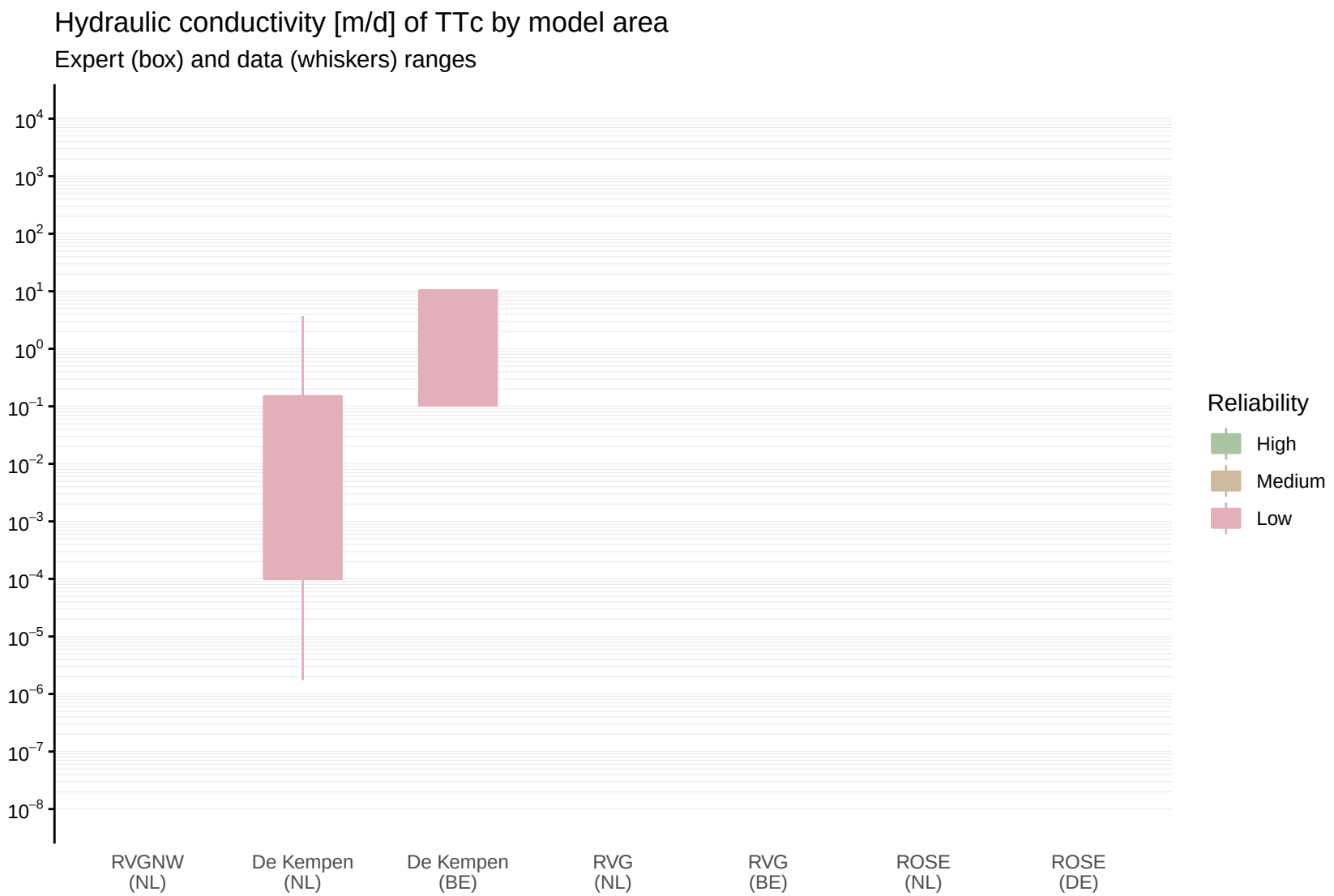
Hydraulic conductivity [m/d] of TTc by model area
Expert (box) and data (whiskers) ranges
10^{4}
10^{3}
10^{2}
10^{1}
10^{0}
10^{-1}
10^{-2}
10^{-3}
10^{-4}
10^{-5}
10^{-6}
10^{-7}
10^{-8}
RVGNW (NL)
De Kempen (NL)
De Kempen (BE)
RVG (NL)
RVG (BE)
ROSE (NL)
ROSE (DE)
Reliability
High
Medium
Low

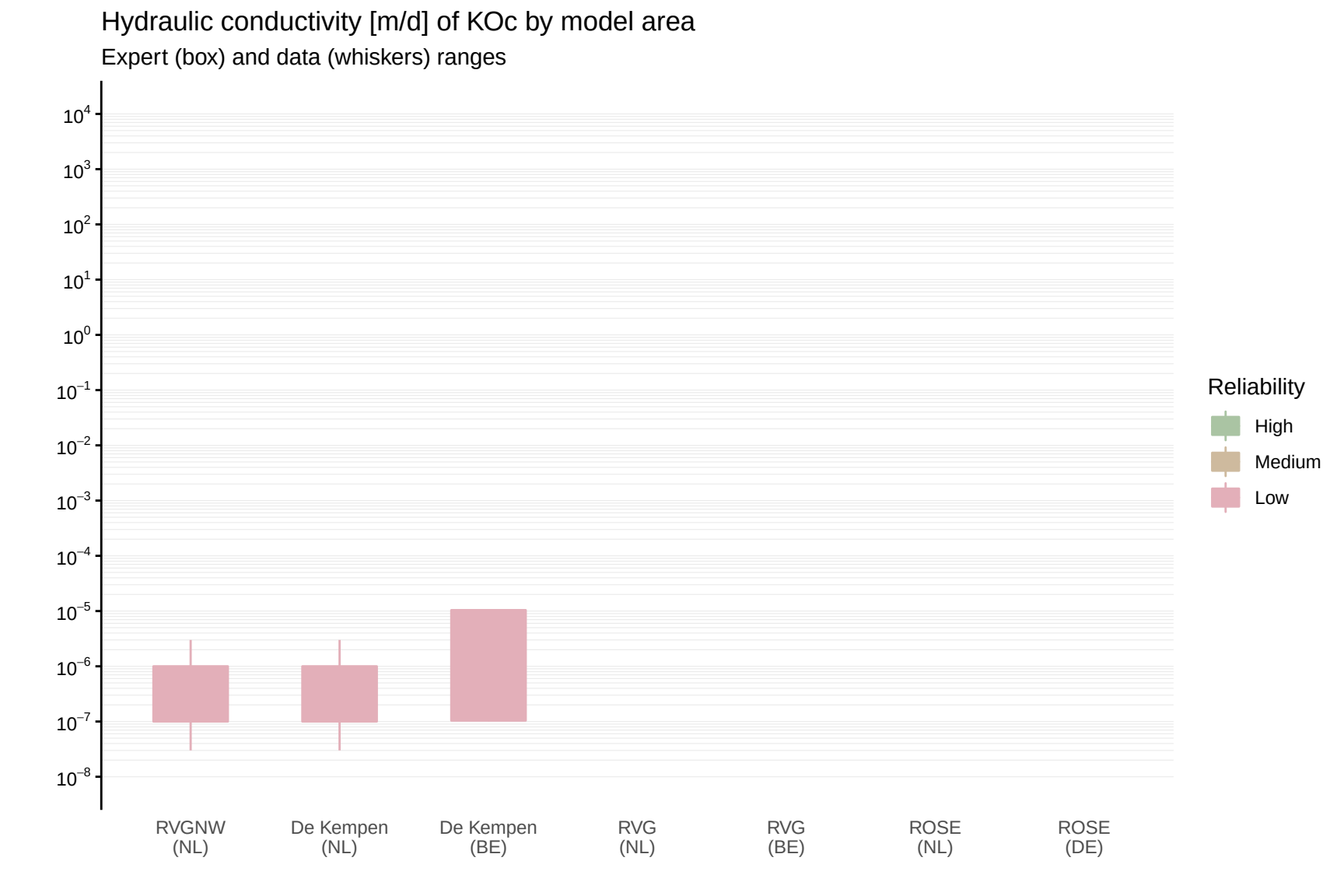
Hydraulic conductivity [m/d] of KOc by model area
Expert (box) and data (whiskers) ranges
10^{4}
10^{3}
10^{2}
10^{1}
10^{0}
10^{-1}
10^{-2}
10^{-3}
10^{-4}
10^{-5}
10^{-6}
10^{-7}
10^{-8}
RVGNW (NL)
De Kempen (NL)
De Kempen (BE)
RVG (NL)
RVG (BE)
ROSE (NL)
ROSE (DE)
Reliability
High
Medium
Low

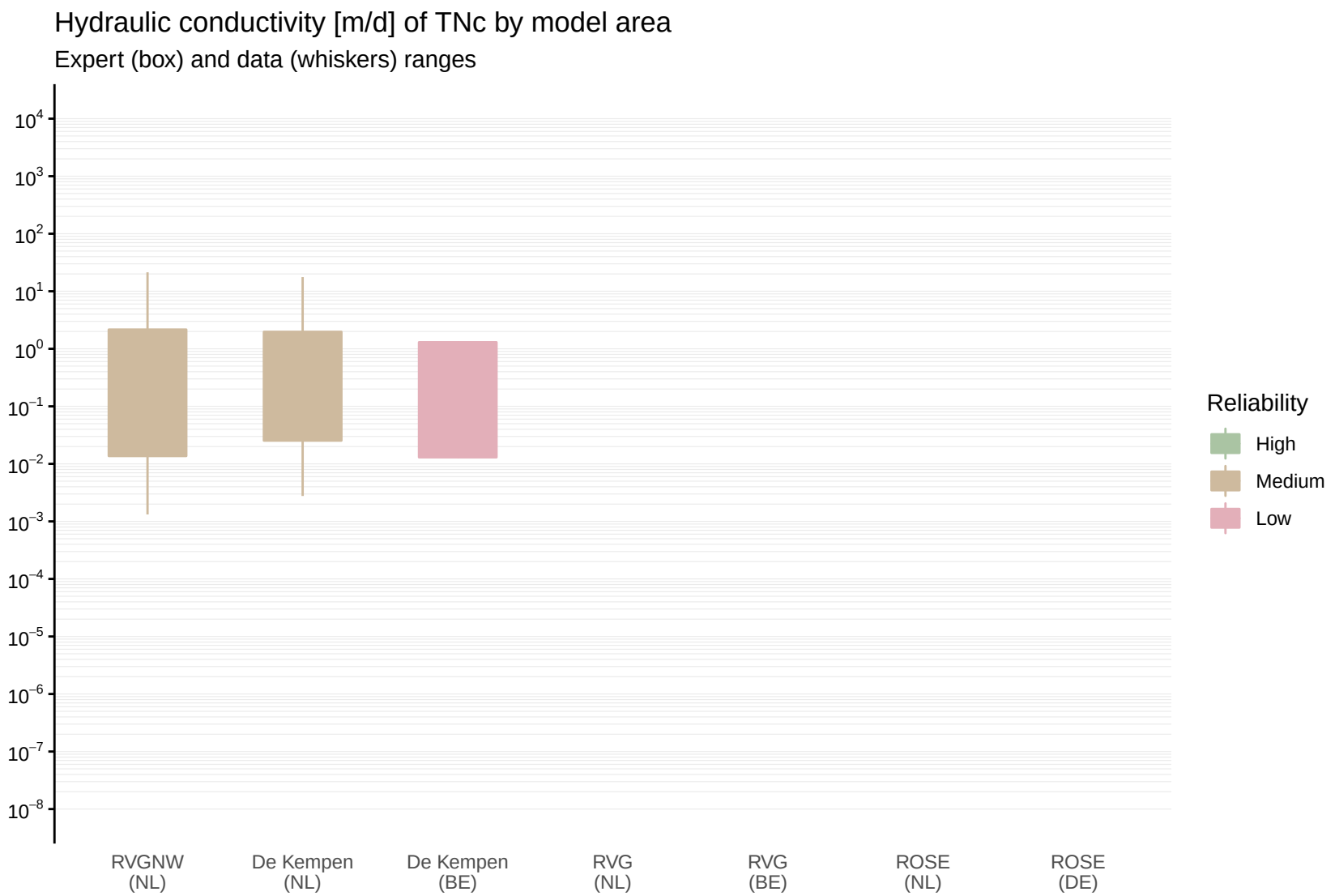
Hydraulic conductivity [m/d] of TNc by model area
Expert (box) and data (whiskers) ranges
10^{4}
10^{3}
10^{2}
10^{1}
10^{0}
10^{-1}
10^{-2}
10^{-3}
10^{-4}
10^{-5}
10^{-6}
10^{-7}
10^{-8}
RVGNW (NL)
De Kempen (NL)
De Kempen (BE)
RVG (NL)
RVG (BE)
ROSE (NL)
ROSE (DE)
Reliability
High
Medium
Low

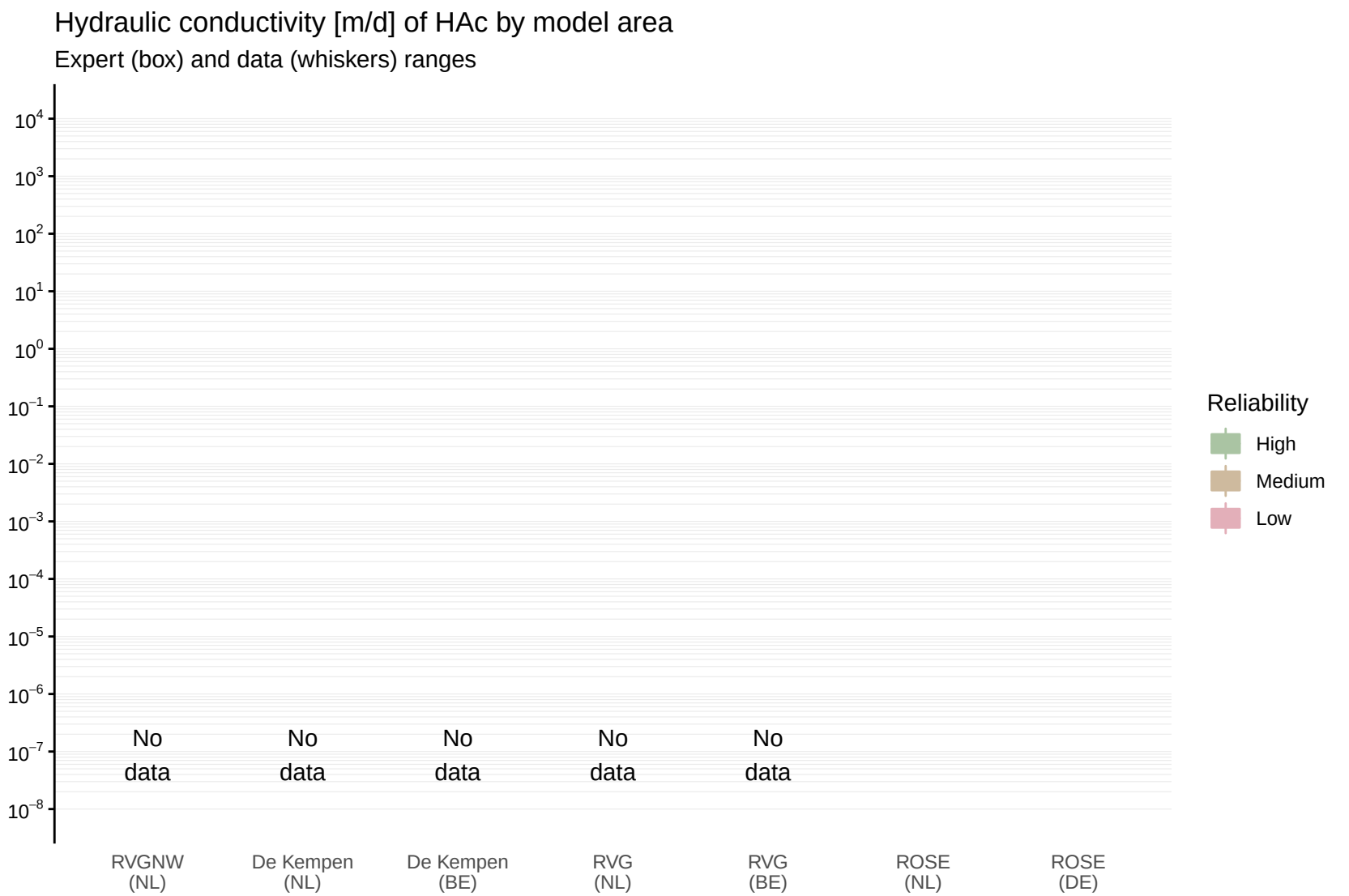
Hydraulic conductivity [m/d] of HAc by model area
Expert (box) and data (whiskers) ranges
10^{4}
10^{3}
10^{2}
10^{1}
10^{0}
10^{-1}
10^{-2}
10^{-3}
10^{-4}
10^{-5}
10^{-6}
10^{-7}
10^{-8}
No data
No data
No data
No data
No data
RVGNW (NL)
De Kempen (NL)
De Kempen (BE)
RVG (NL)
RVG (BE)
ROSE (NL)
ROSE (DE)
Reliability
High
Medium
Low

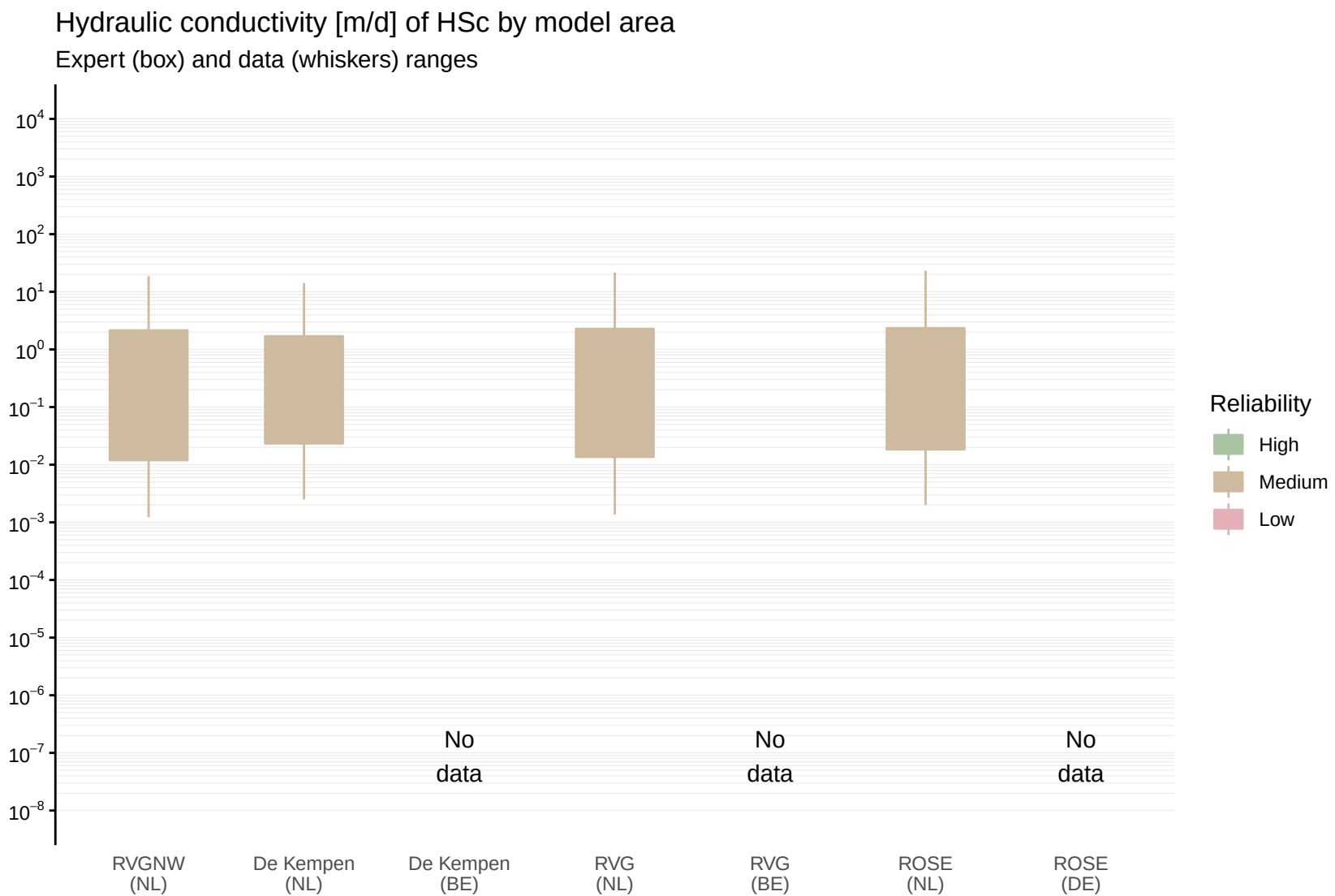
Hydraulic conductivity [m/d] of HSc by model area
Expert (box) and data (whiskers) ranges
10^{4}
10^{3}
10^{2}
10^{1}
10^{0}
10^{-1}
10^{-2}
10^{-3}
10^{-4}
10^{-5}
10^{-6}
10^{-7}
10^{-8}
No data
No data
No data
RVGNW (NL)
De Kempen (NL)
De Kempen (BE)
RVG (NL)
RVG (BE)
ROSE (NL)
ROSE (DE)
Reliability
High
Medium
Low


Hydraulic conductivity [m/d] of OPc by model area
Expert (box) and data (whiskers) ranges
10^{4}
10^{3}
10^{2}
10^{1}
10^{0}
10^{-1}
10^{-2}
10^{-3}
10^{-4}
10^{-5}
10^{-6}
10^{-7}
10^{-8}
No data
No data
RVGNW (NL)
De Kempen (NL)
De Kempen (BE)
RVG (NL)
RVG (BE)
ROSE (NL)
ROSE (DE)
Reliability
High
Medium
Low